Università degli Studi di Ferrara

DOCTORAL COURSE IN "HUMANITIES"

CYCLE XXXIII

DIRECTOR Prof. Trovato Paolo

BEHAVIOURAL VARIABILITY IN PREHISTORIC SOCIETIES: LINEAR AND GEOMETRIC MORPHOMETRIC APPROACHES ON ENTHESEAL SITES OF METACARPAL AND PHALANGEAL BONES OF ADULT INDIVIDUALS

Scientific/Disciplinary Sector (SDS) L-ANT/01

Candidate
Dott. Calandra Rosamaria

(signature)

Supervisor
Prof. Arzarello Marta

(signature)

Co-Supervisor
Dott. Arnaud Julie

(signature)

Years 2017/2020

Tables of Contents

Chapter 1

Introduction

In archaeological and forensic fields, investigating variations recorded on human bones is necessary for reconstructing occupational profiles of individuals. In archaeological contexts, these analyses allow researchers to reconstruct typical behaviours of ancient population from a biocultural point of view (Mariotti *et al.*, 2004). Physical activity can be considered as a linking nexus between features of technology, economy and social relations (Wallace *et al.*, 2017). According to bioarchaeologists, the morphology and the degree of development of muscle and tendon insertion sites (also known as *entheses*) are informative about levels of physical activity; in particular, they are considered as indicators of habitual muscle use (Noldner, Edgar, 2013; Wallace *et al.*, 2017).

Several anthropological and biomechanical studies conducted during the years concluded that bones are subjected to remodelling processes when exposed to muscular stress (Rauch, 2005; Foster *et al.*, 2014). Over the years, particular attention was given to post-cranial bones (vertebras, bones of the upper and lower limbs), because of their main use during locomotion and physical activities (Mariotti *et al.*, 2004, 2007; Milella *et al.*, 2012; Foster *et al.*, 2014; Macintosh *et al.*,2014; Santana-Cabrera *et al.*, 2015). In this research, the interest is pointed towards the hand bones, mostly to metacarpals and proximal phalanges, which have never been particularly considered except for the last decades. In fact, their small dimensions, particular morphologies, and important morphological variability make hard their identification in archaeological context. As a consequence, they are not considered so much and, for these reasons, finding complete reference collections with the entire set of hand bones is not easy. Furthermore, their intra-specific variability makes hand bones be confused with some faunal osteological remains.

Fortunately, in the last decades, the development and application of new technologies have allowed to develop specific approaches to different skeletal part, multiplying the field of investigation and promoting their preservation. In this context, the introduction of 3D technologies and geometric morphometrics has been really useful allowing to analyse several aspects difficult to consider only macroscopically. In this framework, the application of such analysis on muscular insertion sites of hand bones led to the development of new perspectives of research concerning the reconstruction of manual activity patterns of human populations.

In the present study, different types of investigations will be conducted in order to obtain the most accurate and complete information possible; entheseal surfaces of metacarpals and proximal phalanges will be analysed with both linear and geometric morphometric approaches to evaluate shape variation in human hands, in relation to several human crafts. The main goal is to create activity patterns of recent and ancient populations through the analysis of markers recorded on the bones, reflecting continuous muscle use in agreement with peculiar behaviours and subsistence strategies. The selected sample comes from several osteological collections and different chronologies, from Neolithic to Late Medieval, using the biological known collections as references.

In order to reach the main aim, the different types of the cited technologies and methodologies will be used; all these set of analyses will be conducted on the selected entheses to answer to the following **Research Questions** that can be exposed in this way:

Which is the degree of shape variation of the entheseal surfaces of hand bones of individuals coming from populations of different historical periods? How do the different human groups correlate? Are there differences in 3D entheseal shape and size from a diachronic point of view?

The ensemble of results and answers obtained will help to generally reconstruct the possible manual activities of the ancient and selected populations compared to the reference ones, on the base of different subsistence economies performed by each population. To pursue this goal, it will be important to evaluate the differences of the anthropological collections introduced, due to the nature of the burials and the dispersion of the human remain. The creation of activity patterns will be related to precision and powerful grasping performances conducted during different chronologies; also, both linear and geometric morphometric methodological approaches will be used. These models will be formulated on the base of the muscles utilised in all these kinds of grasping, because of the different typologies of movements and grips realised, according to subsistence activities of human groups (Karakostis, Lorenzo, 2016; Karakostis *et al.*, 2017; Karakostis *et al.*, 2018).

1.1 State of art

The word 'enthesis' – from Greek term *ένθεση* meaning 'insertion' – refers to attachment sites of muscles, tendons and ligaments on bones' surfaces and are commonly subjected to overuse injuries (M Benjamin et al., 2006). In 1959, G. La Cava created the term 'enthesitis' referring to an "inflammation of tendon attachments into bone". Afterwards, J. Ball (1971) and G.A. Niepel and S. Sit'Aj (1979) used two different terms to differentiate the normal ('enthesis') and the pathological conditions ('enthesopathy') of insertion sites (La Cava, 1959; Jurmain, Villotte, 2010).

According to the kind of tissue at the bone-tendon interface, entheses are classified into **fibrous** and **fibrocartilaginous**. Fibrous attachment sites insert on long bones' diaphysis, on the skull and vertebras directly or through the periosteum. They can also be subdivided into two categories: periosteal and bony. On the contrary, fibrocartilaginous entheses attach on bones' epiphyses, short bones, and some parts of vertebras. In this type of insertion sites is possible to differentiate four different histological zones: tendon or ligament, uncalcified fibrocartilage, calcified fibrocartilage and subchondral bone; also, the uncalcified and calcified fibrocartilages are highly vascularized and separated by a calcified layer called *tidemark* (Benjamin *et al.*, 1986; Benjamin, 2000; Benjamin *et al.*, 2002, 2006; Jurmain *et al.*, 2012; Foster *et al.*, 2014).

When subjected to overuse injuries, entheses modify their surface morphology, usually characterized by irregularities (ridges, roughs, remodelling) and determined by their location and functional requirements. It is important to distinguish the 'robusticity' character from the pathological type consequently to muscles' activity. Robusticity represents the 'normal' osseous marking at attachment site; on the contrary, the pathological cases can be subdivided into erosive (*osteolytic enthesopathies*, OL) and proliferative (*osteophytic enthesopathies*, OF) (Mariotti *et al.*, 2004; Benjamin *et al.*, 2006; Jurmain *et al.*, 2012; Foster *et al.*, 2014). The boundary between robusticity and pathology is not clearly well-defined because they depend on several remodelling multifactorial origin (Jurmain, Villotte, 2010; Manzon, 2011; Jurmain *et al.*, 2012).

In not pathological cases, it is possible to talk about **Musculoskeletal Stress Markers** (MSMs) or **Entheseal Changes** (ECs), considered as indicators of activity and biomechanical stress. The expression *Musculoskeletal Stress Marker* was introduced in literature with the work of Hawkey and Merbs (Hawkey, Merbs, 1995); even if several terms and expressions were also used to describe these morphological changes, researchers started talking about ECs, trying to avoid particular references to their aetiology (Jurmain, Villotte, 2010; Jurmain *et al.*, 2012).

Several works about methodological analyses regarding the recognition of ECs and the standardisation of terminologies all over the world about entheseal morphologies were carried out. Other studies take into consideration bones of the upper and lower limbs to reconstruct patterns of physical activities in past and recent populations.

Hawkey and Merbs analysed the human osteological remains (=318 individuals) of two ancient Eskimos populations of two different period (Early and Late Period Thule), coming from the Hudson Bay (Canada). Only adult individuals were analysed in this research, while children and subadults were not introduced. The entheseal surfaces of the bones of the upper limb – clavicles, scapulae, humeri, radii, ulnae – were examined to evaluate and visually score stress markers. For this goal, one of the authors (D.E. Hawkey) created a visual reference system to obtain a standardised scoring method for MSMs. She distinguished three categories – robusticity, stress lesion and ossification – and recognised different visual score (0 = Absent, 1 = Faint, 2 = Moderate, 3 = Strong). Related to the historical periods, authors obtained different results. Concerning the Early Period Thule, results indicated gender-specific activities – even if not evident in the archaeological record. Clothing preparation was a peculiar female activity, while use of umiak and kayak for hunting was typically male (even if probably women used umiak for family transportation and participated in scavenging activities along the shoreline). Concerning the Late Period Thule, an increase of caribou hunting was recorded and a decreasing until disappearance of kayak use was observed after the Early Period, suggesting changes in subsistence strategies though time. (Hawkey, Merbs, 1995).

The research group of the University of Bologna worked on recent identified osteological collections to propose standardised scoring methods for entheses and enthesopathies of the postcranial skeleton

to evaluate the different entheseal morphologies related to age, sex and physical activity (Mariotti *et al.*, 2004; Mariotti *et al.*, 2007; Milella *et al.*, 2012).

In 2004, V. Mariotti, F. Facchini and M.G. Belcastro worked on a sample (=113 individuals) coming from two osteological collections with known sex, age and occupation: 52 males from the Sperino Collection housed in the Institute of Anatomy of the Modena Hospital (late XIX c.) and 61 individuals – 44 males and 17 females – from the Sardinian collection housed in Museum of Anthropology of the University of Bologna (early XX c.). For the analyses, they subdivided the sample in several age classes (YA = Young Adults, MA = Mature Adults, OA = Old Adults) and selected only individuals of the class 'MA' to test sex and age differences. So, the final sample was made of 20 males and 17 females. Their scoring method distinguish 'robusticity' and 'enthesopathy' (both osteophytic and osteolytic), providing 3 possible degrees of entheseal development (1 = weak to moderate; 2 = strong; 3 = very strong) and photographic documentations. The results showed possible effects of sex and age on the degree of development of enthesopathies, considering their multifactorial aetiology. Enthesopathies can be used to reconstruct past occupational activities in ancient populations, even if – in case of prehistoric collections – this kind of analyses could be more difficult because of the lack of exact and accurate individual information about occupations (Mariotti *et al.*, 2004). Another work investigates 23 entheses of several postcranial bones, belonging to both right and left sides, (clavicle, scapula, humerus, radius, ulna, femur, tibia, patella, calcaneus) to understand the relations between the degree of entheseal development and both sex and age and, finally, to describe the development of the analysed entheses (Mariotti *et al.*, 2007). An application of this scoring method was made analysing the effect of age, sex and physical activity on entheseal morphology in a large Italian contemporary skeletal sample (=484 adult individuals – 274 males, 210 females) coming from the Sardinian identified collection (early XX c.). In this case, the authors selected 158 males with known occupational profile to test for influence of biomechanical stress on entheseal changes, then subdivided into two groups – Hard workers (HW: farmers, miners, manual laborers) and Light workers (LW: employees, shoe-makers, painters). As result, sex and age are the major contributors which influence entheseal changes; on the contrary, no significant correlation has been found concerning the influence of physical activity. These results show that the different degrees of entheseal development depend on biological genetic factors (sex and age, for example), not to mechanical ones (Milella *et al.*, 2012).

In 2009, the Workshop in MSMs was organised and held at University of Coimbra (Portugal) to discuss and standardise methodology and terminology used to study both enthesopathies and stress occupational markers in relation to age effect (Henderson *et al.*, 2010; Henderson *et al.*, 2012; Henderson, 2013; Henderson *et al.*, 2016; Henderson *et al.*, 2017; Henderson *et al.*, 2017). Also, a relationship between ECs of postcranial bones and physical stress was investigated (Milella *et al.*, 2015). The results of this work put in evidence different separate occupations related to farming, physically demanding occupations and undemanding activities; also, they are consistent with

differences in biomechanical activities between different occupations related to farming activities (Milella *et al.*, 2015).

1.2 Bilateral asymmetry and sexual division of labour

During the last decades, several studies have pointed out the presence of bilateral individual asymmetry and sexual dimorphism from different points of view – for example, both inter- and intra-specific and both inter- and intra- population.

1.2.1 Examples of bilateral asymmetry

Bilateral asymmetry related to different use of both right and left sides in muscle activity can be recorded after intense and continuous mechanical stress; nowadays, this kind of condition is recognisable, for example, in pro tennis players. In ancient populations, this feature is recorded on long bones of hunter-gatherers using javelins and atlatls or after the introduction of bows and ploughs or starting of forging activities (Molnar, 2006; Sládek *et al.*, 2007; Sparacello *et al.*, 2011; Villotte, Knüsel, 2013; Kubicka *et al.*, 2016; Sládek *et al.*, 2016).

Several studies involving bilateral asymmetry focuses on the bones of the upper limb (Sládek *et al.*, 2007; Sládek *et al.*, 2016; Kubicka *et al.*, 2016; Kubicka *et al.*, 2018). V. Sládek and colleagues analysed asymmetry in external dimensions and asymmetry in size and distribution of cortical tissue of humeri to understand the real nature of the transition period from the Late Eneolithic to Early Bronze Age in Central Europe – if associated with changes in subsistence strategies and gender differences or if may be considered as a continuous process. To test these hypotheses, the authors analysed a sample of a total 67 male and female individuals with both right and left well-preserved humeri, coming from five different archaeological cultures. They observed divergences between males and females, associated with gender-specific activities: entheseal changes recorded on males might be related to asymmetrical manipulation loading (for example, extra-domestic agricultural work), while entheseal changes recorded on females might be associated with symmetrical manipulation loadings (for example, domestic labour). These results also let authors interpret the sexual differences as evidence of gender-specific work (Sládek *et al.*, 2007).
Another study analysing possible bilateral asymmetry of the upper limbs was performed by A.M. Kubicka and colleagues using a combination of linear and geometric morphometric methods. The authors measured clavicles, humeri and scapulae from 100 individuals – 50 males, 50 females – coming from a Medieval Polish population: later, they put landmark and semi-landmark reference system on the 3D reconstruction of the glenoid fossa to investigate shape differences between right and left sides of the same individual between sexes. From an archaeological point of view, males were involved in harder work – building, plowing, agriculture – while females used to be involved

in other kind on work – carrying children or water, helping with the harvest, showing different markers of activity. In this study, authors obtained similar results for both males and females: the similarity of asymmetry between sexes may be due to similar activities performed between men and women, taking into account the hypothesis of similar level of activity performed – not necessary performing the same kind of tasks (Kubicka *et al.*, 2016).

Bilateral asymmetry was also investigated evaluating different types of technologies – for example, grindings – in females of prehistoric groups from Neolithic to Iron Age in Europe. An experimental study was conducted including 36 female volunteers, subdivided into two groups: 16 of them were employed to analyse grinding efficiency, while 20 of them were employed to analyse muscle activity during grinding. Only right-handed women were introduced in the study. The authors tried to assess evidence related to the different use of saddle quern (Neolithic) and rotary quern (Iron Age) using electromyography to measure activity of muscles of the upper limbs and try to reconstruct past activity patterns according to subsistence changes with the introduction of agriculture. Experimental result showed differences in the use of the two kind of querns: the saddle one requires more muscle strength than the rotary quern and showed also symmetrical activity in the muscle involved; on the contrary, experimental tests with the rotary quern showed evident directional asymmetry in particular during bimanual rotation. As a result, saddle quern grinding may have decreased the directional asymmetry in humeral strength in Neolithic agricultural females, while the introduction of the rotary quern may have increased the humeral asymmetry and reduced time related to cereal grinding to realise other manipulative tasks (Sládek *et al.*, 2016).

A recent work analysed bilateral asymmetry of the humerus in Neanderthals, Australian aborigines, and individuals of a medieval population to interpret the functional adaptation of the upper limbs to habits in Palaeolithic and modern hunter-gatherers and farmers (Kubicka *et al.*, 2018). Three different historical samples were compared: CT image data of 5 humeri pairs of adult Neanderthals, 80 humeri pairs belonging to a medieval Polish population (40 males, 40 females) and 15 humeri pairs of 15 modern Australian aborigines (11 males, 4 females). Results showed a more evident directional asymmetry in the medieval sample compared to the Palaeolithic and modern hunter-gatherers. These differences may be related to the different physical efforts of the medieval population – not associated to the shift to agriculture. The observed differences between Neanderthals and modern aborigines can be due to "[…] different habitual behaviour, eco-geographic pattern in body proportions, climatic adaptations, genetic factors, and differences in ontogeny. The low level of directional asymmetry observed in individuals with greater development of the left arm might be explained by their adjustment to the constraints of a right-handed world […]." (Kubicka *et al.*, 2018).

1.2.2 Examples of sexual division of labour and subsistence strategies

Other studies examine in particular sexual dimorphism and gender-specific activity patterns related to changes on subsistence strategies or sexual division of labour (Churchill, Morris, 1998; Derevenski, 2000; Wanner *et al.*, 2007; Macintosh *et al.*, 2014; Santana-Cabrera *et al.*, 2015).

Taking into consideration different prehistoric samples, divergences in manipulative behaviours between men and women have been recorded. Authors investigated asymmetry and variability in humeral lengths of individuals of different transition periods – Early/Middle Neolithic, Early/Middle Bronze Age, Early/Late Iron Age – with similar subsistence strategies characterising the transition to agriculture. Neolithic females showed more variability than males, while a major degree of homogeneity has been observed during the Bronze Age between sexes. If considering the Bronze/Iron Age transition, a reduction of sexual dimorphism and an increasing of morphological changes between males and females have been observed; also, in the transition period Neolithic – Bronze/Iron Age, an increasing of loading activities carried out by females has been recorded (Macintosh *et al.*, 2014).

Consistent results have been obtained for pre-Hispanic populations (a Maya coastal group from Mexico and a human group of Gran Canarias Isle, 11^{th} – 15^{th} c.). Even if different kinds of studies were performed, results concerned sexual division of labour: males' biomechanical activities are related to maritime transport and loading of materials and farming, while females used to perform fine hand movements and process food, such as extraction and processing cereals (Wanner *et al.*, 2007; Santana-Cabrera *et al.*, 2015).

1.3 Focus on entheseal changes of hand bones

When focusing on hand bones and entheseal changes, investigate human manual activities is possible when considering the 'high robusticity' character as indicator of continuous and intense muscular stress (Cashmore, Zakrzewski, 2013; Noldner, Edgar, 2013; Karakostis, 2014-15; Karakostis, Lorenzo, 2016; Karakostis *et al.*, 2018). Cashmore and Zakrzeski analysed the development of MSMs in the human hand creating a presence/absence scoring system for twelve muscular origin and insertion sites of metacarpals and phalanges from an English sample (= 32 individuals from Naval Hospital Cemetery, Greenwich – London). Authors were able to obtain information about bilateral asymmetry comparing hand entheses with humeri of the same individuals (low levels of asymmetry), demonstrating that hand bones and their entheses can be introduced into MSMs research to better understand divergences in cultural behaviour (Cashmore, Zakrzewski, 2013).

Macroscopic methodologies were applied to observe and analyse the entheseal development after intense stress activity using qualitative scoring systems in the previously described works (Hawkey, Merbs, 1995; Mariotti *et al.*, 2004, 2007; Cashmore, Zakrzewski, 2013). Both 2D and 3D methods were developed to quantify entheseal surface areas on hand bones; as written by Noldner and Edgar, "2D areas account for enthesis size, overlooking surface topography, and therefore rugosity. 3D scanning technology provides a way to quantify both enthesis size and rugosity by measuring surface topography within the true boundaries of the insertion sites" (Noldner, Edgar, 2013). Indeed, representing entheses in a 3-dimensional way is useful to evaluate and provide more data regarding their shape and complexity thanks to several software programs (Noldner, Edgar, 2013).

1.4 Applications and examples in prehistoric contexts

In archaeological and paleoanthropological contexts, taking into consideration the entheseal development and the related changes as activity stress marker is useful to better understand the totality of changes in subsistence strategies and cultures. This could be considered the main reason to investigate both the hand and its muscles and entheses to obtain information about its biomechanical potentialities and evolutionary history (Karakostis, 2014-15; Karakostis, Lorenzo, 2016; Karakostis *et al.*, 2017). Nevertheless, some researchers assert that physical labor does not influence entheseal morphology but these changes depend on genetic or biological factors (such as age and body size) (Zumwalt, 2006; Milella *et al.*, 2012; Djukic *et al.*, 2015; Williams-Hatala *et al.*, 2016).

Most of the studies cited above did not focus on 3D entheseal shape, but only on the evaluation of the entheseal size. Thanks to works by A. Karakostis, a repeatable geometric morphometric approach to analyse 3D hand entheseal form (both size and shape) – based on 3D landmark apposition – was developed; the resulting shape variables can be utilized to compare both 3D size and shape of entheses and the relation between them (also known as allometry) from a statistic point of view (Mitteroecker, Gunz, 2009; Karakostis *et al.*, 2018).

Some of the most recent anthropological works investigating hand bones have been carried out by several research groups, particularly focusing on both muscles and entheses and morphology of the bones of the thumb – comparing humans, great apes and fossil hominins – because of its important function in manipulative grips (Maki, Trinkaus, 2011; Bardo *et al.*, 2016; Bardo *et al.*, 2017; Karakostis et al., 2018; Bucchi *et al.*, 2019; Galletta *et al.*, 2019; Karakostis *et al.*, 2019).

In such inter-specific approach, A. Bardo and colleagues compared manual functional abilities belonging to great apes and humans when performing tool use in food collection to investigate if different species used to perform different manual techniques and performances. After experimental

works, they were able to observe different techniques used by each species – humans used bimanual and precision grip techniques also involving fingertips in in-hand movements, gorillas used unimanual grips and simple in-hand movements, orangutans used different kind of strategies, also including mouth. The experimental results can be correlated to the different kind of locomotion and lifestyles of these species (Bardo *et al.*, 2017). When investigating behavioural and functional strategies during tool use in *Pan paniscus*, the results showed that "[…] bonobos were able to develop in-hand movements similar to humans and chimps, demonstrated dynamic manipulation, and they responded to task constraints by selecting and modifying tools appropriately" (Bardo *et al.*, 2016). All these types of experimental investigations are useful to understand and reconstruct the evolution of primate manual abilities and to obtain more information about the evolution of morpho-functional skills of the human hand (Bardo *et al.*, 2016).

In paleoanthropological field, researchers started focusing on morphological characteristics of the thumb comparing modern living individuals and fossil specimens. A. Karakostis and colleagues investigated Neanderthal manual activities using a 3D multivariate analysis on entheseal surfaces of hand bones. They established that Neanderthals did not only performed powerful grasping, but they also performed precision forceful movements thanks to the thumb and the index finger, according to production and use of flake-based industries, suggesting a real complex behaviour (Karakostis *et al.*, 2018). Another 3-dimensional approach was conducted by L. Galletta and colleagues to compare the distal articular surface of the 1st metacarpal in humans, great apes, and fossil hominins; the objective was to analyse different shape morphologies related to human-like forceful opposition and to evaluate if such morphologies are similar between different species – both extant and fossil ones. As results, authors obtained humans differ from great apes because of a flatter distal articular surface of 1st metacarpal, a larger epicondyle surface and a larger radial palmar condyle, suggesting that, if these characteristics are present in fossil specimens, this could be an indication of human-like manipulative actions (Galletta *et al.*, 2019).

Chapter 2

The human hand bones

The human hand represents the distal extremity of each upper limb. It is a complex structure, made up of several bones, articular joints, muscles, and tendons. Its anatomy has been extensively descripted. Before describing the different elements of the hand introduced in this research, it is important to consider the anatomical nomenclature used in the study of the hand for a correct orientation of both bones and enthesis. In particular:

- Anterior = palmar;
- Posterior = dorsal;
- Medial = ulnar = 5^{th} finger side;
- Lateral = radial = 1^{st} finger side.

Also, the different kind of movements (**Figure 1)** a limb can do are subdivided into:

- Flexion: a bending movement that decreases the angle between body parts. When the fingers of a hand are tightly closed in a fist, there is strong flexion of the phalanges on the metacarpal heads;
- Extension: opposite of flexion, a movement that increases the angle between body parts. When the fingers are completely extended, the hand is open;
- Abduction: the movement of a limb away from the sagittal median plane. Concerning the hand, the principal plane is a sagittal plane passing through the third finger;
- Adduction: opposite of abduction, the movement of a limb towards the sagittal plane. Concerning the hand, adduction is the movement of the five digits towards the sagittal plane of the middle finger.

Each hand consists of 27 bones, subdivided into three parts: carpus, metacarpus, and digits (**Figure 2**). **Carpus** is made up of 8 small irregular bones, arranged in two rows. The proximal row includes (considering a radial-ulnar direction) the **scaphoid**, the **lunate**, the **triquetral** and the **pisiform**. The distal row (considering again a radial-ulnar direction) is composed of the **trapezium** (or **greater multangular**), the **trapezoid** (or **lesser multangular**), the **capitate** and the **hamate**.

The dorsal carpal surface is convex while the palmar one is concave and creates a carpal groove. The radial and the ulnar projections of the palmar surface are formed by the pisiform and the hook of the hamate (on the medial side) and the scaphoid and the trapezium (on the lateral side). A fibrous retinaculum – *flexor retinaculum* – is attached to these projections and creates a **carpal tunnel** through which flexor tendons of the wrist pass: this fibrous band makes the carpus stronger and increases flexors' tendons performances. The articulation in correspondence with the carpal bones occurs thanks to different kind of ligaments, as shown below (**Figure 3**) (Gray, 1918; Standring, 2008; White *et al.*, 2012).

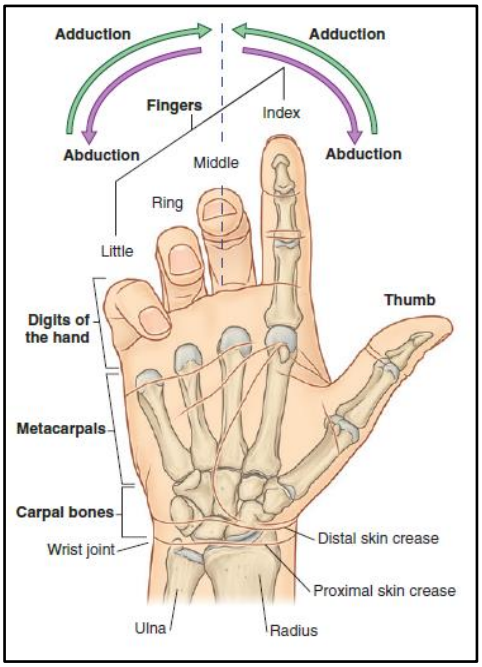

Figure 1 - Right hand. The fingers are shown in a normal resting arcade in which they are flexed. In the anatomical position, the digits are straight and adducted (Drake *et al.*,2019).

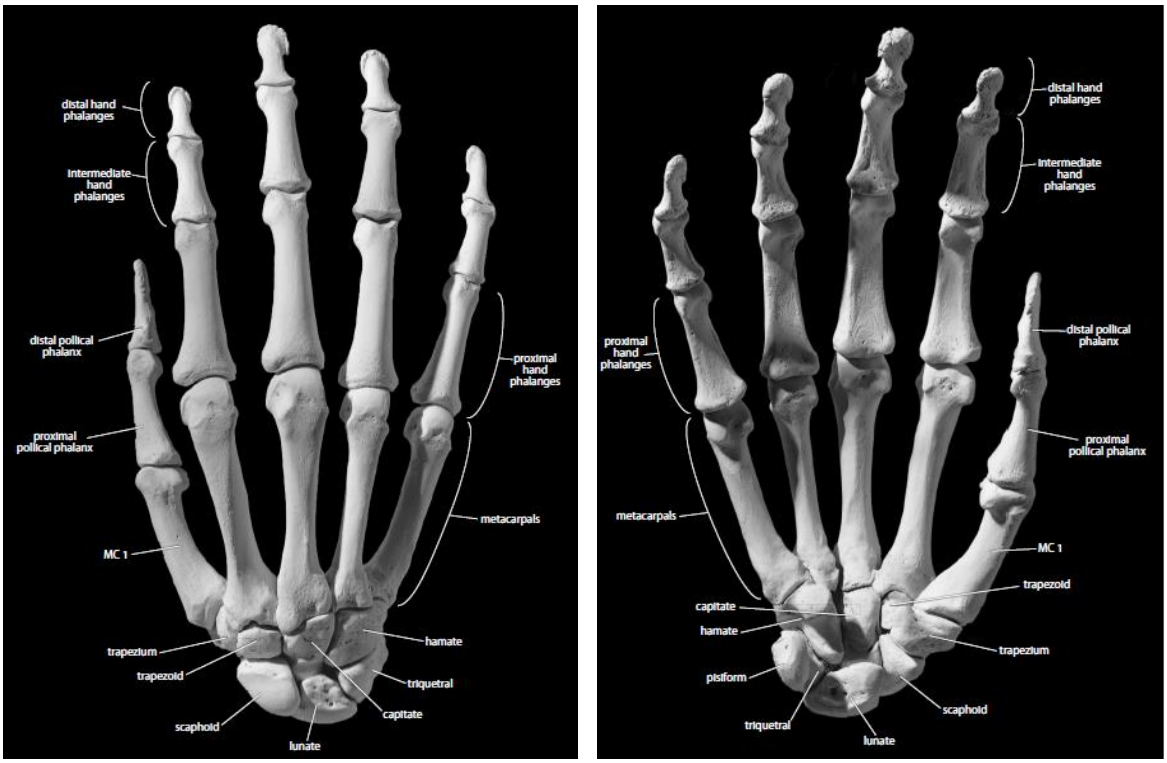

Figure 2 - Right hand. Dorsal (on the left) and palmar (on the right) views. Small sesamoid bones not included (White et al., 2012).

Metacarpus is made up of 5 metacarpal bones, conventionally numbered from 1 to 5 in radio-ulnar order. Metacarpal bones are considered as little long bones: they present two epiphysis (a proximal one and a distal one) and a diaphysis. The distal epiphysis is a rounded **head** that articulates with the correspondent proximal phalange while the **base** articulates with the distal row of the carpus and with each other metacarpal (except for MC1 and MC2). The shaft of each bone is longitudinally curved and allows the insertion of *Palmar Interossei* muscles. Each metacarpal base has a distinctive morphology, and the identification is possible thanks to it. The metacarpals are usually described as parallel, but they converge towards the carpus. They form the so-called *metacarpal interossei spaces* that are occupied by *palmar* and *dorsal interossei* muscles. The articulation between MCs is allowed by different ligaments: *palmar* and *dorsal ligaments* join the base of MC2, MC3, MC4 and MC5 anteriorly and posteriorly, while *interossei ligaments* are at the adjacent surfaces of metacarpal bases (**Figure 3**).

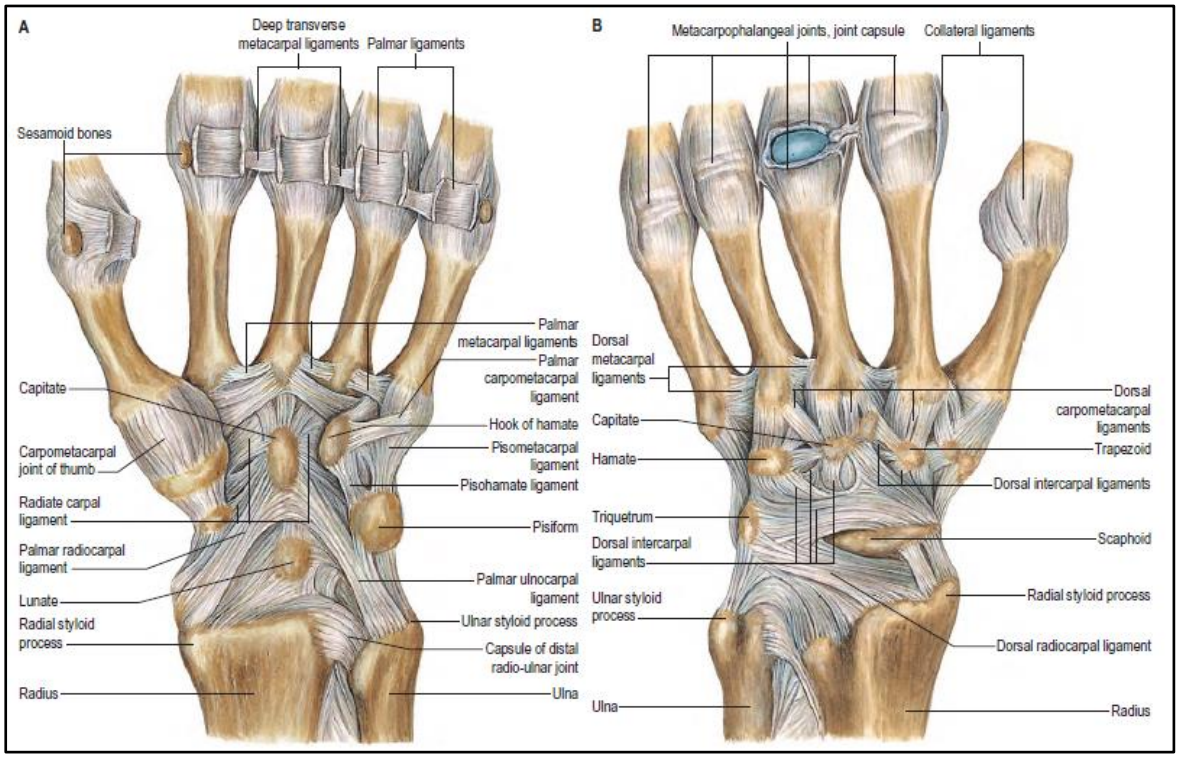

Figure 3 – Joints and ligaments of the left hand. A, palmar aspect. B, dorsal aspect (Standring, 2008).

Digits are made up of 3 phalanges – **proximal**, **intermediate,** and **distal**. The thumb is an exception because it lacks the intermediate one, so it presents only proximal and distal phalanges. Each hand presents a total of 14 phalanges. **Phalanges** are shorter than metacarpals; their shaft is antero-posteriorly flattened, their dorsal surface is transversely convex while the palmar one is flat but

concave anteriorly along the long axis. The proximal epiphysis (the **base**) is larger than the distal end (the **head**). Dorsal surfaces are smooth and rounded while palmar surfaces are flat and roughened along both side of the shaft, because of the insertion of fibrous flexor sheaths (**Figure 4**).

The proximal phalanges are the longest of the hand. Their base is concave and rounded, adapted to the metacarpal heads while their heads articulate with the bases of intermediate phalanges. Also, distal phalanges have a double articular facet that articulates with the head of intermediate phalanges. The distal epiphysis (also called **tuft**) has a **distal phalangeal tuberosity**, to which pulp of fingertips attaches (Standring, 2008).

Different ligaments and muscles insert on phalanges. The tendons of *Flexor Digitorum Profundus* and *Extensor Digitorum* insert on the base of each distal phalange on the palmar and the dorsal surfaces, respectively. The tendons of *Flexor Digitorum Superficialis* and the corresponding fibrous sheaths attach to the palmar sides of each intermediate phalange; also, a part of *Extensor Digitorum* insert to the base dorsally (Standring, 2008).

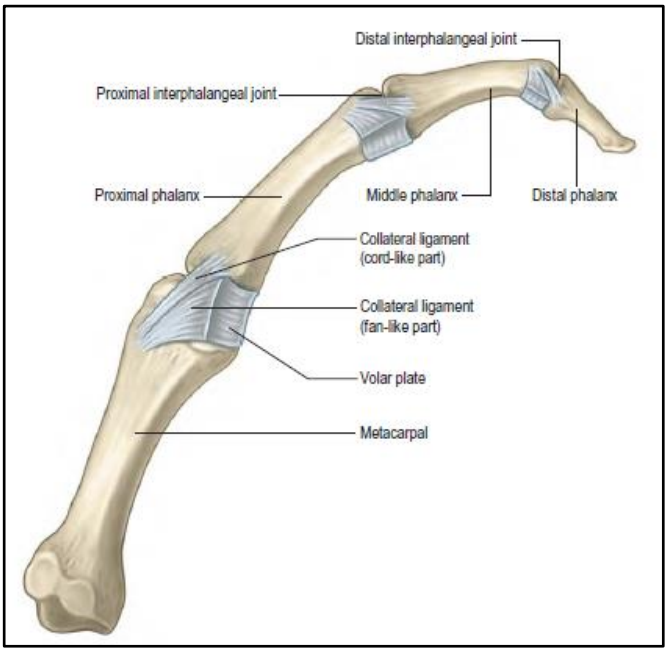

Figure 4 - Metacarpophalangeal and digital joints of the left 3rd finger: medial aspect (Standring, 2008)

2.1 The muscles and movements of the human hand

Muscles can be distinguished in different ways. Based on their origin, it is possible to distinguish **extrinsic** and **intrinsic** muscles. Extrinsic muscles originate from the arm and the forearm while intrinsic muscles originate in correspondence with the wrist and the hand.
Based on the position with respect to the joint, muscles can be distinguished in anterior and posterior. Finally, based on the function they carry out, muscles can be classified into extensors, flexors, abductors, adductors and opposing (Gray, 1918; Standring, 2008).

In this work, muscles will be descripted on the base of their function. In the table shown in Annexes (cf. A1 – 1), both intrinsic and extrinsic muscles of the hand are specified. Below, each muscular insertion considered in this work is described and indicated on the 3D model (**Figure 5**).

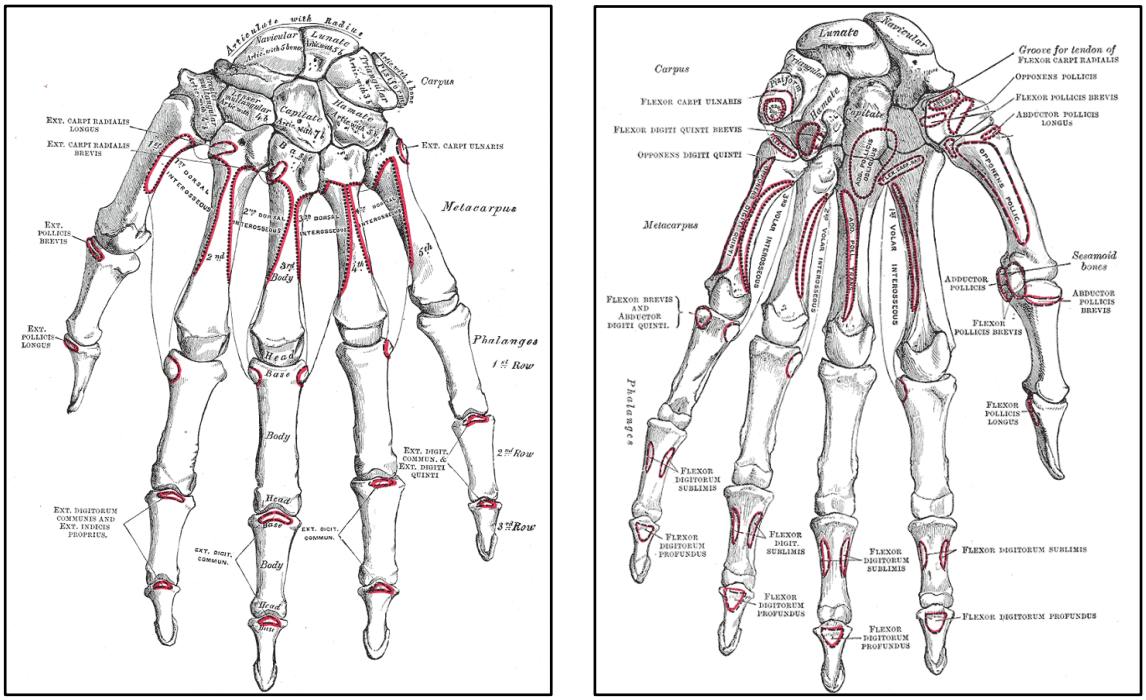

Figure 5 - Bones of the left hand with muscular insertions indicated (Gray, 1918).

2.1.1 **The thumb: muscles and entheses** (Gray, 1918; Standring, 2008)

The **1st metacarpal bone** (or **MC1**) is the shortest metacarpal. The **head** is less convex than in other metacarpals and is broad along its transversal axis. Its **shaft** is broader and more robust than the other metacarpals' shaft. The palmar surface is concave and is divided into a larger lateral (anterior) part and a smaller medial (posterior) one. MC1 articulates with the **1st proximal phalange** (or **PP1**); the latter articulates with the **1st distal phalange** (or **DP1**) (**Figure 6**).

Figure 6 – The entheseal surfaces on the 3D model of MC1, PP1 a DP1 (right hand). From left to right:

- MC1 – OP (on the lateral side of the shaft), ABL (on the lateral side of the base), DI1 (on the medial side of the shaft);
- PP1 – ADP (on the medial side of the base), EPB (on the dorsal surface of the base), ABP+FBP (on the lateral side of the base);
- DI1 – EPL (on the dorsal surface of the base), FPL (on the palmar surface of the base)

Opponens Pollicis – OP is the largest muscle of the thenar eminence. It arises from the tubercle of the trapezium and the adjacent *flexor retinaculum*. It inserts along the entire length of the lateral border and adjacent palmar surface of the MC1 shaft.

Abductor Pollicis Longus – ABL arises from the posterior surface of the shaft of the ulna, from interossei membrane and from the middle third of the radius. Its muscle fibres converge in a tendon that end proximal to the wrist. This tendon continues in a groove on the lateral side of the distal end of the radius, together with the *Extensor Pollicis Brevis* tendon. Then, it splits in two: one extremity inserts on the lateral base of MC1, while the other one is attached on the trapezium.

Dorsal Interosseous 1 – DIs are the most dorsal intrinsic muscles of the hand. They consist of four bipennate muscles, each arising from the adjacent sides of the metacarpal bones. DI1 is the largest one; it arises from the shafts of MC1 (on the ulnar side) and MC2 and inserts on the radial side of the 2nd proximal phalange.

Adductor Pollicis – ADP has two origin. The **oblique head** originates from *flexor retinaculum*, the capitate and the adjacent bases of MC2 and MC3. The **transverse head** originates from the palmar ridge on the distal two-thirds of the shaft of MC3. These heads converge towards the lateral side of the hand to a tendon which inserts on both the medial side of the base of PP1 and into the extensor hood.

Abductor Brevis Pollicis and *Flexor Brevis Pollicis* – ABP is one the muscle of the thenar eminence. It originates from the *flexor retinaculum*; some fibres arise from the scaphoid and the trapezium and from the tendon of ABL. FBP is medial in relation to ABP. It has two origins. The **superficial head** originates from *flexor retinaculum* and the distal part of the tubercle of trapezium; the **deep head** arises from the trapezoid and the capitate and from palmar ligaments of the distal carpal row.
ABP and FBP join and insert on the radial base of PP1.

Extensor Pollicis Brevis – EPB originates from the posterior surface of the radius and from the interosseous membrane. Its tendon inserts on the dorsal surface of DP1.

Flexor Pollicis Longus – FPL arises from the interosseous membrane and the anterior surface of the radius. Its tendon passes behind the *flexor retinaculum*, between OP and the oblique head of ADP. It inserts on the palmar surface of DP1.
Extensor Pollicis Longus – EPL is larger than EPB. It originates from the lateral part of the shaft of the ulna, in correspondence of the middle third of its posterior surface, and from the interosseous membrane. It inserts on the dorsal surface of the base of DP1.

2.1.2 **The index finger: muscles and entheses** (Gray, 1918; Standring, 2008)

The **2nd metacarpal bone** (**MC2**) is the longest metacarpal and has the largest base. It articulates with the trapezoid, the trapezium, the capitate and MC3 at the base. The tubercles on both sides on its head are attachment sites for the *collateral ligaments*. Its shaft is prismatic in section, curved in longitudinal direction, dorsally convex and concave towards the palm. The head of MC2 articulates with the **2nd proximal phalange** (or **PP2**) (**Figure 7**).

Figure 7 - The entheseal surfaces on the 3D model of MC2 and PP2 (right hand). From left to right:

- MC2 – DI2+PI1 (on the medial side of the shaft), FCR (on the palmar surface of the base), DI1 (on the lateral side of the shaft), ECRL (on the lateral side of the base);
- PP2 – PI1 (on the medial side of the base), DI1 (on the lateral side of the base).

Extensor Carpi Radialis Longus – ECRL originates from the distal part of the supracondylar crest and the lateral epicondyle of the humerus. Its tendon inserts on the dorsal surface of the base of the bone, just above the facet for the trapezium.

Flexor Carpi Radialis – FCR originates from the medial epicondyle of the humerus. Its tendon continues under the *flexor retinaculum* and inserts on a small tubercle on the palmar surface of the base of MC2 (on the radial side).

Dorsal Interosseous 1 – DIs are the most dorsal intrinsic muscles of the hand. They consist of four bipennate muscles, each arising from the adjacent sides of the metacarpal bones. DI1 is the largest one; it arises from the shafts of MC1 and MC2 (on the radial side) and inserts on the radial side of the 2nd proximal phalange.

Dorsal Interosseous 2 and *Palmar Interosseous 1* – DI2 and PI1 originate from the medial surface of the shaft of MC2. Concerning PIs, they are unipennate muscles and originates from the MCs' shafts, anterior in relation to the DIs.

2.1.3 **The middle finger: muscles and entheses** (Gray, 1918; Standring, 2008)

The **3rd metacarpal bone** (**MC3**) lies at the base of the middle finger. It has a **styloid process** projecting proximally from the radial side of the dorsal surface. At the base, it articulates with the capitate MC2 (laterally) and MC4 (medially). Its shaft is like that of MC2; it is attachment site for several muscles and the extensor tendon inserts on the dorsal surface. The head of MC3 articulates with the **3rd proximal phalange** (or **PP3**) (**Figure 8)**.

Figure 8 – The entheseal surfaces on the 3D model of MC3 and PP3 (right hand). From left to right:

- MC3 – ECRB (on the dorsal surface of the base), DI2 (on the lateral side of the shaft), DI3+ADP (on the medial side of the shaft), ADP (on the palmar surface of the base);
- PP3 – DI3 (on the medial side of the base), DI2 (on the lateral side of the base).

Adductor Pollicis – ADP has two origin. The **oblique head** originates from *flexor retinaculum*, the capitate, and the adjacent bases of MC2 and MC3. The **transverse head** originates from the palmar ridge on the distal two-thirds of the shaft of MC3. These heads converge towards the lateral side of the hand to a tendon which inserts on both the medial side of the base of PP1 and into the extensor hood.

Dorsal Interosseous 2 – the ulnar head of DI2 originates from the adjacent sides of MC2 and MC3 (on lateral side of its shaft). It inserts on the lateral base of the 3rd proximal phalange.

Dorsal Interosseous 3 – the radial head of DI3, together with the transverse head of ADP, originate on the medial side of the shaft of MC3. DI3 inserts on the medial base of the 3rd proximal phalange.

Extensor Carpi Radialis Brevis – ECRB originates from the lateral humeral epicondyle; its tendon, together with the ECRL's one, passes under the *flexor retinaculum* and inserts on the dorsal surface of the base of MC3, towards the facets for capitate and MC2, beyond the styloid process.

2.1.4 **The ring finger: muscles and entheses** (Gray, 1918; Standring, 2008)

The **4th metacarpal bone** (**MC4**) is shorter and thinner than MC3 and MC2. It articulates with the capitate (sometimes), the hamate, MC3 and MC5. The shaft is like MC2, but they differ because of a presence of a little crest on the lateral surface which separates the attachments of PI2 and DI3. The head of MC4 articulates with the **4th proximal phalange** (or **PP4**) (**Figure 9**).

Figure 9 – The entheseal surfaces on the 3D model of MC4 and PP4 (right hand). From left to right:

- MC4 – DI3+PI2 (on the lateral side of the shaft), DI4 (on the medial side of the shaft);
- PP4 – DI4 (on the medial side of the shaft), PI2 (on the lateral side of the shaft).

Dorsal Interosseous 3 and *Palmar Interosseous 2* – the ulnar head of DI3 and PI2 originate from the radial side of the shaft of MC4. They insert on the lateral side of the base of PP4.

Dorsal Interosseous 4 – DI4 originates from the adjacent shafts of MC4 and MC5. Its radial head is attached to the ulnar side of the shaft of MC4. DI4 inserts on the medial side of the base of PP4.

2.1.5 **The little finger: muscles and enthesis** (Gray, 1918; Standring, 2008)

The **5th metacarpal bone** (or **MC5**) is the base for the little finger. It is the thinnest and the shortest of the metacarpals constituting the palm (except of the thumb). MC5 articulates only with the hamate and MC4. On its medial bone surface, a non-articular tubercle for the *Extensor Carpi Ulnaris* is present. On the dorsal surface of the shaft, there is a triangular area almost reaching the base. The lateral surface inclines dorsally towards the proximal epiphysis; it is divided by a crest into a palmar strip (for the attachment of PI3) and a dorsal one (for the attachment of DI4). The head of MC5 articulates with the **5th proximal phalange** (or **PP5**) (**Figure 10**).

Figure 10 – The entheseal surfaces on the 3D model of MC5 and PP5 (right hand). From left to right:

- MC5 – ODM (on the medial side of the shaft), ECU+FCU (on the medial side of the base), DI4+PI3 (on the lateral side of the shaft);
- PP5 – ADM+FDM (on the medial side of the base), PI3 (on the lateral side of the base).

Opponens Digiti Minimi – ODM originates from the hook of the hamate and the *flexor retinaculum*. It is attached to the medial surface of the MC5.

Dorsal Interosseous 4 and *Palmar Interosseous 3* – DI4 originates from the adjacent shafts of MC4 and MC5. Its ulnar head is attached to the lateral surface of MC5 and inserts on the medial side of PP4. Also, PI3 originates from the lateral surface of MC5 but is attached to the lateral base of PP5.

Extensor Carpi Ulnaris and *Flexor Carpi Ulnaris* – ECU originates from the lateral humeral epicondyle and inserts on the non-articular tubercle of the medial side of the base of MC5. FCU originates from the olecranon and the posterior border of the ulna and from the medial humeral

epicondyle. The muscle fibres converge into a tendon which attaches to the pisiform bone; from here, the **piso-hamate** and **piso-metacarpal ligaments** inserts to the hamate and to the base of MC5.

Abductor Digiti Minimi and *Flexor Digiti Minimi* – ADM originates from the pisiform, the tendon of FCU and the piso-hamate ligament. The terminal part of its tendon is divided in two: one is attached on the ulnar side of the base of PP5, the other one joins the tendon of *Extensor Digiti Minimi*. FDM arises from the palmar surface of the *flexor retinaculum* and the convex surface of the hook of the hamate. It inserts to the ulnar base of PP5, together with ADM.

Chapter 3

Materials and methods

3.1 The selection of bones and entheses

The entire material analysed in this PhD research was sampled on the base of the characteristics of the bone surface – for example, they should not have taphonomic alterations (erosion or damage) in correspondence of entheseal area. It should be mentioned that these insertion or origin muscle sites correspond both intrinsic and extrinsic muscles. The surface areas differ between the entheses: for example, little surface areas are characterized by bony elevation; on the contrary, the action of muscles such as DIs and PIs on metacarpals' shafts, tends to modify the morphology of the bone, which is characterized by depressed areas (Gray, 1918; Standring, 2008).
In some cases, distinguish and differentiate some entheses was not so easy: the main reason is that entheseal surfaces of some muscles overlap with those of other muscles (Gray, 1918). Consequently, it is not possible to certainly discriminate between different enthesis. Following, the entheseal surfaces have been considered together, as unique surface:

- DI2+PI – on the medial side of the 2nd metacarpal shaft;
- DI3+ADP – on the medial side of the shaft and on the palmar surface of the base of the 3rd metacarpal bone;
- DI3+PI2 – on the lateral side of the 4th metacarpal shaft;
- DI4+PI3 – on the lateral side of the shaft of the 5th metacarpal bone;
- ABP+FBP – on the lateral side of the base of the 1st proximal phalange;
- ADM+FDM – on the medial side of the base of 5th proximal phalange.

Some muscular insertion was not included in the analyses because of their difficult identification and delimitation on the 3D surface of the bone, although their easy macroscopic identification – FCR (on the base of 2nd metacarpal) and ECU+FCU (on the base of 5th metacarpal). Also, the distal phalange of the thumb was not introduced in the research because of the reduced number of specimens within the whole sample.
Several groups were created to analyse the differences among the archaeological and reference samples. Also, both right and left elements were considered to evaluate variation between the two sides of the same group.
In the San Pablo reference sample, on the base of the work of A. Karakostis (Karakostis, 2015; Karakostis, Lorenzo, 2016), a comparison between both right and left sides of same individuals should be done to evaluate possible significant bilateral asymmetry (Cashmore, Zakrzewski, 2013).

3.2 The anthropological collections

The whole osteological sample can be subdivided into two groups:

- the reference one coming from the collection of *Museo di Antropologia ed Etnografia* of Turin (Piedmont, Italy) and from the San Pablo cemetery (Burgos, Spain);
- the archaeological samples coming from the prehistoric collections of *Musée de l'Homme* (Paris, France) and IPHES (Tarragona, Spain).

This subdivision was made in function of the availability and presence of information regarding the biological profile of the individuals. Concerning the archaeological collections, the whole sample correspond to collective burials: so, no information about sex and age of the individuals were available. On the contrary, the reference collections were selected because of the known biological data of the sample.

3.2.1 The reference collections

3.2.1.1 The Predynastic and Dynastic collections

The osteological sample of the "Collezione Marro" is part of the collection of the *Museo di Antropologia ed Etnografia dell'Università degli Studi di Torino*. This sample comes from the Egyptian sites of Gebelein and Assuan (**Figure 12**), from Predynastic and Dynastic periods respectively of the Upper Egypt (Masali,Chiarelli, 1972; Torre *et al.*, 1980; Boano *et al.*,2013).
During a short period of 10 days at the *Dipartimento di Scienze della Vita e Biologia dei Sistemi* (University of Turin), a total of 86 well-preserved bones from both right and left sides was scanned. They were sampled from 7 different boxes but the NMI is 9.
In the box with individual 513EPG, 2 right MC5 and 2 left PP1 were recovered; in the box with individual 512EPG, 2 left MC1, 2 left MC3, 2 left MC4, 2 left MC5, 2 left PP3 and 2 left PP4 were recovered. See **Table 1** and **Table 2** for the whole sample.
Also, information about sex and age were recovered from the paper archive of the "Collezione Marro" at *Dipartimento di Scienze della vita e Biologia dei Sistemi* (University of Turin).
Pathological and demographic studies were conducted on this collection (Masali,Chiarelli, 1972; Torre *et al.*, 1980). No particular information about occupational profiles of individuals is available, but it is possible to know something more thanks to historical sources. Concerning Egyptian subsistence strategies during the Predynastic and Dynastic periods, hunting-gathering activities were gradually substituted by agriculture and farming and long-distance/trade exchanges of exotic materials were recorded. Furthermore, specialised crafts activities increased – jewels, stone palettes, chert knives, metallurgy, buildings (Bard, 2015).

3.2.1.2 The collection of San Pablo, Burgos (IPHES)

The medieval sample of San Pablo cemetery (Burgos, Spain) consists of 50 individuals (all individual graves), dated between 13th-15th century AD (see **Table 3**, **Figure 11**). They were selected for the good preservation of hand bones primarily, and cranium and pelvis for the identification of sex and age. The sample is subdivided into three age groups: **young** (approximately between 18 and 30 years of age), **middle-aged** (approximately between 30 and 50 years of age), **aged** (over 50 years of age) (Karakostis, Lorenzo, 2016).

Even in this case, there is no information about occupational profiles of each individual but historical sources can help. During the Late Medieval in Burgos the main occupational strategies were agriculture and general activities related to an agricultural economy, but trading and commercial activities were described too. Furthermore, specialised craftsmen, manual specialised and unspecialised manual workers also lived in the city, related to the increase of urbanisation. Concerning women of low or middle socioeconomic status, the majority had an occupation: in particular, they took care of children and houses and, at the same time, they helped their husbands in agricultural or farming activities (Estepa-Diez, Barruque, 1984; Montenegro, Duque, 1987; Stuard, 1989; Gerli, 2003).

		MC1	MC2	MC3	MC4	MC5	PP1	PP2	PP3	PP4	PP5	
513 (F)	R	1	1	-	1	2	-	-	1	-	-	6
	L	-	1	1	1	1	2	-	-	1	-	7
	R+L	1	2	1	2	3	2	0	1	1	0	13
512 (M)	R	1	1	1	-	-	-	1	-	-	1	5
	L	1	-	1	1	1	-	2	2	2	-	10
	R+L	2	1	2	1	1	0	3	2	2	1	15
521 (M)	R	-	-	1	1	-	-	-	-	-	-	2
	L	1	1	1	1	1	-	1	1	1	1	9
	R+L	1	1	2	2	1	0	1	1	1	1	11
529 (F)	R	-	-	-	-	-	1	1	-	-	-	2
	L	-	-	-	-	1	1	-	-	-	-	2
	R+L	0	0	0	0	1	2	1	0	0	0	4
475 (M)	R	1	1	1	1	1	-	1	1	-	1	8
	L	1	1	1	1	-	-	1	-	1	-	6
	R+L	2	2	2	2	1	0	2	1	1	1	14

Table 1 - The total amount of the skeletal elements of the Gebelein collection of Museo di Antropologia ed Etnografia (Turin) separated by individual and laterality.

		MC1	MC2	MC3	MC4	MC5	PP1	PP2	PP3	PP4	PP5	
3_16710 (F)	R	1	1	1	1	-	1	-	-	1	1	7
	L	-	-	1	-	-	-	-	1	-	1	3
	R+L	1	1	2	1	0	1	0	1	1	2	10
4_16714 (M)	R	1	1	1	1	1	-	1	1	1	1	9
	L	1	1	1	1	1	1	1	1	1	1	10
	R+L	2	2	2	2	2	1	2	2	2	2	19

Table 2 - The total amount of the skeletal elements of the Assuan collection of Museo di Antropologia ed Etnografia (Turin) separated by individual and laterality.

Male Individuals (SP)	5	8	10	12	33	48	59	60	72	81	86	88	90	100	121	130	142	155	156	175	194	210	215	172a	172b
Female Individuals (SP)	16	24	25	26	28	31	52	55	61	66	68	74	78	95	103	120	128	132	133	139	161	162	163	207	219

Table 3 - The individuals of the San Pablo collection (IPHES).

3.2.2 The archaeological samples

The whole archaeological sample was selected in function of the good conservation of the metacarpal and phalangeal bones in one hand and in the other, the good preservation of the entheseal surfaces. As written before, the biological information (i.e. biological profile of the individual) could not be taken into consideration due to the nature of the burials and the dispersion of the remains (collective burials with individuals not in anatomical connection).

3.2.2.1 The collections of *Musée de l'Homme*

The Neolithic archaeological sample of the *Musée de l'Homme* comes from different areas and sites (**Figure 11**): *Belle-Haie, Oise; Parc Pinterville – Eure; Grotte du Courjeonnet, vallée du Petit Morin; Bray-sur-Seine, Seine-et-Marne; dolmen Verdoline, Saint-Vallier-de-Thiey; dolmen de Meudon, Hauts-de-Seine; Grotte sépulcrale de Campniac, Périgueux, Dordogne; dolmen de Novis; Roches Rousses, Lozère* (Baye (de), 1874; Roland, 1911; Marquer, 1954; Larroque & Riquet, 1966; Dastugue, 1973).

A total of 192 pieces of these collections were scanned. The osteological material was subdivided into several bags recognised by different archive numbers: each number refers to a defined archaeological site. Before start scanning, well-preserved both right and left metacarpal and phalangeal bones were sampled.

Shown below, the total amount of the elements, divided by archaeological site, bone type and laterality (**Table 4**).

3.2.2.2 The "El Mirador" collection of IPHES

El Mirador cave is in the southern side of the archaeological complex sites of *Sierra de Atapuerca* (Burgos, Spain) (**Figure 11**). Three funerary episodes were recorded in different levels (Cáceres *et al.*, 2007; Rodríguez, 2015):

- the episode in **MIR4** (*Sondeo Central*) is characterized by the accumulation of non-articulated human remains and other dispersed individuals in the levels MIR2 and MIR3, (Bronze age, 4400-4100 BP);

- the episode in **MIR106** (Sector 100) is characterized by a single burial of a male individual of 15 years of age (between 1870-1850 cal BC and 1780-1670 cal BC);
- the last episode in **Sector 200** is characterized by a collective burial where at least 22 individuals have been buried (male, female, young and adult) (Chalcolithic, 4760-4200 cal BC).

A total of 239 bones of this collection were scanned. In **Table 5** the total amount of the elements, divided by bone type and laterality.

A series of interdisciplinary studies were carried out regarding archaeobotanical, archaeological and archaeozoological deposits that allowed research groups to obtain information about subsistence economies – agricultural and livestock practises, farming (Vergès *et al.*, 2016).
In *El Mirador* cave, gastronomic cannibalism events have been recorded and described – after identification of cutmark, human toothmarks, cooking damage and intentional breakage of bones (Cáceres *et al.*, 2007). No information about individuals of the sample is available.

		MC1	MC2	MC3	MC4	MC5	PP1	PP2	PP3	PP4	PP5	
Belle-Haie, Oise	R	3	2	5	1	-	-	-	-	-	-	11
	L	2	1	-	1	1	-	-	1	1	-	7
25157	R+L	5	3	5	2	1	0	0	1	1	0	18
Une grotte de la vallée du Pétit Morin	R	-	-	-	-	1	-	-	-	-	1	2
	L	-	-	-	-	-	-	-	1	-	-	1
21628	R+L	0	0	0	0	1	0	0	1	0	1	3
Dolmen Verdoline	R	1	-	-	-	-	-	1	1	1	2	6
	L	-	-	-	1	-	1	3	1	-	2	8
25271	R+L	1	0	0	1	0	1	4	2	1	4	14
Bray-sur-Seine (Seine et Marne)	R	1	1	1	1	1	1	1	1	1	1	10
	L	1	1	1	1	1	1	1	1	1	1	10
26046	R+L	2	2	2	2	2	2	2	2	2	2	20
Roches Rousses, Lozère	R	-	-	-	-	-	-	-	-	-	-	0
	L	-	-	-	-	-	1	-	-	1	-	2
24751	R+L	0	0	0	0	0	1	0	0	1	0	2
Dolmen de Novis	R	-	-	-	-	1	1	2	-	-	1	5
	L	-	-	-	-	-	-	1	2	-	1	4
24725	R+L	0	0	0	0	1	1	3	2	0	2	9
Grotte sépulcrale de Campniac	R	-	-	-	-	1	1	2	-	-	1	5
	L	-	-	-	-	-	-	1	2	-	1	4
25179	R+L	0	0	0	0	1	1	3	2	0	2	9
Grotte de Courjeonnet	R	-	-	-	-	-	-	-	-	-	-	0
	L	-	1	2	-	-	-	-	-	-	-	3
26071-bis	R+L	0	1	2	0	0	0	0	0	0	0	3
Dolmen du Meudon, Hauts-de-Seine	R	1	1	2	2	-	1	3	-	2	1	13
	L	3	4	1	2	-	-	-	1	4	1	16
25192	R+L	4	5	3	4	0	1	3	1	6	2	29
Allée sépulcrale du Parc Pinterville (EUR)	R	10	7	11	7	4	-	-	-	-	-	39
	L	-	2	-	-	1	-	-	-	-	-	3
24824D	R+L	10	9	11	7	5	0	0	0	0	0	42
Allée sépulcrale du Parc Pinterville (EUR)	R	1	2	-	-	-	-	-	-	-	-	3
	L	10	9	7	8	6	-	-	-	-	-	40
24824G	R+L	11	11	7	8	6	0	0	0	0	0	43

Table 4 - The total amount of the Neolithic archaeological sample of MH (Paris) separated by site, skeletal and laterality

Site Code/Level			MC1	MC2	MC3	MC4	MC5	PP1	PP2	PP3	PP4	PP5	
		R	1	4	2	4	6	3	-	1	1	2	24
	Mir201	L	-	2	-	2	-	1	1	1	1	1	9
		R+L	1	6	2	6	6	4	1	2	2	3	33
		R	-	-	-	-	-	-	-	-	-	-	0
At09	Mir202	L	-	1	-	-	-	-	-	-	-	-	1
		R+L	0	1	0	0	0	0	0	0	0	0	1
		R	-	-	1	-	-	-	-	-	-	1	2
	Mir203	L	-	2	2	-	-	-	1	-	-	-	5
		R+L	0	2	3	0	0	0	1	0	0	1	7
		R	-	1	-	3	-	-	-	1	1	3	9
	Mir201	L	-	-	1	-	1	1	2	-	-	1	6
		R+L	0	1	1	3	1	1	2	1	1	4	15
At10													
		R	-	-	1	-	-	-	-	-	-	-	1
	Mir202	L	-	-	-	-	-	-	-	-	-	-	0
		R+L	0	0	1	0	0	0	0	0	0	0	1
		R	-	-	-	3	-	-	-	-	-	-	3
	Mir201	L	1	1	-	-	-	-	-	-	-	-	2
		R+L	1	1	0	3	0	0	0	0	0	0	5
At11													
		R	-	-	-	-	-	-	2	-	-	-	2
	Mir202	L	2	-	-	-	-	1	-	-	-	1	4
		R+L	2	0	0	0	0	1	2	0	0	1	6
		R	1	6	4	3	5	5	7	5	8	7	51
	Mir201	L	1	6	6	5	3	5	5	1	3	4	39
		R+L	2	12	10	8	8	10	12	6	11	11	90
		R	-	-	2	-	-	-	-	-	-	-	2
At12	Mir202	L	-	1	-	-	-	-	-	-	1	2	4
		R+L	0	1	2	0	0	0	0	0	1	2	6
		R	-	2	2	1	2	2	1	2	3	2	17
	Mir203	L	-	-	-	1	-	-	1	1	2	-	5
		R+L	0	2	2	2	2	2	2	3	5	2	22

Table 5 – The total amount of the 'El Mirador' collection (IPHES), subdivided by code/level, bone type and laterality

		R	-	-	-	1	-	-	2	-	-	1	4
	Mir201	L	-	1	-	1	-	1	1	1	-	-	5
		R+L	0	1	0	2	0	1	3	1	0	1	9
		R	-	1	-	-	-	-	1	-	1	3	6
At13	Mir202	L	1	-	1	1	1	-	-	1	-	1	6
		R+L	1	1	1	1	1	0	1	1	1	4	12
		R	1	1	-	-	-	-	-	1	-	-	3
	Mir203	L	1	1	1	-	-	-	-	1	1	-	5
		R+L	2	2	1	0	0	0	0	2	1	0	8
		R	-	1	-	-	1	-	2	-	1	-	5
At14	Mir202	L	1	1	-	-	-	-	3	-	1	-	6
		R+L	1	2	0	0	1	0	5	0	2	0	11
		R	1	-	-	-	-	-	-	-	1	-	2
At16	Mir202	L	-	-	-	-	-	2	1	-	-	-	3
		R+L	1	0	0	0	0	2	1	0	1	0	5
		R	1	-	2	1	1	-	-	-	-	-	5
At17	Mir202	L	-	-	-	-	-	-	-	-	-	-	0
		R+L	1	0	2	1	1	0	0	0	0	0	5
		R	1	-	-	-	-	-	1	-	-	-	2
	Mir202	L	-	-	-	-	-	-	-	-	-	-	0
		R+L	1	0	0	0	0	0	1	0	0	0	2
At18													
		R	-	-	-	-	-	-	-	-	-	1	1
	Mir206	L	-	-	-	-	-	-	-	-	-	-	0
		R+L	0	0	0	0	0	0	0	0	0	1	1

Table 5 – Continued.

Figure 11 - Geographical position of the sites from *Musée de l'Homme* and IPHES osteological collections:

1) Oise, Belle-Haie; **2)** Pinterville, EUR; **3)** Courjeonnet, Marne (Petit Morin); **4)** Bray-sur-Seine, Seine-et-Marne; **5)** dolmen Verdoline, Saint-Vallier-de-Thiey; **6)** dolmen de Meudon, Hauts-de-Seine; **7)** Campniac, Périgueux, Dordogne; **8)** dolmen de Novis, Midi-Pyrénées; **9)** Roches Rousses, Lozère; **10)** Burgos; **11)** Sierra de Atapuerca, Burgos.

Figure 12 - Geographical position of the Predynastic and Dynastic sites from University of Turin osteological collections

3.3 Methods

3.3.1 The scanning process

The total amount of the sample was scanned with a NextEngine 3D Scanner Ultra HD and a Breuckmann SmartScan 3d^{-duo}.

The **NextEngine Scanner Ultra HD** uses **laser triangulation technology**. Its maximum resolution and measurement accuracy are 0.1 mm and 0.13 mm, respectively. It was used to obtain the 3D models of the archaeological collections of *Musée de l'Homme* and IPHES.

Before scans were started, all the parameters of the associated software 'ScanStudio HD Pro' were set, such as scan positioning, number of scans, number of points for each scan, exposure to light in relation to the bone surface, range of scanning mode. For each element, a total of 7 HD scans were taken along 360° using 'Macro' range.

The final 3D model for each element was saved and extracted as '.ply' format for a better processing with the 'MeshLab – v1.3.3' software (Cignoni et al., 2008).

The **Breuckmann SmarScan^{3d}-duo** uses **a structured light** technology, with high resolution (from ± 9 µm to ± 45 µm). It was used to obtain the 3D models of the reference collections of *Museo di Antropologia ed Etnografia dell'Università degli Studi di Torino* and IPHES (Tarragona, Spain). The Neolithic collection of the University of Turin was scanned with the Breuckmann SmartScan of TekneHub of University of Ferrara; for the San Pablo collection, the Breuckmann SmartScan of IPHES was utilized (Karakostis, 2015; Karakostis & Lorenzo, 2016).

Concerning the Neolithic 3D models, all the parameters of the software 'Optocat 2011' were set. To capture the 3D scans, the 9 µm lens were used; also, the parameter 'Maximum Data' was selected to acquire as much 3D quality information as possible. Finally, the 3D file was saved and exported in a '.ply' format with 'texture and colour information' for the next processing with 'MeshLab'.

3.3.2 The identification and delimitation of the entheseal surfaces

The identification of the entheseal surfaces is the most meticulous part of the entire work. Recognizing the position of origin and insertion sites of muscles and tendons is difficult because of the small dimensions of the hand bones; nevertheless, it is possible thanks to both textual and graphic data obtained by anatomical studies on humans and cadavers (Gray, 1918; Standring, 2008). To see which entheses have been considered in this work, see **Figures 6 – 10**.

The protocol for the processing on 3D models can be summarized in few steps: macroscopic analysis of the bone, macroscopic identification of the entheseal surface area and identification of the entheses on the 3D model (Karakostis, Lorenzo, 2016). Once the entheseal surface has been recognized -

thanks to texture, morphology, crests and other surface bone characteristics (Cashmore, Zakrzewski, 2013) – 'MeshLab' can be used for the entheseal delimitation process.

In the following figures (**Figures 13 – 14**), the different steps for the delimitation of each enthesis are indicated and shown.

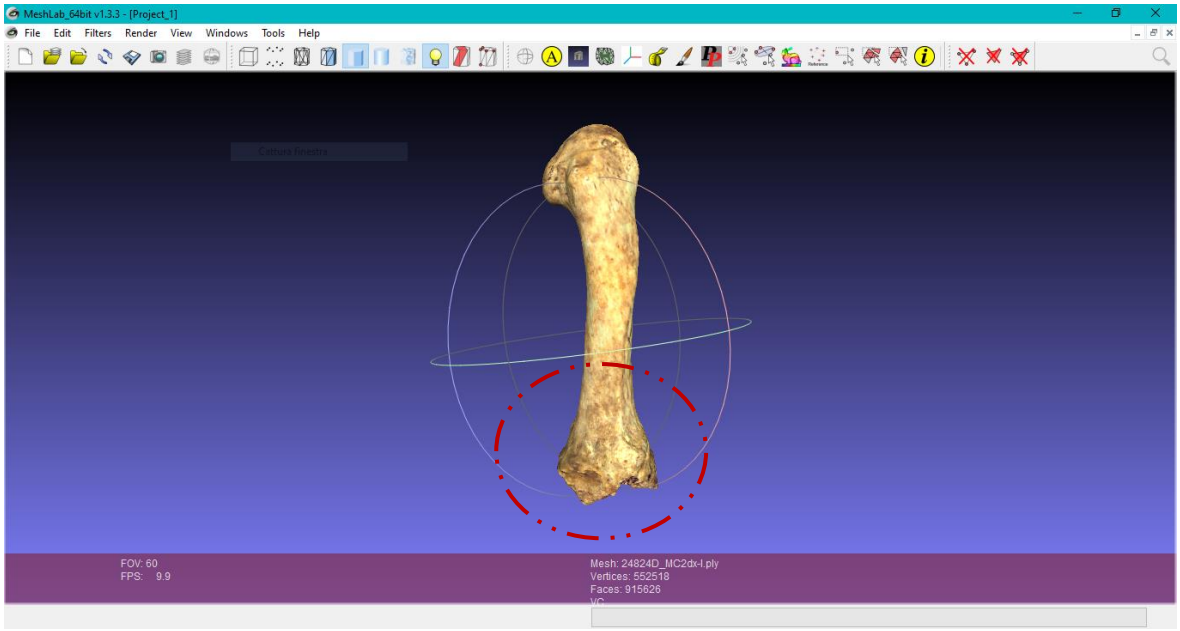

Figure 13 - Identification of the entheseal area of ECRL on a random right MC2.

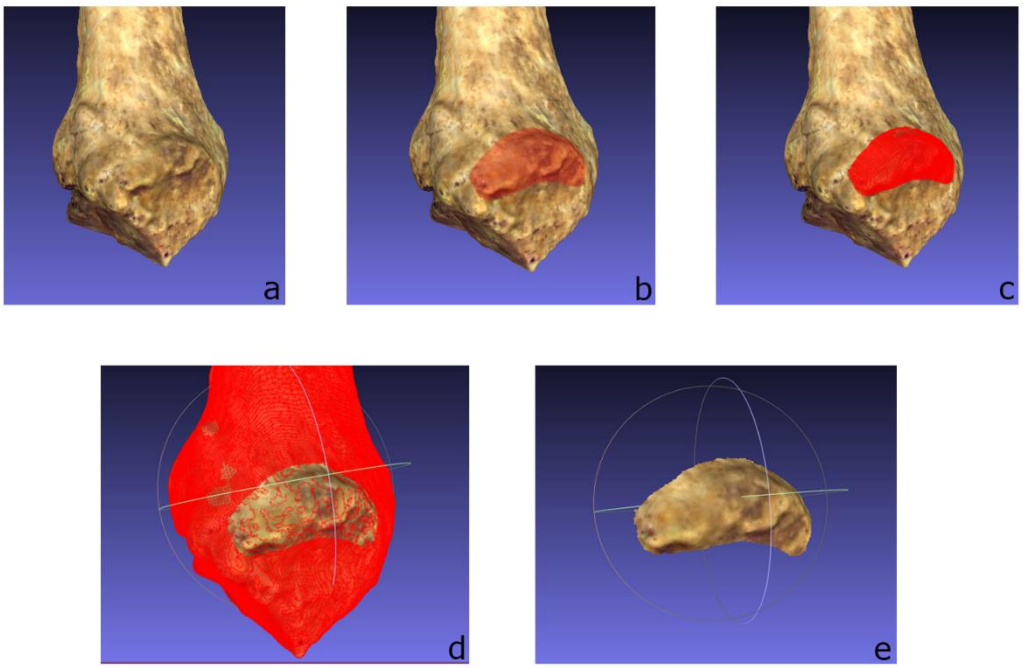

Figure 14 – **a)** detail of the proximal epiphysis of a random MC2 where ECRL inserts; **b)** selection of the enthesis with Z-painting tool; **c)** selection of the enthesis with Select vertices from faces tool; **d)** inversion of the selection with Invert selection tool; **e)** Delete selection. The remaining part of the 3D model will be the delimitated muscular insertion site.

3.3.3 Measurements

Two different kind of dimensions were calculated. Firstly, a total of five linear measurements were taken with an electronic sliding calliper with a resolution of 0.1mm/0.5" and accuracy of ±0.2mm/0.01". Based on these measurements, two **robusticity indexes** were calculated for each bone - using Antero-Posterior Width at Midshaft (APWM) and Medio-Lateral Width at Midshaft (MLWM) and dividing them by Maximum Length (ML). This ratio, that may be expressed as numeric or percentage value, is usually described as an indicator of bone robusticity (Bush *et al.*, 1982; Cashmore, Zakrzewski, 2009; Garrido Varas, Thompson, 2011; White *et al.*, 2012) (**Table 6**).

Maximum Length	**ML**
Antero-Posterior Width at Midshaft	**APWM**
Medio-Lateral Width at Midshaft	**MLWM**
Robusticity Indexes	**APWM/ML**
	MLWM/ML

Table 6 – The linear measurements taken for each skeletal element (Bush et al., 1982; Cashmore, Zakerzewski, 2009; Garrido Varas, Thompson, 2011; White et al., 2012).

Another measurement obtained from the 3D scans is the Index of **Entheseal Relative Size** (indicated from now on as **ERS**) (Karakostis, 2015; Karakostis, Lorenzo, 2016): it can be defined as the ratio between the raw size of the single enthesis and the total bone surface size. The MeshLab tool 'Quality Measure and Computations' is used to calculate raw size and total bone surface size.

3.3.4 The landmark protocol

A specific reference system of landmarks and semi-landmarks was created for each enthesis in relation to their different shape morphologies to cover the entire surface and obtain as much information as possible. Different packages of the 'R!' software (version '4.0.3') were used to process and analyse the entire sample. The preliminary step was to create the landmark template using the 'geomorph' package (v. '3.3.2') – Geometric Morphometric Analyses of 2D/3D Landmark Data (Adams & Otárola-Castillo, 2013).

Two types of points were chosen according to Bookstein's definitions. Landmarks of **Type 2** (defined as geometric points) and **Type 3** or **pseudo-landmarks** (defined according to their relative position) were used to build the reference templates for each enthesis (Bookstein, 1991; Mitteroecker, Gunz,

2009; Slice, 2005; Bardua *et al.*,2019). They were made of several fixed points placed along the outline of each insertion: they were defined as homologous and described according to their geometric position; landmark information about name, Type and descriptions are indicated in tables inserted in the Annexes. For a detailed definition of each landmark pattern, see Annexes (cf. A2 – 1 to A2 – 10). Also, a pattern of 40 or 50 surface semi-landmarks were automatically and equidistantly placed on each 3D entheseal surface (Slice, 2005; Mitteroecker, Gunz, 2009).

After the landmarks and semi-landmarks template was built on the first individual, it was applied to all the other specimens of the sample; later, a Generalized Procrustes Analysis (indicated as GPA) was performed using the *gpagen* function from the 'geomorph' R! package. This analysis involves three different steps: **translation**, **scaling**, **rotation**. GPA translates all landmarks configurations to the origin of the coordinate system, **scales** them to the unit-Centroid Size and **rotates** them to optimally align the corresponding points. The resulting *Procrustes shape coordinates* represent the shape of each specimen, projected in a curved space related to Kendall's shape space (Kendall, 1984).

3.4 Main statistical analyses

3.4.1 Univariate analyses

To test the distribution of the variables, a **Shapiro-Wilk test** was performed for each skeletal element on all the different variables of the sample.

For each enthesis of each skeletal element, correlation tests between entheseal size (raw and ERS), ML and Robusticity Indexes (RIs) were performed. It is important to consider that several studies (Pawar, Dadich, 2012) showed correlation between hand bones' length and body length (Krishan, Sharma, 2007). Also, bone length is not subjected to biomechanical stress but is influenced by genetic factors during growth of individual (Gaskin *et al.*, 2011; Nolte, Wilczak, 2013).This means that if statistical correlation exists between entheseal size (raw and ERS) and ML, so the entheseal surface modification is caused by genetics. But if statistical correlation exists between entheseal size (raw and ERS) and RIs, this means that the entheseal surface is influenced by biomechanical stress (Ruff, Runestad, 1992; Rauch, 2005; Karakostis, 2015).

3.4.2 Multivariate analyses

For the multivariate analyses, both PAST (v. 4.0) and R! were used (Hammer *et al.*, 2001). Different kinds of PCAs were performed with PAST using linear and entheseal measurements for each bone using different combinations of variables. Several Principal Component Analyses were conducted to investigate the statistical correlation between entheseal surface (raw size and ERS indexes) and ML and RIs: the purpose is about to understand the nature of the entheseal change, if genetic or biomechanical. The results will be described later.

For the morphometric analyses with ‘geomorph’ R! package, after the GPA was performed, the resulting *Procrustes shape coordinates* were used to conduct PCAs for each single enthesis, using the function *gm.prcomp*. The resulting data were therefore plotted, using the function *autoplot* of ‘ggplot2’ package. Later, shape differences between the reference specimen and the target one were illustrated using *PlotRefToTarget* function; in this way, it was possible to see the shape variation between both maximum and minimum values of the first principal component (PC1 max and PC1min) (Mitteroecker *et al.*, 2004; Karakostis, 2015).

In the table in the Annexes (cf. A3 – 1), the functions used to analyse the 3D sample are shown and described.

Chapter 4

Results

In this chapter, results for each bone are described separately and subdivided into several paragraphs on the base of the different number of enthesis. The description of the results will follow the same structure for each section: discussion of descriptive statistics, normality tests and correlation analyses for each bone to investigate the relation between raw size/ERS of each enthesis and both total surface area of the 3D bone and bone dimensions. Results and brief discussion of the geometric morphometrics analysis of each enthesis will be described; here, the most relevant morpho spaces are presented, allowing to highlight the main differences between groups. The remaining plots will be shown in the 'Annexes' chapter.

As previously explained, sexual dimorphism between male and female individuals cannot be investigated because of nature of burials and dispersion of the human remains (collective burials with individuals not in anatomical connection).
Each group – corresponding to each collection – has been defined with a proper acronym: **UoT** (University of Turin collections), **MH** (*Musée de l'Homme* collection), **EM** (El Mirador collection from IPHES) and **SP** (San Pablo collection from IPHES).

4.1 Analyses of 1st metacarpal bones

4.1.1 Right MC1 – Descriptive statistics, normality test and correlation tests

	raw size - DI1	ERS - DI1	raw size - ABL	ERS - ABL	raw size - OP	ERS - OP	APWM/ML*	MLWM/ML*	ML*
N	67	65	66	62	62	61	71	71	71
Min	80,79	0,06	29,81	0,02	55,42	0,03	0,15	0,19	35,64
Max	298,33	0,17	102,93	0,05	239,11	0,12	0,23	0,34	48,59
Mean	191,34	0,11	56,54	0,03	147,62	0,08	0,19	0,27	42,65
Stand. dev	50,97	0,03	16,80	0,01	45,87	0,02	0,02	0,03	2,68

Table 7– Summary statistics for both 3D size and linear measurements of right MC1
Raw size is calculated in mm^2, ML in calculated in mm. **APWM/ML**: Antero-Posterior Robusticity Index. **MLWM/ML**: Medio-Lateral Robusticity Index. **ML**: Maximum Length

	raw size - DI1	ERS - DI1	raw size - ABL	ERS - ABL	raw size - OP	ERS - OP	APWM/ML*	MLWM/ML*	ML*
N	67	65	66	62	62	61	71	71	71
Shapiro-Wilk W	0,9584	0,9672	0,9532	0,969	0,9823	0,9781	0,9875	0,9921	0,9922
p(normal)	0,02488	0,08227	0,01421	0,1181	0,5122	0,3426	0,7064	0,9381	0,9415

Table 8 – Shapiro-Wilk test for each variable of right MC1.

	raw size - DI1	ERS - DI1	raw size - ABL	ERS - ABL	raw size - OP	ERS - OP
APWM/ML*		0,16	0,10	-0,11	0,19	0,08
MLWM/ML*		0,13	0,17	0,04	0,21	0,12
ML*		-0,03		0,18		-0,00004

Table 9 – Correlation tests between 3D bone sizes and linear dimensions for right MC1.

In **Tables 7 – 9**, descriptive statistics, correlation tests and normal distribution tests for all the variables used in this work are summarized.

The set of values of enthesis DI1 are the highest among the entheses of MC1, according to their dimensions and nature of muscular origin sites on metacarpal shafts. With regard to normality tests for each variable of right MC1, the Shapiro-Wilk's test has verified a normal distribution with a *p-value* > 0.05 for all variables, except for raw size of DI1 and ABL entheses.

Correlation tests were performed: positive relations have been recorded between raw size of each enthesis and total surface size of all entheses. About relation between entheseal size (raw and ERS) and bone dimensions, ERS indexes of all entheses correlate with all linear measurements (with negative correlation between ERS of DI1 and OP entheses and maximum bone length, and between ERS of ABL enthesis with antero-posterior RI).

4.1.1.1 ABL enthesis

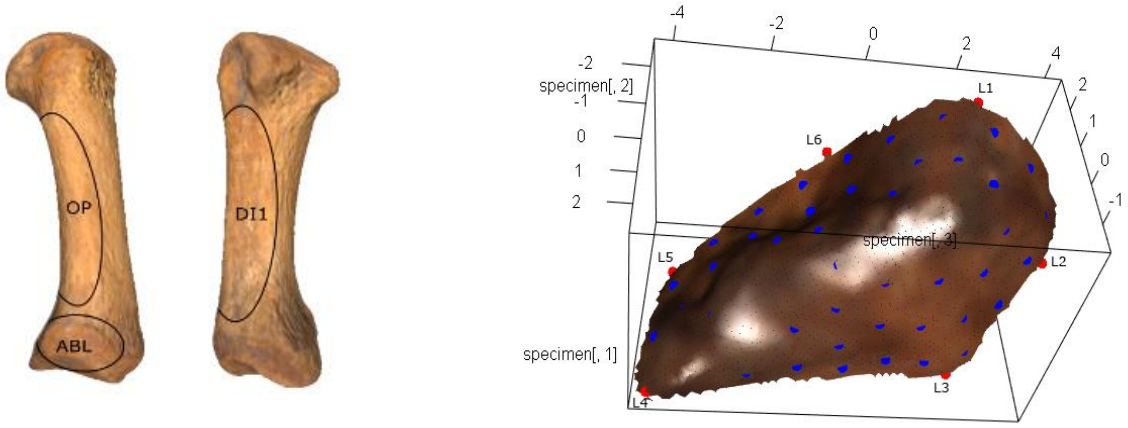

Figure 15 – On the left, the MC1 bone with delimited enthesis.
On the right, the landmarks (red spots) and semi-landmarks (blue spots) on the 3D model of the surface of ABL.
For the landmarks' definitions, see Annexes (cf. A2 – 1)

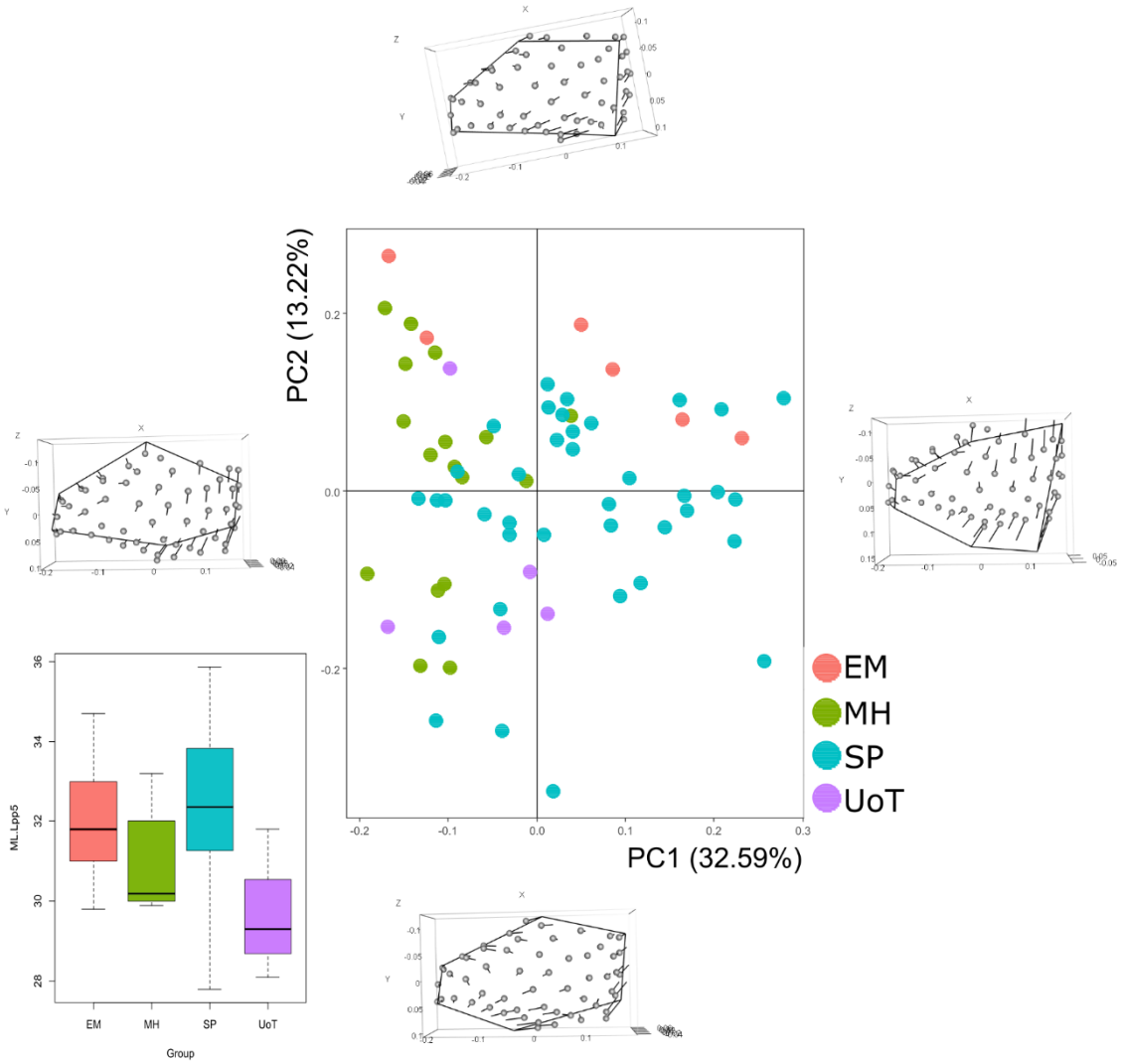

Figure 16 – Principal Component Analysis on the entire set of landmarks and shape configuration at the extremes of PC1 and PC2 for right ABL

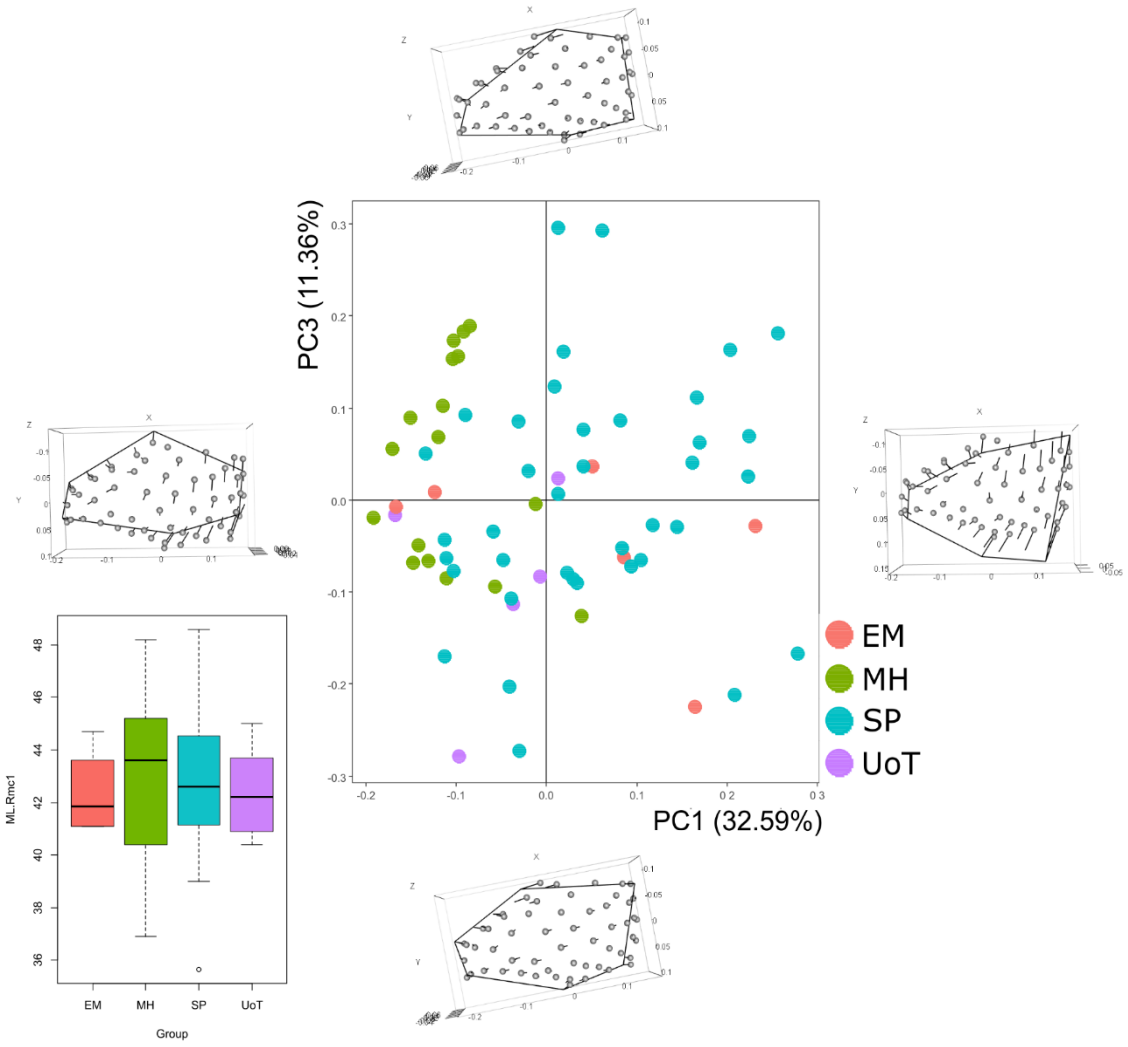

Figure 17 – Principal Component Analysis on the entire set of landmarks and shape configuration at the extremes of PC1 and PC3 for right ABL.

For the analyses of ABL of right MC1 (**Figure 15**), a total of 66 specimens were available. Here, the first four PCs were analysed, representing almost the 67% of the total variance.

Regarding shape variation on PC1, an increasing in correspondence of the dorsal aspect of the entheseal outline is recorded, due to relocation of both fixed and surface landmarks: L1 and L2 move distally and proximally, respectively, with L2 also moving to a medial direction, L3 moves to proximal and medial directions, L4 goes medially, and L5 and L6 both move proximally, towards the centre of the enthesis. About the surface semi-landmarks, those located in correspondence of the proximal and dorsal aspect of the entheseal outline move to a most proximal position, while some lying on the central portion of the enthesis move to a distal direction. With regard to PC2, major variation is along the proximal and dorsal portions of the outline, caused by relocation of landmarks lying on these outlines: L1 partially moves towards the palmar surface, L2 and L3 move to opposite direction – palmar and dorsal, respectively – along the same entheseal outline, L4 and L5 both move medially and L6 moves to a lateral direction. About surface semi-landmarks, those located on the proximal aspect of the outline move towards the dorsal surface, those lying on the dorsal outline (between L1 and L2) move proximally, while others located near the distal and palmar outline move to a most palmar position. With regard to PC3, variation is recorded on the dorsal and palmar portions of the entheses, caused by relocations of fixed pseudo-landmarks: L1 and L4 move to a medial direction, L2 moves towards the dorsal surface but to a partial medial direction, L3 moves both distally and laterally, L5 moves both proximally and dorsally, and L6 moves towards the dorsal surface, to a lateral direction. About surface semi-landmarks, most variation is in correspondence of the palmar aspect of the distal outline, going towards the centre of the enthesis. Regarding PC4, variation is recorded in antero-posterior direction, caused by repositioning of fixed pseudo-landmarks: L1 moves proximally, L2 and L3 both move towards the palmar surface, L4 moves to a dorsal direction, L5 moves proximally and L6 relocates to a most lateral position. About surface semi-landmarks, those lying in correspondence of the central portion move to a dorsal direction, while others located on the dorsal aspect of the proximal outline move both to distal and palmar directions.

In **Figure 16** and **Figure 17** similar distributions can be seen, with EM specimens changing positions along the y-axis. Distinction between groups is evident: MH group is distributed for negative values of PC1, but only one specimen is distributed for positive values of the same PC, while general distribution is along PC2 and PC3; UoT group has the same distribution of MH, but for negative values of each PCs. When PC1 and PC4 are considered, the same distribution as **Figure 17** shown; for this reason, this plot is introduced in the Annexes (cf. A4 – 1).

4.1.1.2 DI1 enthesis

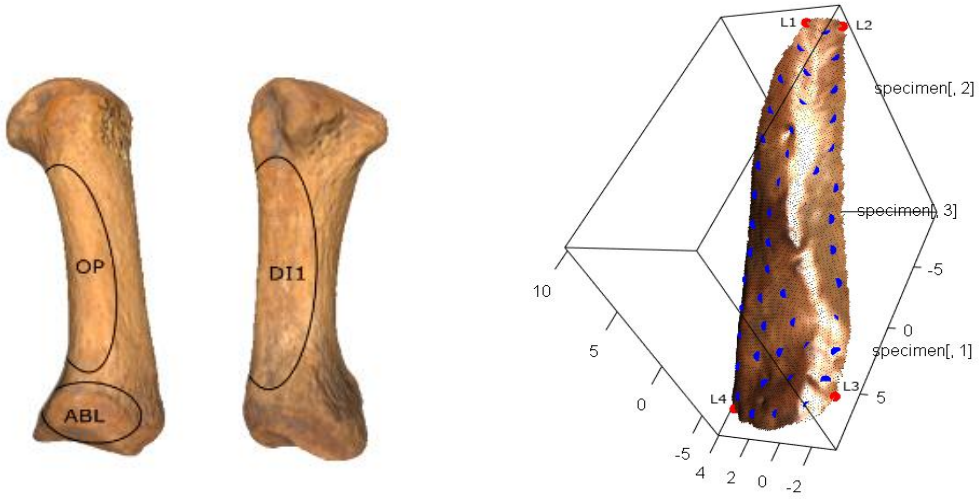

Figure 18 – On the left, the MC1 bone with delimited entheses.
On the right, the landmarks (red spots) and semi-landmarks (blue spots) on the 3D model of the surface of DI1.
For the landmarks' definitions, see Annexes (cf. A2 – 1).

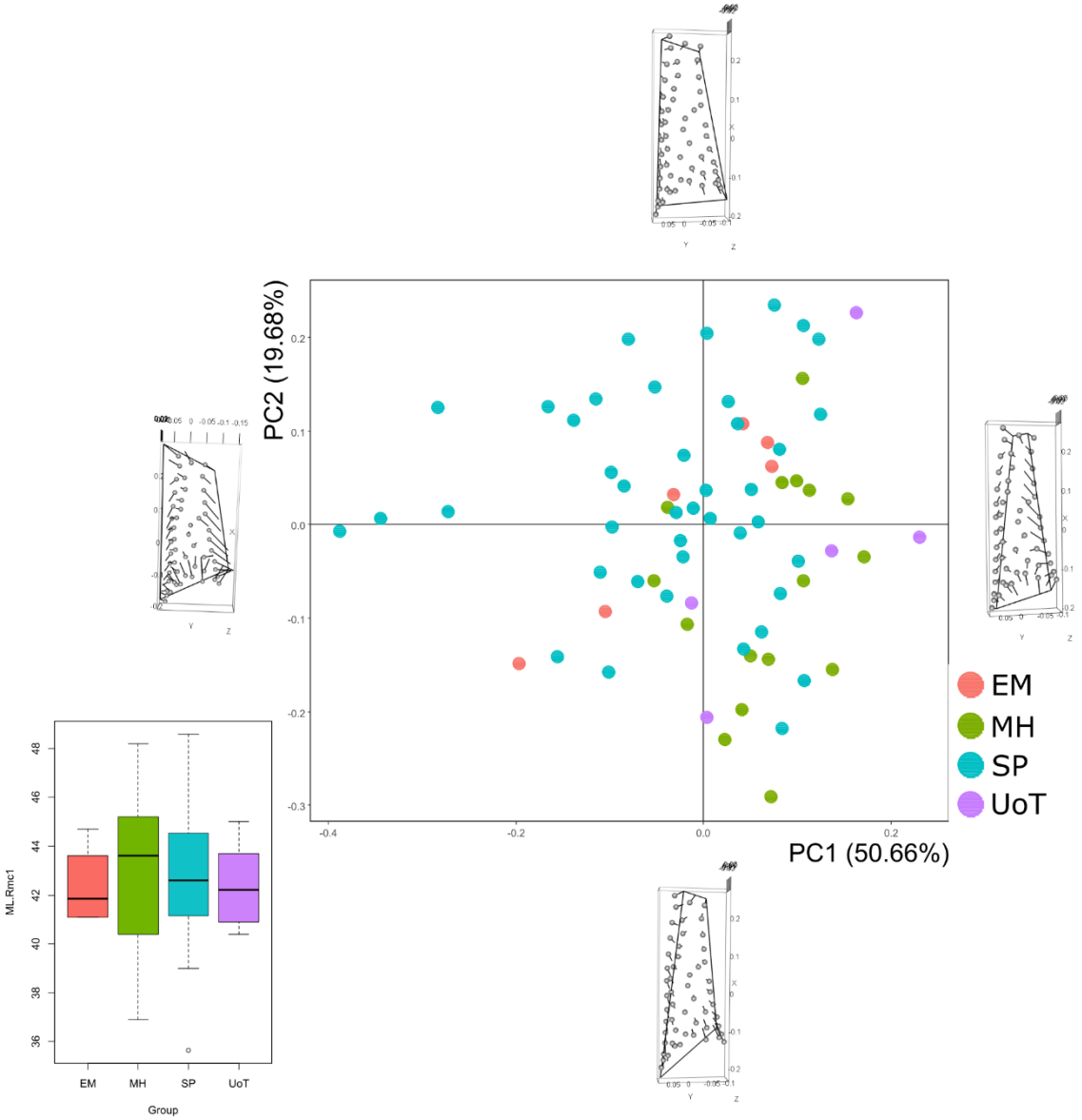

Figure 19 - Principal Component Analysis on the entire set of landmarks and shape configuration at the extremes of PC1 and PC2 for right DI1

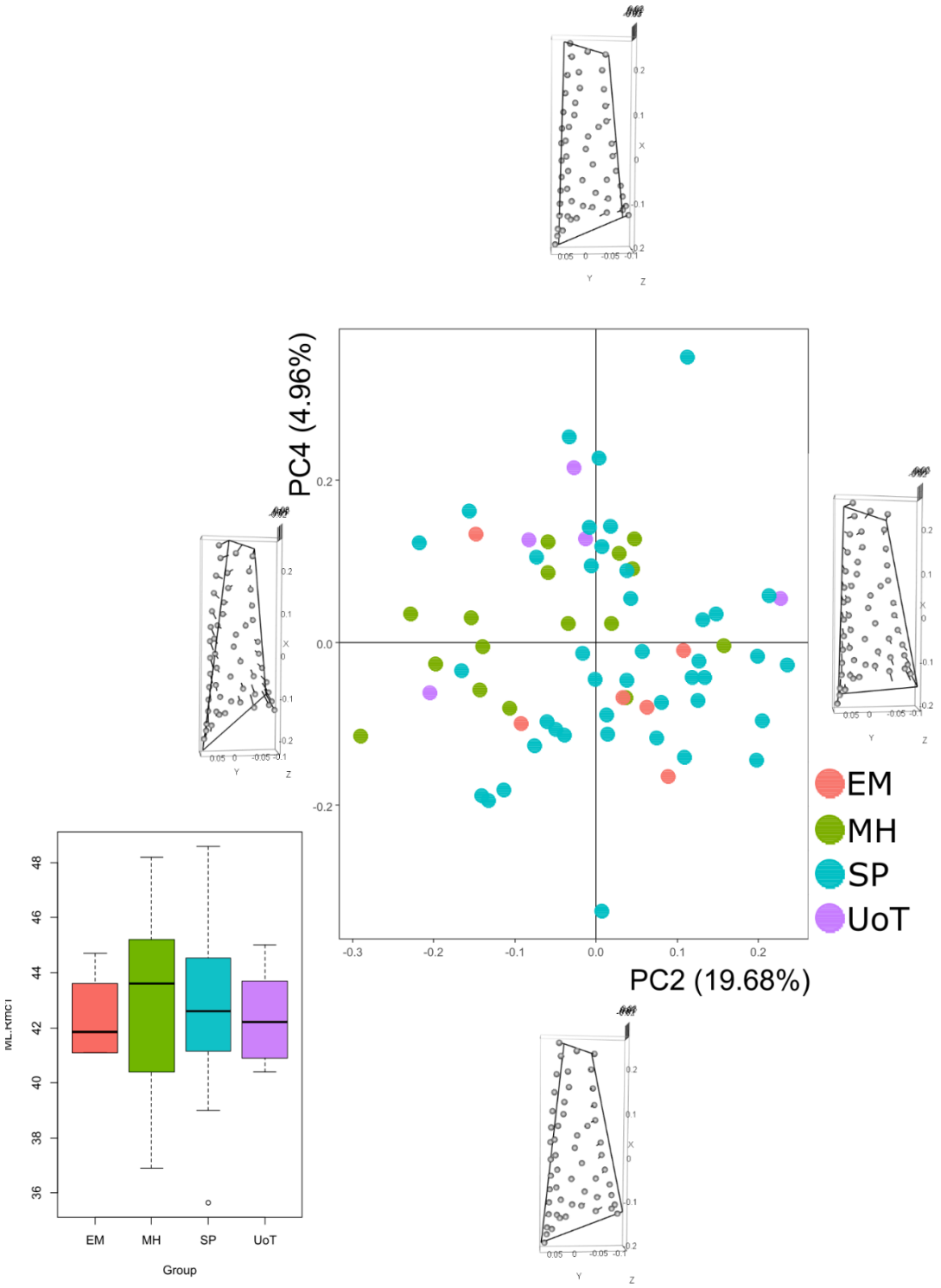

Figure 20 – Principal Component Analysis on the entire set of landmarks and shape configuration at the extremes of PC2 and PC4 for right DI1.

For the analyses of DI1 of right MC1 (**Figure 18**), a total of 68 specimens were available. Here, the first four PCs were analysed, representing almost the 89% of the total variance.

Analysing shape variation on PC1, a decreasing in antero-posterior direction is recorded due to relocation of both fixed and surface landmarks – these latter all moving towards the centre of the enthesis: L1 and L2 both move in opposite directions, going to palmar and dorsal directions respectively, L3 moves proximally, towards the dorsal surface, and L4 going medially. With regard to PC2, an increasing in antero-posterior direction in correspondence of the proximal portion of the enthesis, caused by relocation of L3, moving to proximal and palmar directions – along with surroundings surface semi-landmarks. Other pseudo-landmarks also relocate: L1 moves towards the dorsal surface, L2 moves proximally and towards the centre of the enthesis, while L4 moves distally, along the outline towards L1. About surface semi-landmarks, those lying on the dorsal aspect of the entheseal outline move to a most distal direction. With regard to PC3, a decreasing and an increasing in antero-posterior and proximo-distal directions, respectively: L1 moves distally, both L2 and L3 moves towards the dorsal surface – along with the surface semi-landmarks lying along the entire entheseal outline – and L4 moves towards the palmar surface; also, surface semi-landmarks located on the dorsal aspect of the entheseal outline – all moving to a palmar direction. About PC4, most variation is in correspondence of the distal aspect of the entheseal outline – a decreasing can be seen for repositioning of both L1 and L2, going medially and laterally respectively; also, L3 moves to a lateral direction, while no variation occurs on L4. About surface semi-landmarks, some of them lying in correspondence of palmar aspect of the entheseal outline move to a medial direction.

In **Figure 19** previously shown, a homogenous distribution of the entire sample can be seen, even if separation between MH and UoT and SP groups is evident: in particular, MH specimens are spread for positive values of PC1, distinct from the most part of SP. Also, MH is separated by EM, located between the previous cited groups. Similar distribution can be seen in **Figure 20**, with MH and EM groups distinct for different values of PC4: a peculiarity is one specimen from EM, falling into the MH group, distributed for negative and positive values for PC2 and PC4, respectively.

4.1.1.3 OP enthesis

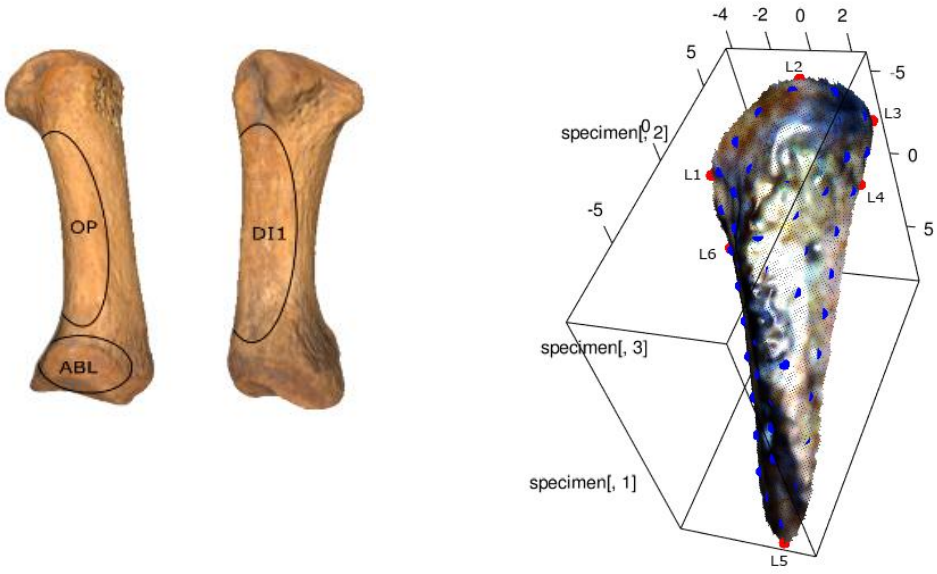

Figure 21 - On the left, the MC1 bone with delimited entheses.
On the right, the landmarks (red spots) and semi-landmarks (blue spots) on the 3D model of the surface of OP.
For the landmarks' definitions, see Annexes (cf. A2 – 1).

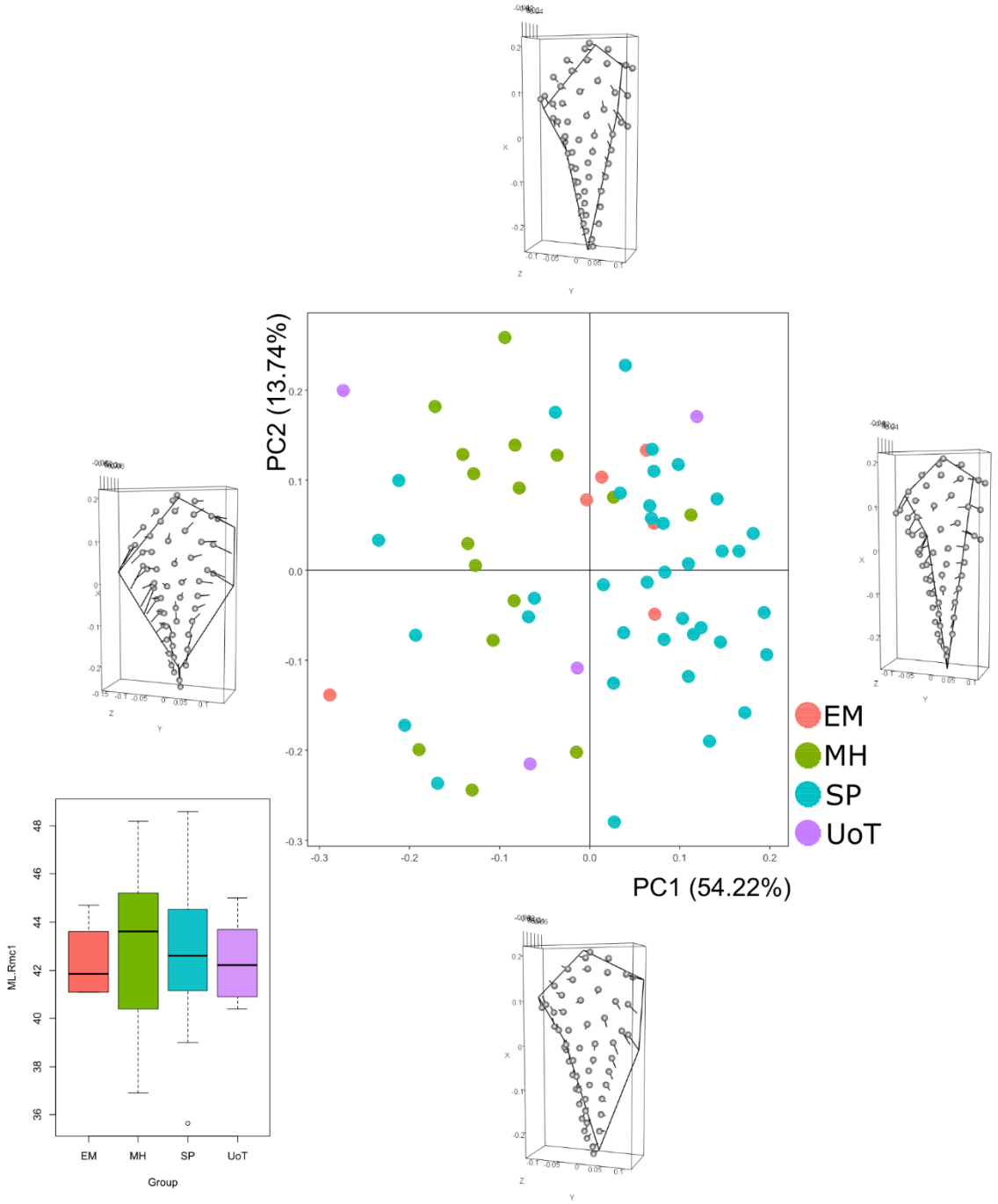

Figure 22 - Principal Component Analysis on the entire set of landmarks and shape configuration at the extremes of PC1 and PC2 for right OP.

For the analyses of OP of right MC1 (**Figure 21**), a total of 63 specimens were available. Here, the first four PCs were analysed, representing almost the 84% of the total variance.

Analysing shape variation along PC1, an increasing in length and a reduction in an antero-posterior direction are recorded, due to relocation of both fixed and surface landmarks, in particular L1, L3, L4, L5 and L6: both L1 and L6 move to a most distal position, towards the centre of the enthesis and to a dorsal direction, L3 and L4 both move distally and towards the centre of the enthesis but, in this case, towards the palmar surface of the bone, and L5 moves to a most proximal direction, determining the increasing in a proximo-distal way. With regard to surface semi-landmarks, some of them located in correspondence of both dorsal and palmar aspects of the entheseal outlines, all proceeding to a most dorsal direction. Along PC2, the morphology of the entheseal outline is the same but a decreasing in antero-posterior way is recorded, due to fixed pseudo-landmarks L1, L3 and L4 – moving to proximal, palmar, and distal directions, respectively. Also, L2 and L5 change position, going dorsally and medially, respectively. About surface semi-landmarks, only some of them lying along the distal and dorsal aspects of the entheseal outline move to a central position. With regard to PC3, an increasing in an antero-posterior direction in correspondence of the distal portion of the enthesis can be seen, due to repositioning of L3 and L4, which move distally, while some surface semi-landmarks located close to the distal extremity go towards the centre of the enthesis. About PC4, an increasing in antero-posterior way is recorded, along with a modification of the dorsal and distal aspect of the entheseal outline between L3 and L4, because of relocation of L3 to a most proximal and dorsal position; also, L2 and L5 both move proximally, while L4 and L6 move distally. With regard to surface semi-landmarks, some of them move towards the centre of the enthesis.

Taking into account **Figure 22**, the main visible separation is evident between MH and most of SP, whose subdivision is for different values of PC1 – negative and positive ones, respectively. In particular, specimens from MH are characterised by more reduced entheseal morphologies than the big group of SP. The rest of the sample is homogenously distributed all over the graph. Similar distributions can be seen also in figures shown in the Annexes (cf. A4 – 2, A4 – 3).

4.1.2 Left MC1 – Descriptive statistics, normality tests and correlation analyses

	raw size - DI1	ERS - DI1	raw size - ABL	ERS - ABL	raw size - OP	ERS - OP	APWM/ML*	MLWM/ML*	ML*
N	69	69	68	68	69	68	72	72	72
Min	68,76	0,04	18,95	0,01	52,16	0,04	0,15	0,22	37,70
Max	349,01	0,17	88,56	0,05	197,17	0,11	0,23	0,33	48,50
Mean	194,65	0,11	53,82	0,03	107,99	0,06	0,19	0,26	42,55
Stand. dev	62,15	0,03	18,09	0,01	35,37	0,02	0,02	0,02	2,45

Table 10 - Summary statistics for both 3D size and linear measurements of left MC1. Raw size is calculated in mm^2, ML in calculated in mm. **APWM/ML**: Antero-Posterior Robusticity Index. **MLWM/ML**: Medio-Lateral Robusticity Index. **ML**: Maximum Length.

	raw size - DI1	ERS - DI1	raw size - ABL	ERS - ABL	raw size - OP	ERS - OP	APWM/ML*	MLWM/ML*	ML*
N	69	69	68	68	69	68	72	72	72
Shapiro-Wilk W	0,97	0,93	0,98	0,99	0,94	0,94	0,99	0,99	0,98
p(normal)	0,14	0,001051	0,19	0,70	0,004001	0,003495	0,81	0,76	0,53

Table 11 - Shapiro-Wilk test for each variable of left MC1.

	raw size - DI1	ERS - DI1	raw size - ABL	ERS - ABL	raw size - OP	ERS - OP
APWM/ML*		0,21			0,01	-0,17
MLWM/ML*		0,16		0,24	0,14	0,02
ML*		0,06		-0,08		0,27

Table 12 - Correlation tests between 3D bone sizes and linear dimensions for left MC1.

In **Tables 10 – 12**, descriptive statistics, correlation tests and normal distribution tests for all the variables used in this work are summarized.

The set of values of enthesis DI1 are the highest among the entheses of MC1, according to their dimensions and nature of muscular origin sites on metacarpal shafts. With regard to normality tests for each variable of left MC1 the Shapiro-Wilk's test has verified a normal distribution with a *p-value* > 0.05 for all variables, except for OP entheses and ERS of DI1 and OP entheses.

Correlation tests were performed: positive relations have been recorded between raw size and ERS indexes of each enthesis and total surface size. About relation between entheseal size (raw and ERS) and bone dimensions, ERS indexes of DI1 and OP entheses correlate with all linear dimensions (with a negative value between ERS of OP and antero-posterior RI), ERS of ABL enthesis correlates with medio-lateral RI and bone length, positively and negatively, respectively, while raw size of OP enthesis also correlates with both Robusticity Indexes.

4.1.2.1 ABL enthesis

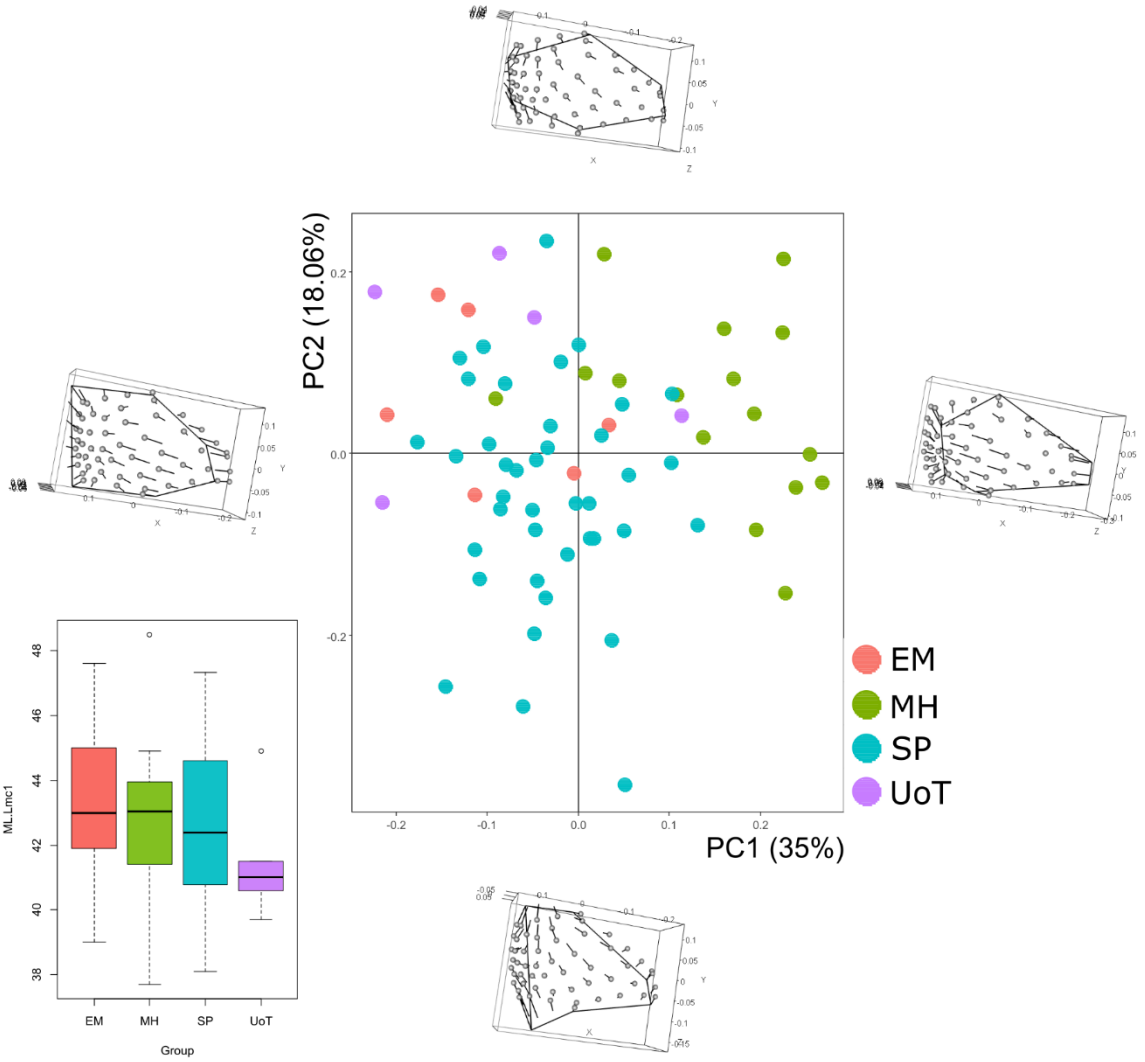

Figure 23 - Principal Component Analysis on the entire set of landmarks and shape configuration at the extremes of PC1 and PC2 for left ABL.

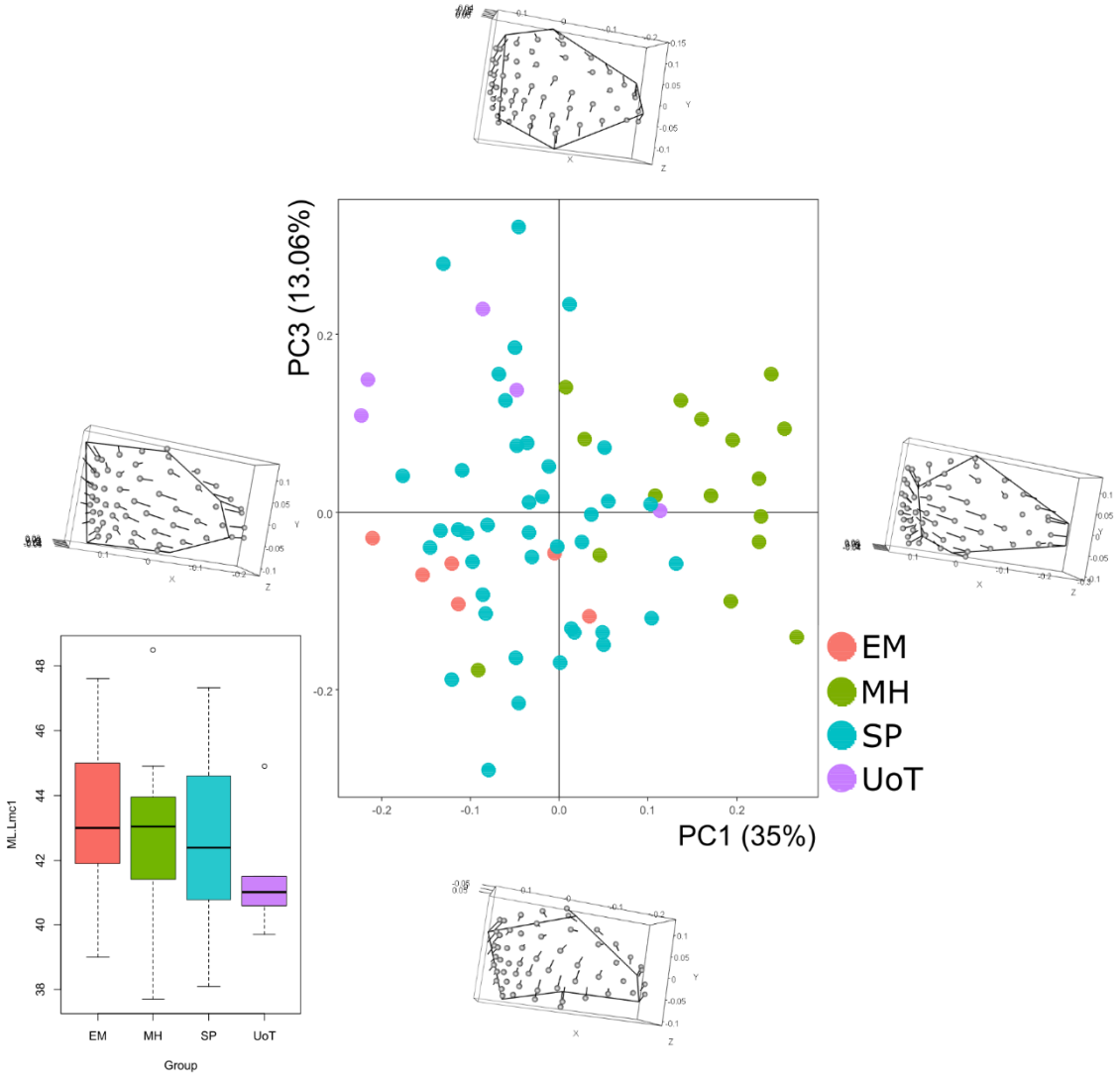

Figure 24 - Principal Component Analysis on the entire set of landmarks and shape configuration at the extremes of PC1 and PC3 for left ABL.

For the analyses of ABL of left MC1, a total of 67 specimens were available. Here, the first four PCs were analysed, representing almost the 76% of the total variance.

Regarding shape entheseal variation on PC1, increasing in antero-posterior direction is recorded, along with an increasing in proximo-distal way in correspondence of the dorsal aspect of the entheseal outline. These variations are due to relocation of fixed pseudo-landmarks: L1 and L2 both move towards the centre of the enthesis, proximally and distally respectively, L3 moves to a dorsal direction, along the outline towards L2, L4 and L5 both move to a palmar direction; L6 does not relocate. About surface semi-landmarks, most of them move towards a central point close to the dorsal surface of the bone, while some semi-landmarks lying in correspondence of the palmar aspect of the entheseal outline continue proceeding to a palmar direction. With regard PC2, a decreasing in correspondence of the dorsal aspect of the entheseal outline can be seen, which causes also shape changes along the outline due to relocation of fixed pseudo-landmarks: L1 and L2 both move dorsally and towards the centre of the outline between these two points – moving proximally and distally, respectively – L3 does not relocate, L4 and L5 both move laterally and to a distal direction, partially, while L6 move medially. Even in this case, surface semi-landmarks' repositioning is related to movements towards the mid-point of the entheseal outline between L1 and L2, while surface semi-landmarks lying in correspondence of the centre of the enthesis move towards a palmar direction. Regarding PC3, an increasing in proximo-distal direction is recorded due to a proximal relocation of L3 and a distal repositioning of L1 and L6, moving distally but in opposite directions, palmar and dorsal, respectively; also, L2, L4 and L5 all move medially and distally, partially, while L3 move towards the proximal epiphysis. About surface semi-landmarks, those lying close to dorsal and palmar aspects of the entheseal outline move distally, while those located on the central part move proximally. With regard to shape variation on PC4, a decreasing in proximo-distal direction close to the palmar surface is recorded, caused by relocation of fixed pseudo-landmarks: L1 and L2 both move to a most distal position, L3 moves towards the palmar surface, L4 and L5 also move to a palmar direction but distally and proximally, respectively, while L6 moves proximally to a dorsal direction. About surface semi-landmarks, those lying in correspondence of the dorsal aspect of the entheseal outline move distally, those lying along the proximal outline move to a palmar direction, and those located along the distal and palmar aspects of the enthesis move distally, towards the centre of the enthesis.

In **Figure 23**, distinction between MH group and the rest of the sample is evident – MH has a distribution for positive values of PC1 while UoT and EM are distributed for negative values for the same PC; also, SP is spread all over the graph but results distinct from MH. As a result, specimens from MH are characterised by reduced entheseal morphologies on the dorsal aspect of the outline in proximo-distal way and increasing in antero-posterior direction. Similar distribution has shown in **Figure 24**:in this case, separation between UoT and EM groups is also recorded, for positive and

negative values of PC3, respectively. This situation put in evidence the different entheseal morphologies between groups, where UoT has characterised by larger entheses in proximo-distal direction than EM.

4.1.2.2 DI1 enthesis

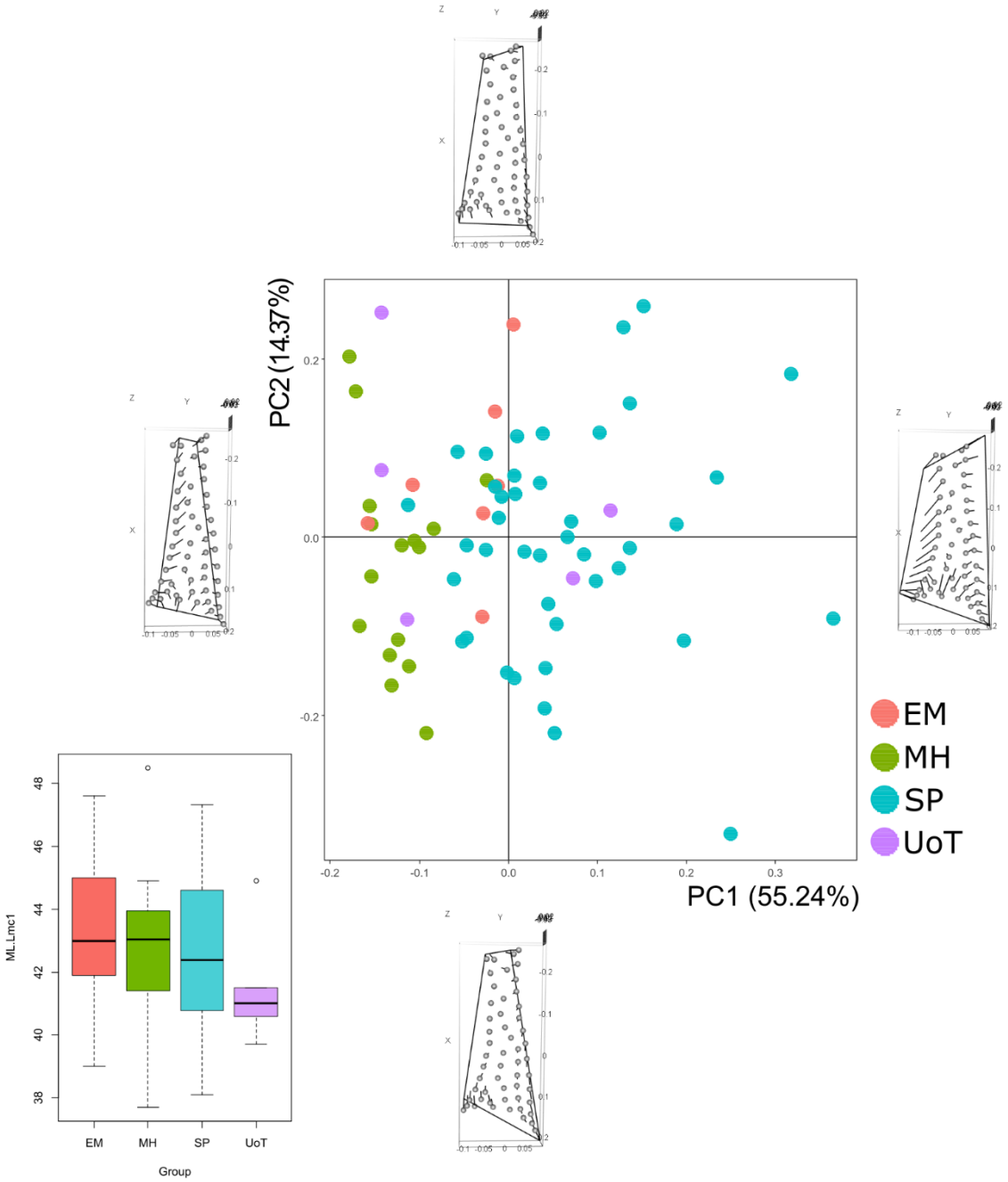

Figure 25 - Principal Component Analysis on the entire set of landmarks and shape configuration at the extremes of PC1 and PC2 for left DI1.

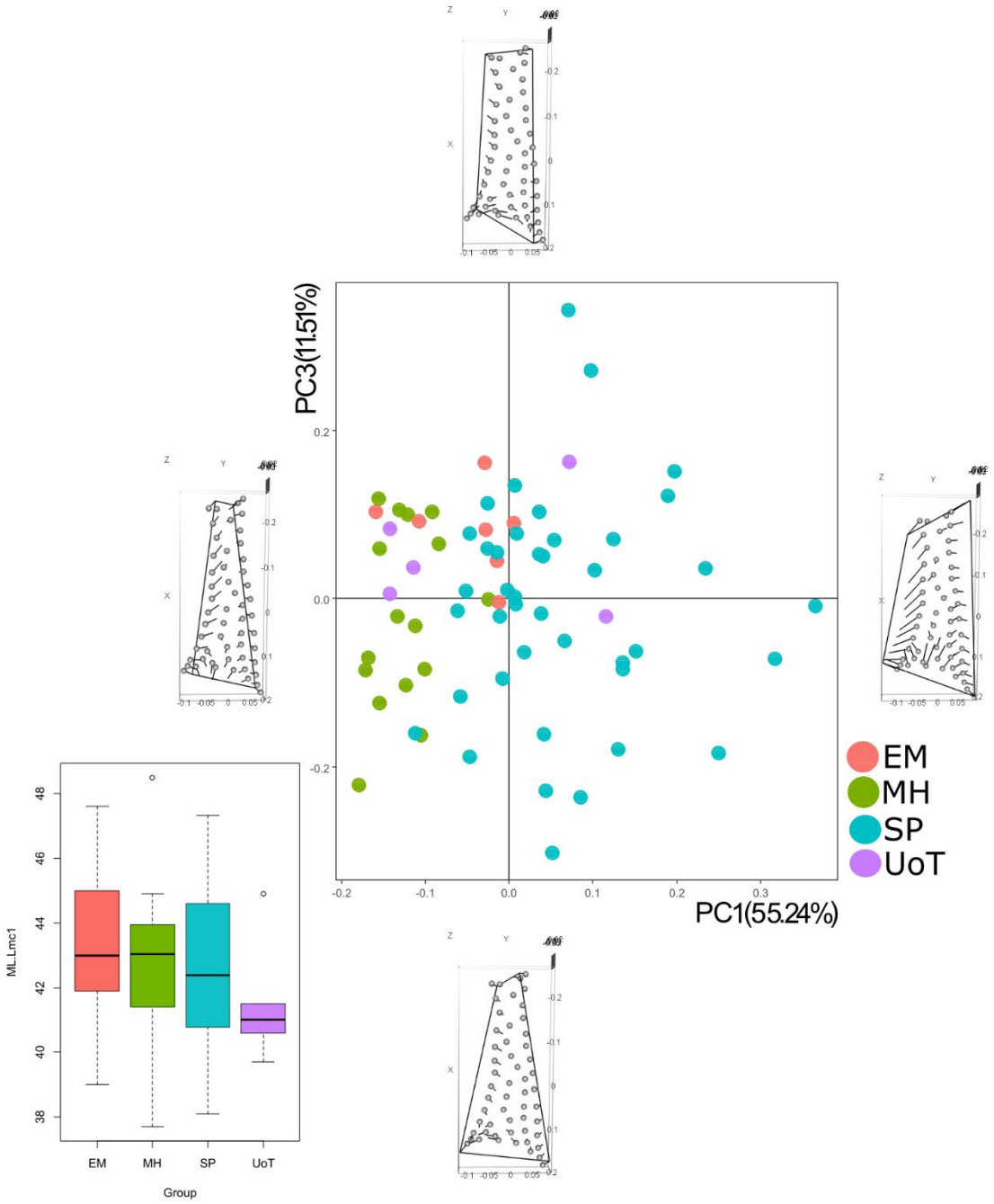

Figure 26 - Principal Component Analysis on the entire set of landmarks and shape configuration at the extremes of PC1 and PC3 for left DI1.

For the analyses of DI1 of left MC1, a total of 69 specimens were available. Here, the first four PCs were analysed, representing almost the 89% of the total variance.

Regarding shape variation along PC1, an increasing in antero-posterior direction is recorded, due to relocation of both fixed and surface landmarks: L1 and L4 both move towards the dorsal surface of the bone, going distally and proximally, respectively, while L2 and L3 both move towards the palmar surface of the bone, going proximally and distally, respectively. About surface semi-landmarks, those lying along the dorsal and palmar entheseal outlines proceed going to dorsal and palmar directions, also proximally, while some of them located in correspondence of the proximal outline between L3 and L4 move to a distal direction. With regard to PC2, an increasing in correspondence of the palmar entheseal outline between L2 and L3 can be seen, along with a decreasing of the dorsal outline between L4 and L1: these modifications are caused by relocation of L1, moving dorsally, L2 partially moving proximally, and L3 and L4 moving in opposite directions, proximal and distal respectively. About surface semi-landmarks, those located along the dorsal entheseal outline move distally and dorsally (starting from the base to the distal extremity) and some lying close to L3 move to a proximal direction. With regard to PC3, an increasing and a decreasing in both distal and proximal extremities of the enthesis, respectively, are recorded, due to fixed pseudo-landmarks: L1 moves towards a dorsal direction, L2 moves towards the palmar surface, L3 moves distally and dorsally, L4 moves to both proximal and palmar directions. About surface semi-landmarks, those located in correspondence of the proximal entheseal outline create a sort of curve going from L3 to L4.

In **Figure 25** and **Figure 26**, separation between different groups is recorded, with MH, EM and UoT samples mostly distributed for negative values of PC1 – except for two specimens from UoT which are in the positive side of PC1. Also, in **Figure 26** separation between EM and MH can be seen – distributed for positive and negative values of PC3, respectively. This distinction can be due to different entheseal morphologies between each group, with the archaeological samples characterised by smaller entheses than SP ones.

4.1.2.3 OP enthesis

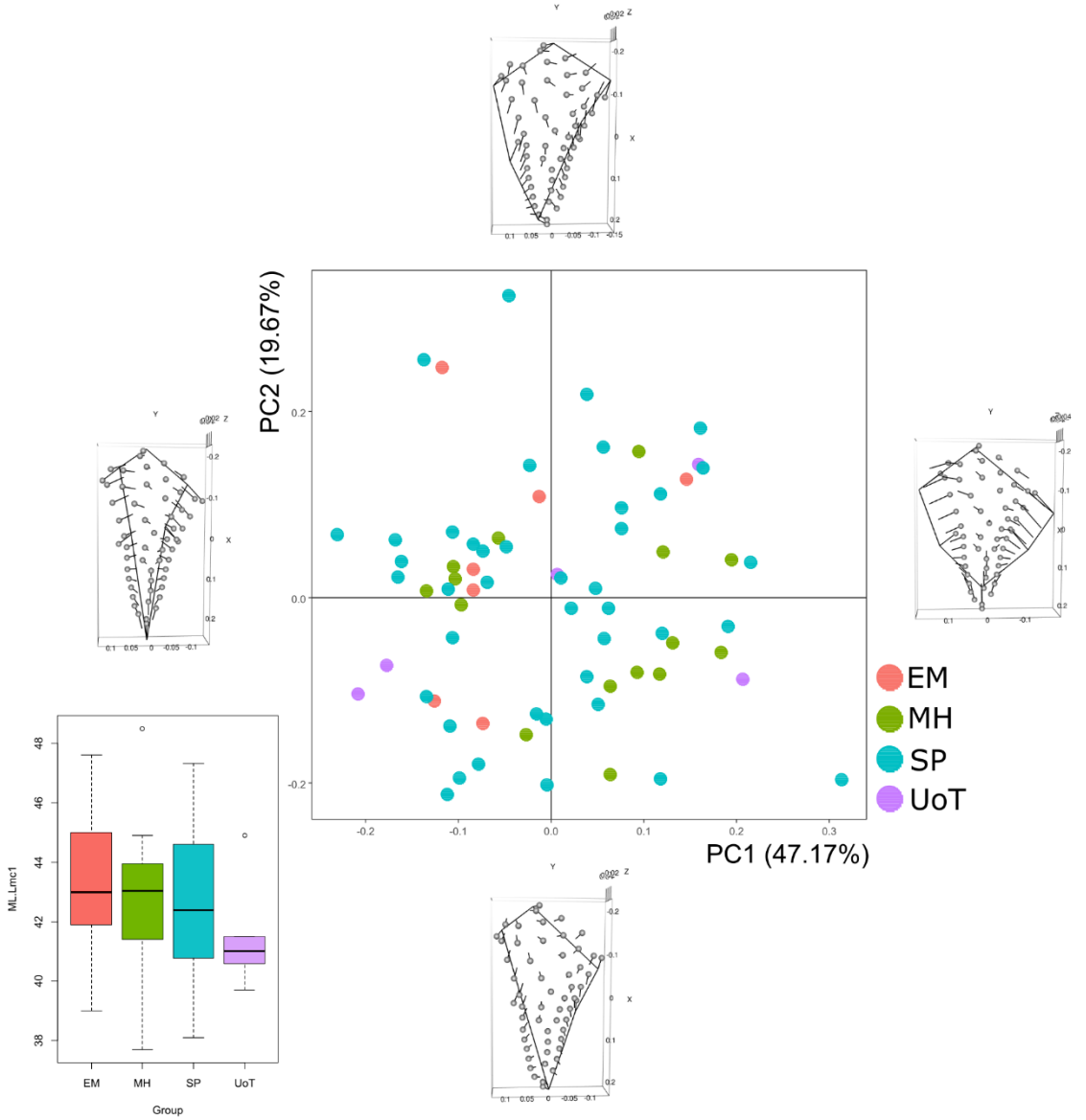

Figure 27 - Principal Component Analysis on the entire set of landmarks and shape configuration at the extremes of PC1 and PC2 for left OP.

For the analyses of OP of left MC1, a total of 68 specimens were available. Here, the first two PCs were analysed, representing almost the 67% of the total variance.

Concerning shape variation, an increasing in antero-posterior direction and a reduction in proximo-distal way are recorded along both PCs. Along PC1, both fixed and surface semi-landmarks relocate: in particular, most variation is due to L1 and L6, which both move towards a palmar direction, L3 and L4, both moving dorsally, and L5 which moves to a most distal position. With regard to surface semi-landmarks, those lying close to the dorsal and palmar aspects of the entheseal outline move towards the dorsal and palmar surfaces, respectively, while those landmarks located in correspondence of the proximal extremity of the bone. About PC2, the entheseal morphological changes are in correspondence of fixed pseudo-landmarks L1 and L6, both moving distally, L2 moving to a palmar direction, L3 and L4, moving both laterally and proximally, L5 partially moves to both distal and dorsal directions. With regard to surface semi-landmarks, those lying close to dorsal aspect of the outline move to a most dorsal position, while others lying in correspondence of the proximo-palmar side of the outline move distally.

Here in **Figure 27**,the subdivision of groups is not evident, and the entire sample is homogenously distributed all over the plot, even if shape variation is recorded. One consideration can be made about EM: it is mostly distributed for negative values of PC1, except for one individual which is in the positive side of the same PC. Along PC2, one specimen from UoT has a distribution for positive values of PC2, while most of them has negative values for PC2. No peculiar consideration can be made for MH and SP.

4.2 Analyses of 2nd metacarpal bones

4.2.1 Right MC2 – Descriptive statistics, normality tests and correlation analyses

	raw size - DI1	ERS - DI1	raw size - DI2+PI1	ERS - DI2+PI1	raw size - ECRL	ERS - ECRL	APWM/ML*	MLWM/ML*	ML*
N	80	72	78	71	72	66	72	72	72
Min	245,03	0,12	294,70	0,13	21,33	0,01	0,10	0,02	56,19
Max	605,88	0,26	565,52	0,25	85,21	0,03	0,16	0,16	74,60
Mean	400,91	0,16	439,41	0,18	47,62	0,02	0,14	0,12	63,89
Stand. dev	77,33	0,02	66,88	0,02	12,41	0,005	0,01	0,02	3,38

Table 13 - Summary statistics for both 3D size and linear measurements of right MC2. Raw size is calculated in mm^2, ML in calculated in mm. **APWM/ML**: Antero-Posterior Robusticity Index. **MLWM/ML**: Medio-Lateral Robusticity Index. **ML**: Maximum Length.

	raw size - DI1	ERS - DI1	raw size - DI2+PI1	ERS - DI2+PI1	raw size - ECRL	ERS - ECRL	APWM/ML*	MLWM/ML*	ML*
N	80	72	78	71	72	66	72	72	72
Shapiro-Wilk W	0,98	0,95	0,97	0,97	0,99	0,98	0,99	0,77	0,99
p(normal)	0,42	0,008	0,13	0,05	0,69	0,22	0,73	0,000003	0,61

Table 14 - Shapiro-Wilk test for each variable of right MC2.

	raw size - DI1	ERS - DI1	raw size - DI2+PI1	ERS - DI2+PI1	raw size - ECRL	ERS - ECRL
APWM/ML*		0,04				0,14
MLWM/ML*	0,06	0,03	0,08	0,09	0,01	0,01
ML*		0,12		-0,08		-0,08

Table 15 - Correlation tests between 3D bone sizes and linear dimensions for right MC2.

In **Tables 13 – 15**, descriptive statistics, correlation tests and normal distribution tests for all the variables used in this work are summarized.

The set of values of enthesis DI2+PI1 and DI1 are the highest among the entheses of MC2, according to their dimensions and nature of muscular origin sites on metacarpal shafts. With regard to normality tests for each variable of right MC2, the Shapiro-Wilk's test has verified a normal distribution with a *p-value* > 0.05 for all variables, except for ERS of enthesis DI1 and medio-lateral RI.

Correlation tests were performed: positive relations have been recorded between raw size of each enthesis and total surface size, while negative or neutral relations have been recorded when analysing ERS indexes. About relation between entheseal size (raw and ERS) and bone dimensions, raw size and ERS of all entheses of MC2 correlate with medio-lateral RI; only ERS – DI1 and ERS – ECRL correlate with both antero-posterior RI and ML. Also, ERS indexes of DI2+PI1 and ECRL entheses correlate negatively with maximum length.

4.2.1.1 ECRL enthesis

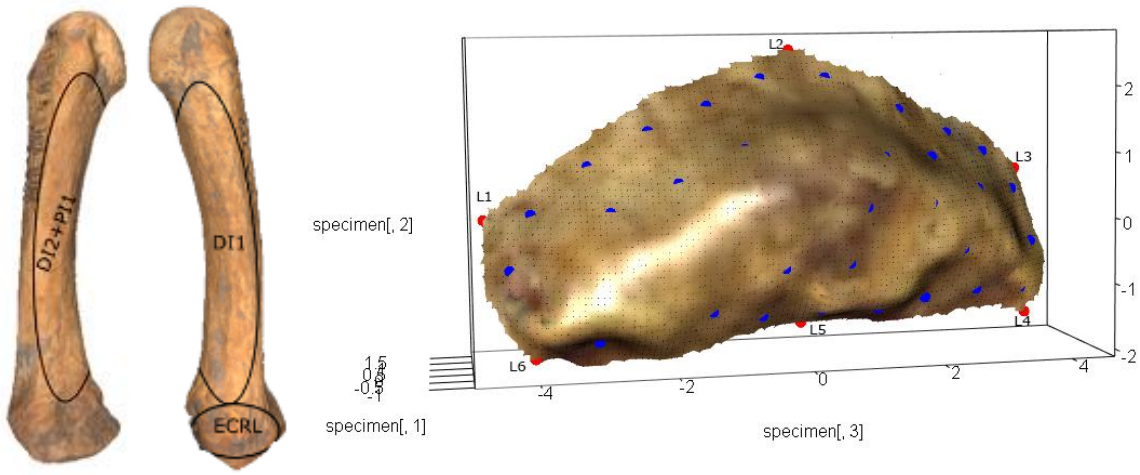

Figure 28 - On the left, the MC2 bone with delimited entheses.
On the right, the landmarks (red spots) and semi-landmarks (blue spots) on the 3D model of the surface of ECRL.
For the landmarks' definitions, see Annexes (cf. A2 – 2).

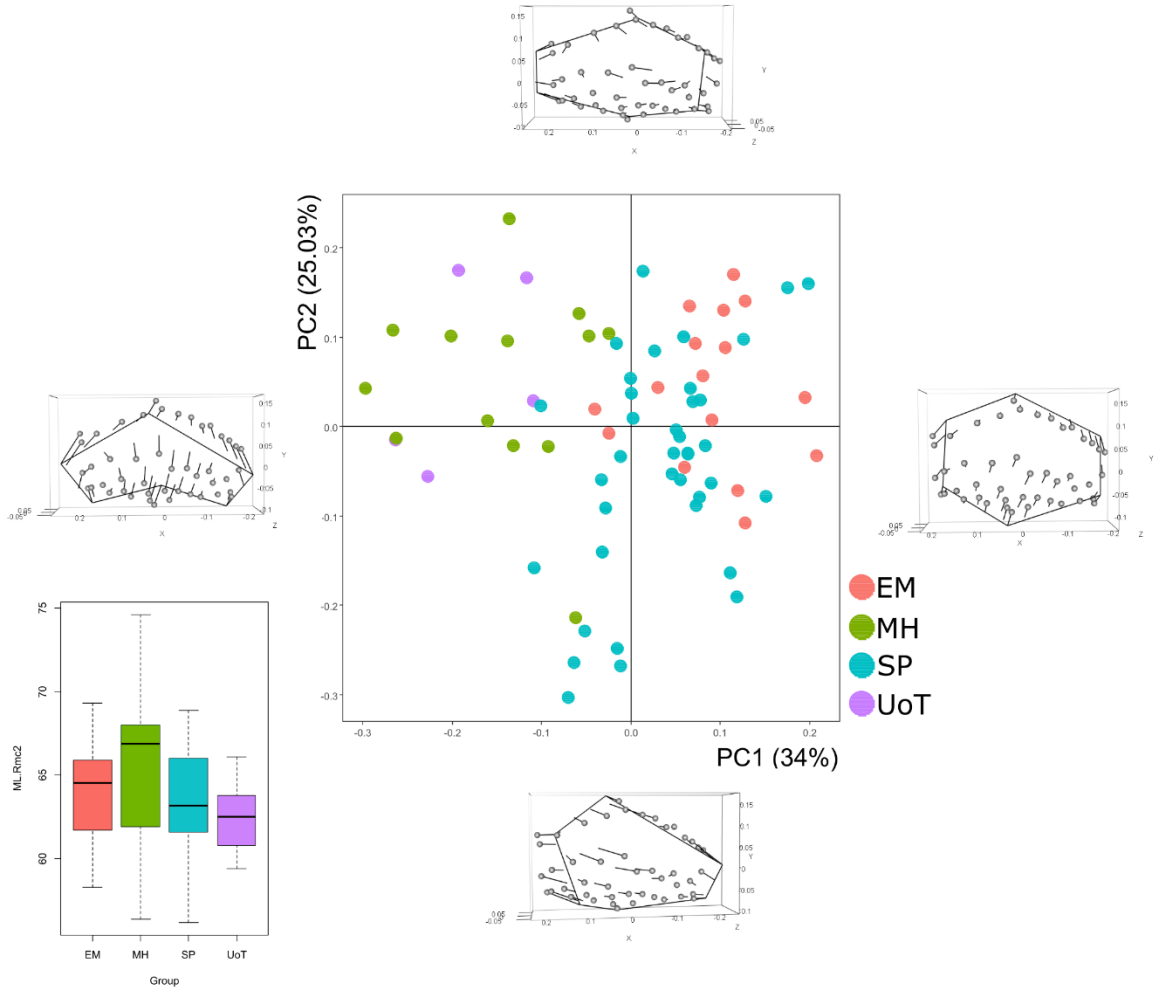

Figure 29 - Principal Component Analysis on the entire set of landmarks and shape configuration at the extremes of PC1 and PC2 for right ECRL.

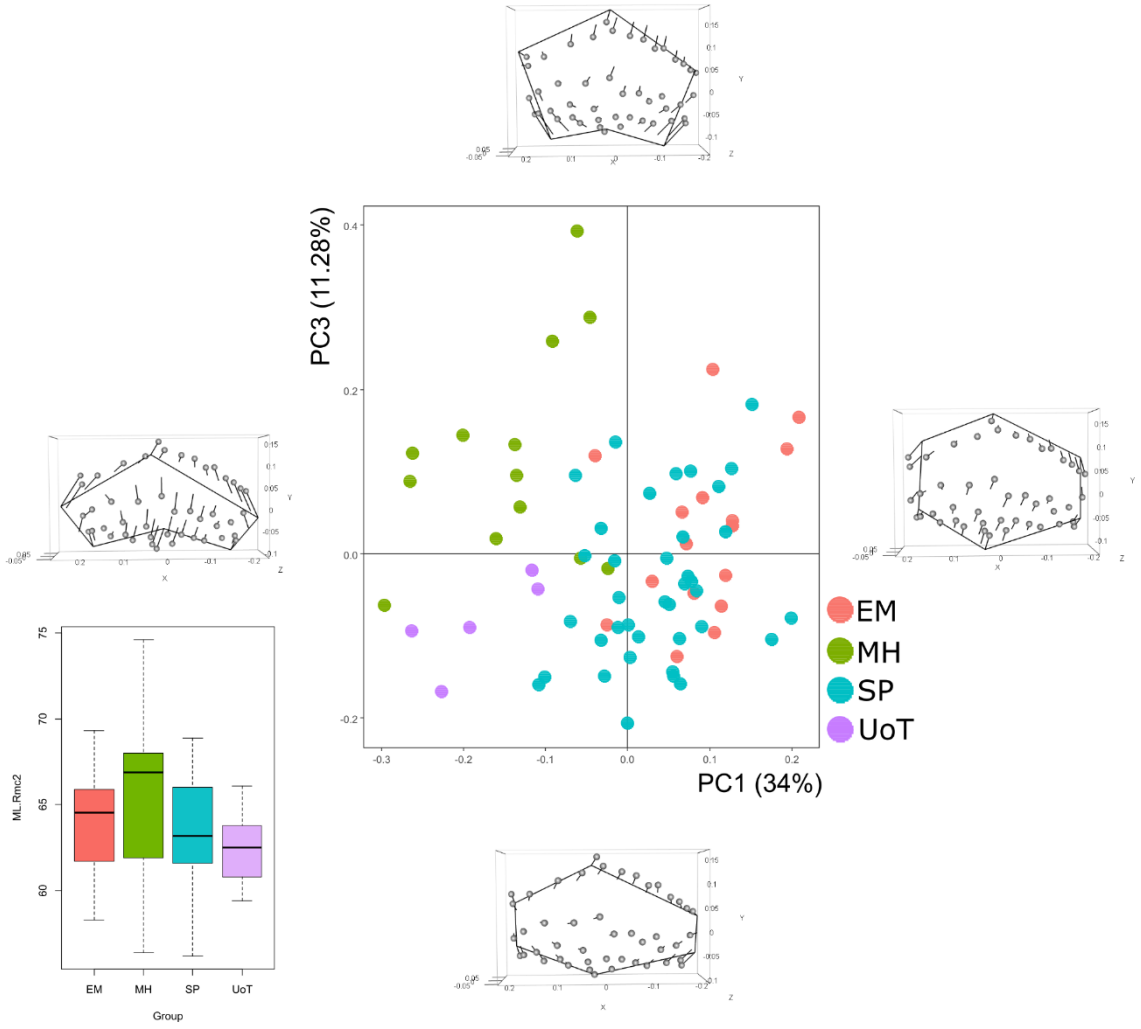

Figure 30 - Principal Component Analysis on the entire set of landmarks and shape configuration at the extremes of PC1 and PC3 for right ECRL.

For the analyses of ECRL of right MC2 (**Figure 28**), a total of 72 specimens were available. Here, the first four PCs were analysed, representing almost the 80% of the total variance.

Regarding shape variation on PC1, an increasing in antero-posterior and proximo-distal directions can be observed in correspondence of both fixed pseudo-landmarks and surface semi-landmarks: L1 and L3 move distally, along the entheseal outline towards L2, while L5 moves towards the proximal epiphysis of the bone. About surface semi-landmarks, they move towards the centre of the enthesis, following the relocation of the landmarks delimiting the outline. With regard to PC2, a shift from a palmar to a dorsal position is observable, along with relocation of surface semi-landmarks located at the centre of the enthesis. About other fixed landmarks, L2, L3, L5 and L6 all move to a palmar direction, causing an increasing in an antero-posterior way. With regard to PC3, variation can be observed in correspondence of fixed landmarks L4 and L6 – moving to a proximal direction, which cause an increasing in proximo-distal direction in correspondence of both palmar and dorsal aspects of the entheseal outlines.
Considering PC4, the variation evident in antero-posterior direction, due to relocation of fixed pseudo-landmarks: L2 moves towards the dorsal surface, L3 and L4 both move distally and to a palmar direction, partially, L6 moves medially.

When describing shape spaces previously shown, in **Figure 29** differences between groups can be seen, according to the different entheseal morphologies: MH and UoT are in the negative side of PC1 axis, for the most distributed for positive values of PC2, while SP and EM groups have a distribution for positive values of PC1 – with EM most spread for positive values of both PC1 and PC2. These groups are characterised by two different entheseal morphologies – specimens from MH and UoT have reduced entheses in proximo-distal direction, with the distal portion directed towards the palmar surface, while the SP and EM are characterised by wider entheses in proximo-distal way. Similar distribution can be seen when considering PC1 and PC4 (Annexes, cf. A4 – 4). With regard to **Figure 30**, MH and UoT are distributed for negative values of PC1 but they are also distinct between them: in particular, specimens from MH have a distribution for positive values of PC4, while those from UoT are distributed for negative values of the PC4. This means that specimens from UoT are characterised by wider entheses in a proximo-distal way, while entheses belonging to specimens from MH are wider in an antero-posterior way.

4.2.1.2 DI1 enthesis

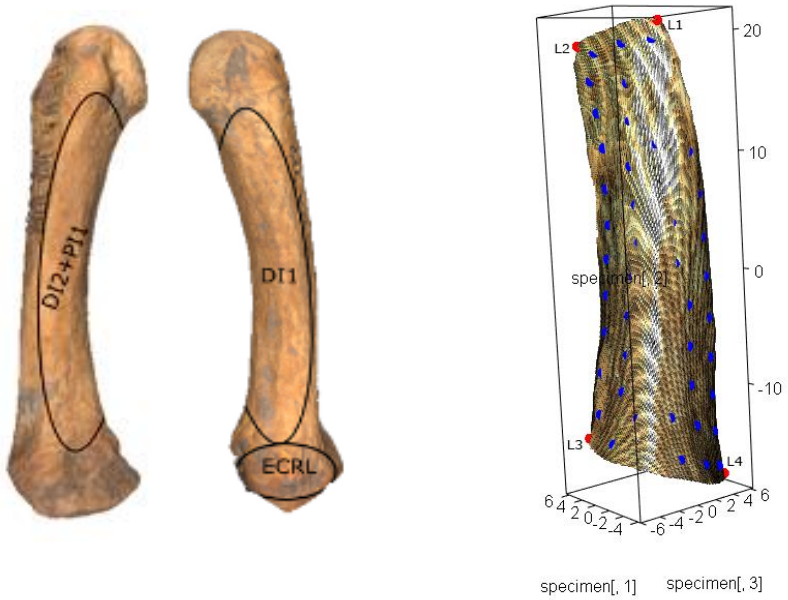

Figure 31 - On the left, the MC2 bone with delimited entheses.
On the right, the landmarks (red spots) and semi-landmarks (blue spots) on the 3D model of the surface of DI1.
For the landmarks' definitions, see Annexes (cf. A2 – 2).

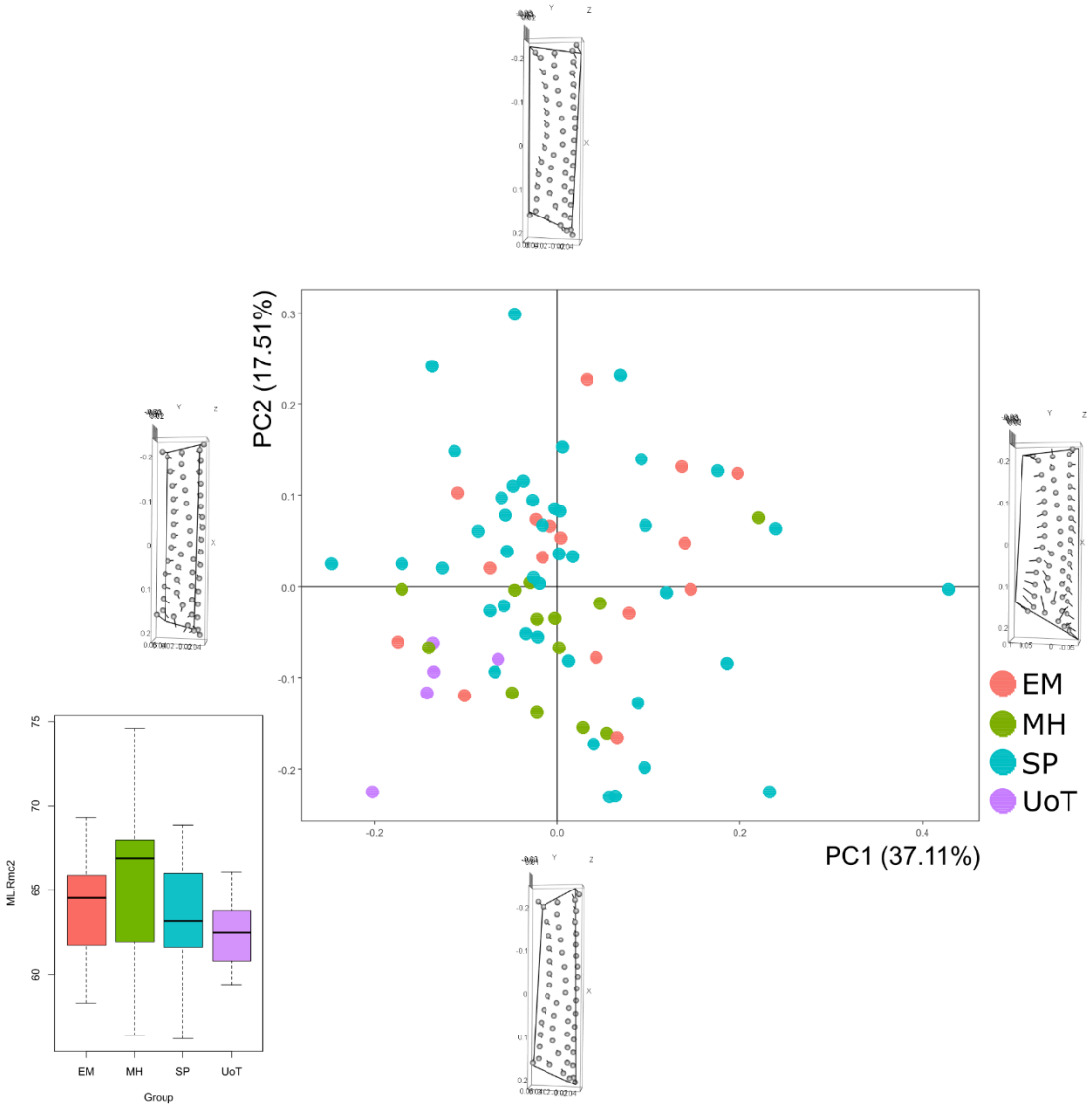

Figure 32 - Principal Component Analysis on the entire set of landmarks and shape configuration at the extremes of PC1 and PC2 for right DI1.

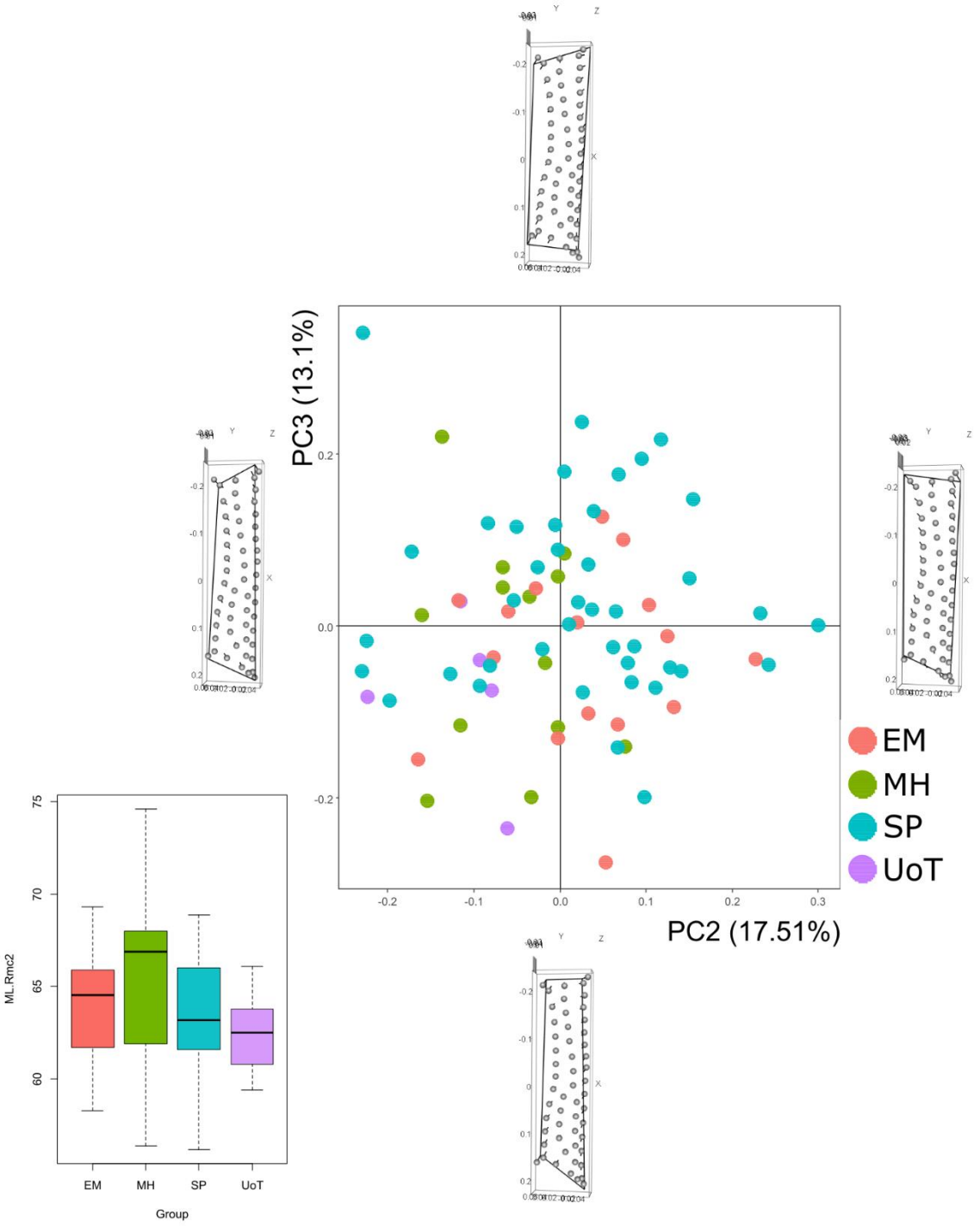

Figure 33 - Principal Component Analysis on the entire set of landmarks and shape configuration at the extremes of PC2 and PC3 for right DI1.

For the analyses of DI1 of right MC2 (**Figure 31**), a total of 75 specimens were available. Here, the first three PCs were analysed, representing almost 70% of the total variance.

Analysing shape variation, along PC1 the morphology of the enthesis is modified, due to changes in position of L3 – it moves medially, causing a modification of the position of the surface semi-landmarks, some going distally, others medially. When discussing about PC2, fixed pseudo-landmarks L1 and L2 move proximally and distally respectively: this means that the entheseal shape become wider at the distal portion, causing an increasing in correspondence of the distal aspect of the entheseal outline. Same kind of considerations can be done for PC3: increasing at the distal portion of the enthesis and in correspondence at the proximal extremity are recorded, so the palmar entheseal outline is longer than the dorsal one.

In **Figure 32** analysis shows a uniform distribution for most of the sample, except for UoT, located in the 3rd quarter of the plane, with negative values for both PCs. Even if distinct groups are not evident, it is possible to highlight some differences between MH and EM – generally distributed for negative and positive values along PC2, respectively. In **Figure 33**, a similar distribution is shown: the only difference is about MH group whose specimens are all distributed for negative values of PC2.

4.2.1.3 DI2+PI1 enthesis

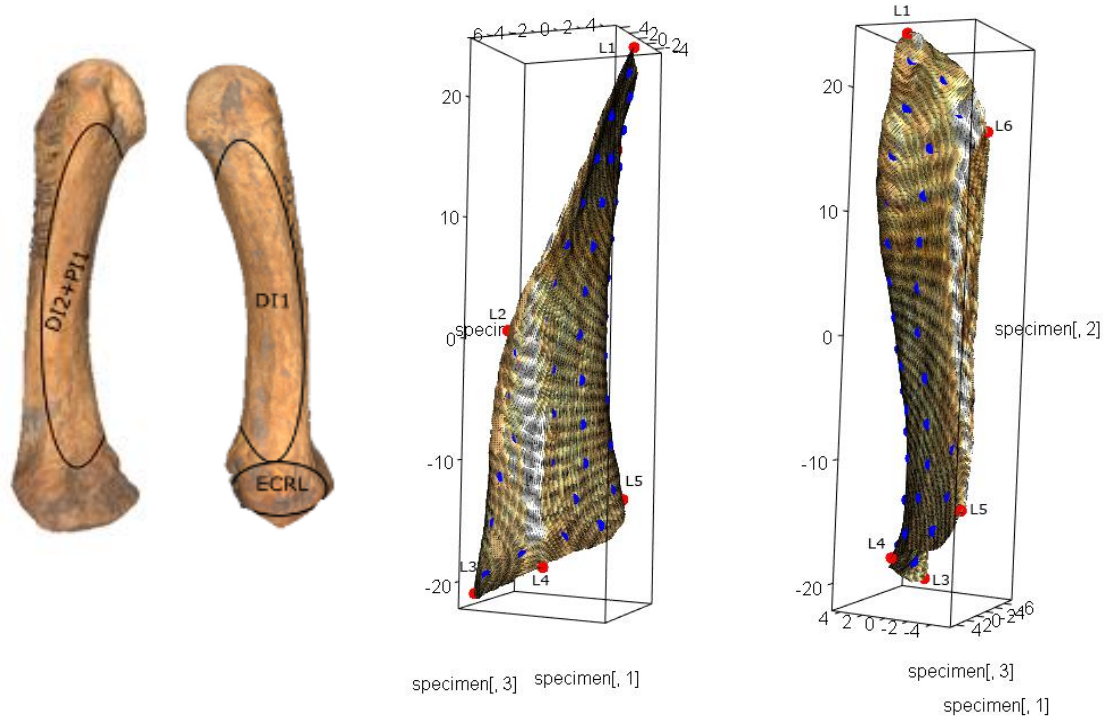

Figure 34 - On the left, the MC2 bone with delimited entheses.
On the right, the landmarks (red spots) and semi-landmarks (blue spots) on the 3D model of the surface of DI2+PI1. For the landmarks' definitions, see Annexes (cf. A2 – 2).

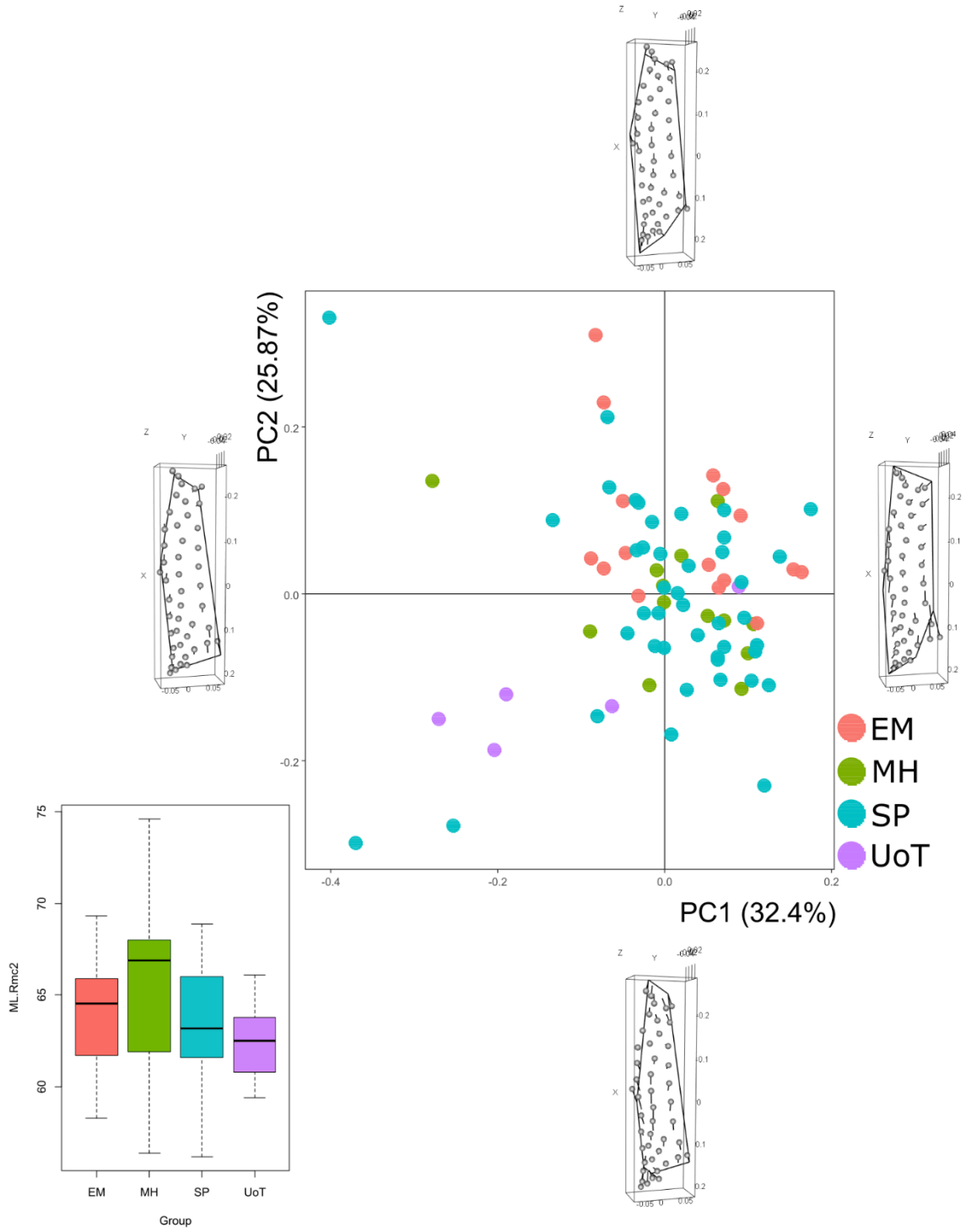

Figure 35 - Principal Component Analysis on the entire set of landmarks and shape configuration at the extremes of PC1 and PC2 for right DI2+PI1

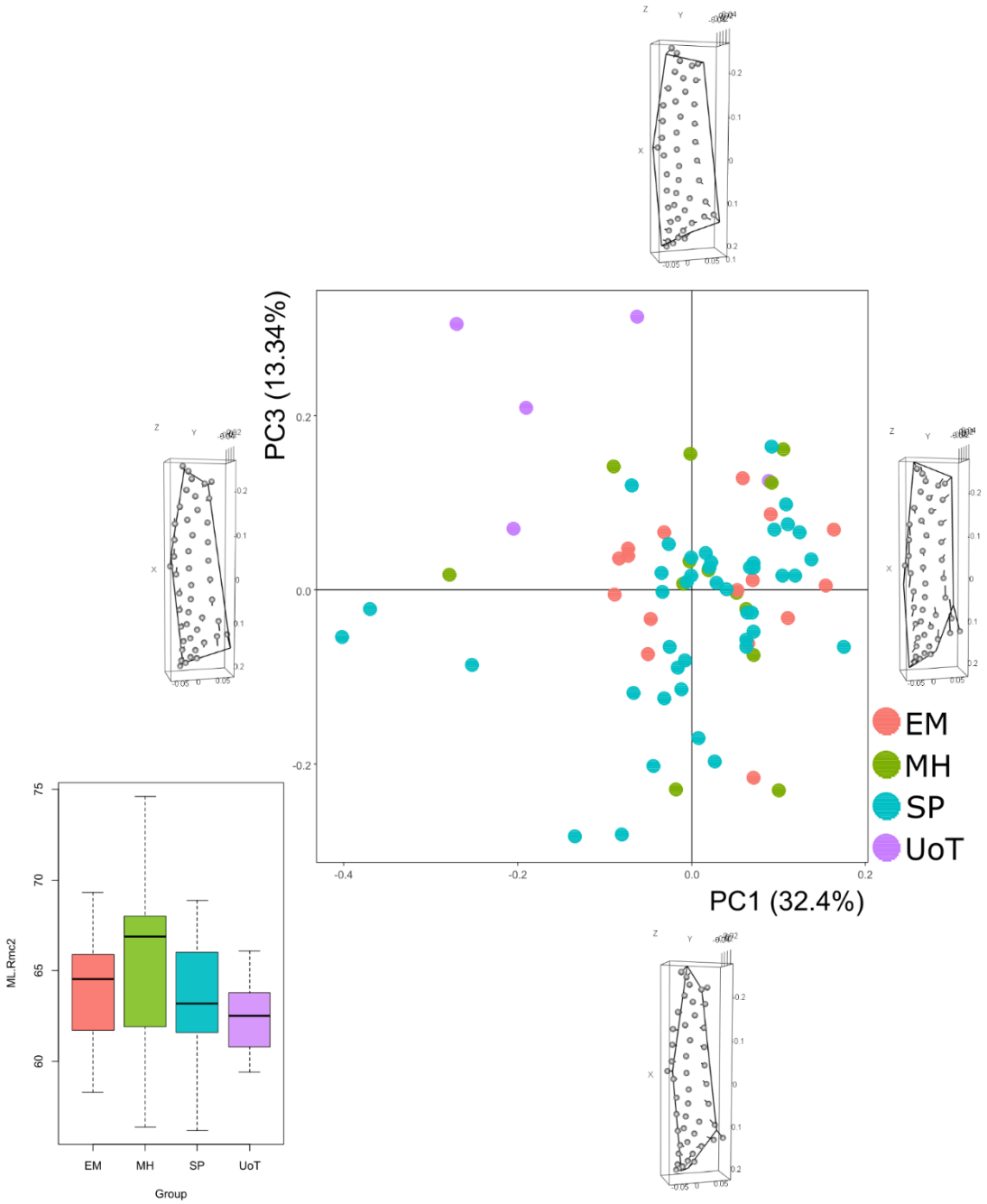

Figure 36 - Principal Component Analysis on the entire set of landmarks and shape configuration at the extremes of PC1 and PC3 for right DI2+PI1.

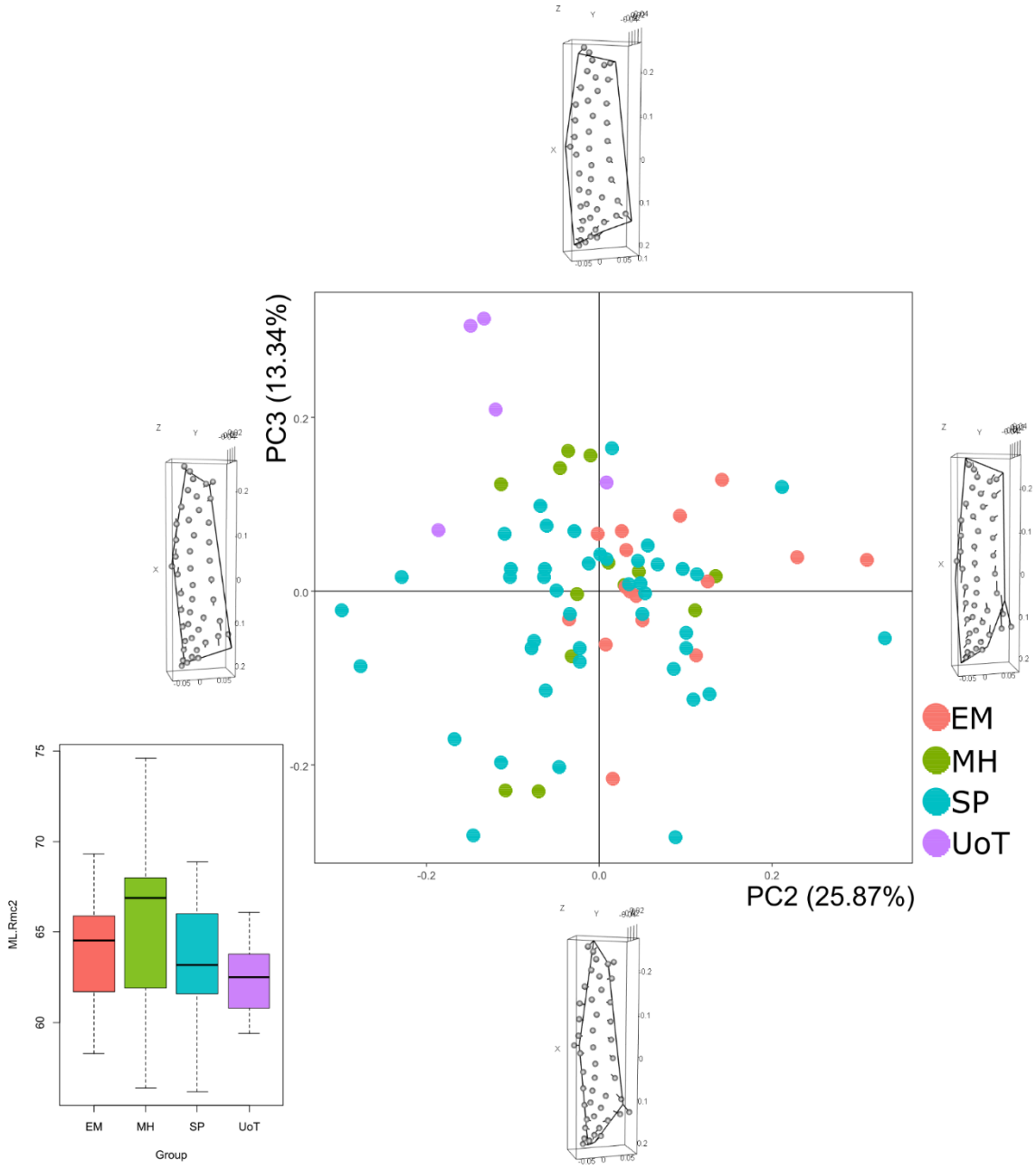

Figure 37 - Principal Component Analysis on the entire set of landmarks and shape configuration at the extremes of PC2 and PC3 for right DI2+PI1.

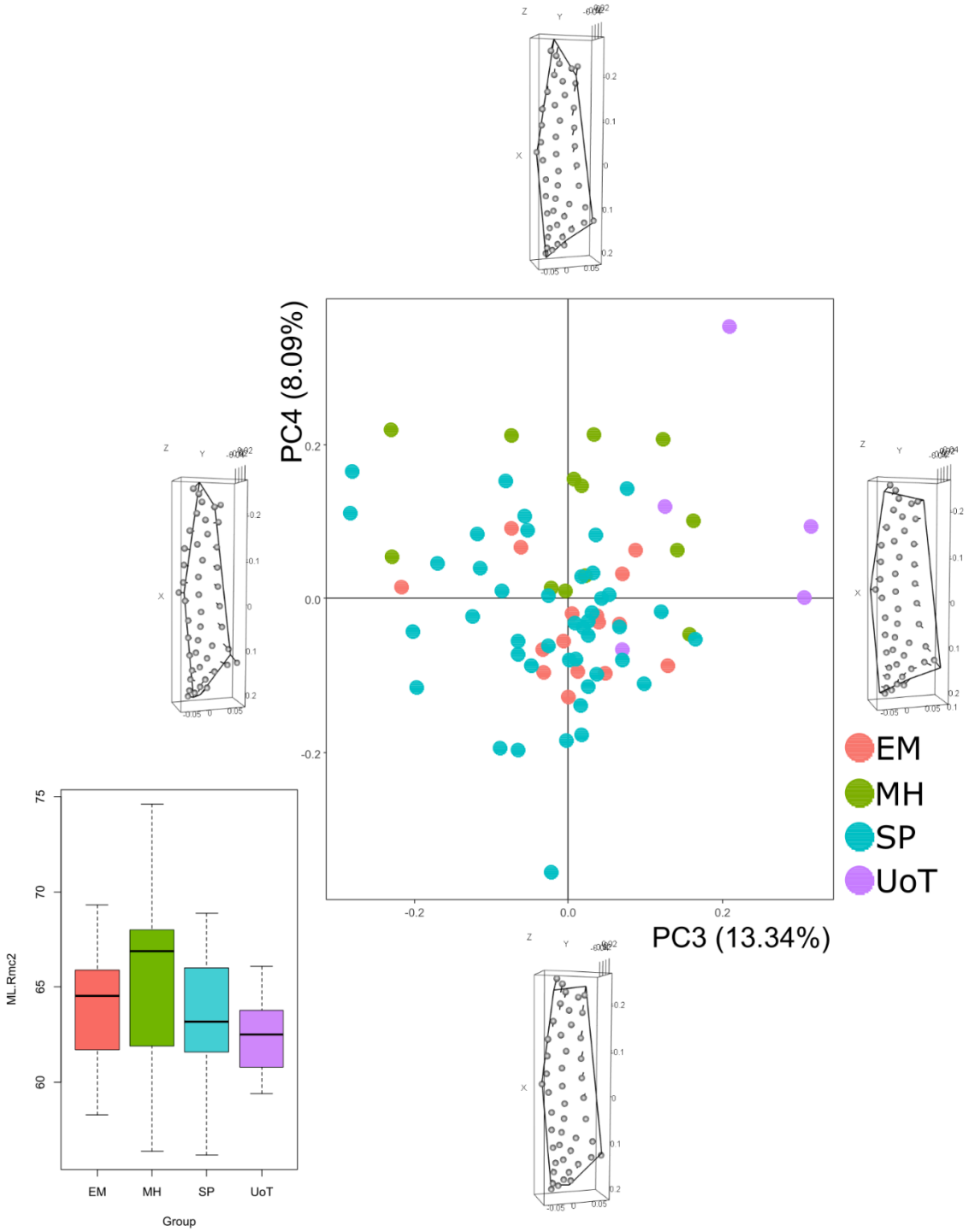

Figure 38 - Principal Component Analysis on the entire set of landmarks and shape configuration at the extremes of PC3 and PC4 for right DI2+PI1

For the analyses of DI2+PI1 of right MC2 (**Figure 34**), a total of 77 specimens were available. Here, the first four PCs were analysed, representing almost the 80% of the total variance.

Regarding PC1, changes in position of fixed pseudo-landmarks L2, L4 and L5 are recorded, causing variation in correspondence of the proximo-palmar aspect of the entheseal outline: a decreasing in length can be seen for the outline between L5 and L6, along with a minimum increasing in correspondence of the distal portion. With regard to PC2, it is possible to observe different entheseal morphologies due to relocation of fixed landmarks L2 and L5, moving distally, and L4, moving proximally: these changes cause modifications of both distal and proximal entheseal portions. Regarding PC3, L1 moves towards L2 and L5 moves proximally, causing an increasing of the size of the enthesis in an antero-posterior direction, not only modification of the outline. Considering PC4, fixed pseudo-landmarks – L1, L4 and L6 – change their positions, with L1 moving distally, L4 moving towards the centre of the enthesis and L6 moving proximally, consequently determining a reduction in length for the palmar entheseal outline between L5 and L6.

Analysing shape space shown in **Figure 35**, the sample is distributed all over the graph, except for four specimens of UoT, three specimens of SP and one from MH. EM sample is distributed for positive values of PC2 and is distinct from UoT sample. In **Figure 36**, the peculiarity is about specimens from UoT, which move along PC3 towards the positive side of this PC but has negative values for PC1 (with one individual falling into the group constituted by the rest of the sample). Even in **Figure 37** UoT is separated from the rest of the sample and EM has a distribution for positive values of PC2. Also, MH is divided into three groups: two specimens have negative values for both PCs and are characterised by the smallest entheseal morphology, the second group is distributed for values near to zero, while the third group has a distribution for negative and positive values for PC2 and PC3, respectively, and is constituted by specimens with widest entheses in both proximal and distal extremities. Finally, in **Figure 38**, UoT is distributed for positive values of both PC3 and PC4, while MH has a distribution for positive values of PC4, with specimens characterised by entheses reduced in correspondence of the distal portion.

4.2.2 Left MC2 – Descriptive statistics, normality tests and correlation analyses

	raw size - DI1	ERS - DI1	raw size - DI2+PI1	ERS - DI2+PI1	raw size - ECRL	ERS - ECRL	APWM/ML*	MLWM/ML*	ML*
N	82	81	82	81	77	76	82	82	83
Min	223,51	0,09	290,71	0,14	10,68	0,003	0,105	0,10	55,60
Max	596,31	0,21	585,11	0,21	78,97	0,031	0,17	0,16	73,80
Mean	392,33	0,16	423,23	0,18	46,13	0,019	0,13	0,12	63,81
Std. error	8,47	0,00	7,13	0,00	1,84	0,00	0,00	0,00	0,41
Stand. dev	76,67	0,023	64,59	0,016	16,17	0,006	0,014	0,011	3,74

Table 16 - Summary statistics for both 3D size and linear measurements for left MC2. Raw size is calculated in mm^2. ML is calculated in mm. **APWM/ML**: Antero-Posterior Robusticity Index. **MLWM/ML**: Medio-Lateral Robusticity Index. **ML**: Maximum Length.

	raw size - DI1	ERS - DI1	raw size - DI2+PI1	ERS - DI2+PI1	raw size - ECRL	ERS - ECRL	APWM/ML*	MLWM/ML*	ML*
N	82	81	82	81	77	76	82	82	83
Shapiro-Wilk W	0,99	0,98	0,99	0,99	0,98	0,98	0,98	0,95	0,99
p(normal)	0,82	0,35	0,77	0,59	0,36	0,16	0,20	0,0021	0,53

Table 17 - Shapiro Wilk test for each variable of left MC2.

	raw size - DI1	ERS - DI1	raw size - DI2+PI1	ERS - DI2+PI1	raw size - ECRL	ERS - ECRL
APWM/ML*	0,13	-0,11		0,12		
MLWM/ML*	0,13	-0,04	0,19	-0,09		
ML*		0,18		0,09		-0,01

Table 18 - Correlation tests between 3D bone sizes and linear dimensions for left MC2.

In **Tables 16 – 18**, descriptive statistics, correlation tests and normal distribution tests for all the variables used in this work are summarized. The set of values of enthesis DI2+PI1 and DI1 are the highest among the entheses of MC2, according to their dimensions and nature of muscular origin sites on metacarpal shafts. With regard to normality tests for each variable of left MC2, the Shapiro-Wilk's tests verified a normal distribution with a *p-value* > 0.05 for all variables, except for medio-lateral Robusticity Index.

Correlation tests were performed: positive relations have been recorded for both raw size and ERS of each enthesis and total surface size. About relation between entheseal size (both raw and ERS) and bone dimensions, raw size and ERS of DI1 and DI2+PI1 entheses correlate with medio-lateral RI, while ERS of both DI1 and DI2+PI1 correlate also with the other linear dimensions: in particular, negative correlation are recorded between antero-posterior RI and ERS of DI1 enthesis and medio-lateral RI and ERS of both DI1 and DI2+PI1 entheses. Regarding ECRL enthesis, only its ERS shows a low value of negative correlation with maximum length.

4.2.2.1 ECRL enthesis

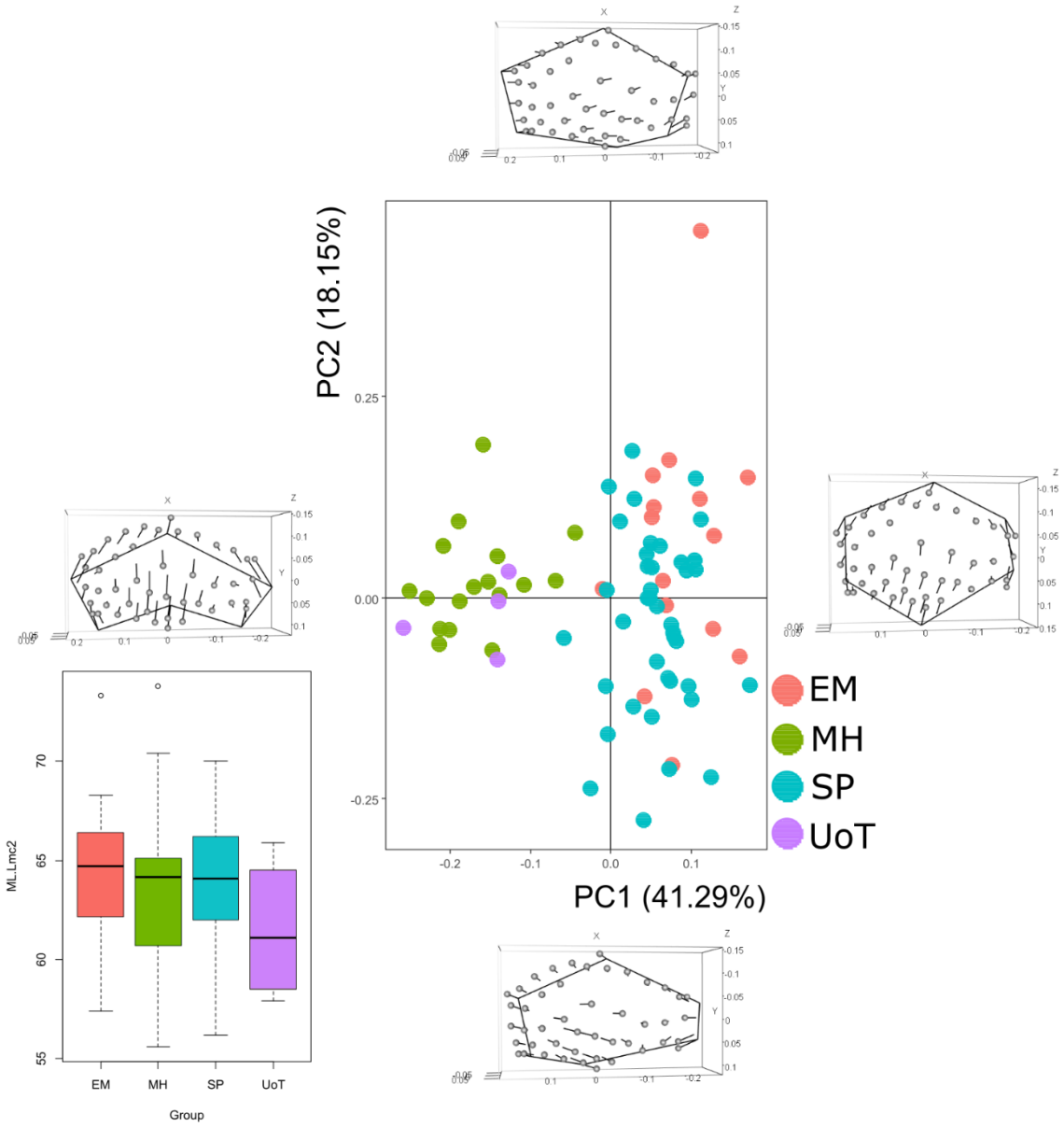

Figure 39 - Principal Component Analysis on the entire set of landmarks and shape configuration at the extremes of PC1 and PC2 for left ECRL

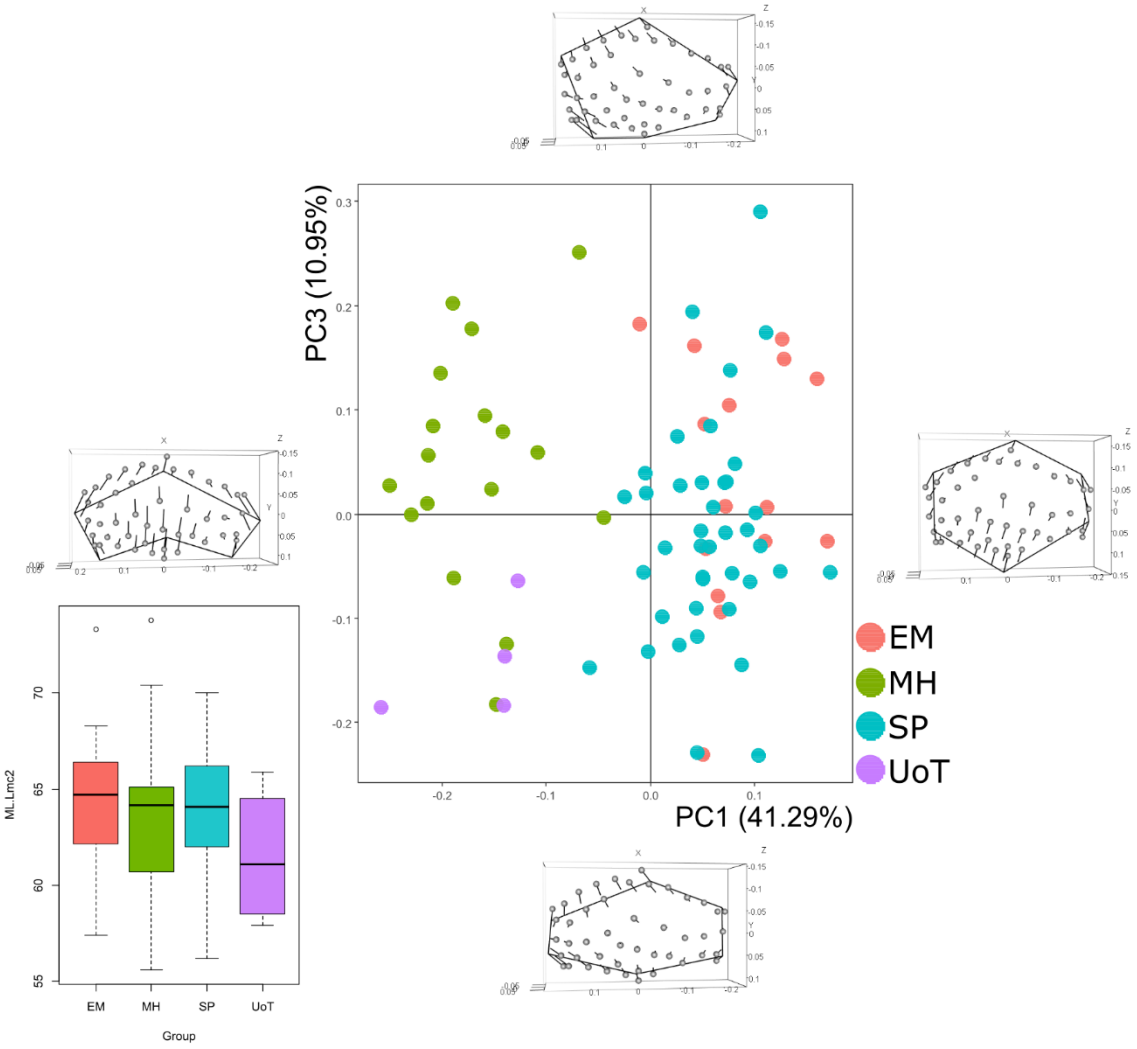

Figure 40 - Principal Component Analysis on the entire set of landmarks and shape configuration at the extremes of PC1 and PC3 for left ECRL

For the analyses of ECRL of left MC2, a total of 76 specimens were available. The first four PCs were analysed, representing almost the 80% of the total variance.

Regarding shape differences along PC1, L1, L3, L4 and L6 move in a distal direction, L2 moves towards the distal epiphysis and L5 moves in the opposite direction than L2 – determining an increasing of the entheseal shape in proximo-distal direction. With regard to PC2, shape variation occurs in correspondence of the outline, caused by a shift of L5 – which moves to a palmar direction – and the other fixed pseudo-landmarks which move to a dorsal direction. About surface semi-landmarks, those located close to the distal, dorsal, and palmar outlines move towards the dorsal surface, while those located at the centre of the enthesis go to a palmar direction. About PC3, an increasing of the dorsal aspect of the entheseal outline can be seen, due to repositioning of L3 and L4 – with L3 moving distally and L4 moving proximally, along the proximal outline towards L5. Also, L2 and L5 move in opposite directions – distally and proximally, respectively. About surface semi-landmarks, major degree of variation occurs close to the dorsal surface of the bone. Regarding PC4, the portion of the enthesis between L3 and L4 moves to palmar direction with the two fixed landmarks moving towards the dorsal surface, and L5 moving in the opposite direction; here, an increasing in antero-posterior direction can be seen in correspondence of the proximal portion of the outline.

Describing the resulting shape spaces previously shown in **Figure 39** and **Figure 40**, a clear distinction between EM and SP – at one side – and UoT and MH – on the other one – is shown, due to variation in correspondence of PC1. As a result, two distinct groups can be distinguished: MH and UoT are distributed for negative values of PC1, and EM and SP groups have positive values for the same PC. When considering PC3, similar distribution is evident, even if UoT group is distinct from MH: according to this separation, specimens from UoT are characterised by smaller entheses in proximo-distal direction, with a reduced dorsal outline. No distinction is evident between EM and SP. Similar distribution is also evident for PC1 and PC4: for this reason, this plot has been included in the Annexes (cf. A4 – 5).

4.2.2.2 DI1 enthesis

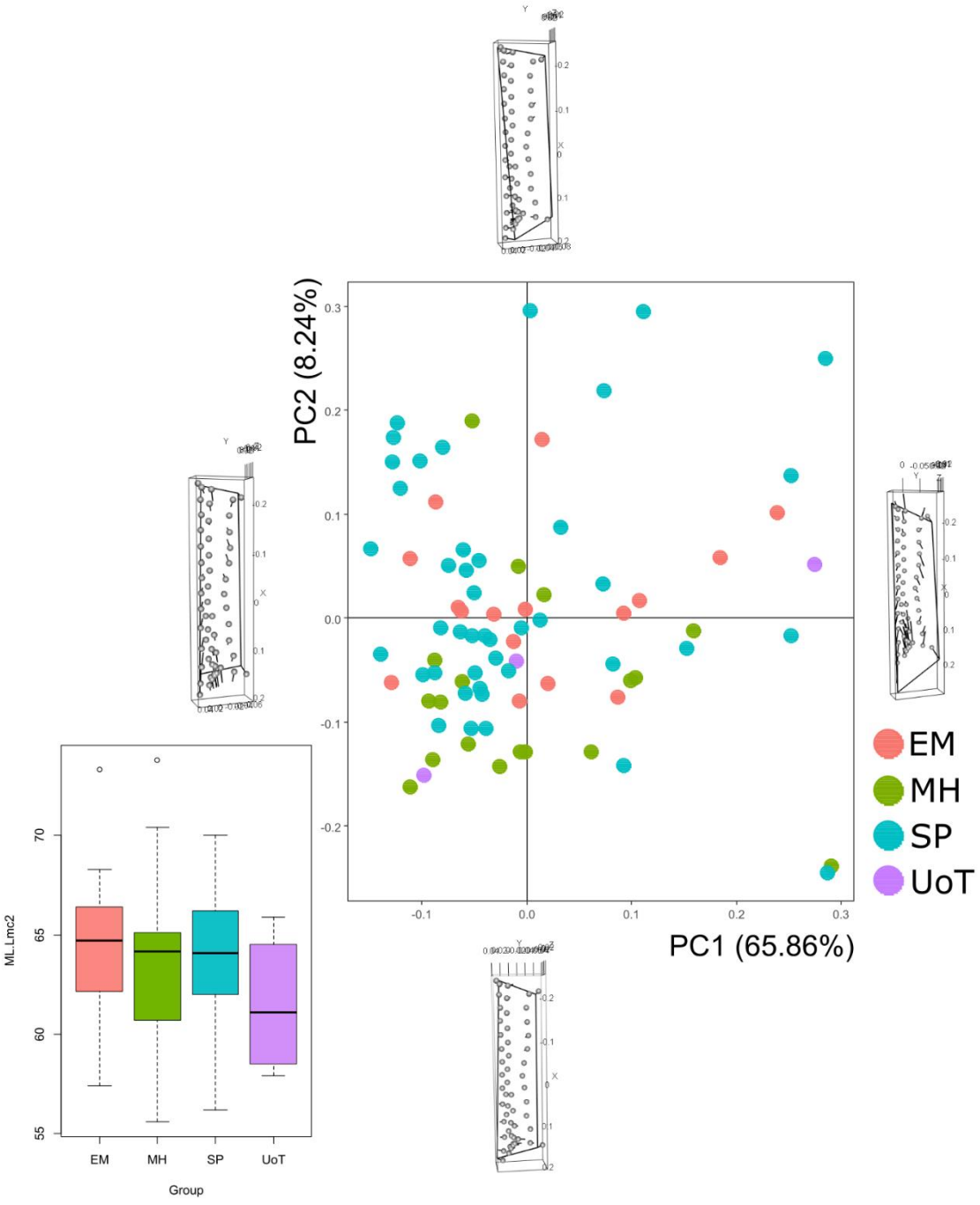

Figure 41 - Principal Component Analysis on the entire set of landmarks and shape configuration at the extremes of PC1 and PC2 for left DI1.

For the analyses of DI1 of left MC2, a total of 80 specimens were available. Here, the first two PCs were analysed, representing almost 75% of the total variance.

When analysing PC1 and PC2, variation occurs in correspondence of surface semi-landmarks, determining variation of the entheseal surface structure. For this reason, only one plot is shown: in **Figure 41**, the distribution of the entire set of samples according to PC1 and PC2 is shown. No particular groups are evident, even if a different distribution of the entire set of landmarks is recorded. Other PCs are not considered, because of similar disposition of landmarks in correspondence of the entheseal surface. So, plots considering other PCs are not included and shown.

4.2.2.3 DI2+PI1 enthesis

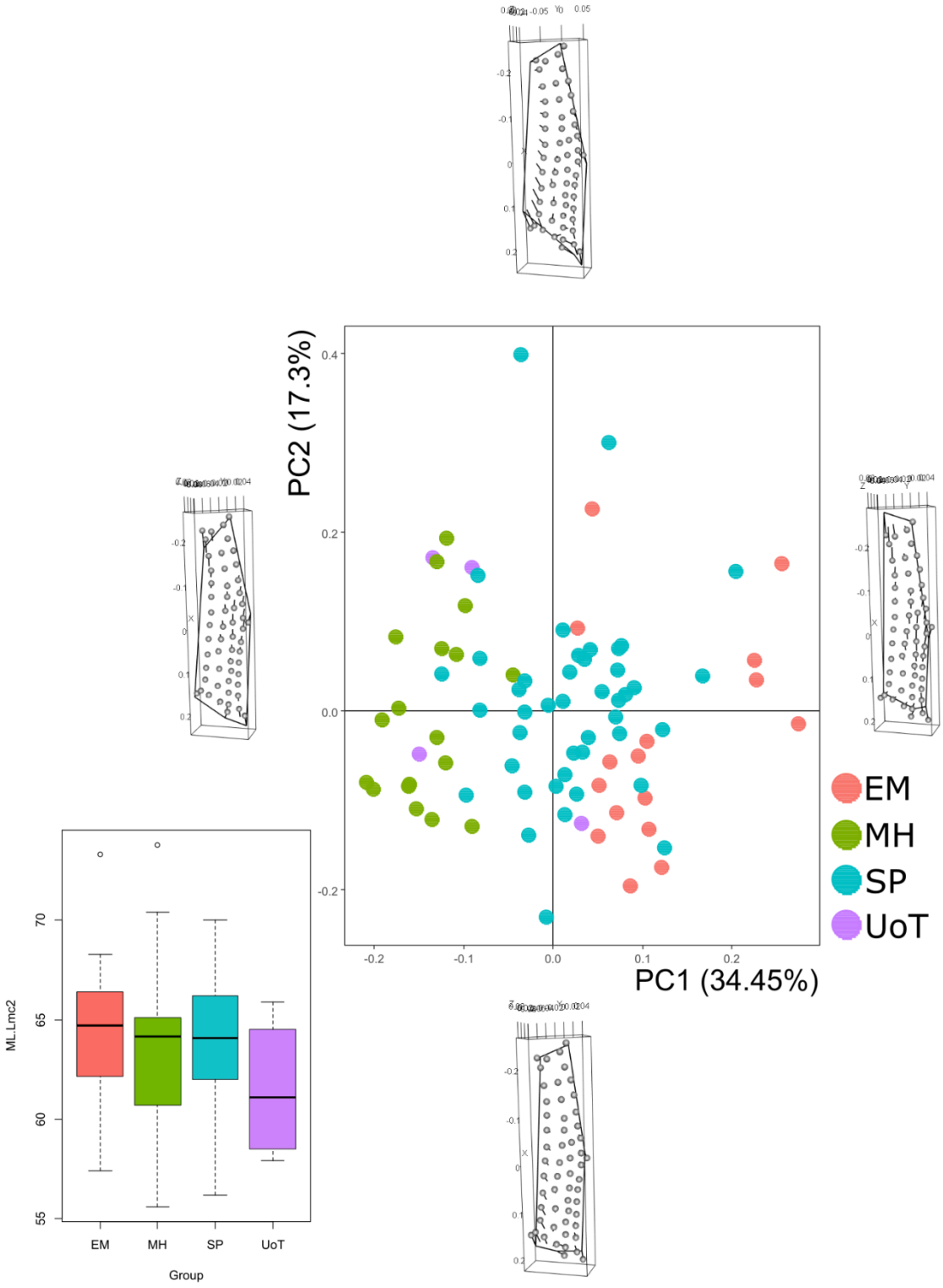

Figure 42 - Principal Component Analysis on the entire set of landmarks and shape configuration at the extremes of PC1 and PC2 for left DI2+PI1.

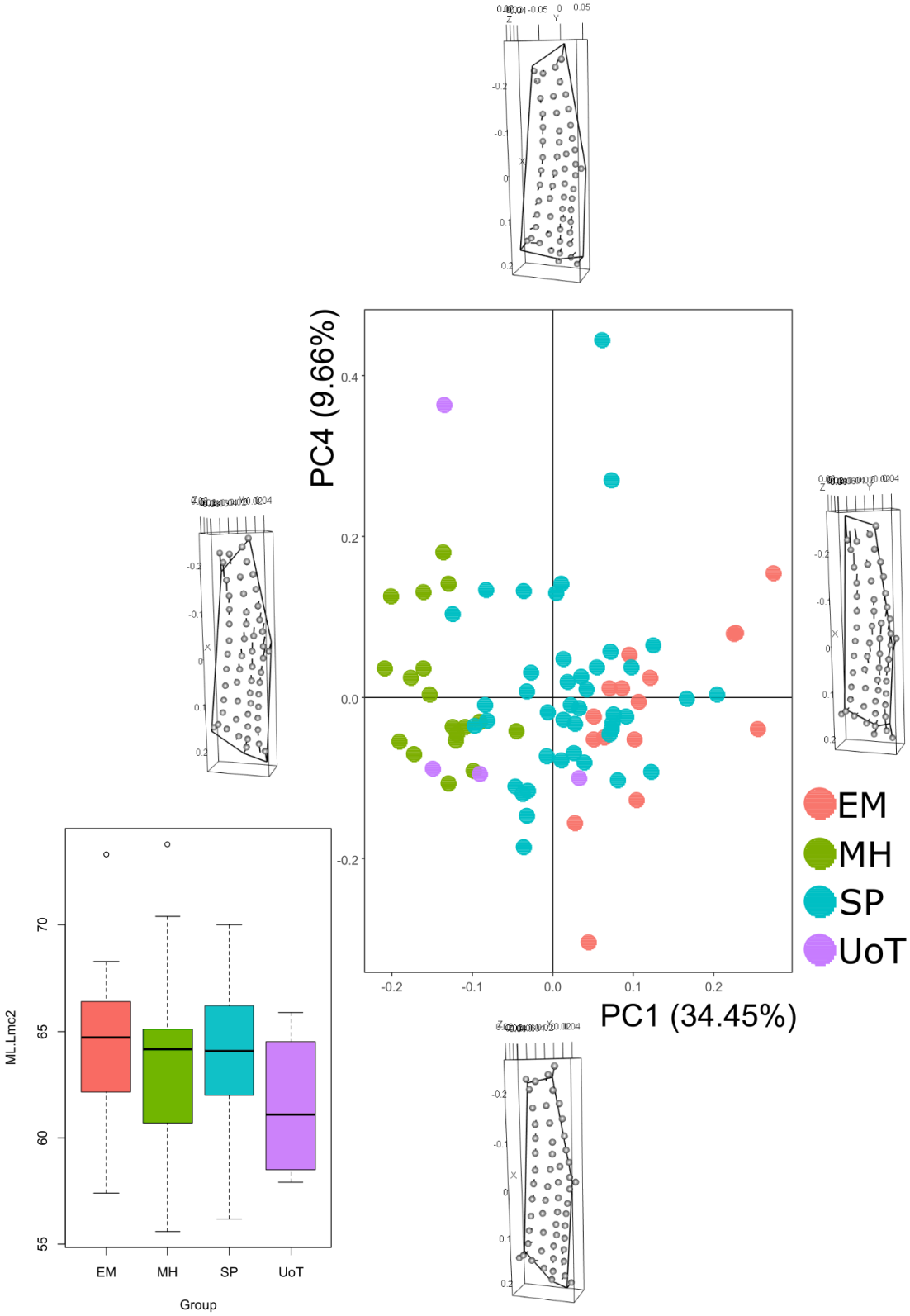

Figure 43 - Principal Component Analysis on the entire set of landmarks and shape configuration at the extremes of PC1 and PC4 for left DI2+PI1.

For the analyses of DI2+PI1 of left MC2, a total of 81 specimens were available. Here, only three PCs were considered (PC1, PC2 and PC4), representing 75% of the total variance. When considering PC1, fixed pseudo-landmarks relocates, causing modification in correspondence of both distal and proximal portions of the entheseal outline: L2 moves proximally, while L3, L4 and L6 move distally. With regard to PC2, the most important variation concerns landmarks from L3 to L5 – L3 and L4 moving both proximally and dorsally, while L5 moving distally. About surface semi-landmarks, some of them lying close to the palmar outline of the enthesis relocate, going in both distal and palmar direction, determining an increasing in an antero-posterior way. Discussing about PC4, variation occurs in correspondence of L1, going distally, L3, moving both distally and dorsally, and L5, going both proximally and in a palmar direction.

In graphs in **Figure 42** and **Figure 43** the same subdivision can be seen: the entire sample is subdivided into two groups with SP and EM samples on the right – characterised by positive values for PC1 – and the other two samples on the left – with negative values for the same PC. The other PCA plots are not introduced here because no variation is evident, but the totality of the sample is distributed uniformly all over the graph. This means that all the variation is due to shape variation on PC1.

4.3 Analyses of 3rd metacarpal bones

4.3.1 Right MC3 – Descriptive statistics, normality tests and correlation analyses

	raw size - ECRB	ERS - ECRB	raw size - DI2	ERS - DI2	raw size - DI3+ADP	ERS - DI3+ADP	APWM/ML*	MLWM/ML*	ML*
N	83	75	84	78	83	77	78	78	78
Min	27,06	0,01	185,14	0,07	322,02	0,10	0,11	0,10	54,00
Max	96,44	0,04	562,23	0,20	763,18	0,27	0,17	0,16	72,80
Mean	59,47	0,02	373,90	0,16	532,69	0,23	0,14	0,13	62,76
Stand. dev	15,94	0,01	82,50	0,03	86,33	0,03	0,01	0,01	3,69

Table 19 - Summary statistics for both 3D size and linear measurements for right MC3. Raw size is calculated in mm^2, ML is calculated in mm. APWM/ML: Antero-Posterior Robusticity Index. MLWM/ML: Medio-Lateral Robusticity Index. ML: Maximum Length

	raw size - ECRB	ERS - ECRB	raw size - DI2	ERS - DI2	raw size - DI3+ADP	ERS - DI3+ADP	APWM/ML*	MLWM/ML*	ML*
N	83	75	84	78	83	77	78	78	78
Shapiro-Wilk W	0,98	0,99	0,98	0,94	0,99	0,88	0,98	0,97	0,99
p(normal)	0,21	0,54	0,41	0,0009072	0,74	4,02E-03	0,14	0,09	0,91

Table 20 - Shapiro-Wilk test for each variable of right MC3.

	raw size - ECRB	ERS - ECRB	raw size - DI2	ERS - DI2	raw size - DI3+ADP	ERS - DI3+ADP
APWM/ML*		0,21				0,11
MLWM/ML*		0,21				0,01
ML*		-0,04		-0,03		0,06

Table 21 - Correlation tests between 3d bone size and linear dimensions for right MC3.

In **Tables 19 – 21**, descriptive statistics, correlation tests and normal distribution tests for all the variables used in this work are summarized.

The set of values for DI3+ADP are the highest among the entheses of MC3, according to the dimension of the insertion sites for the two muscles.

With regard to normality tests for each variable of right MC3, the Shapiro-Wilk's tests verified a normal distribution with a *p-value* > 0.05 for all variables, except for ERS of entheses DI2 and DI3+ADP.

Correlation tests were performed: positive relations have been recorded between raw size of each enthesis and the total surface size, while negative relations have been recorded when analysing ERS indexes. About relation between entheseal size (raw and ERS) and bone dimensions, ERS of ECRB and DI3+ADP entheses correlate with all linear measurements (ERS index of ECRB with negative correlation), while ERS of DI2 enthesis negatively correlates with ML.

4.3.1.1 ECRB enthesis

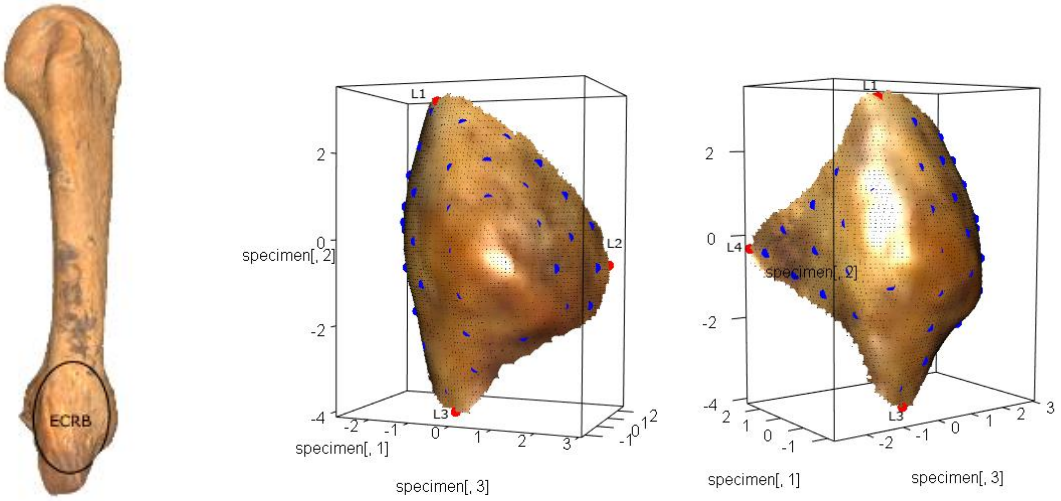

Figure 44 - On the left, the MC3 bone with delimited entheses.
On the right, the landmarks (red spots) and semi-landmarks (blue spots) on the 3D model of the surface of ECRB.
For the landmarks' definitions, see Annexes (cf. A2 – 3).

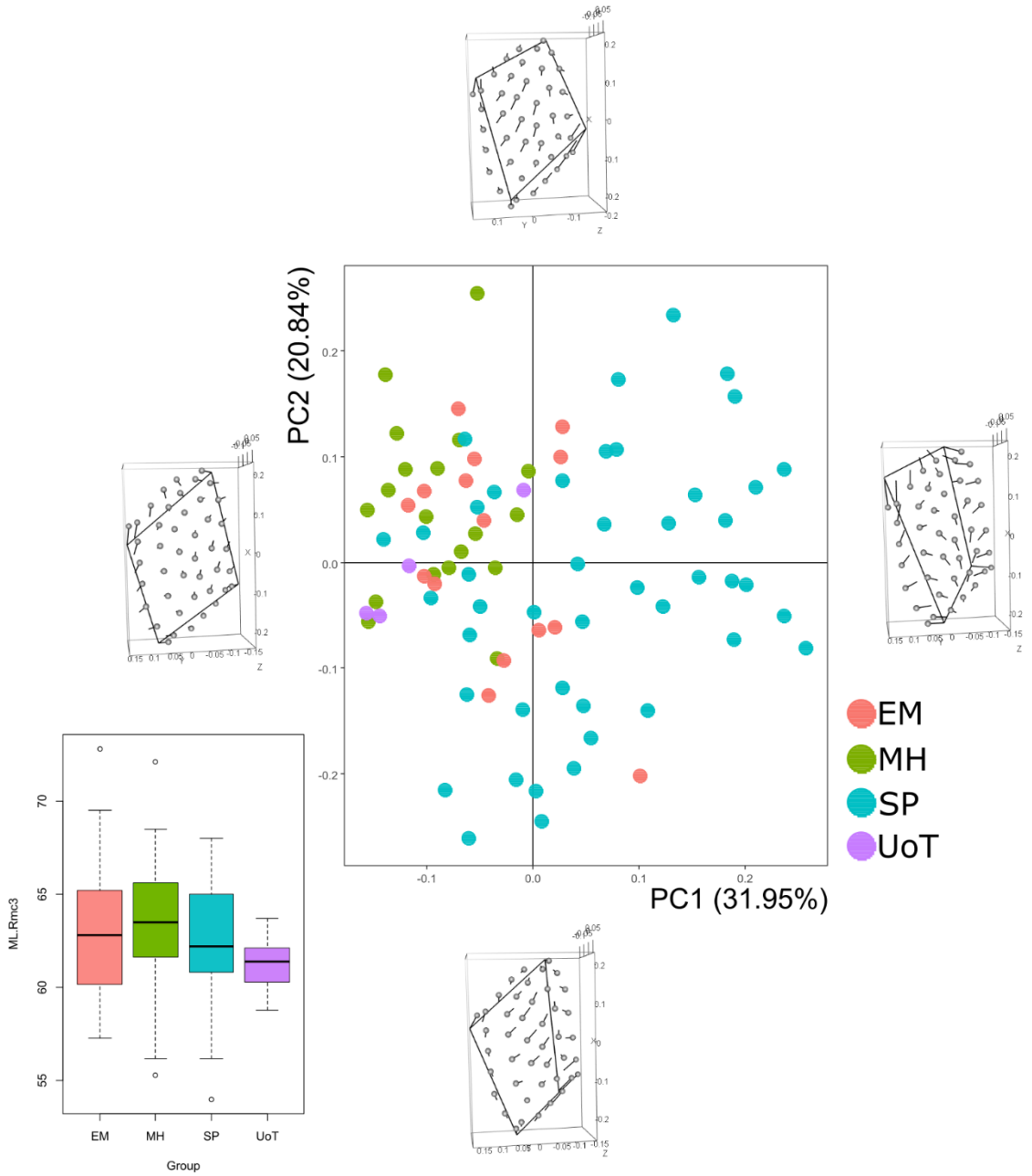

Figure 45 - Principal Component Analysis on the entire set of landmarks and shape configuration at the extremes of PC1 and PC2 for right ECRB.

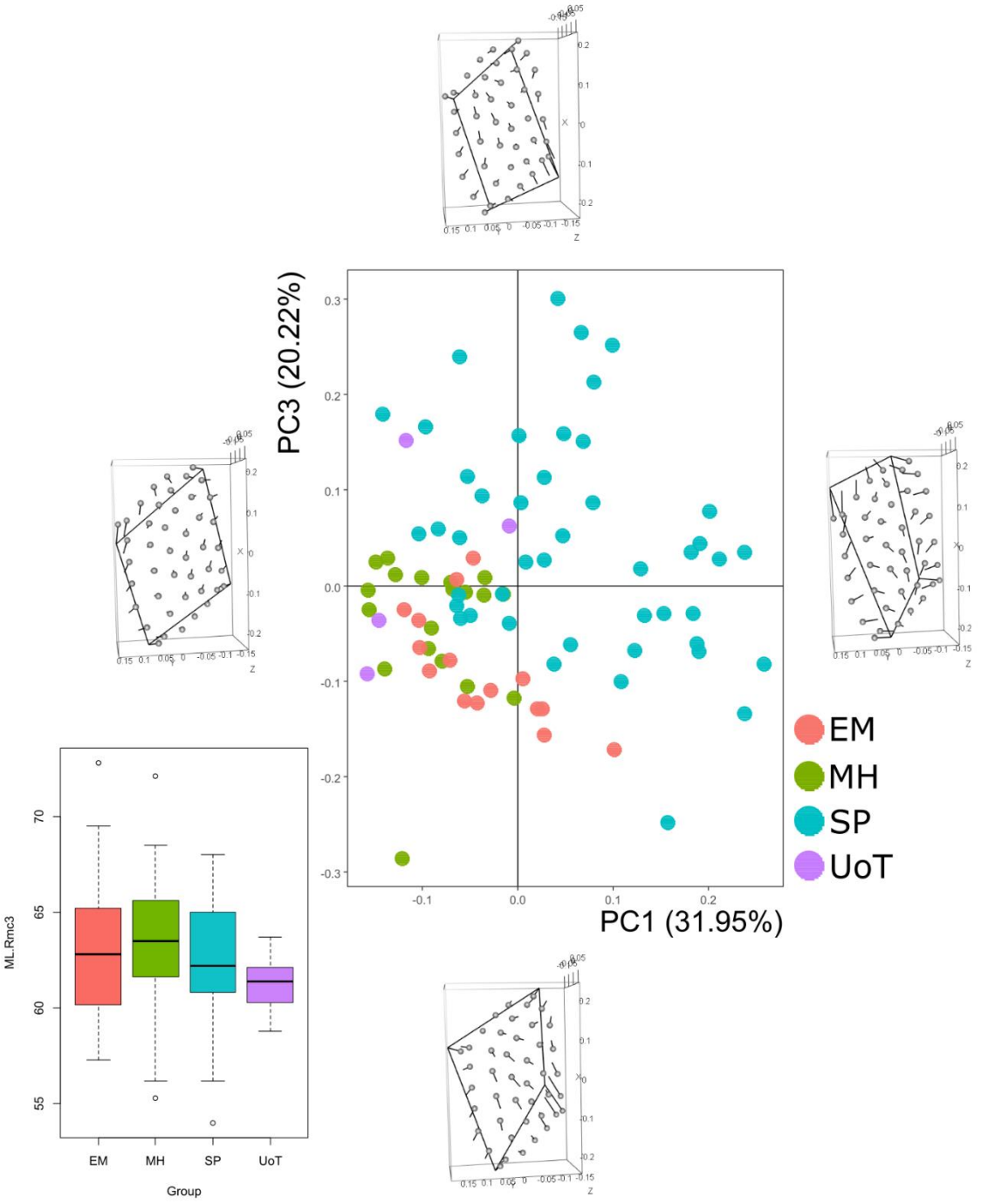

Figure 46 - Principal Component Analysis on the entire set of landmarks and shape configuration at the extremes of PC1 and PC3 for right ECRB.

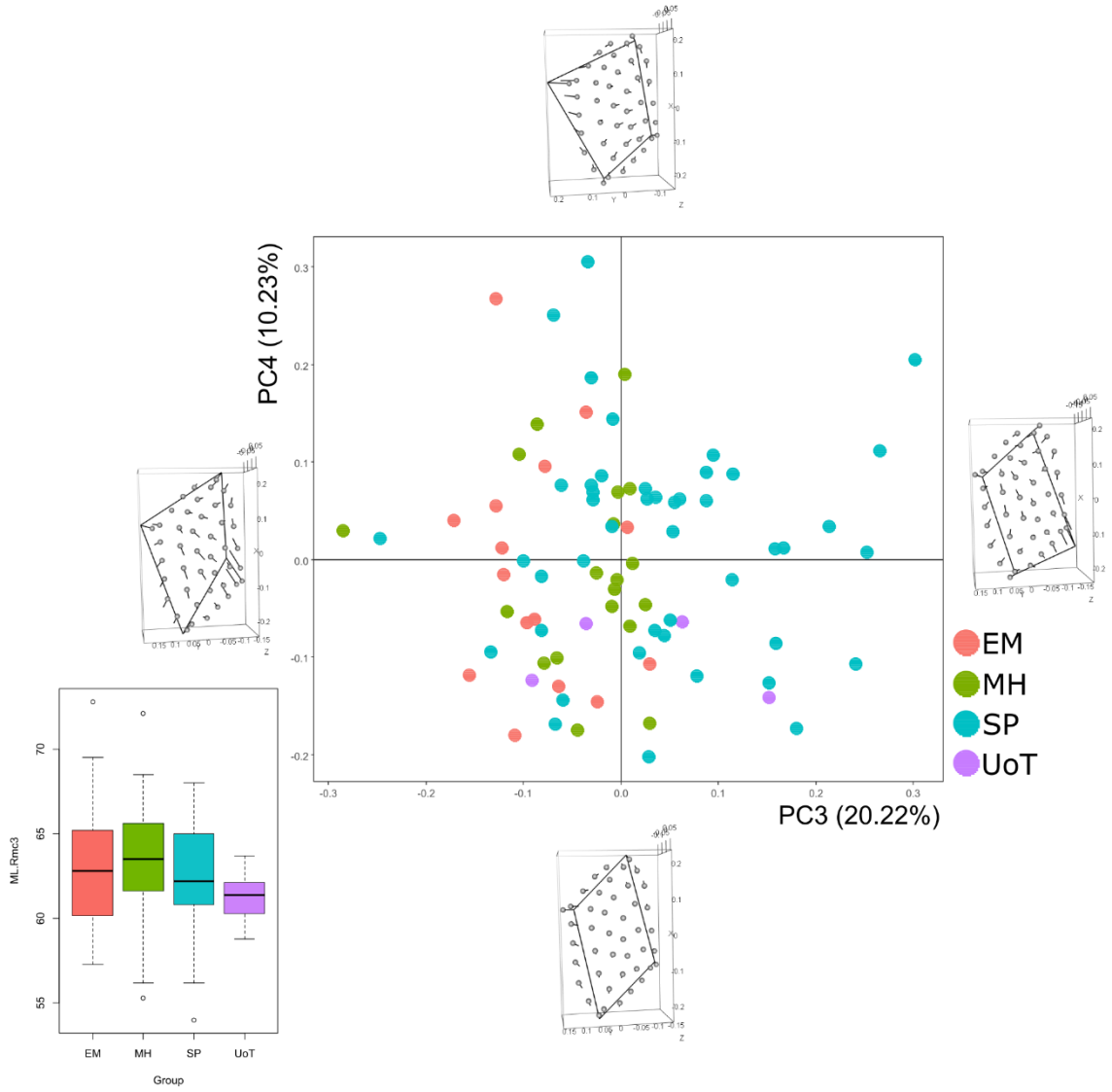

Figure 47 - Principal Component Analysis on the entire set of landmarks and shape configuration at the extremes of PC3 and PC4 for right ECRB.

For the analyses of ECRB of right MC3 (**Figure 44**), a total of 83 specimens were available. Here, the first four PCs were analysed, representing almost the 85% of the total variance.
Regarding shape differences on PC1, variation can be observed in correspondence of fixed pseudo-landmarks: L1 and L2 move in a palmar direction, L3 moves towards the dorsal surface of the bone and L4 moves distally. Also, relocation of surface semi-landmarks is evident, moving towards the centre of the enthesis. On PC2, variation is observable on both fixed pseudo-landamarks and surface semi-landmarks, causing changes in the entheseal shape. From PC2 min to max, L1 and L2 move proximally, while L4 moves in a palmar direction: these changes cause an increasing of the shape of the enthesis in an antero-posterior way. When analysing shape variation on PC3, relocation of fixed pseudo-landmarks determines modification of the entheseal shape in the distal portion. This variation is due to changes in position of L2, L3 and L4: L2 moves both proximally and dorsally, while L3 and L4 move towards the centre of the enthesis. Surface semi-landmarks change position too, causing modification of the shape of the surface bony projection. With regard to PC4, the major modification of the entheseal shape is caused by relocation of L4 which moves distally.

In **Figure 45** and **Figure 46**, same kind of distribution has shown, with the entire sample subdivided into two groups: most of the specimens from SP have positive values for PC1 and the remaining part of this collection – along with the rest of the sample – is on the other side of the same PC. The main variation between these two plots is due to the different distribution of the specimens according to PC2 and PC3. With regard to PC2, the major distribution is for positive values of this component, while, with regard to PC3, specimens are distributed for negative values of the PC (**Figure 45** and **Figure 46**). On the contrary, no subdivision has evident when analysing PC3 and PC4, with the entire sample homogeneously distributed on the plot: the peculiarity is UoT which is in the negative part of PC4 and the majority of EM is on the negative side of PC3. Also, only specimens of SP are in the 1st quarter of the plane, along with one specimen from EM and two specimens from MH (**Figure 47**).

4.3.1.2 DI2 enthesis

Figure 48 - On the left, the MC3 bone with delimited entheses.
On the right, the landmarks (red spots) and semi-landmarks (blue spots) on the 3D model of the surface of DI2.
For the landmarks' definitions, see Annexes (cf. A2 – 3).

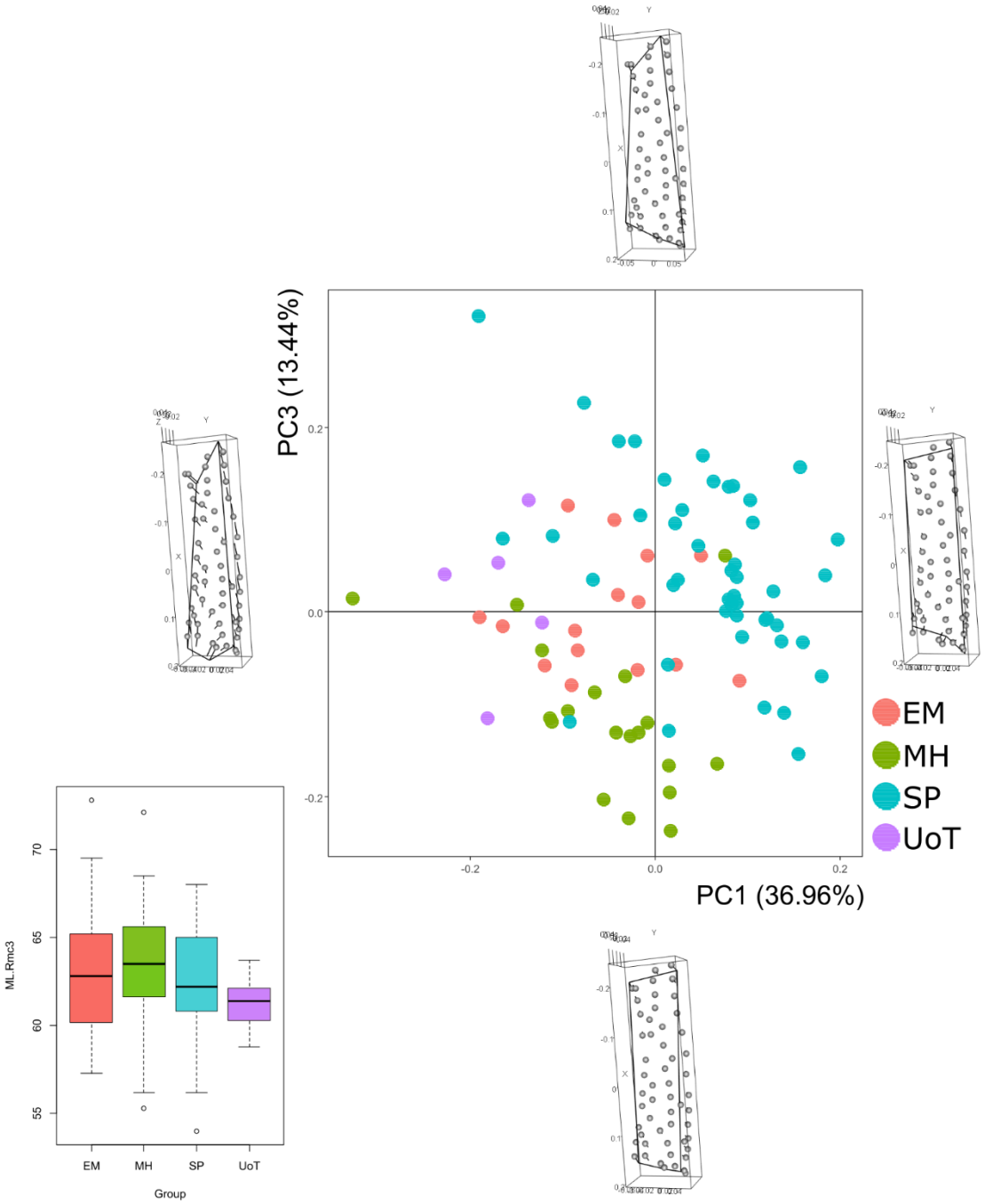

Figure 49 - Principal Component Analysis on the entire set of landmarks and shape configuration at the extremes of PC1 and PC3 for right DI2.

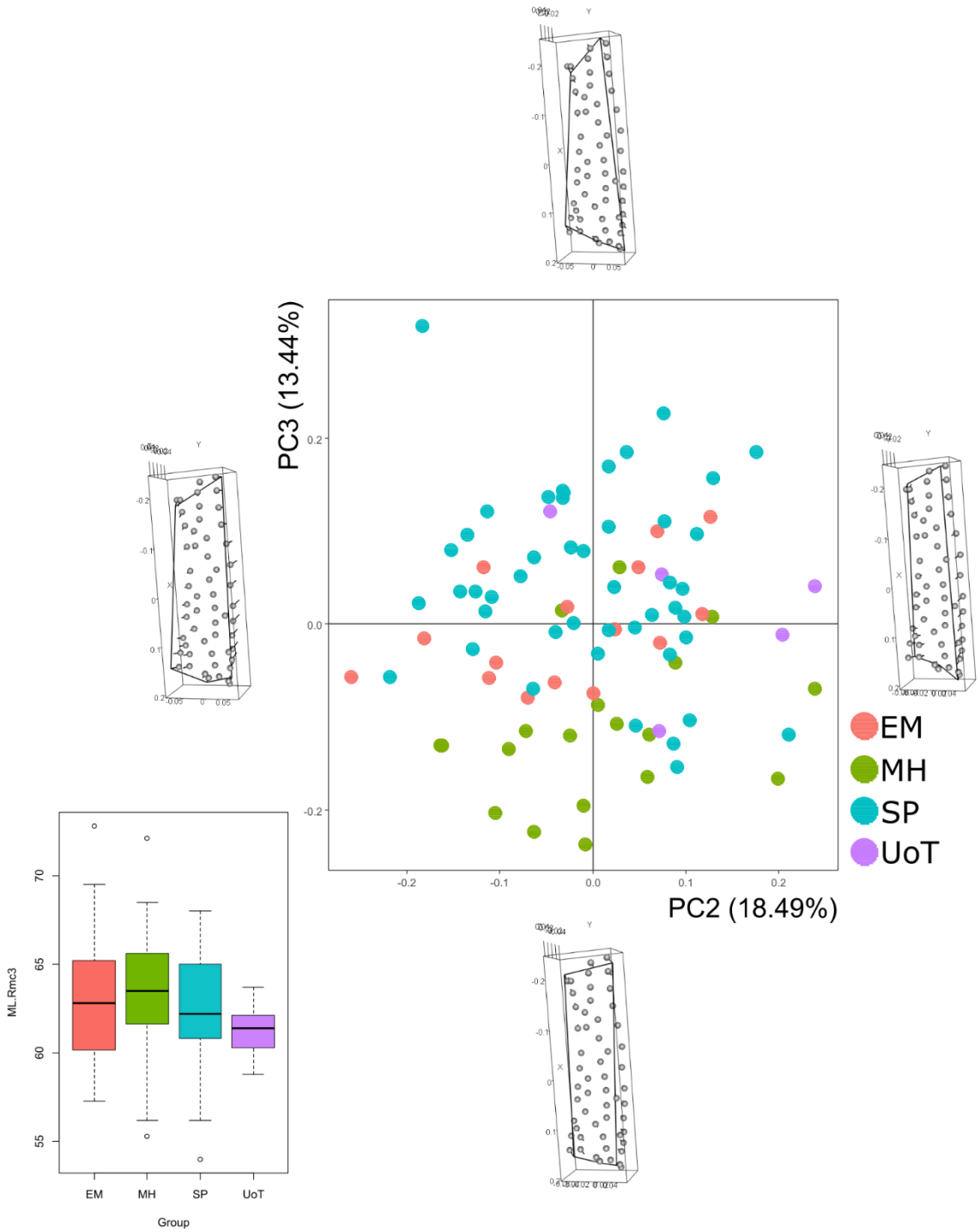

Figure 50 - Principal Component Analysis on the entire set of landmarks and shape configuration at the extremes of PC2 and PC3 for right DI2.

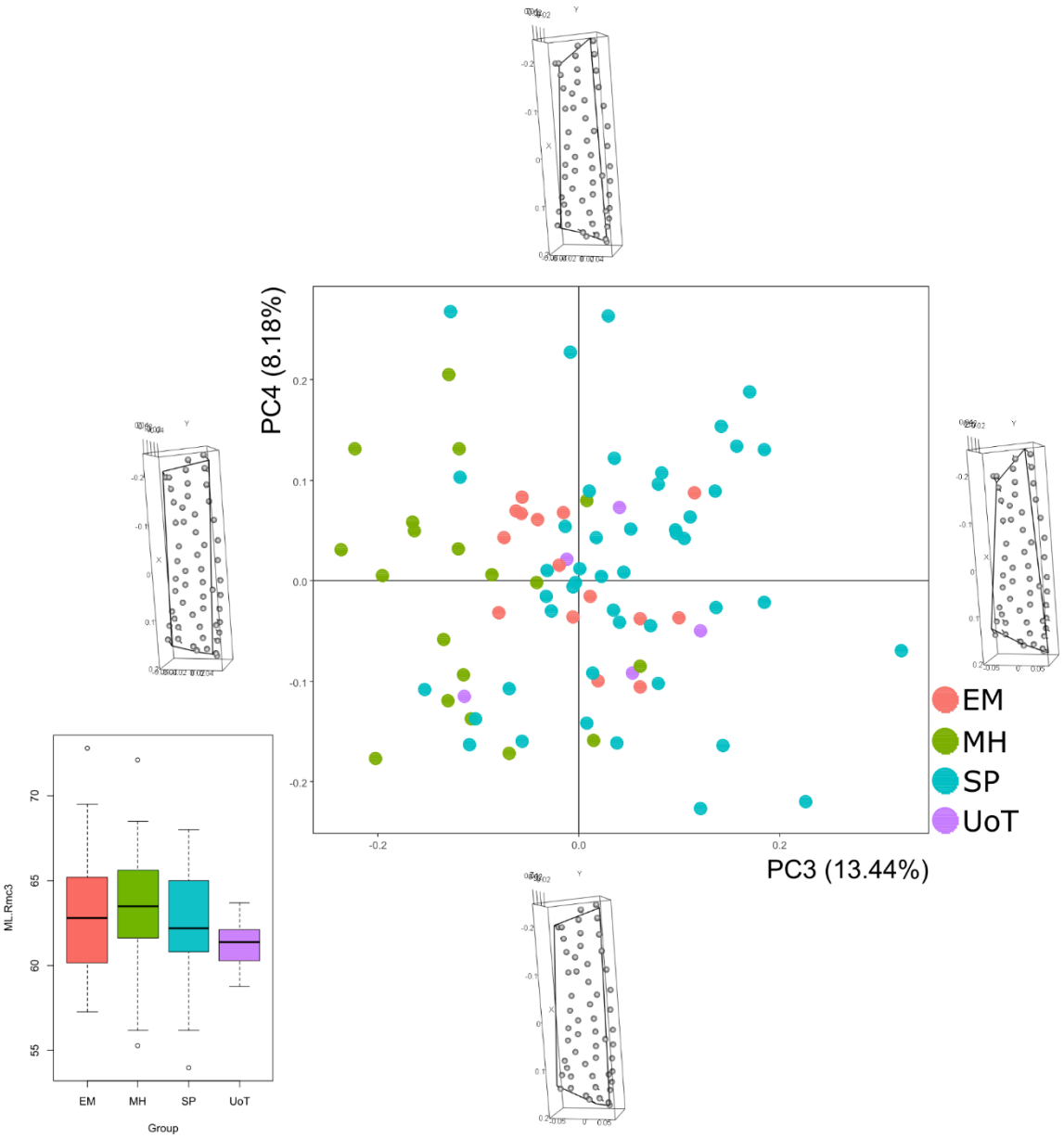

Figure 51 - Principal Component Analysis on the entire set of landmarks and shape configuration at the extremes of PC3 and PC4 for right DI2.

For the analyses of DI2 of right MC3 (**Figure 48**), a total of 85 specimens were available. The first four PCs were selected for the analyses, representing the 77% of the total variance.

With regard to shape variation along PC1, fixed pseudo-landmarks modify their position along the axis: L1 moves towards the centre of the enthesis, in a proximal direction, also L2 moves proximally, L3 relocates its position in a distal direction, towards the centre of the enthesis too, L4 moves distally, and L5 moves both distally and in a palmar direction. These modifications of position of landmarks cause variation in the entheseal shape – in correspondence of L3 and L5 – and determine a different morphology in correspondence of proximal and distal extremities, respectively. With regard to PC2, the most evident variation occurs on all fixed pseudo-landmarks except for L1: L2 moves both proximally and medially, L3 moves distally, towards the centre of the enthesis, L4 moves towards L2, in a dorsal direction, while L5 moves both distally and dorsally, along the outline connecting L5 and L1. About PC3, the most important variation is in correspondence of the distal portion of the enthesis, due to the relocation of L5 – moving to a distal direction. Also, L2 moves dorsally, determining an increase in size of the proximal portion. The same consideration can be made for PC4: in this case, also L3 relocates distally.

In **Figure 49**, the entire sample is homogenously distributed on the graph, with each group partially distinct from the others. Specimens from SP are distributed for positive values of PC1 while the remaining part of the total sample has a negative distribution for the same PC. Also, MH group has negative values for PC3 than EM and UoT ones.
Even in **Figure 50**, MH is distinct from the others for negative values of PC3 – except for three specimens with positive values – and most of SP has a positive distribution for the same PC. Also, when considering PC3 and PC4 (**Figure 51**), PC3 is the component which determine variation and the separation between MH and the remaining part of the sample, resulting homogenously distributed.

4.3.1.3 DI3+ADP enthesis

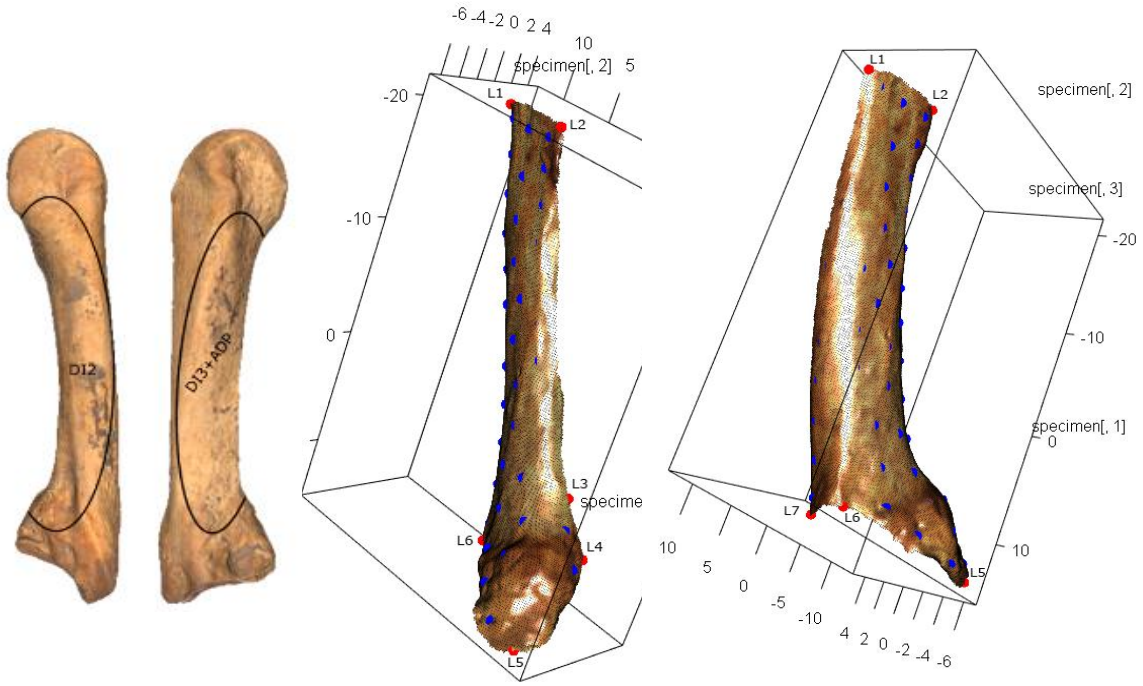

Figure 52 - On the left, the MC3 bone with delimited entheses.
On the right, the landmarks (red spots) and semi-landmarks (blue spots) on the 3D model of the surface of DI3+ADP. For the landmarks' definitions, see Annexes (cf. A2 – 3).

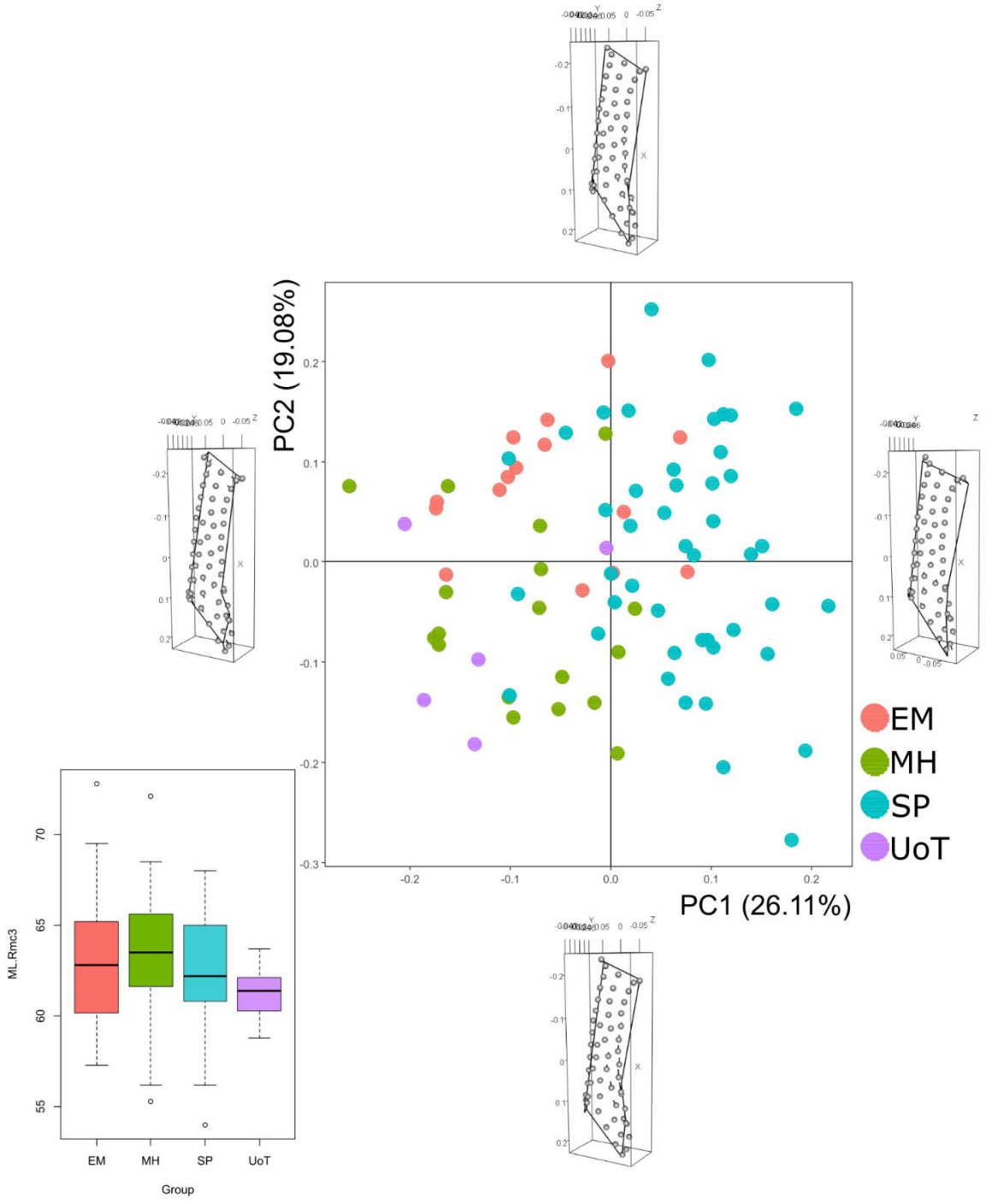

Figure 53 - Principal Component Analysis on the entire set of landmarks and shape configuration at the extremes of PC1 and PC2 for right DI3+ADP.

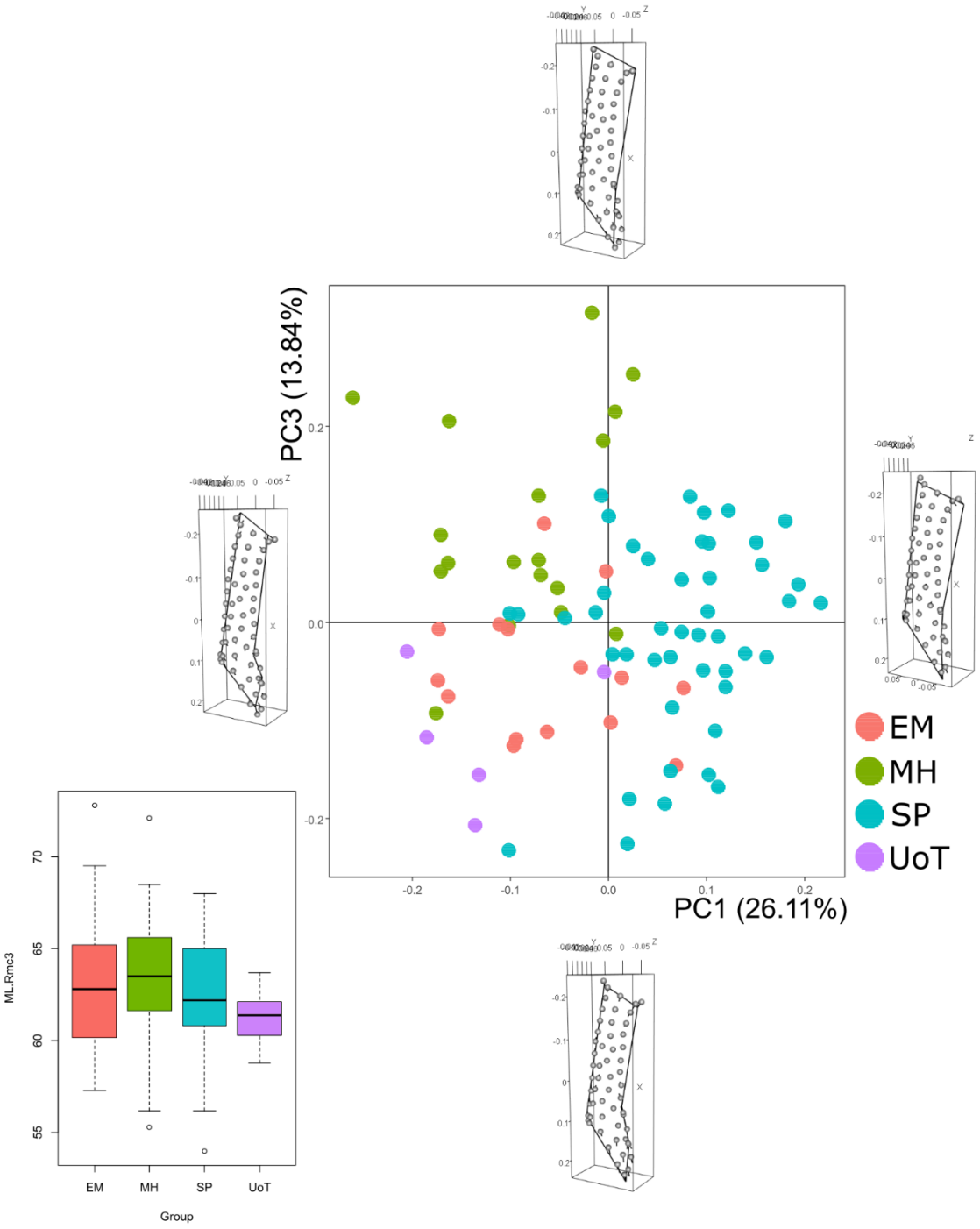

Figure 54 - Principal Component Analysis on the entire set of landmarks and shape configuration at the extremes of PC1 and PC3 for right DI3+ADP.

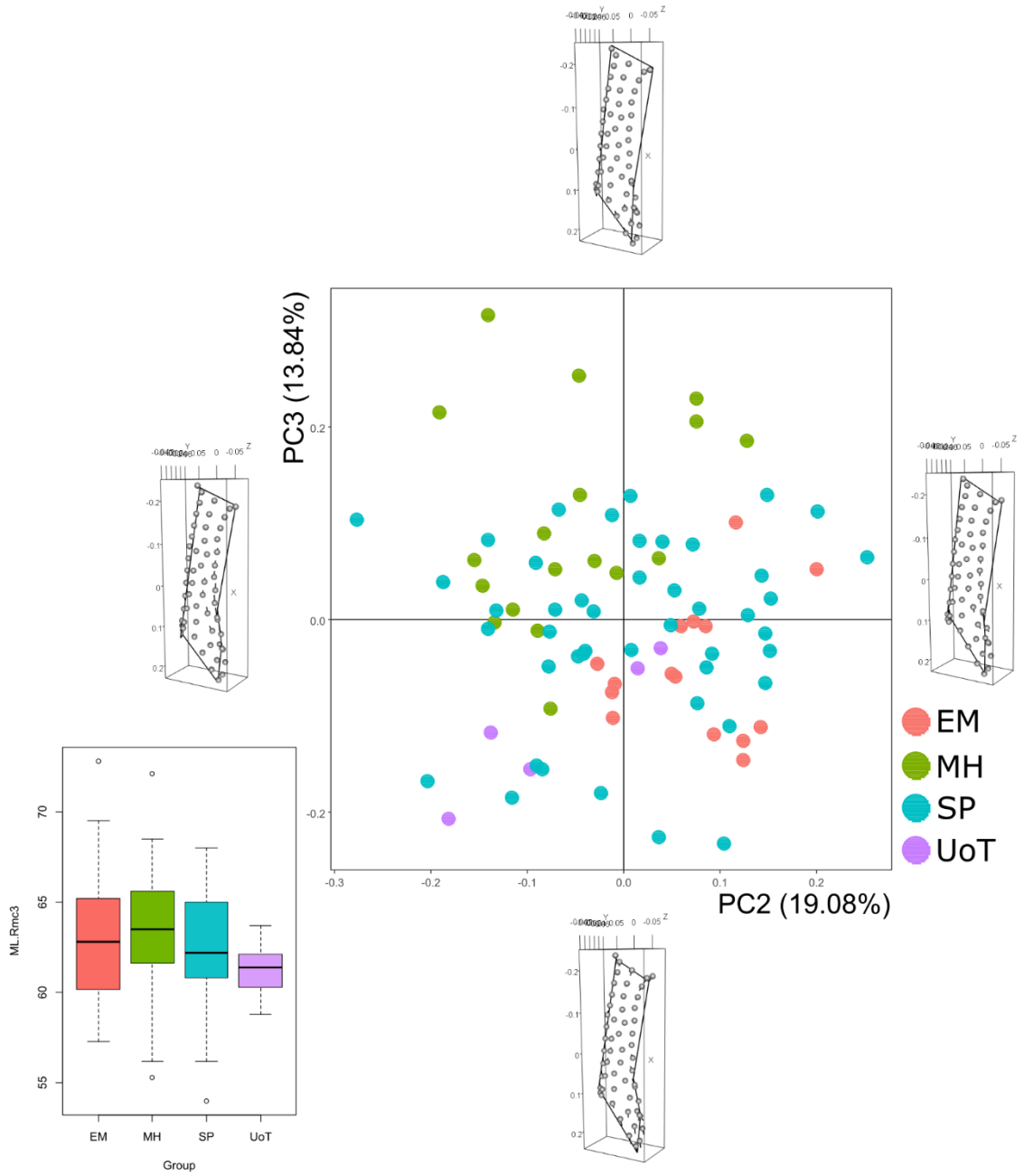

Figure 55 - Principal Component Analysis on the entire set of landmarks and shape configuration at the extremes of PC2 and PC3 for right DI3+ADP.

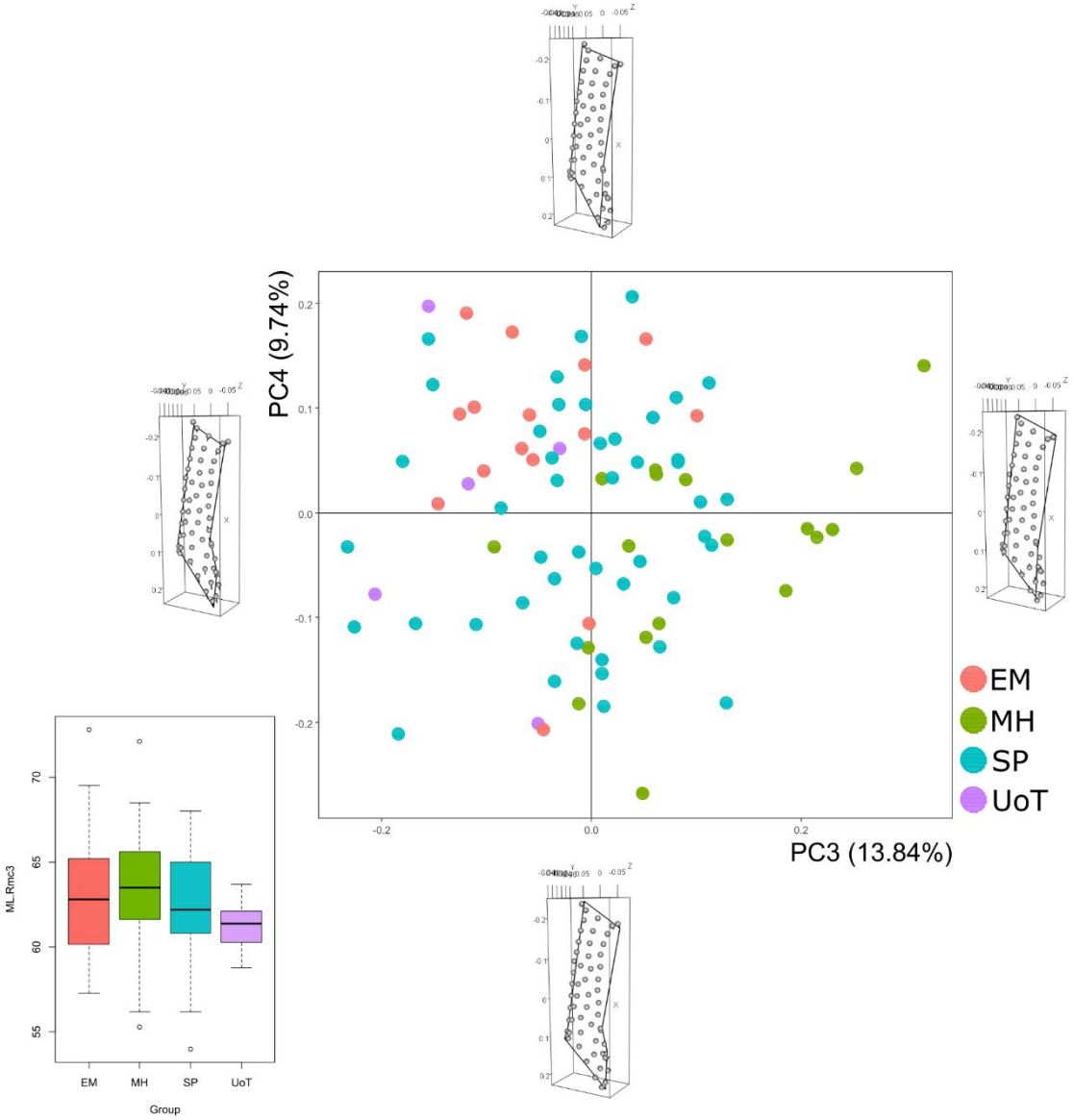

Figure 56 - Principal Component Analysis on the entire set of landmarks and shape configuration at the extremes of PC3 and PC4 for right DI3+ADP.

For the analyses of DI3+ADP of right MC3 (**Figure 52**), a total of 83 specimens were available. The first four PCs were selected for the analyses, representing almost the 70% of the total variance.

Regarding shape differences on PC1, the most important variation is due to fixed pseudo-landmarks L2 (moving in a palmar direction), L4 (moving laterally), L5 and L7 (both moving proximally). When analysing variation on PC2, shape differences can be observed in correspondence of fixed pseudo-landmarks L3, moving towards the proximal epiphysis, L6 and L7, which both move distally. Also, a minimum variation is visible for L5, distally too. About shape variation on PC3, the major variation is caused by relocation of fixed pseudo-landmarks L1 and L5 (moving both medially and distally), L2 (moving both laterally and distally, L3 (towards L4, in a proximal direction), L4 (moving laterally), L7 (also moving in a proximal direction). Also surface semi-landmarks modify their position, reducing the bony projection in correspondence of the base – from PC3 min to max. Regarding variation on PC4, a reduction in shape from minimum to maximum visualization can be seen, due to a minimum relocation of landmarks.

About descriptions of shape spaces shown in **Figures 53 – 56**, three groups can be distinguished: SP with some specimens from EM and MH (on the right), MH (in the 3rd quarter of the plot), EM in the 2nd quarter of the plane. Individuals from sample from UoT have negative values for PC1 and are also mixed with other groups. Even in **Figure 54**, groups are evident but the distribution is different than PC1 and PC2: groups from EM and MH are inverted in position respect to PCA in **Figure 53**, with EM located in the 3rd quarter while MH sample is in the 2nd one. No changes are recorded for UoT, which lies with both negative values for PC1 and PC3. Similar distribution is shown when considering PC2 and PC3 (**Figure 55**), with a clear distinction between specimens from MH and EM, characterized by positive and negative values for PC3, respectively. When analysing PC3 and PC4, only distinction between groups from EM and MH is evident: the first one has distributed for positive values of PC4 and negatives for PC3, while the dispersal of the second group is wider than EM and the most part is distributed for negative values of PC4 (**Figure 56**).

4.3.2 Left MC3 – Descriptive statistics, normality tests and correlation analyses

	raw size - ECRB	ERS - ECRB	raw size - DI2	ERS - DI2	raw size - DI3+ADP	ERS - DI3+ADP	APWM/ML*	MLWM/ML*	ML*
N	73	72	76	75	74	73	74	74	75
Min	25,44	0,01	205,61	0,10	291,91	0,16	0,11	0,09	50,50
Max	111,20	0,04	538,00	0,20	670,15	0,26	0,18	0,16	73,40
Mean	64,01	0,03	378,50	0,17	511,37	0,22	0,14	0,13	62,35
Stand. dev	19,22	0,01	74,13	0,02	84,39	0,02	0,01	0,01	3,86

Table 22 - Summary statistics for both 3D size and linear measurements of left MC3. Raw size is calculated in mm^2, ML in calculated in mm. **APWM/ML**: Antero-Posterior Robusticity Index. **MLWM/ML**: Medio-Lateral Robusticity Index. **ML**: Maximum Length.

	raw size - ECRB	ERS - ECRB	raw size - DI2	ERS - DI2	raw size - DI3+ADP	ERS - DI3+ADP	APWM/ML*	MLWM/ML*	ML*
N	73	72	76	75	74	73	74	74	75
Shapiro-Wilk W	0,99	0,97	0,99	0,93	0,97	0,97	0,99	0,99	0,99
p(normal)	0,57	0,10	0,58	0,0004523	0,14	0,07	0,56	0,73	0,84

Table 23 - Shapiro-Wilk test for each variable of left MC3.

	raw size - ECRB	ERS - ECRB	raw size - DI2	ERS - DI2	raw size - DI3+ADP	ERS - DI3+ADP
APWM/ML*				0,13		0,22
MLWM/ML*				0,15		0,19
ML*	-0,04	-0,12		0,02		0,13

Table 24 - Correlation tests between 3D bon size and linear dimensions for left MC3.

In **Tables 22 – 24**, descriptive statistics, correlation tests and normal distribution tests for all the variables used in this work are summarized.

The set of values for DI3+ADP are the highest among the entheses of MC3, according to the dimension of the insertion sites for these muscles. With regard to normality tests for each variable of left MC3, the Shapiro-Wilk's tests verified a normal distribution with a *p-value* > 0.05 for all variables, except for ERS of entheses DI2.

Correlation tests were performed: positive relations have been recorded between both raw size of each enthesis and ERS of ECRB and DI3+ADP entheses and total surface size, except for ERS of DI2, characterised by a negative relation. About entheseal size (raw and ERS) and bone dimensions, ERSs of DI2 and DI3+ADP entheses correlate with all linear measurements – but ERS of DI2 highly correlates with maximum length – except for ECRB enthesis (both raw size and ERS) which negatively correlates with bone length only.

4.3.2.1 ECRB enthesis

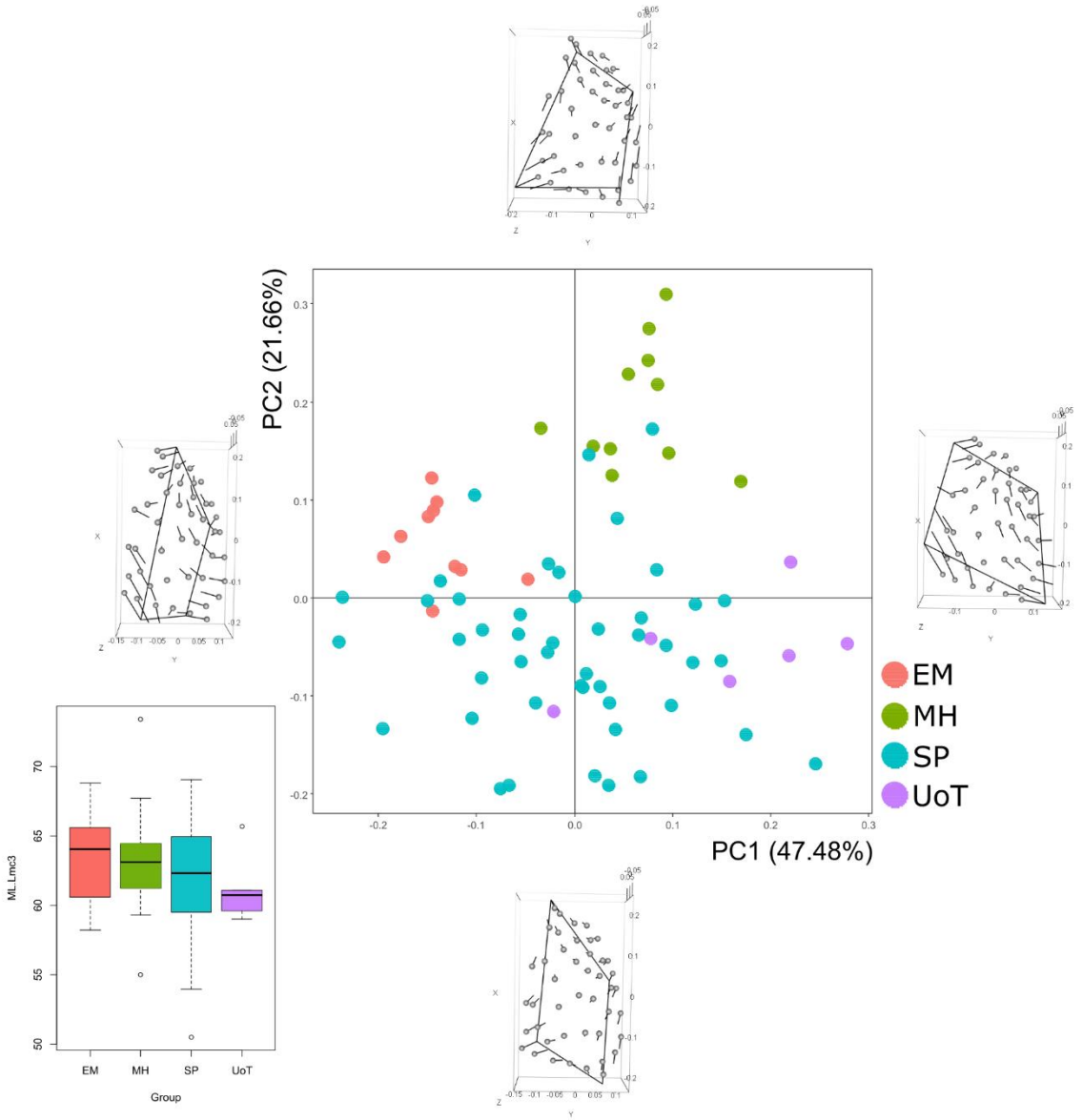

Figure 57 - Principal Component Analysis on the entire set of landmarks and shape configuration at the extremes of PC1 and PC2 for left ECRB.

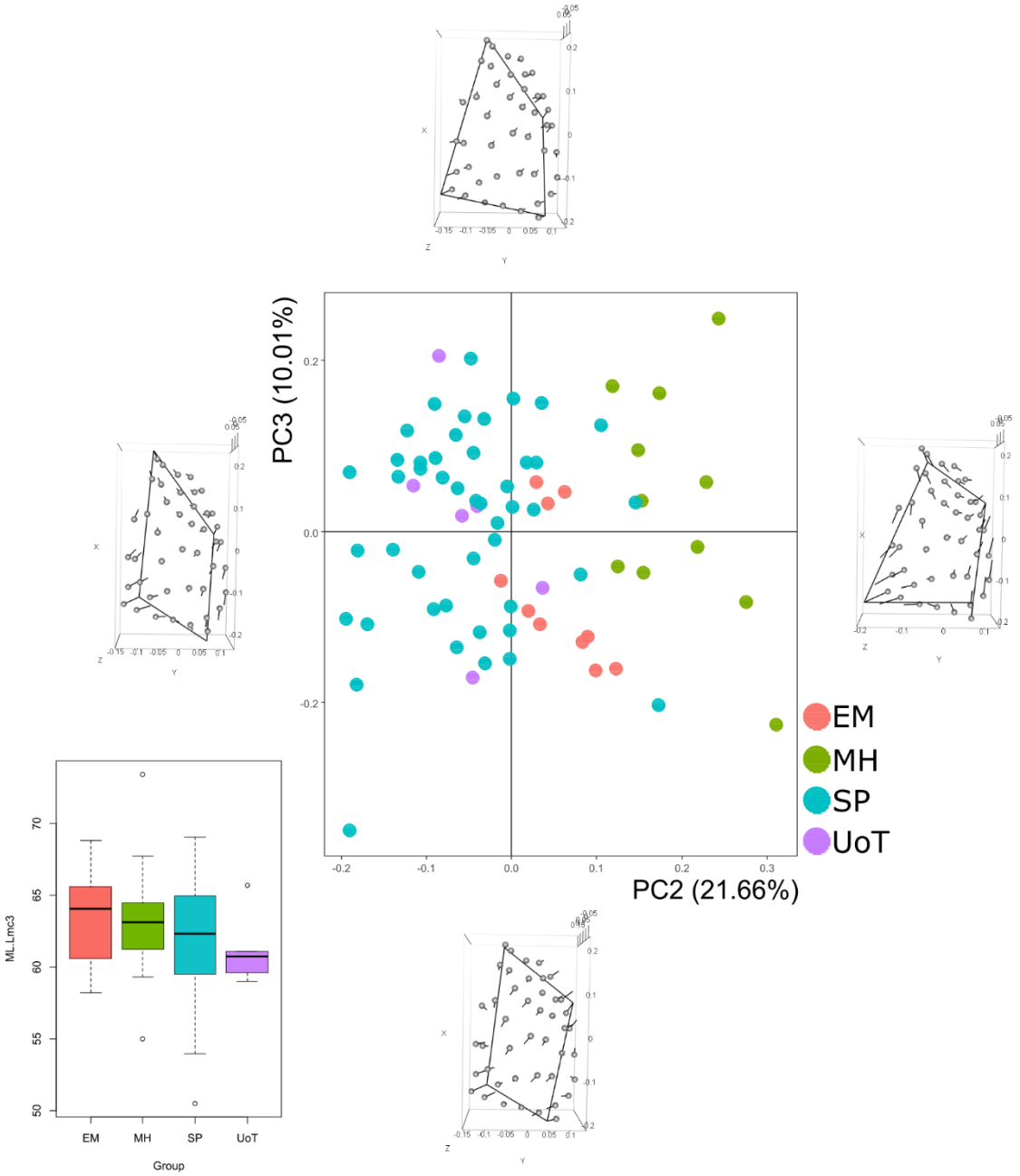

Figure 58 - Principal Component Analysis on the entire set of landmarks and shape configuration at the extremes of PC2 and PC3 for left ECRB.

For the analyses of ECRB of left MC3, a total of 73 specimens were available. Here, the first four PCs were analysed, representing more than 85% of the total variance.

Regarding PC1, great variation in shape and size is evident, caused by repositioning of the four fixed pseudo-landmarks: L1 moves towards the dorsal side of the bone, L2 moves distally, L3 moves in a palmar direction and L4 also moves distally. In this scenario, comparisons between the two structures of PC1 show different morphologies, characterized by increasing in size in an antero-posterior way. With regard to PC2, both fixed pseudo-landmarks and surface semi-landmarks change position, determining also changes in shape and size: L1 moves proximally, L2 moves towards the dorsal surface of the bone, L3 moves in a distal direction and L4 moves both distally and in a palmar direction. About relocation of surface landmarks, reduction in length and increasing in an antero-posterior direction are recorded. No particular distinct groups can be seen in PCA regarding components PC3 and PC4 – for this reason, PCA plot is not shown – even if shape variation for both PCs is visible. About PC3, variation is clear on both fixed and surface landmarks: L2 and L4 move posteriorly in a dorsal direction, L3 moves anteriorly towards the palmar surface, while the surface semi-landmarks relocate towards the centre of the enthesis. Regarding PC4, the major variation is due to relocation of L4, which moves along the outline between L1 and L4, towards the distal extremity of the enthesis.

Distinct groups are clear and can be described as follows. In **Figure 57**, MH results distinct from the remaining group – with both positive values for both PCs – and EM has a distribution for negative values of PC1 and positive ones for PC2, close to SP. With regard to specimens from UoT, they fall in the SP group, distinct from the archaeological samples. Similar description can be done for plots in figures shown in Annexes (cf. A4 – 6, A4 – 7), according to separation between the archaeological collections: they lie into the big distribution of the reference group of SP but result distinct for different values of PC1. For these reasons, these plots are not shown here but can be found in the Annexes chapter. Regarding plot in **Figure 58**, even in this case three distinct groups are evident, with specimens from MH and EM characterised by positive values of PC2 – but MH with more positive values than the other one – and both SP and UoT with negative values for PC2, completely distinct from MH.

4.3.2.2 DI2 enthesis

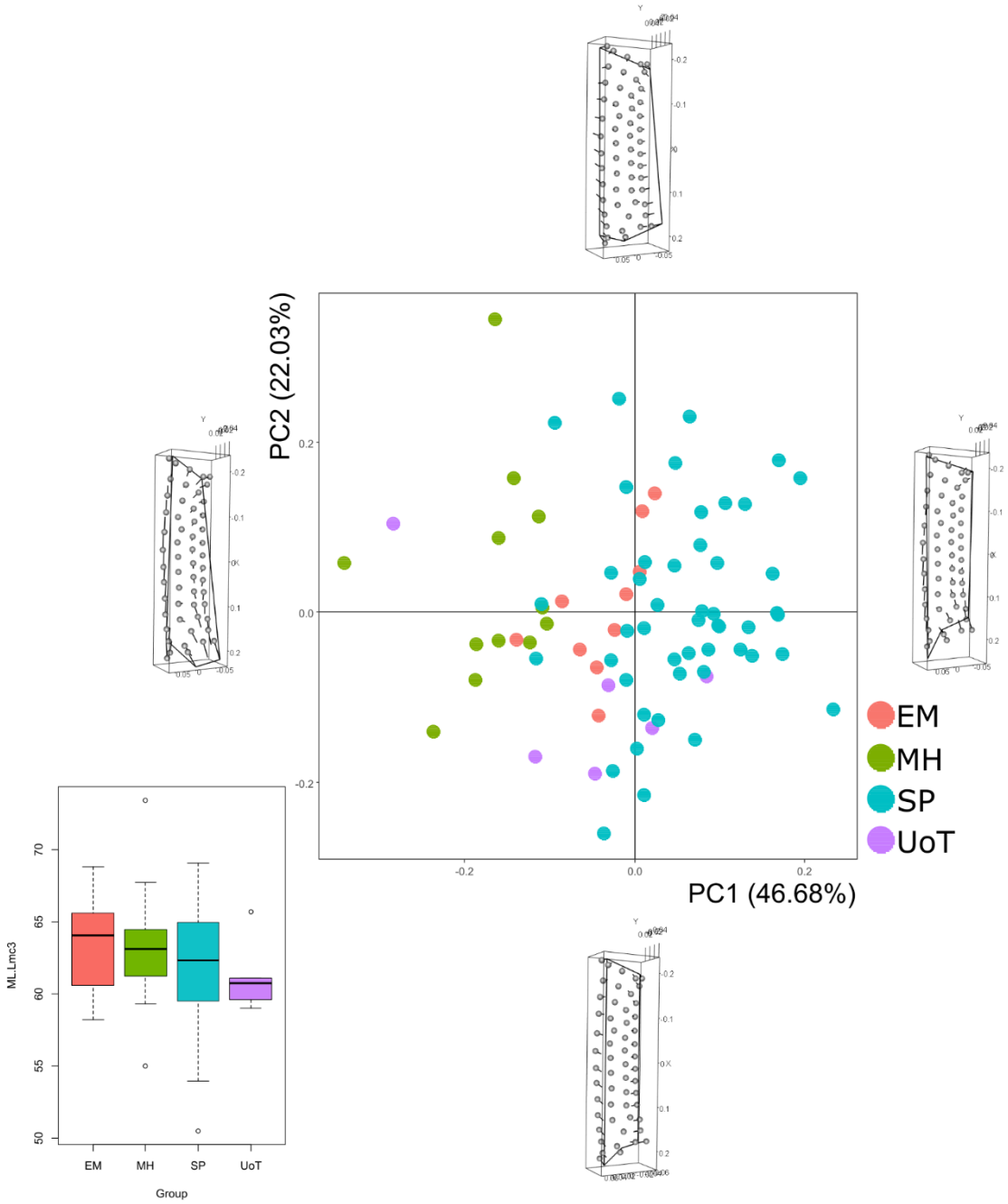

Figure 59 - Principal Component Analysis on the entire set of landmarks and shape configuration at the extremes of PC1 and PC2 for left DI2.

For the analyses of DI2 of left MC3, a total of 76 specimens were available. Here, the first four PCs were analysed, representing almost the 85% of the total variance.

Regarding shape variation on PC1, changes in correspondence of the proximal entheseal extremity are due to relocation of fixed landmarks: L1 moves in a dorsal direction, L2 moves towards the proximal epiphysis, L3 and L4 both move distally, L5 moves in a palmar direction. About surface ones, semi-landmarks located in correspondence of the dorsal surface of the bone (on the entheseal outline between L1 and L2) all move proximally, while landmarks positioning on proximal epiphysis move in a distal direction. With regard to PC2, an increasing of size is evident due to relocation of fixed landmarks: L1 and L5 move in opposite direction, dorsal and palmar respectively, L2 move dorsally and distally, L3 relocates dorsally and proximally and L4 moves in both palmar and medial direction. As PC1, also when considering PC3, shape variation causes increasing in size – in this case in correspondence of the distal entheseal end and a shift of the proximal extremity to a distal position. About fixed pseudo-landmarks, L1 and L5 relocate, moving distally and proximally respectively, with reposition of L5 determining most of the outline variation. Also, L2 moves opposite than L3 and L4, these latter going distally. About PC4, only L3 and L4 can be taken into consideration for analysis of shape variation – they move in opposite direction, distally and proximally respectively.

The resulting PCAs show similar results for PC1 to PC4 (**Figure 59**; Annexes, cf. A4 – 8, A4 – 9), where separation between SP and MH is evident: the first is on the right side of the graph, while the latter has negative values for PC1. The specimens from UoT are mixed with SP ones, with negative values of PC2 – except for one specimen located among MH. About EM, it lies between SP and MH.

4.3.2.3 DI3+ADP enthesis

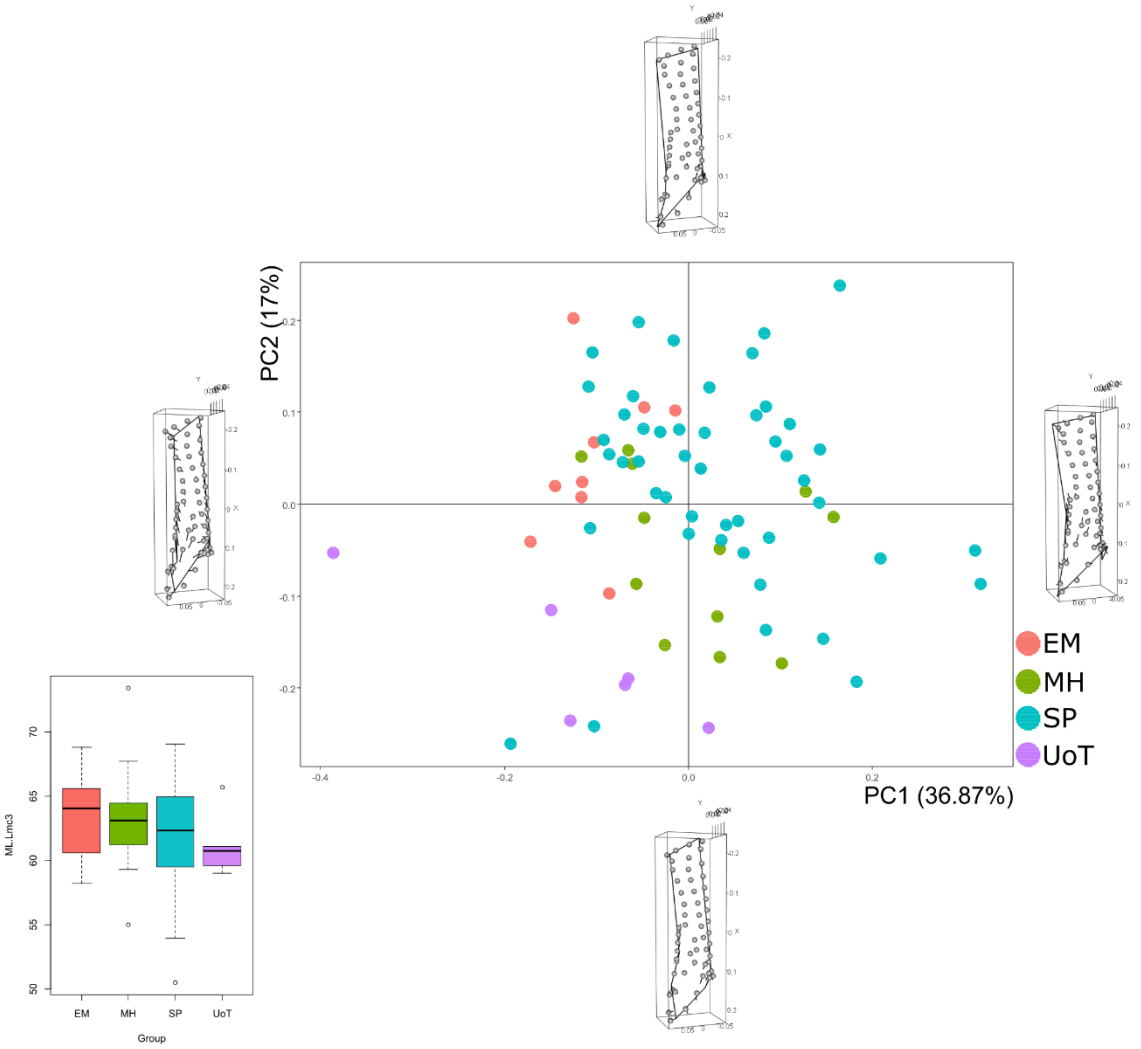

Figure 60 - Principal Component Analysis on the entire set of landmarks and shape configuration at the extremes of PC1 and PC2 for left DI3+ADP.

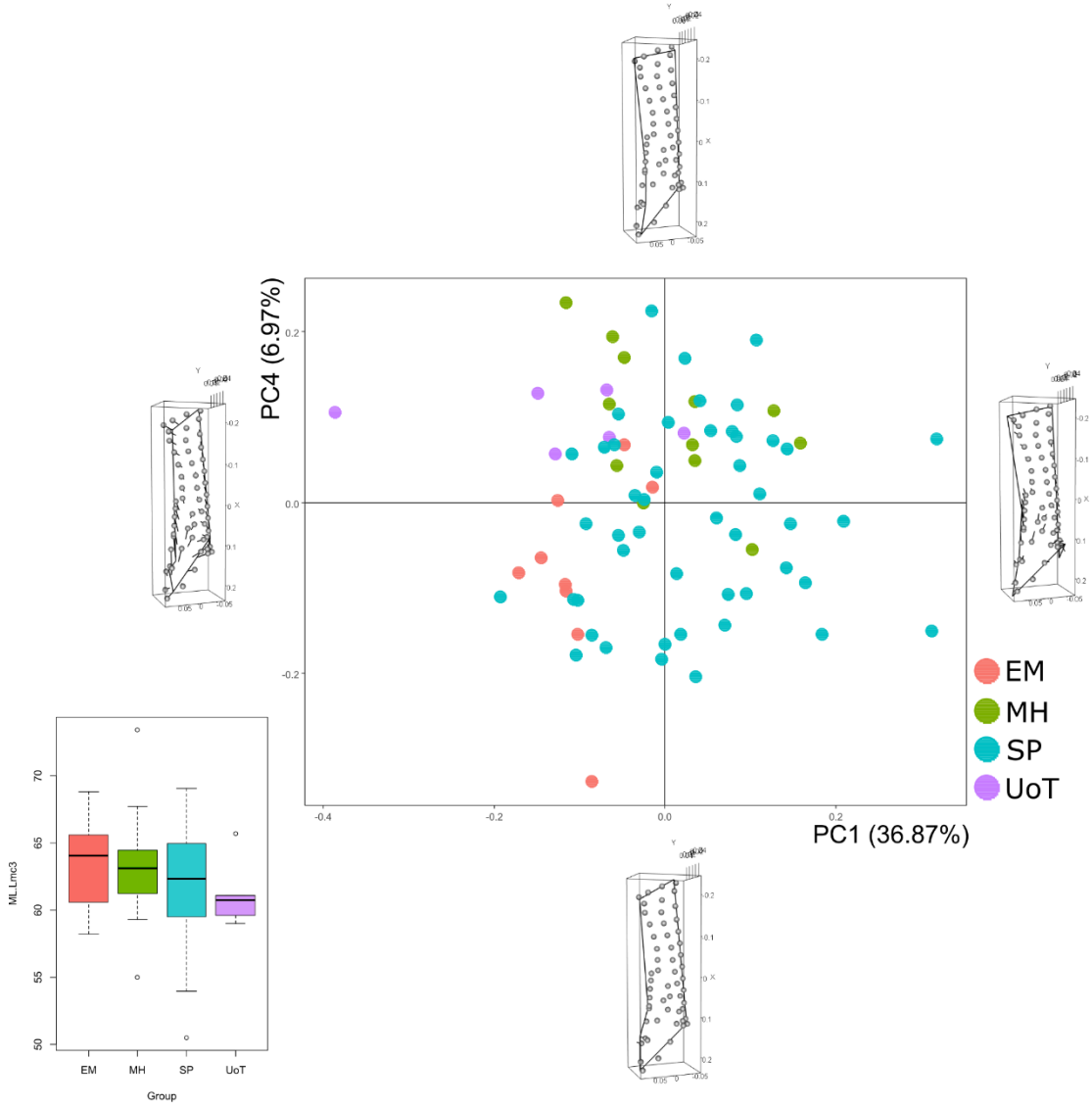

Figure 61 - Principal Component Analysis on the entire set of landmarks and shape configuration at the extremes of PC1 and PC4 for left DI3+ADP.

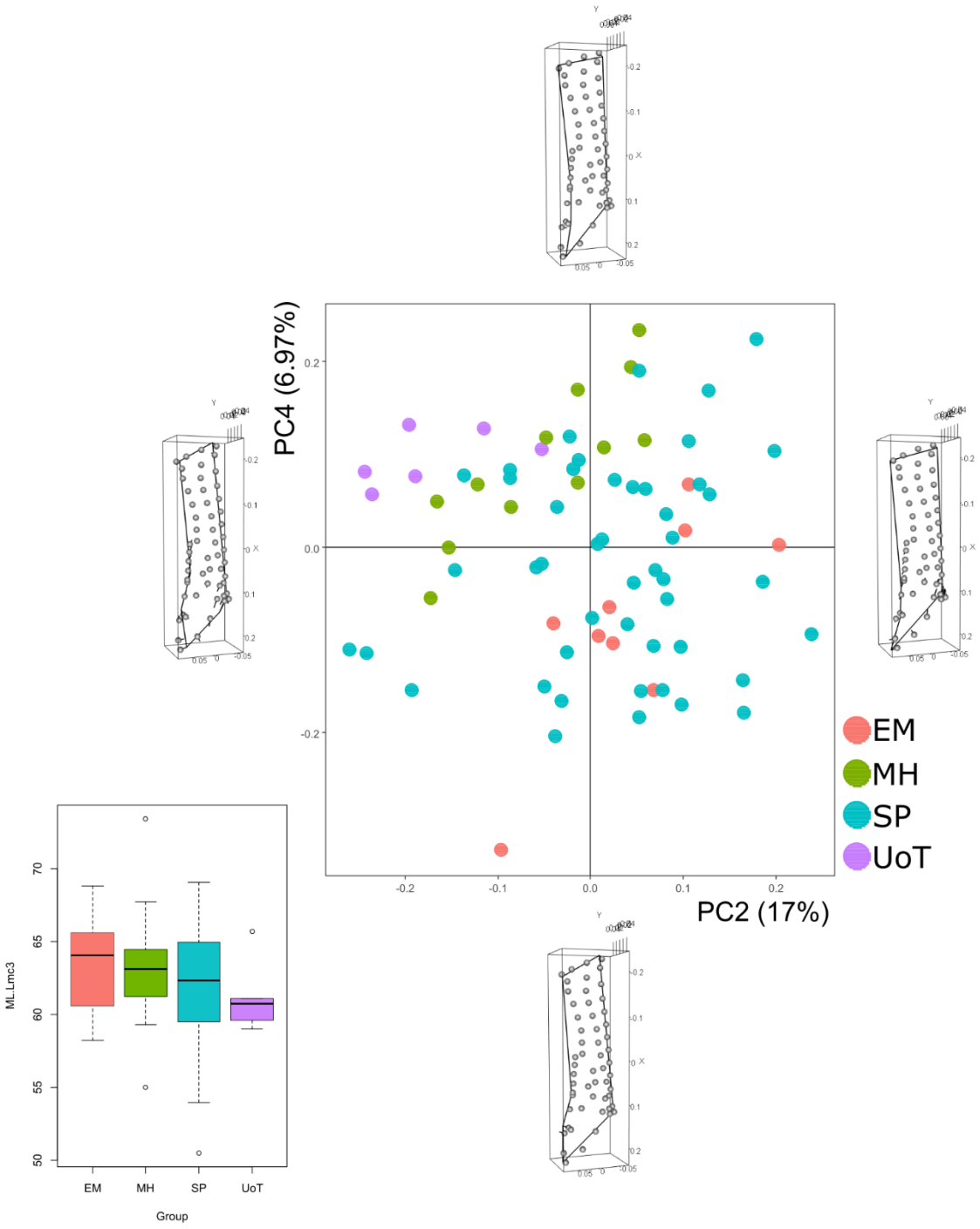

Figure 62 - Principal Component Analysis on the entire set of landmarks and shape configuration at the extremes of PC2 and PC4 for left DI3+ADP.

For the analyses of DI3+ADP of left MC3, a total of 74 specimens were available. Here, the first four PCs were analysed, representing almost the 75% of the total variance.

About shape differences on PC1, the major variation is due to fixed pseudo-landmarks and to the surface semi-landmarks on proximal epiphysis: L2 moves both palmar and distally, L3 moves distally, L4 goes in a medial direction, L5 goes both proximally and partially medially, L6 moves dorsally, L7 goes proximally, and finally, surface semi-landmarks of the proximal part of the enthesis move in a distal direction. As a result, for positive values of PC1, specimens have a more elongated shape in the portion of the palmar section of the bone and an elongated process in correspondence of the entheseal outline between landmarks L5 to L7. Same considerations can be made about shape variation on PC2: in this case, L3 goes towards L4, which moves proximally, L5 moves in a palmar direction and L6 goes towards a distal one. The relocation of L6 causes changes in the shape of the proximal portion of the enthesis, resulting more stretched out. Analysing shape differences on PC3, repositioning of semi-landmarks causes surface variation between the two forms of PC3 (min to max). Finally, regarding PC4, only L1 and L4 move, going both laterally.

In **Figure 60**, SP and MH are equally distributed on the graph, even if only one individual from MH is in the 1st sector of the plane. EM group is in the left side of the plot, with positive values of PC2 and negative ones for PC1 – except for two specimens with negative values for both PC1 and PC2. The six specimens from UoT have all negative values for PC1 and PC2 – exception for one individual with positive PC1. An opposite situation is shown in **Figure 61**, related to variation on PC4: the major difference between these two graphs is about the different position of samples from UoT and MH – in this case, they are distributed for positive values of PC4, but different values for PC1, negative and positive, respectively.
Another distribution is shown in **Figure 62**, where PC2 and PC4 are considered. In this case, UoT is distributed for negative values of PC1 and positive ones for PC2 and is distinct from the other groups. Also, MH and EM groups continue to be separated for PC2 – specimens from MH are distributed for positive values of PC4, while specimens from EM are distributed with negative values of PC4. Separation between EM and MH is clear also when analysing PC3 and PC4, with a similar distribution of specimens as **Figure 61**; for this reason, this plot has not been included here but has been included in the Annexes (cf. A4 – 10).

4.4 Analyses of 4th metacarpal bones

4.4.1 Right MC4 - Descriptive statistics, normality tests and correlation analyses

	raw size - DI3+PI2	ERS - DI3+PI2	raw size - DI4	ERS - DI4	APWM/ML*	MLWM/ML*	ML*
N	76	70	77	71	69	69	69
Min	223,22	0,13	180,30	0,12	0,10	0,10	47,80
Max	565,82	0,27	378,26	0,23	0,17	0,16	61,70
Mean	366,56	0,21	274,64	0,16	0,14	0,12	53,87
Stand. dev	69,96	0,03	46,82	0,02	0,01	0,01	3,16

Table 25 - Summary statistics for both 3D size and linear dimensions for right MC4. Raw size is calculated in mm^2, ML is calculated in mm. **APWM/ML**: Antero-Posterior Robusticity Index. **MLWM/ML**: Medio-Lateral Robusticity Index. **ML**: Maximum Length.

	raw size - DI3+PI2	ERS - DI3+PI2	raw size - DI4	ERS - DI4	APWM/ML*	MLWM/ML*	ML*
N	76	70	77	71	69	69	69
Shapiro-Wilk W	0,98	0,97	0,99	0,92	0,94	0,89	0,98
p(normal)	0,30	0,07	0,52	0,0003903	0,003604	0,02654	0,49

Table 26 - Shapiro-Wilk test for each variable of right MC4.

	raw size - DI3+PI2	ERS - DI3+PI2	raw size - DI4	ERS - DI4
APWM/ML*		0,05		0,03
MLWM/ML*	0,17	-0,01	0,17	-0,04
ML*		0,00004		-0,02

Table 27 - Correlation tests between 3D bone sizes and linear dimensions for right MC4.

In **Tables 25 - 27**, descriptive statistics, correlation tests and normal distribution tests for all the variables used in this work are summarized. The set of values of the two entheses of MC4 are similar, according to their dimensions and nature of muscular origin sites on metacarpal shafts. With regard to normality tests for each variable of right MC4, the Shapiro-Wilk's test has verified a normal distribution with a *p-value* > 0.05 for all variables, except for ERS of enthesis DI4 and both antero-posterior and medio-lateral RIs.

Correlation tests were performed: positive relations have been recorded between raw size of each enthesis and total surface size, while negative relations have been recorded when analysing ERS indexes. About relation between entheseal size (raw and ERS) and bone dimensions, ERS of both entheses highly correlate with all linear dimensions (both positive and negative relations), while raw size of both entheses only correlate with medio-lateral RI.

4.4.1.1 DI3+PI2 enthesis

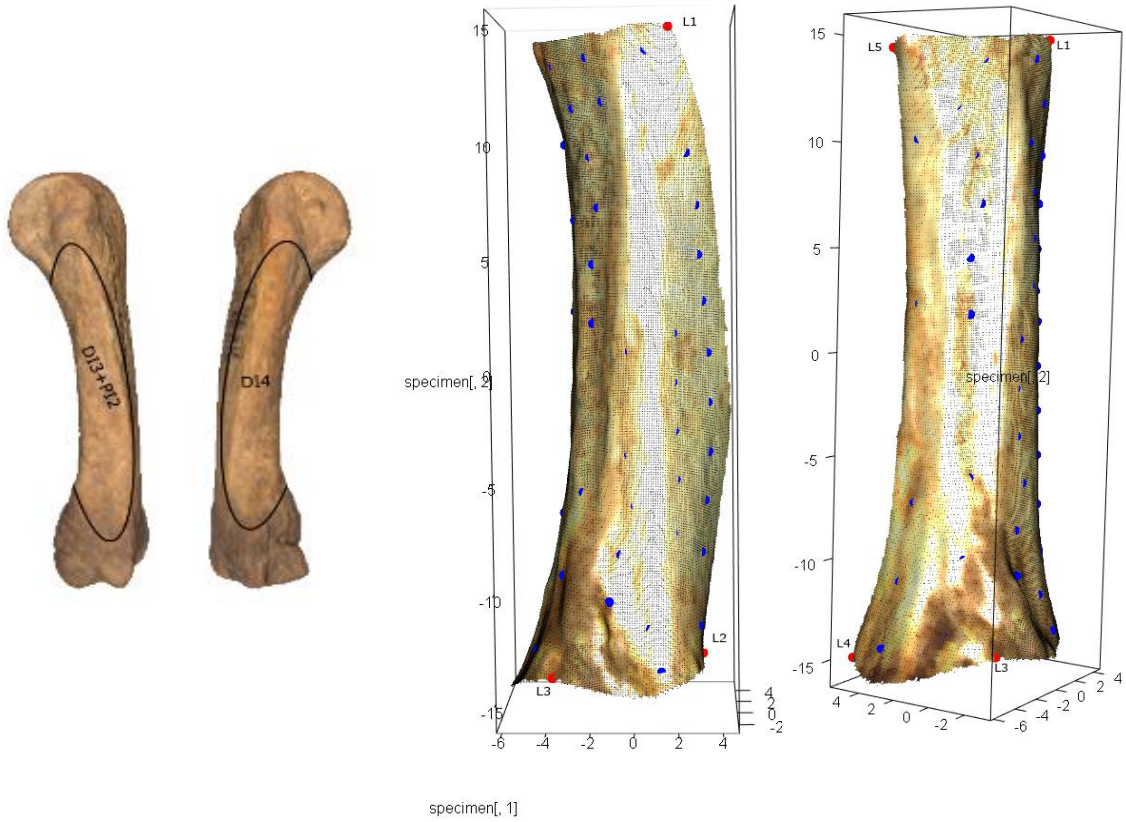

Figure 63 - On the left, the MC4 bone with delimited entheses.
On the right, the landmarks (red spots) and semi-landmarks (blue spots) on the 3D model of the surface of DI3+PI2.
For the landmarks' definitions, see Annexes (cf. A2 – 4).

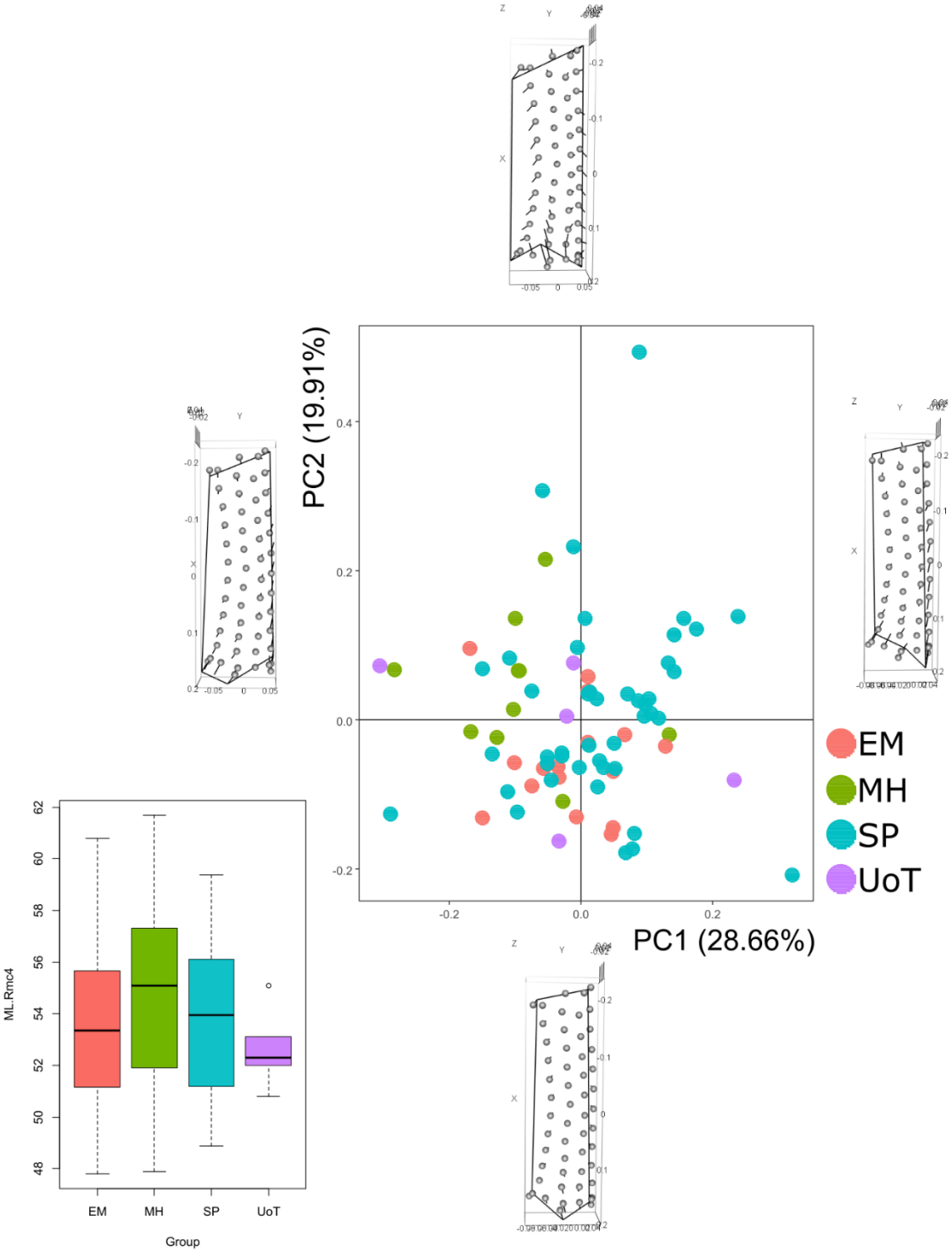

Figure 64 - Principal Component Analysis on the entire set of landmarks and shape configuration at the extremes of PC1 and PC2 for right DI3+PI2.

For the analyses of DI3+PI2 of right MC4 (**Figure 63**), a total of 75 specimens were available. Here, the first three PCs were analysed, representing the 65% of the total variance.

With regard to PC1, some of five fixed pseudo-landmarks change position: L2 move towards the proximal epiphysis, both L3 and L4 move distally and partially in a dorsal direction, and L5 move also distally. About surface semi-landmarks, some of them lying on the dorsal outline of the enthesis move proximally, while others lying in correspondence of the proximal epiphysis go towards the centre of the enthesis. Regarding PC2, the major shape variation is due to relocation of fixed landmarks L2, moving towards the dorsal surface of the bone, L3 which goes distally and both L4 and L5 moving proximally – with L4 moving also towards the palmar surface. About PC3, variation is evident for fixed landmarks L3, L4 and L5 – most of variation is due to L4, moving both distally and in a palmar direction; also, some surface landmarks lying in correspondence of the palmar entheseal outline move towards the palmar surface.

Even if shape variation is evident between the different morphologies of each PC, a general separation between samples from MH and EM is shown, distributed for positive and negative values of PC2, respectively, and negative values for PC1 (**Figure 64**). Similar distribution is visible when considering PC1 and PC3: for this reason, the resulting PCA plot is not shown here but is added in the Annexes (cf. A4 – 11).

4.4.1.2 DI4 enthesis

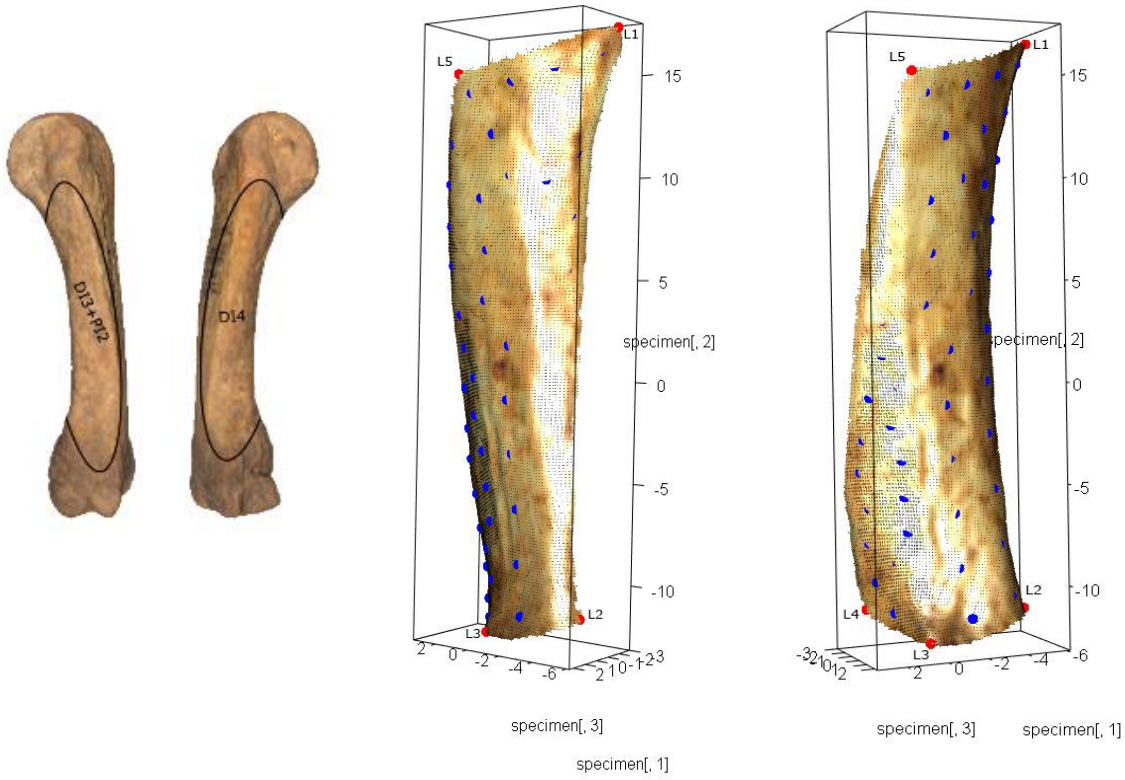

Figure 65 - On the left, the MC4 bone with delimited entheses.
On the right, the landmarks (red spots) and semi-landmarks (blue spots) on the 3D model of the surface of DI4.
For the landmarks' definitions, see Annexes (cf. A3 – 4).

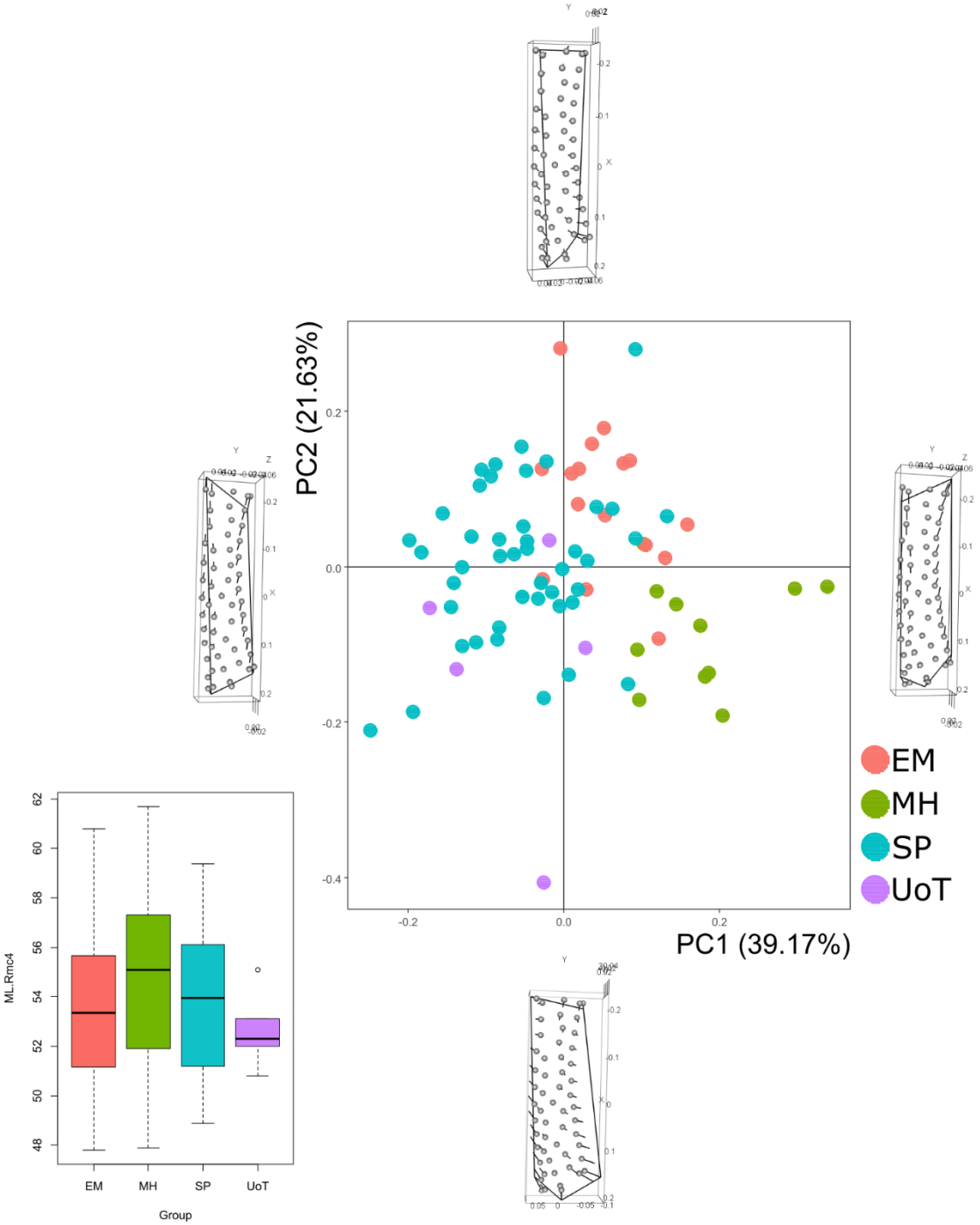

Figure 66 - Principal Component Analysis on the entire set of landmarks and shape configuration at the extremes of PC1 and PC2 for right DI4.

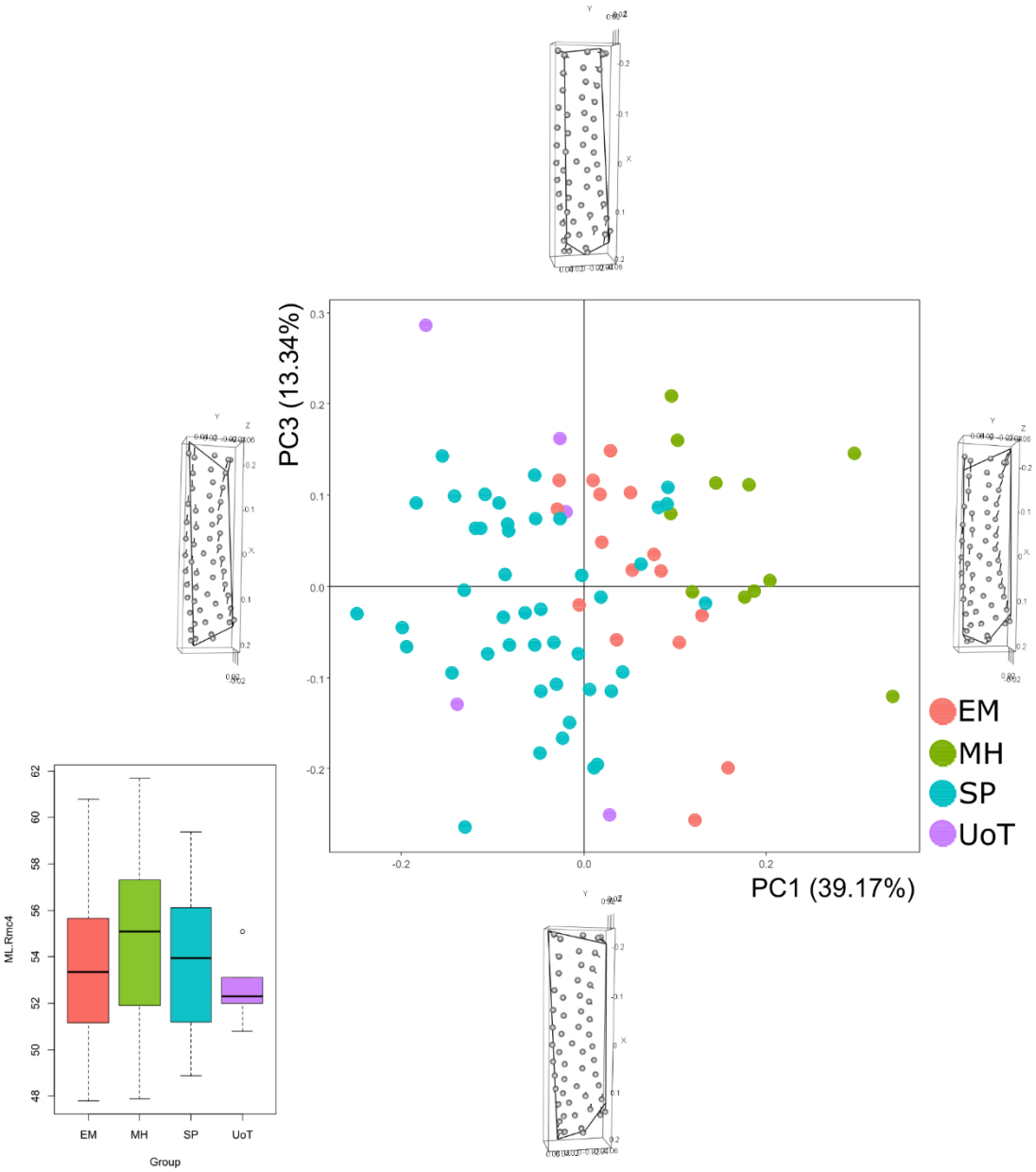

Figure 67 - Principal Component Analysis on the entire set of landmarks and shape configuration at the extremes of PC1 and PC3 for right DI4.

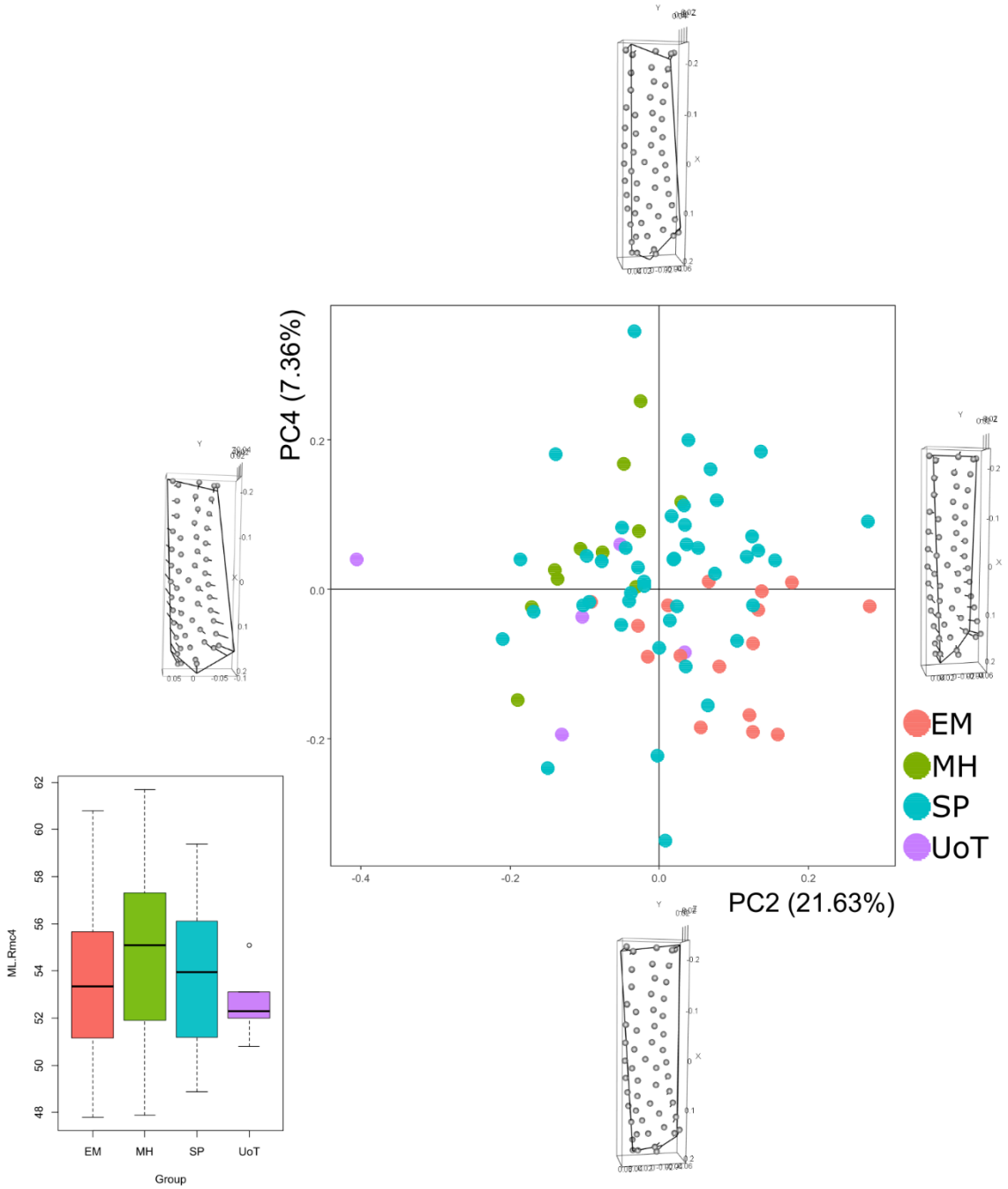

Figure 68 - Principal Component Analysis on the entire set of landmarks and shape configuration at the extremes of PC2 and PC4 for right DI4.

For the analyses of DI4 of right MC4 (**Figure 65**), a total of 76 specimens were available. Here, the first four PCs were analysed, representing almost the 82% of the total variance.
Analyses of shape variation along the different PCs is described. Regarding PC1, both fixed pseudo-landmarks and surface landmarks change position: in particular, L1 and L5 on the distal entheseal outline relocate, going to opposite directions – distally and proximally, respectively. Also, L3 partially moves in a medial way, causing changes in correspondence of the proximal entheseal portion. About surface semi-landmarks, some of them lying on the dorsal outline between L5 and L4 move towards the proximal epiphysis, while others lying close to the palmar surface go distally. About PC2, most of variation is due to relocation of surface semi-landmarks, going towards the centre of the enthesis from both palmar and dorsal entheseal outlines. With regard to fixed pseudo-landmarks, L2, L3 and L5 determine changes along the proximal entheseal portion: L2 moves dorsally, towards the centre of the enthesis, L3 moves distally and L4 moves both proximally and medially. About PC3, variation is in correspondence of L1, L2, L4 and L5. L1 moves along the distal entheseal outline, going towards the dorsal surface of the bone, L2 move along the proximal entheseal outline, towards L3, while both L4 and L5 move towards the centre of the enthesis, going proximally and distally respectively. Regarding PC4, no significant variation is evident due to minimum relocation of all landmarks: L1 and L4 move in a medial direction, L3 moves towards L4 and proximally, and L2 and L5 move in a lateral direction. Relocation of surface semi-landmarks is not determining for changes in shape morphology.

When describing PCA plots, in **Figure 66** separation between groups is evident along both PCs. EM and MH samples are distributed for positive values of PC1 but different values of PC2 – positive and negative, respectively. On the contrary, SP and UoT are distributed for negative values of PC1. These grouping are due to different morphologies of PCs along axes. With positive values of PC1, variation in correspondence of both distal and proximal portions of the enthesis is shown, making clear the separation between the reference samples and the archaeological ones. Along PC2, specimens distributed for negative values are characterised by entheses with wider proximal portions – this is the case of MH, with larger entheses than EM. A reverse distribution for the archaeological groups is visible when analysing PC4 – its PCA plot is added in the Annexes (cf. A4 – 12). In **Figure 67**, a different distribution is shown but similar groups are present: separation between SP and UoT groups and the archaeological samples is shown along PC1, with EM lying between the other ones. Along PC3, no grouping is recorded but a different distribution for EM and MH can be observed. Another different distribution is shown in **Figure 68**, where EM is distinct from MH for opposite values of PC2 and PC4 – the first distributed for negative values of both PCs and MH with positive values for PC4 and negatives' for PC2.

4.4.2 Left MC4 - Descriptive statistics, normality tests and correlation analyses

	raw size - DI3+PI2	ERS - DI3+PI2	raw size - DI4	ERS - DI4	APWM/ML*	MLWM/ML*	ML*
N	75	74	74	74	75	75	75
Min	237,16	0,14	171,19	0,12	0,1	0,1	43,98
Max	572,64	0,28	347,86	0,21	0,16	0,15	60,2
Mean	360,66	0,212	258,64	0,15	0,13	0,12	53,66
Stand. dev	70,26	0,034	42,33	0,018	0,013	0,012	3,29

Table 28 - Summary statistics for both 3D size and linear dimensions for right MC4. Raw size is calculated in $mm^{2,}$ ML is calculated in mm. **APWM/ML**: Antero-Posterior Robusticity Index. **MLWM/ML**: Medio-Lateral Robusticity Index. **ML**: Maximum Length.

	raw size - DI3+PI2	ERS - DI3+PI2	raw size - DI4	ERS - DI4	APWM/ML*	MLWM/ML*	ML*
N	75	74	74	74	75	75	75
Shapiro-Wilk W	0,97	0,98	0,99	0,96	0,94	0,92	0,98
p(normal)	0,12	0,19	0,61	0,01166	0,001475	0,0001256	0,34

Table 29 - Shapiro-Wilk test for each variable of right MC4.

	raw size - DI3+PI2	ERS - DI3+PI2	raw size - DI4	ERS - DI4
APWM/ML*	0,20	-0,05		0,009
MLWM/ML*	0,19	-0,05	0,16	-0,13
ML*		-0,04		0,03

Table 30 - Correlation tests between 3D bone size and linear dimensions for left MC4.

In **Tables 28 – 30**, descriptive statistics, correlation tests and normal distribution tests for all the variables used in this work are summarized.

The set of values of the two entheses of MC4 are similar, according to their dimensions and nature of muscular origin sites on metacarpal shafts. With regard to normality tests for each variable of left MC4, the Shapiro-Wilk's test has verified a normal distribution with a *p-value* > 0.05 for all variables, except for ERS of enthesis DI4 and both antero-posterior and medio-lateral RIs.

Correlation tests were performed: positive relations have been recorded between raw size of each enthesis and total surface size, while negative relations have been recorded when analysing ERS indexes. About relation between entheseal size (raw and ERS) and bone dimensions, ERS of the two entheses correlate with all linear dimensions (all negative values are recorded for ERS of DI3+PI2 and a negative correlation also between ERS of DI4 and medio-lateral RI), while raw size of both entheses do not correlate with maximum length but correlate with medio-lateral RI.

4.4.2.1 DI3+PI2 enthesis

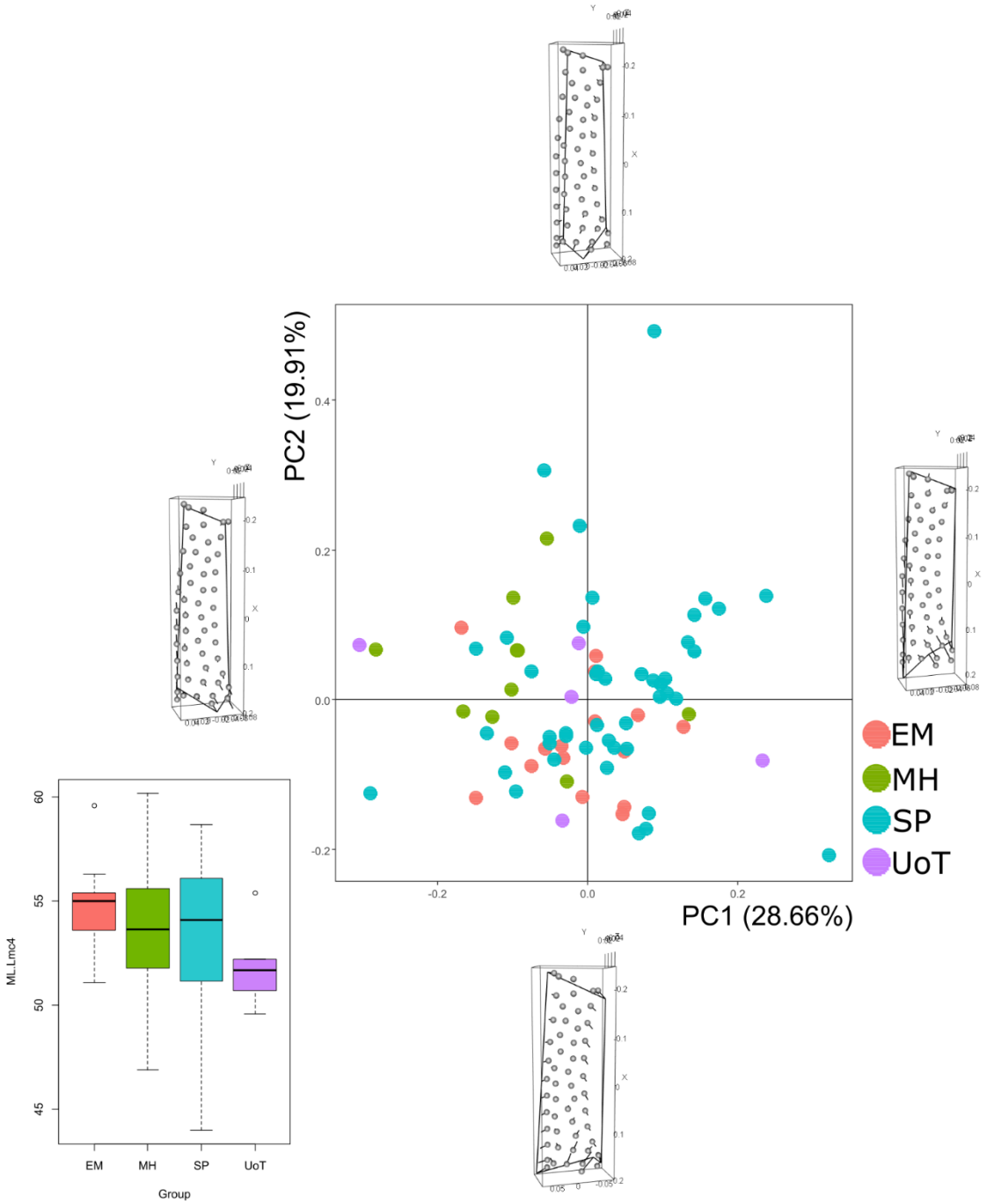

Figure 69 - Principal Component Analysis on the entire set of landmarks and shape configuration at the extremes of PC1 and PC2 for left DI3+PI2.

For the analyses of DI3+PI2 of left MC4, a total of 74 specimens were available. Here, the first two PCs were analysed, representing almost the 47% of the total variance.

Only shape variation along PC1 and PC2 is described. Regarding PC1, fixed pseudo-landmarks from L2 to L5 relocates, determining variation in correspondence of the proximal entheseal section: L2 moves in a proximal and lateral direction, L3 and L4 both move distally and towards the dorsal surface of the bone, while L5 moves in a palmar direction. About surface semi-landmarks, some of them lying close to the dorsal entheseal outline proceed in a proximal direction, others lying on the entheseal outline between L2 and L3 move distally. About PC2, L1 and L5 move in opposite directions along the entheseal outline where they lie, L2 moves towards the palmar surface, L3 moves both proximally and dorsally, and L4 moves laterally, along the outline towards L3. With regard to surface semi-landmarks, some of them lying along the dorsal entheseal outline move in a lateral direction, some semi-landmarks lying on the palmar outline move towards the centre of the enthesis, while some points close to the proximal epiphysis move proximally.

Even if shape variation is clearly evident along each PCs – in particular in correspondence of the bony projection on the proximal epiphysis – separation between groups is not recorded and shown; for this reason, only PC1 and PC2 were before described. Indeed, a homogeneous distribution is shown in **Figure 69**.

4.4.2.2 DI4 enthesis

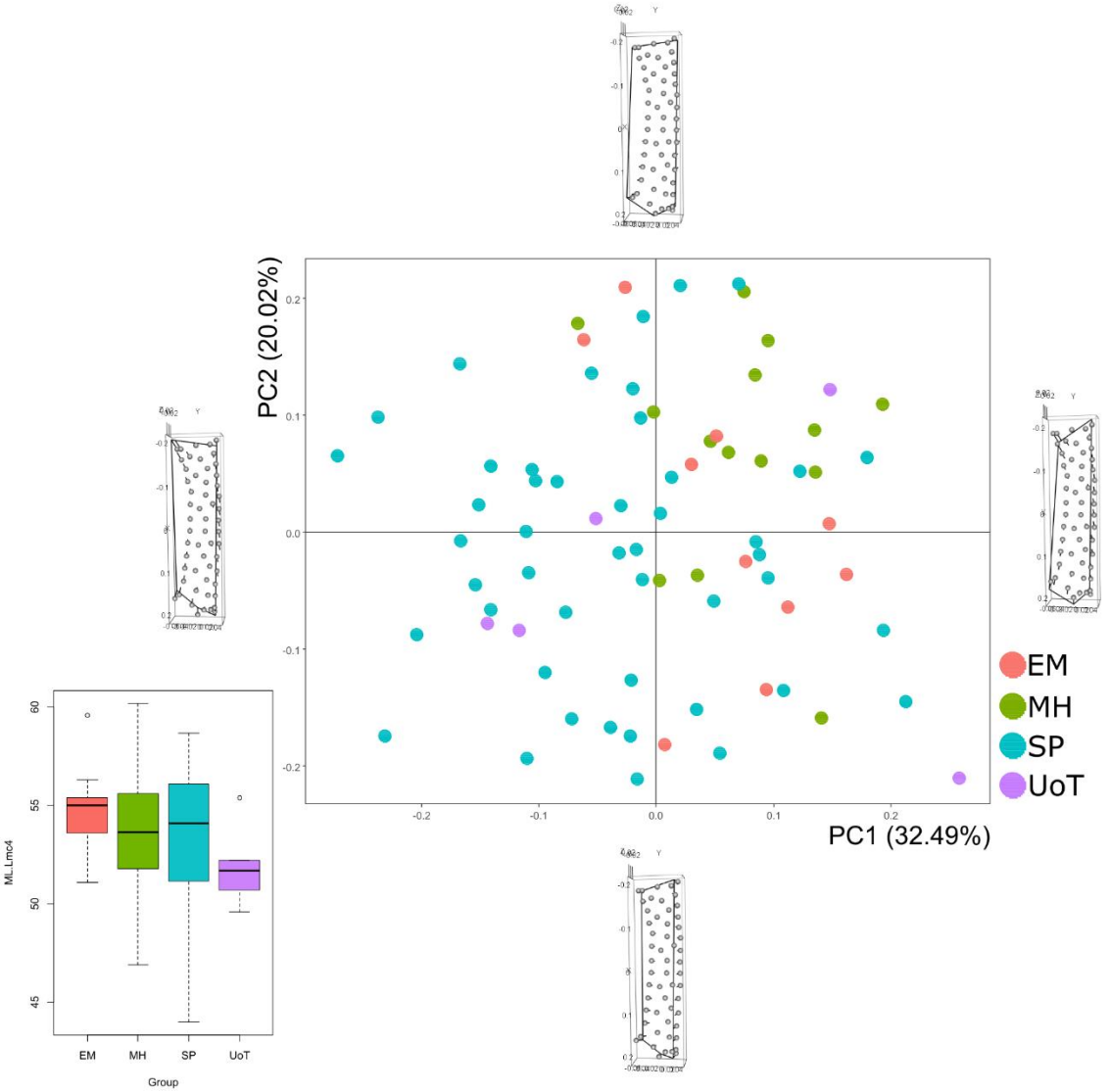

Figure 70 - Principal Component Analysis on the entire set of landmarks and shape configuration at the extremes of PC1 and PC2 for left DI4.

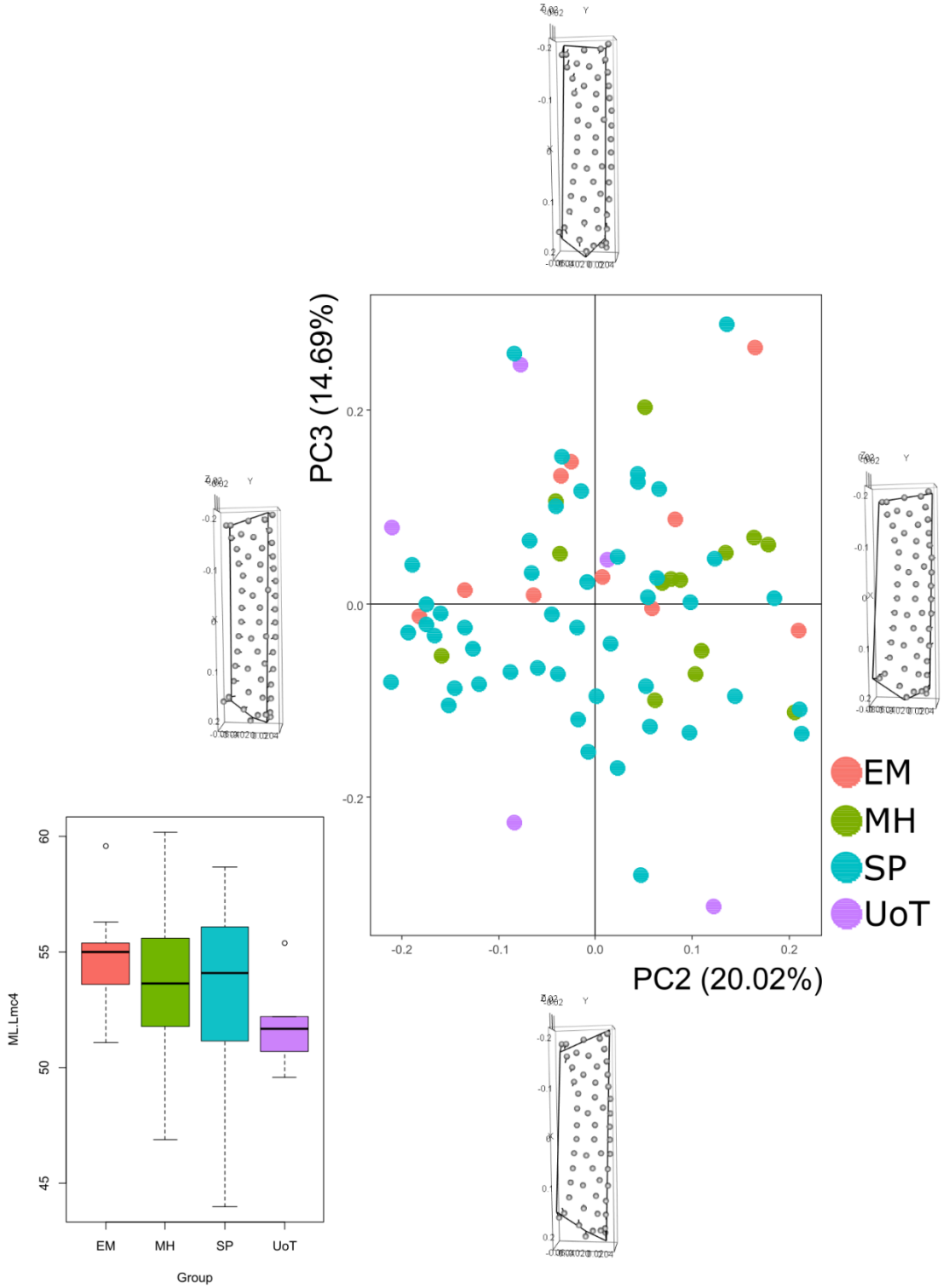

Figure 71 - Principal Component Analysis on the entire set of landmarks and shape configuration at the extremes of PC1 and PC3 for left DI4.

For the analyses of DI4 of left MC4, a total of 75 specimens were available. Here, the first four PCs were analysed, representing about the 76% of the total variance.

Regarding shape variation along PC1, relocation of both fixed and surface landmarks determines similar but different entheseal morphologies, which do not allow clear separation between groups. L1 and L2 and L3 move proximally, with L1 going towards the centre of the enthesis, and L4 and L5 both move towards the distal epiphysis. About surface semi-landmarks, those lying on the dorsal and palmar outlines move distally and proximally, respectively. About PC2, the main visible variation is in correspondence of the proximal portion, with L2 moving in a palmar direction, L3 going proximally and L4 moving laterally. With regard to PC3, L1 moves distally and laterally, L2 moves along the outline towards L3 – which goes in a proximal direction – and L4 moves both distally and dorsally. Entheseal surface modification is not recorded, because of a minimum variation of surface semi-landmarks. Along PC4, a reduced variation of the entheseal morphology can be observed in correspondence of the distal extremity, due to relocation of L1 and L4 – L1 moves along the distal entheseal outline towards L5, while L4 moves in a lateral direction.

Even in presence of shape variation along the different PCs, a collective distribution can be seen in the several PCAs obtained. The unique consideration that can be made concerns the distribution of the archaeological samples (EM and MH) on the right side of the plot in **Figure 70**,for positive values of PC1; same kind of distribution is shown in the Annexes, where plots considering PC3 and PC4 are shown (cf. A4 – 13, A4 – 14). Different arrangements for EM and MH appeared when PC1 is not considered: in **Figure 71**, specimens from EM are distributed for positive values of PC3, and MH ones are in positive side of PC2, and a reverse situation is visible when PC3 and PC4 are evaluated (cf. A4 – 15).

4.5 Analyses of 5th metacarpal bones

4.5.1 Right MC5 - Descriptive statistics, normality tests and correlation analyses

	raw size - DI4+PI3	ERS - DI4+PI3	raw size - ODM	ERS - ODM	APWM/ML*	MLWM/ML*	ML*
N	73	68	72	67	68	68	68
Min	204,81	0,15	136,71	0,09	0,10	0,12	41,63
Max	519,48	0,26	361,99	0,20	0,17	0,18	56,80
Mean	344,98	0,22	238,26	0,15	0,13	0,15	50,70
Stand. dev	62,37	0,026	46,03	0,025	0,015	0,015	2,95

Table 31 - Summary statistics for both 3D size and linear dimensions for right MC5. Raw size is calculated in mm^2. ML is calculated in mm. **APWM/ML**: Antero-Posterior Robusticity Index. **MLWM/ML**: Medio-Lateral Robusticity Index. **ML**: Maximum Length.

	raw size - DI4+PI3	ERS - DI4+PI3	raw size - ODM	ERS - ODM	APWM/ML*	MLWM/ML*	ML*
N	73	68	72	67	68	68	68
Shapiro-Wilk W	0,99	0,97	0,99	0,99	0,98	0,98	0,98
p(normal)	0,67	0,05	0,88	0,62	0,29	0,52	0,29

Table 32 - Shapiro-Wilk test for each variable of right MC5.

	raw size - DI4+PI3	ERS - DI4+PI3	raw size - ODM	ERS - ODM
APWM/ML*		-0,04		-0,11
MLWM/ML*		0,06	0,13	-0,12
ML*		0,05		0,05

Table 33 - Correlation tests between 3D bone sizes and linear dimensions for right MC5.

In **Tables 31 – 33,** descriptive statistics, correlation tests and normal distribution tests for all the variables used in this work are summarized.

The set of values for the entheses of MC5 are similar, according to their dimensions and insertion areas on metacarpal shafts. With regard to normality tests for each variable of right MC5, the Shapiro-Wilk's test has verified a normal distribution with a *p-value* > 0.05 for all variables.

Correlation tests were performed: positive relations have been recorded between both raw size and ERS of both entheses and total surface size, except for ERS index of ODM, characterized by a negative correlation. About relation between entheseal size (raw and ERS) and bone dimensions, ERS indexes of all entheses correlate with all linear measurements with both positive and negative values, while a minimum relation is recorded between raw size of ODM enthesis and corresponding medio-lateral Robusticity Index.

4.5.1.1 DI4+PI3 enthesis

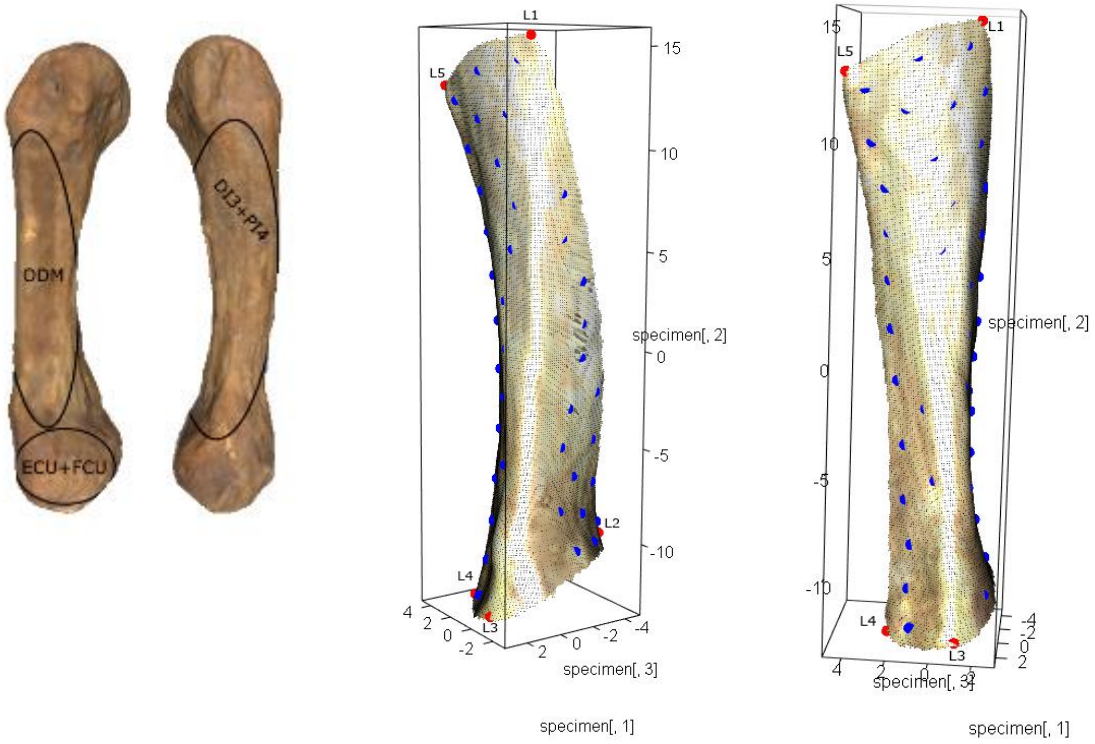

Figure 72 - On the right, the MC5 bone with delimited entheses.
On the left, the landmarks (red spots) and semi-landmarks (blue spots) on the 3D model of the surface of DI4+PI3.
For the landmarks' definitions, see Annexes (cf. A2 – 5).

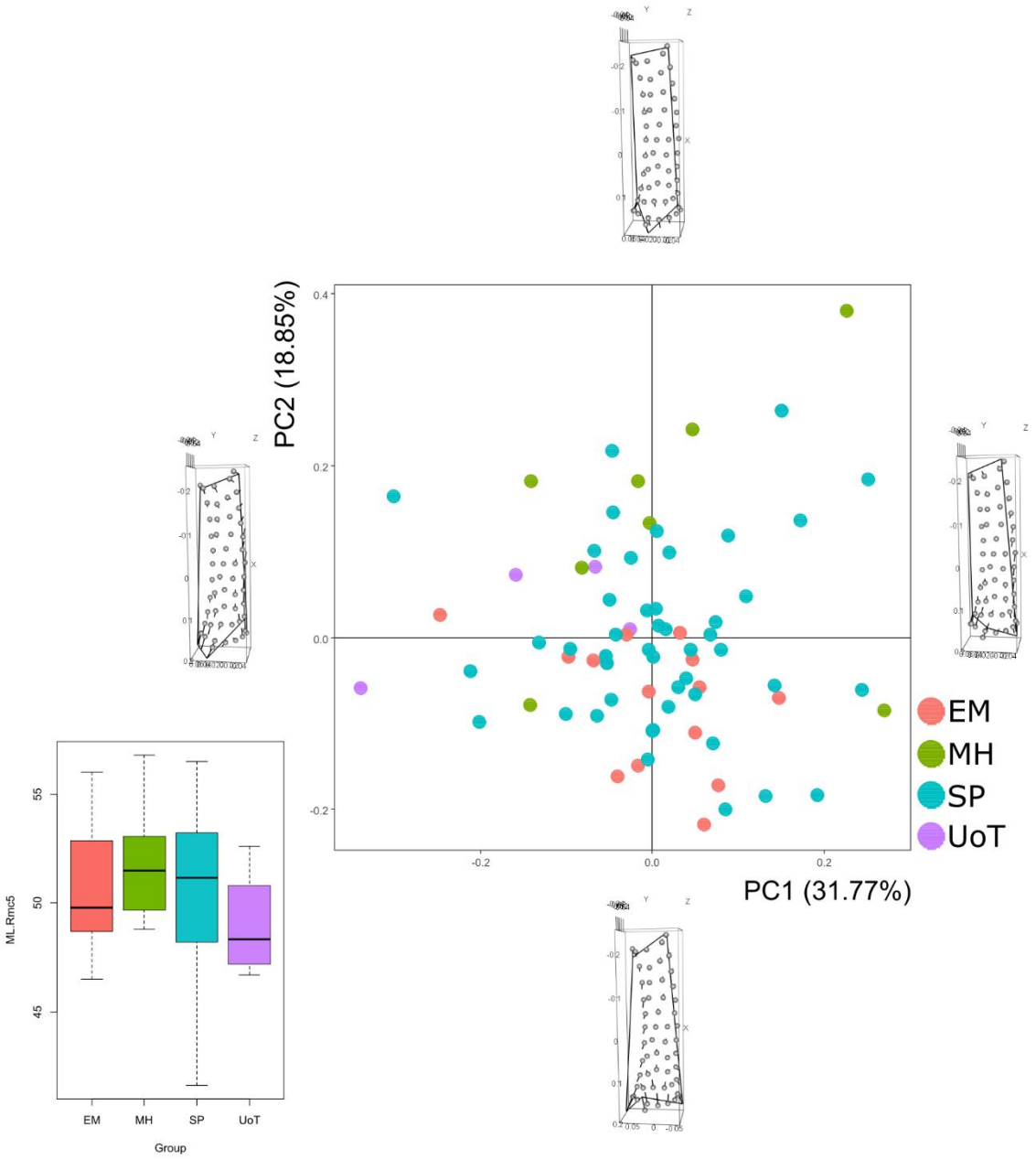

Figure 73 - Principal Component Analysis on the entire set of landmarks and shape configuration at the extremes of PC1 and PC2 for right DI4+PI3.

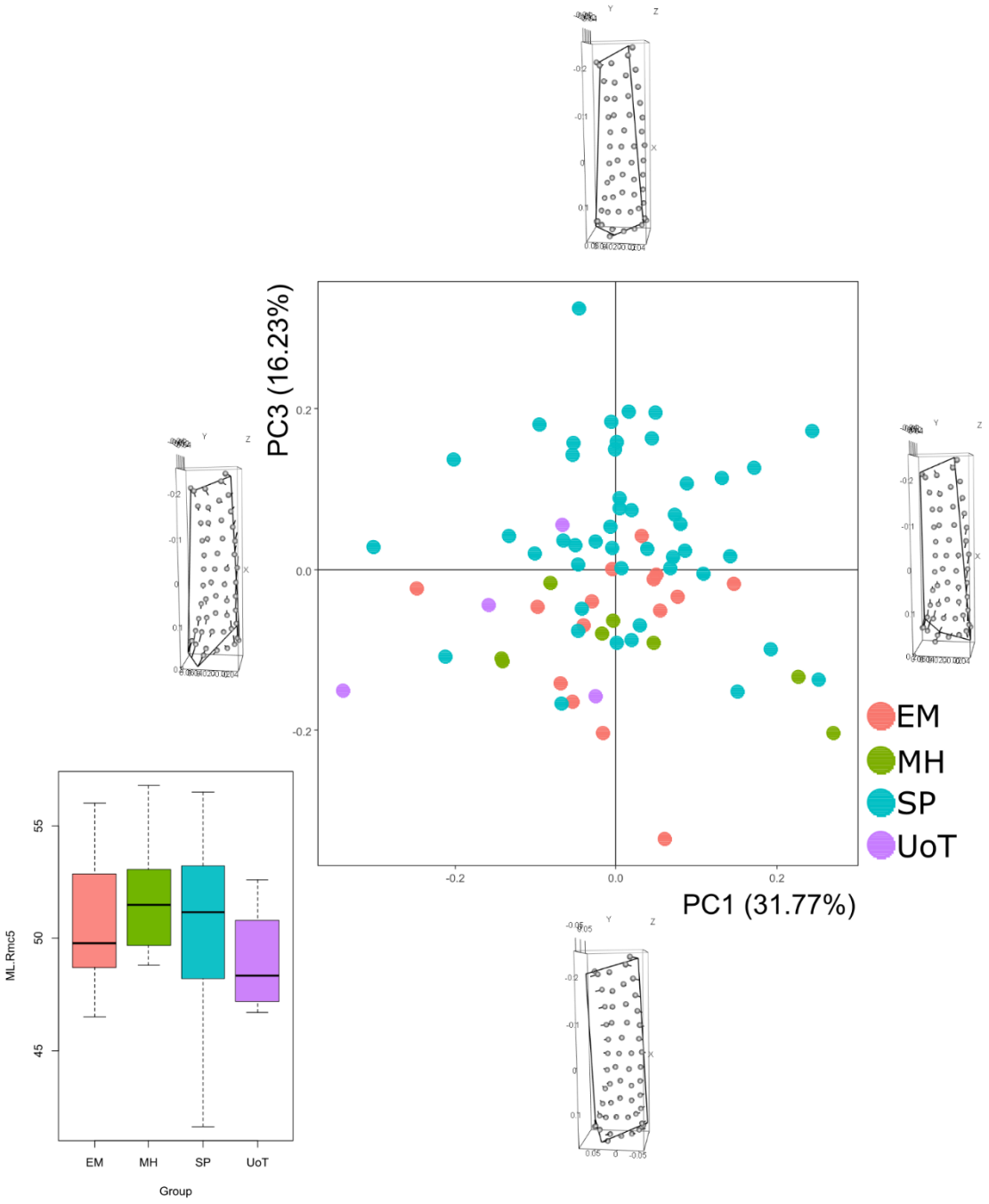

Figure 74 - Principal Component Analysis on the entire set of landmarks and shape configuration at the extremes of PC1 and PC3 for right DI4+PI3.

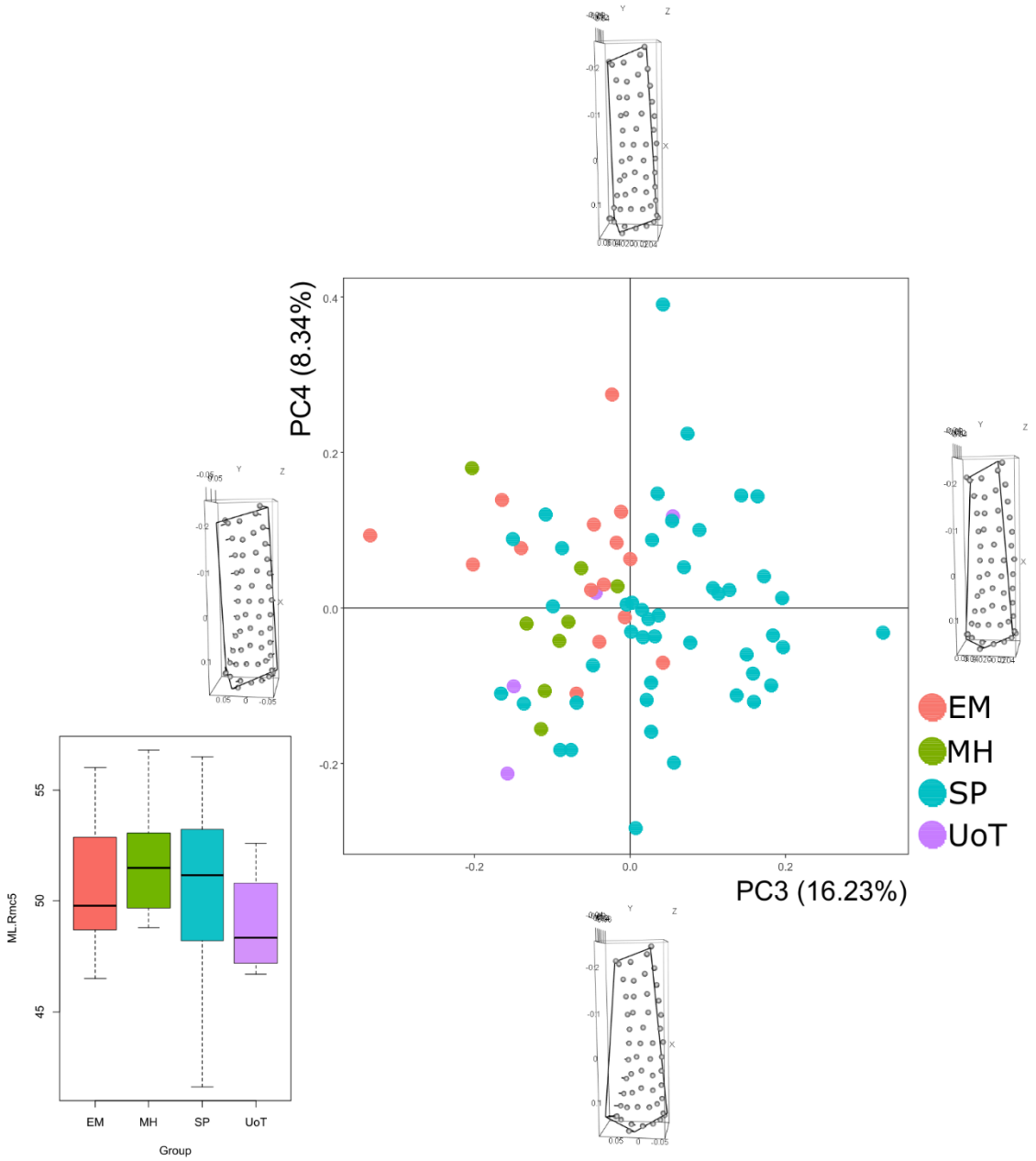

Figure 75 - Principal Component Analysis on the entire set of landmarks and shape configuration at the extremes of PC3 and PC4 for right DI4+PI3.

For the analyses of DI4+PI3 of right MC5 (**Figure 72**), a total of 73 specimens were available. Here, the first four PCs were analysed, representing almost the 76% of the total variance.

Regarding shape variation on PC1, both fixed pseudo-landmarks and surface semi-landmarks relocate: L1 and L5 move in opposite directions, medially and laterally respectively, L2 moves towards the proximal epiphysis and L3 and L4 both move towards the distal extremity. About surface semi-landmarks, some lying along the dorsal entheseal outline move in a proximal direction, while some landmarks located close to the proximal epiphysis on the palmar side go towards the distal extremity. Regarding PC2, most degree of shape variation is in correspondence of the proximal end, caused by a proximal relocation of L3; furthermore, L2 and L4 move distally and towards the centre of the enthesis. Movements of surface semi-landmarks located in correspondence of the base cause an increasing in length of the entheseal shape and an increasing in a medio-lateral way. About PC3, relocation of both fixed pseudo-landmarks and surface semi-landmarks causes a dimensional reduction of the entheseal shape. Same considerations can be made for PC4, but only relocation of L4 determine shape variation – it goes towards the dorsal surface of the bone.

When describing PCA plots, homogenous distribution can be observed for all samples, even if specimens from the two archaeological collections result distinct between them. In **Figure 73**, EM is distributed for negative values of PC2, while most of MH lies on the positive side of PC2 axis: exceptions are the two specimens from MH close to EM group.
Different situation can be observed when PC3 is introduced, showing separation between groups. MH and EM have the same distribution for negative values of this component in all the PCA plots regarding this PC (**Figure 74**; **Figure 75**; Annexes, cf. A4 – 16).

4.5.1.2 ODM enthesis

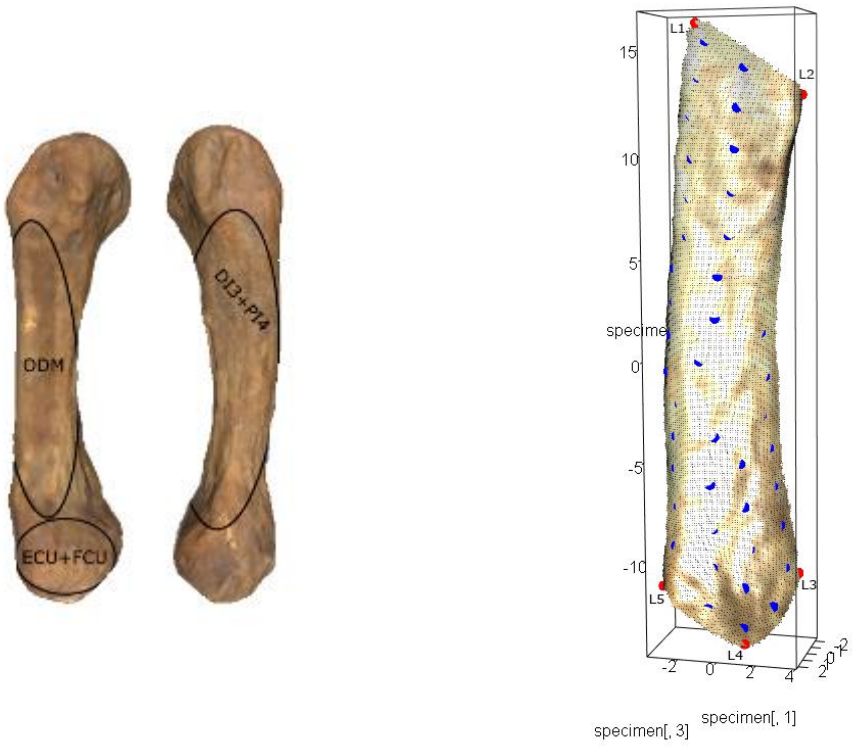

Figure 76 - On the left, the MC5 bone with delimited entheses.
On the right, the landmarks (red spots) and semi-landmarks (blue spots) on the 3D model of the surface of ODM.
For the landmarks' definitions, see Annexes (cf. A2 – 5).

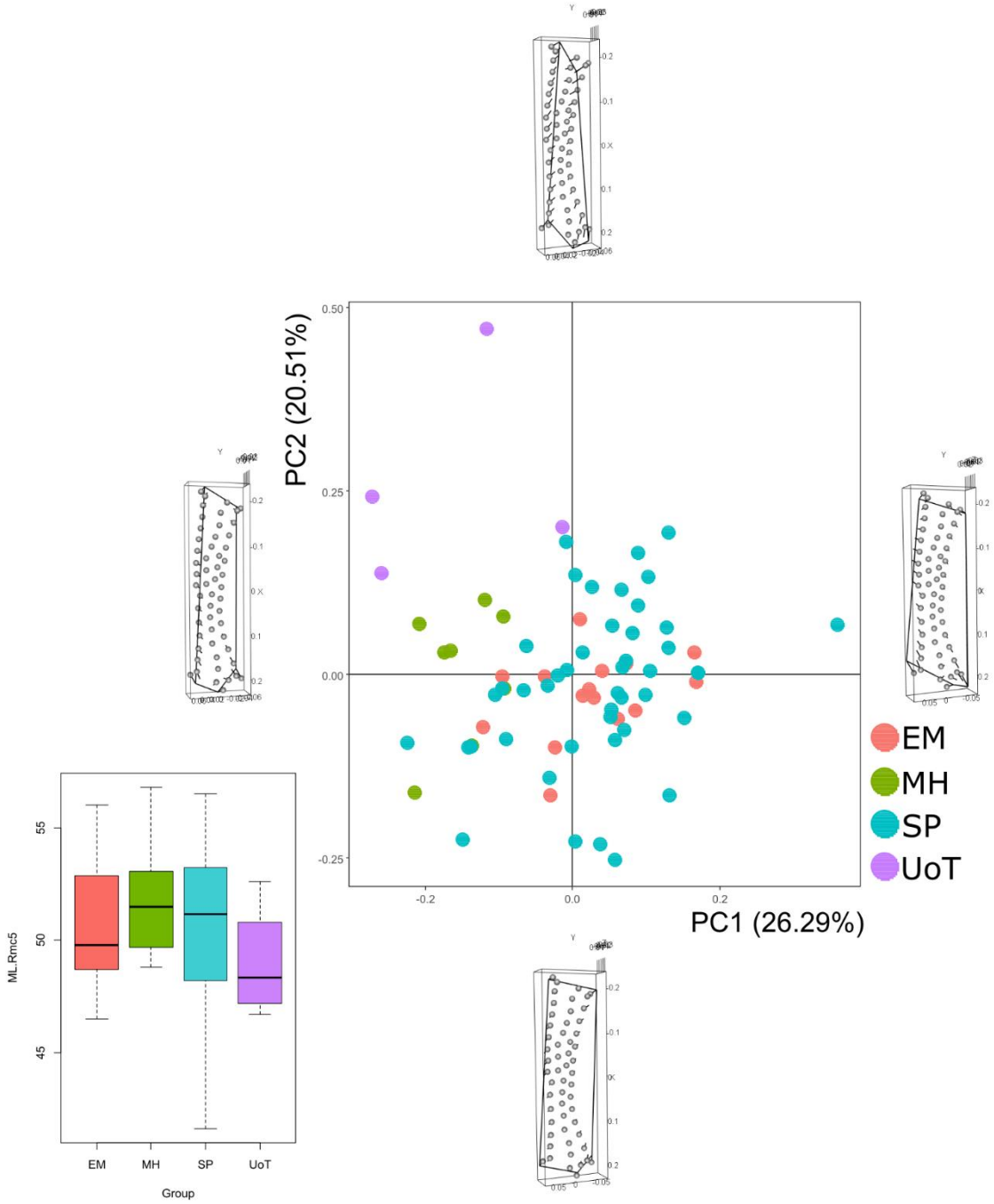

Figure 77 - Principal Component Analysis on the entire set of landmarks and shape configuration at the extremes of PC1 and PC2 for right ODM.

For the analyses of ODM of right MC5 (**Figure 76**), a total of 72 specimens were available. Here, the first four PCs were analysed, representing almost the 70% of the total variance.

Analysing shape variation with regard to PC1, relocating of fixed pseudo-landmarks determine variation in correspondence of proximal extremity near the base; this is due to landmarks from L3 to L5 – with L3 and L5 moving in opposite directions, proximally and distally respectively. Concerning surface semi-landmarks located on the dorsal entheseal outline, they move towards the dorsal surface of the bone and determine an increasing of the surface dimension in an antero-posterior way. About PC2, most variation is due to fixed pseudo-landmarks L2 and L5, moving towards the centre of the enthesis, L3, moving proximally, whose movements determine a reduction in size in an antero-posterior direction and an increasing in length in the proximal area. Regarding PC3, a partial increasing in medio-lateral direction is recorded in correspondence of L3 and L4, moving in lateral and palmar directions, respectively. Along PC4, variation occurs on L2 – moving towards the distal extremity – and L4 – moving along the entheseal outline towards L3.

In **Figure 77**, separation between samples is shown: SP and EM samples are distributed all over the graph except for positive values of PC2, in the 2nd quarter of the plane, where only MH and UoT are. These latter are characterised by specimens with more elongated distal extremities and narrower shape in antero-posterior way. Similar distributions were obtained when PC3 and PC4 have been considered; for these plots, see Annexes (cf. A4 – 17, A4 – 18, A4 - 19).

4.5.2 Left MC5 - Descriptive statistics, normality tests and correlation analyses

	raw size - DI4+PI3	ERS - DI4+PI3	raw size - ODM	ERS - ODM	APWM/ML*	MLWM/ML*	ML*
N	63	63	62	62	64	64	64
Min	180,05	0,16	116,35	0,104	0,09	0,11	41,85
Max	445,84	0,27	361,43	0,20	0,17	0,18	55,42
Mean	331,91	0,22	227,69	0,148	0,13	0,14	49,99
Stand. dev	56,44	0,024	47,68	0,022	0,014	0,015	3,05

Table 34 - Summary statistics for both 3D size and linear dimensions for left MC5. Raw size is calculated in mm^2, ML is calculated in mm. **APWM/ML**: Antero-Posterior Robusticity Index. **MLWM/ML**: Medio-Lateral Robusticity Index. **ML**: Maximum Length.

	raw size - DI4+PI3	ERS - DI4+PI3	raw size - ODM	ERS - ODM	APWM/ML*	MLWM/ML*	ML*
N	63	63	62	62	64	64	64
Shapiro-Wilk W	0,99	0,99	0,99	0,98	0,98	0,99	0,97
p(normal)	0,73	0,84	0,92	0,38	0,38	0,94	0,20

Table 35 - Shapiro-Wilk test for each variable of left MC5.

	raw size - DI4+PI3	ERS - DI4+PI3	raw size - ODM	ERS - ODM
APWM/ML*		0,21		
MLWM/ML*	0,21	0,07	0,10	-0,04
ML*		-0,004		0,19

Table 36 - Correlation tests between 3D bone size and linear dimensions for left MC5.

In **Tables 34 – 36**, descriptive statistics, correlation tests and normal distribution tests for all the variables used in this work are summarized.

The set of values for the entheses of MC5 are similar, according to their dimensions and insertion areas on metacarpal shafts. With regard to normality tests for each variable of left MC5, the Shapiro-Wilk's test has verified a normal distribution with a *p-value* > 0.05 for all variables.

Correlation tests were performed: positive relations have been recorded between both raw size and ERS of both entheses and total surface size. About relation between entheseal size (raw and ERS) and bone dimensions, all entheseal values correlate with medio-lateral Robusticity Index, while relation is recorded between ERS of ODM enthesis and bone length, and ERS of DI4+PI3 enthesis also correlate with the other dimensions available.

4.5.2.1 DI4+PI3 enthesis

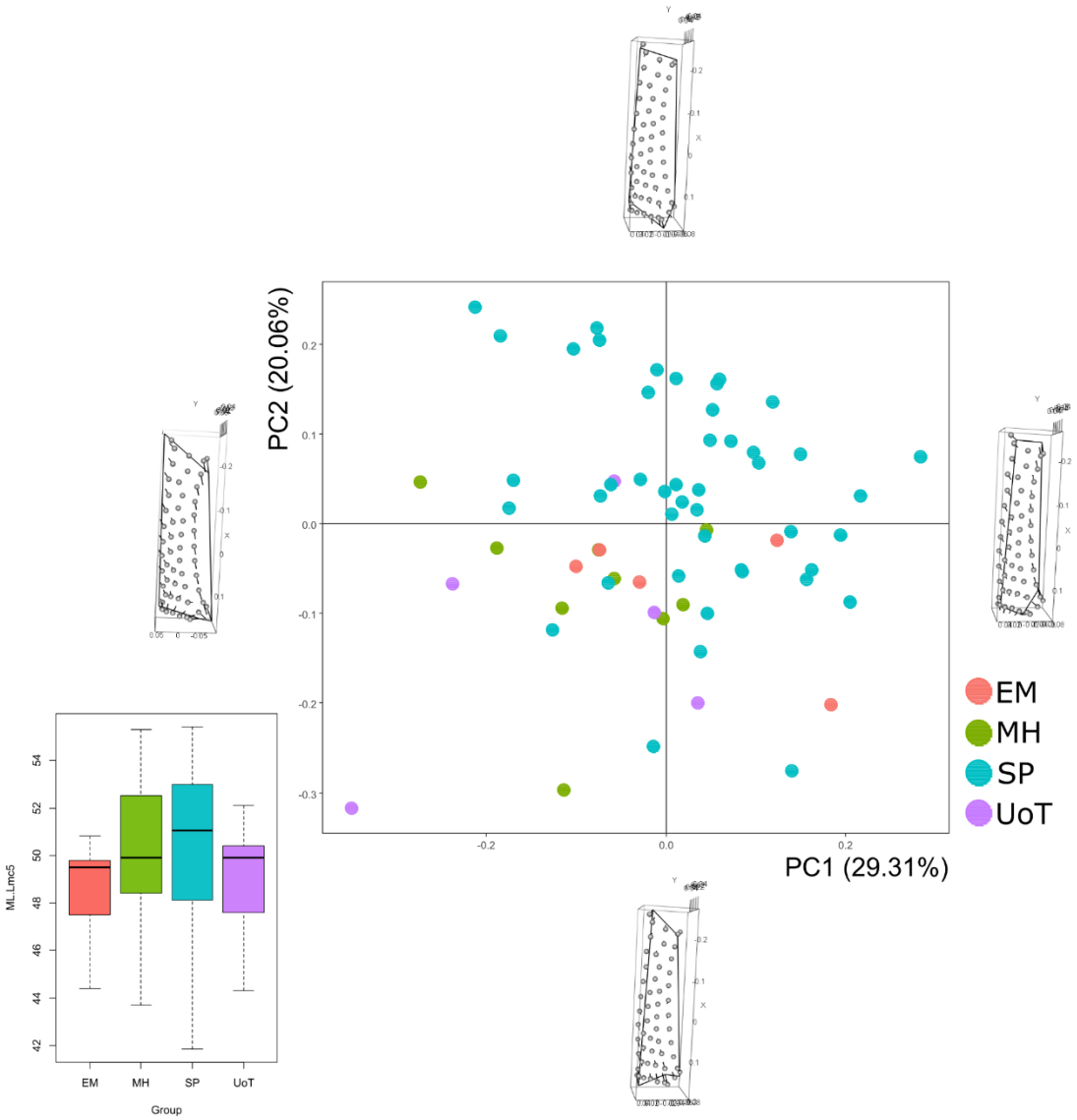

Figure 78 - Principal Component Analysis on the entire set of landmarks and shape configuration at the extremes of PC1 and PC2 for left DI4+PI3.

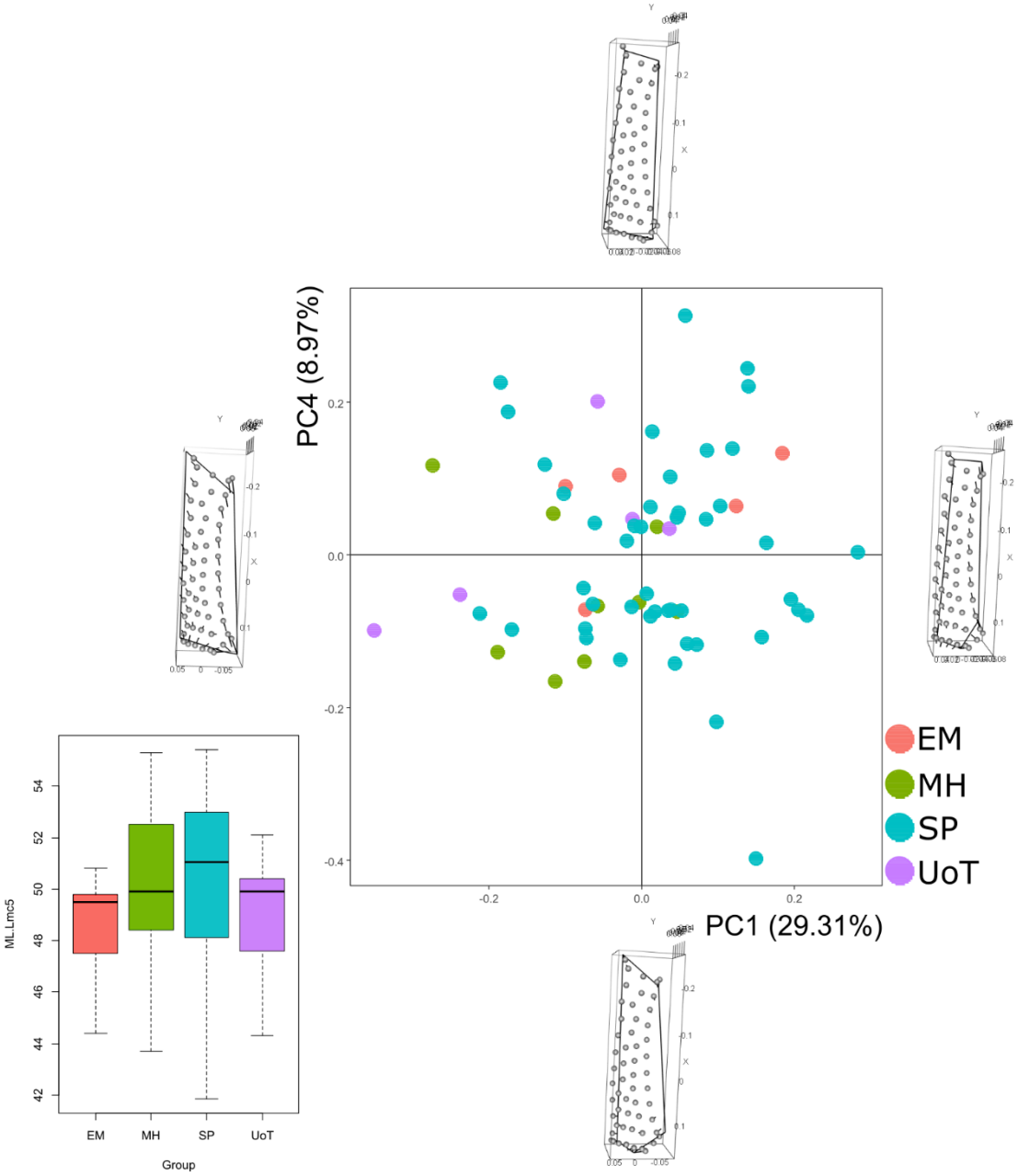

Figure 79 - Principal Component Analysis on the entire set of landmarks and shape configuration at the extremes of PC1 and PC4 for left DI4+PI3.

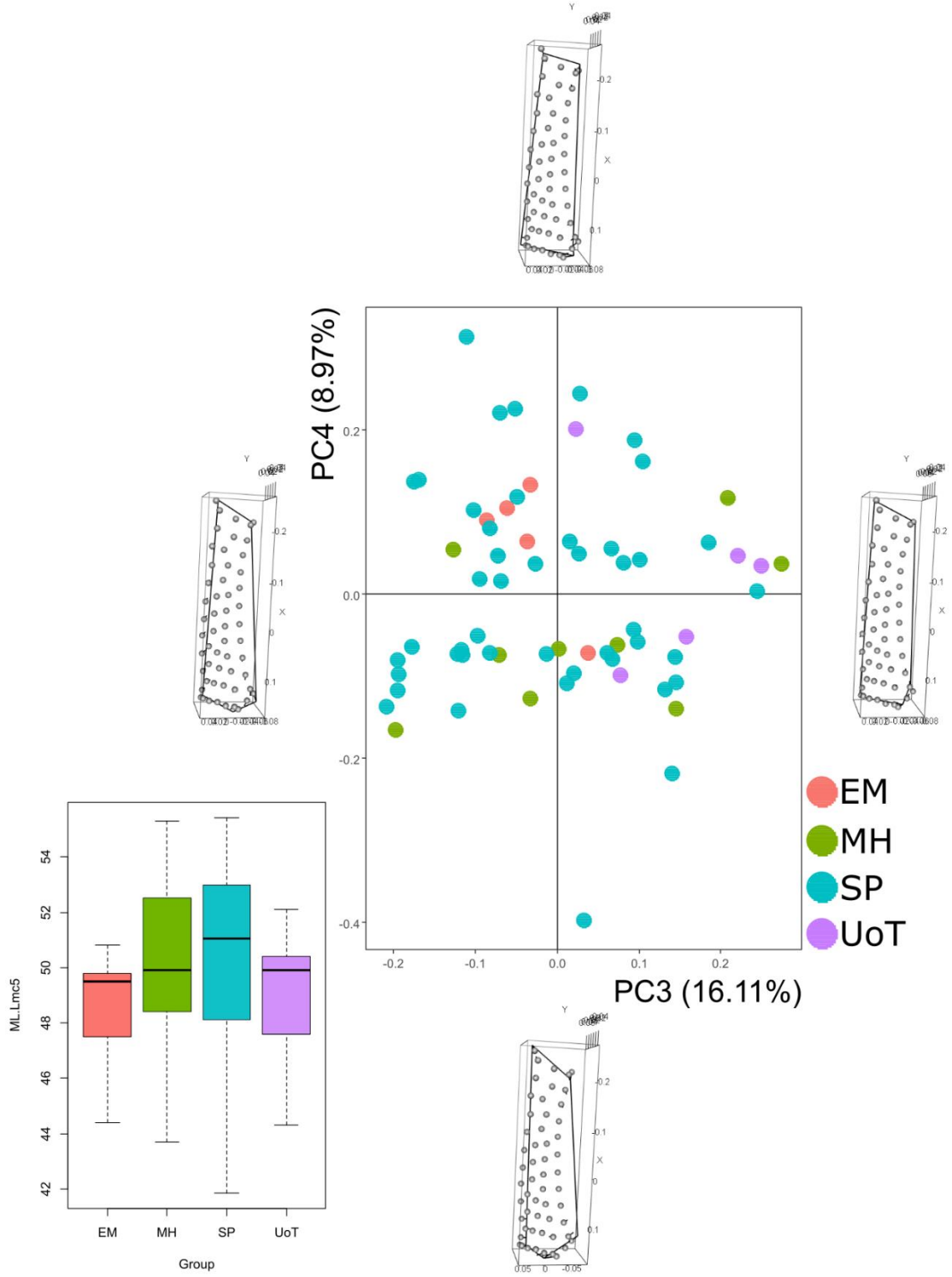

Figure 80 - Principal Component Analysis on the entire set of landmarks and shape configuration at the extremes of PC3 and PC4 for left DI4+PI3.

For the analyses of DI4+PI3 of left MC5, a total of 64 specimens were available. Here, the first four PCs were analysed, representing almost the 75% of the total variance.

Analysing shape variation on PC1, both fixed and surface landmarks determine changes in entheseal shape. About fixed pseudo-landmarks, L1 moves along the distal outline connecting L1 and L5, towards this latter, L2 moves towards L3 and vice versa, and L4 and L5 both move in a distal direction and, in part, dorsally. Furthermore, surface semi-landmarks located close to the dorsal and palmar entheseal outlines move in opposite direction, moving proximally and distally, respectively; other points located along the proximal outline between L2 and L3 move both distally and dorsally and determine an increasing in an antero-posterior way. With regard to PC2, L1 moves in a proximal direction and L2 moves in a distal one, L3 moves both proximally and laterally, and L4 and L5 both move in a medial direction. In this case, surface semi-landmarks disposed along the dorsal outline and close to the base move towards the distal epiphysis, while some of them lying near the base move proximally. About PC3, a minimum shape variation can be observed in correspondence of fixed pseudo-landmarks from L2 to L4, even if variation does not influence shape morphology along this PC. Great variation is evident when analysing PC4, in particular: L2 moves towards the dorsal surface of the bone, L3 move in a palmar direction, L4 moves towards L3, and L5 moves towards L1, dorsally. No changes due to relocation of surface semi-landmarks are recorded. Nevertheless, dimensional reduction in an antero-posterior way can be observed when considering PC4.

Distribution of the samples along PC1 and PC2 can be observed in **Figure 78**: San Pablo's groups is almost completely distinct from the others, while the remaining part of the sample is distributed for negative values for the two PCs. Similar distribution is shown in **Figure 79**, where El Mirador sample moves along PC4 and separates from the MH group, this latter distributed for negative values of both PCs. Separation between the two archaeological samples can be seen when PC3 and PC4 are analysed: El Mirador group is distributed for negative and positive values for PC3 and PC4, respectively, while MH sample spreads negative PC4 (**Figure 80**). Also, specimens from University of Turin's collection are distributed mainly on the right side of the graph, having positive values of PC3.

4.5.2.2 ODM enthesis

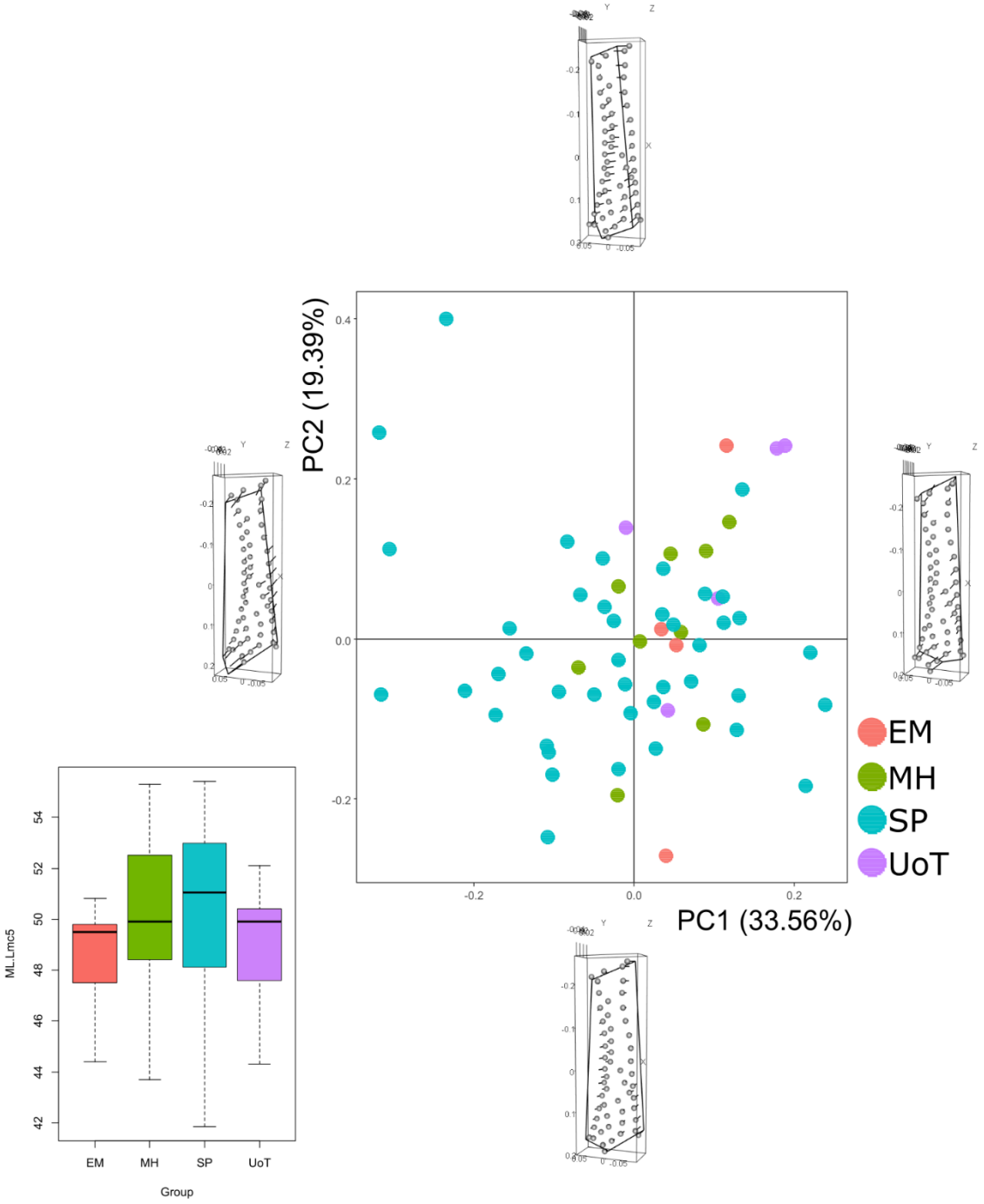

Figure 81 - Principal Component Analysis on the entire set of landmarks and shape configuration at the extremes of PC1 and PC2 for left ODM.

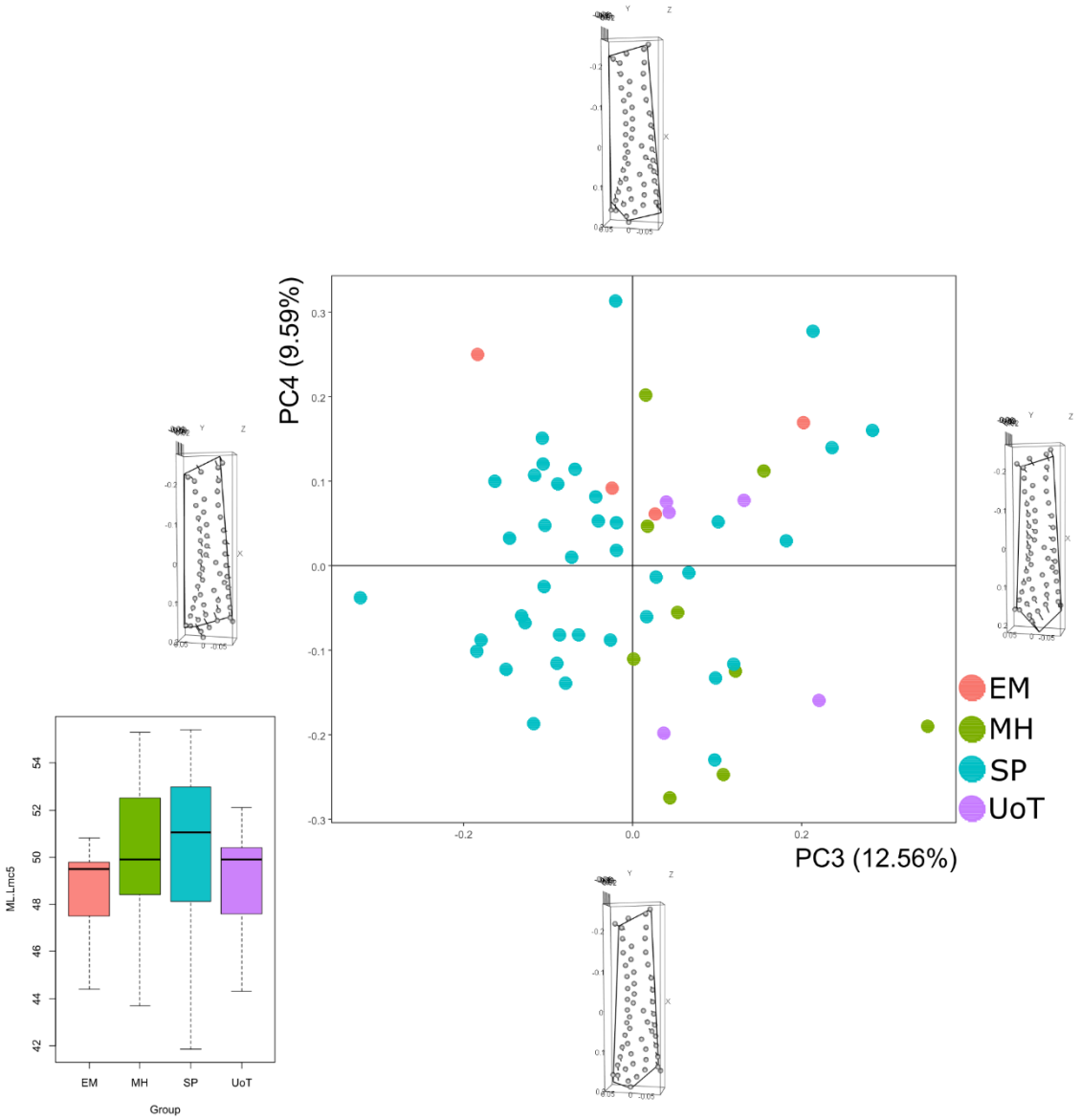

Figure 82- Principal Component Analysis on the entire set of landmarks and shape configuration at the extremes of PC3 and PC4 for left ODM.

For the analyses of ODM of left MC5, a total of 60 specimens were available. Here, the first four PCs were analysed, representing the 75% of the total variance.

Analysing shape variation along PC1, fixed landmarks from L1 to L4 move towards the dorsal surface of the bone, while L5 moves in a medial direction. With regard to surface semi-landmarks, those lying close to the central part of the enthesis move towards the palmar surface, while others located close to extremities move towards the dorsal surface. Along PC2, most of variation is caused by relocation of surface semi-landmarks, which move from the dorsal and palmar outlines towards the centre of the enthesis. About fixed pseudo-landmarks, a minimum variation occurs in correspondence of L1, L3 and L5, all going in a palmar direction. Regarding PC3, fixed landmarks L1, L2 and L4 move in both proximal and dorsal directions, while L5 move also proximally but towards the palmar surface; in this case, surface semi-landmarks on the palmar outline move towards the distal end, while others located in correspondence of both extremities move proximally. About PC4, no particular shape variation is evident when analysing the two entheseal morphologies, even if some fixed pseudo-landmarks relocates: L2 moves anteriorly, L3 moves distally, and L5 moves in a proximal direction.

The resulting analyses shown in **Figure 81** and **Figure 82** allow to observe a homogenous distribution of the entire sample without separation by groups, even if different shape morphologies are recorded along each PC. A partial different situation can be seen in **Figure 82**, where MH and UoT samples are on the right side of the plot, distributed for positive values PC3, while EM has a distribution for positive values of PC4.

4.6 Analyses of 1st proximal phalanges

4.6.1 Right PP1 - Descriptive statistics, normality tests and correlation analyses

	raw size - ABP+FBP	ERS - ABP+FBP	raw size - ADP	ERS - ADP	APWM/ML*	MLWM/ML*	ML*
N	57	52	58	54	56	56	56
Min	48,34	0,04	53,94	0,05	0,16	0,25	26,70
Max	187,71	0,13	167,01	0,12	0,26	0,35	34,18
Mean	113,73	0,10	99,00	0,09	0,21	0,31	29,89
Stand. dev	25,78	0,02	21,23	0,01	0,02	0,02	1,78

Table 37 - Summary statistics for both 3D size and linear dimensions for right PP1. Raw size is calculated in mm^2, ML is calculated in mm. **APWM/ML**: Antero-Posterior Robusticity Index. **MLWM/ML**: Medio-Lateral Robusticity Index. **ML**: Maximum Length.

	raw size - ABP+FBP	ERS - ABP+FBP	raw size - ADP	ERS - ADP	APWM/ML*	MLWM/ML*	ML*
N	57	52	58	54	56	56	56
Shapiro-Wilk W	0,98	0,97	0,98	0,98	0,99	0,99	0,98
p(normal)	0,43	0,15	0,45	0,40	0,87	0,74	0,47

Table 38 - Shapiro-Wilk test for each variable of right PP1.

	raw size - ABP+FBP	ERS - ABP+FBP	raw size - ADP	ERS - ADP
APWM/ML*	0,18	-0,08	0,21	-0,02
MLWM/ML*	0,24	-0,01		0,01
ML*		0,10		-0,04

Table 39 - Correlation tests between 3D bone sizes and linear dimensions for right PP1.

In **Tables 37 – 39**, descriptive statistics, correlation tests and normal distribution tests for all the variables used in this work are summarized.

The set of values for the entheses of right PP1 are similar, according to their comparable dimensions in correspondence of the base of the bone. With regard to normality tests for each variable of right PP1, the Shapiro-Wilk's test has verified a normal distribution with a *p-value* > 0.05 for all variables. Correlation tests were performed: positive relations have been recorded between raw size of both entheses and total surface size, while negative correlations are present between ERS indexes total surface size. About relation between entheseal size (raw and ERS) and bone dimensions, ERS indexes of ABP+FBP and ADP correlate with all measurements (with both positive and negative correlations), while only positive correlations have been recorded between raw size of ABP+FBP enthesis and both RIs and between raw size of ADP and antero-posterior RI.

4.6.1.1 ABP+FBP enthesis

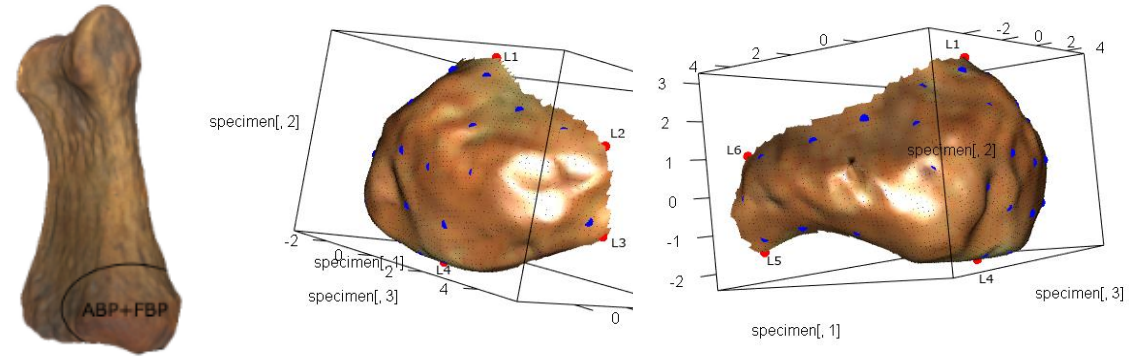

Figure 83 - On the left, PP1 bone with delimited enthesis.
On the right, the landmarks (red spots) and semi-landmarks (blue spots) on the 3D model of the surface of ABP+FBP.
For the landmarks' definitions, see Annexes (cf. A2 – 6).

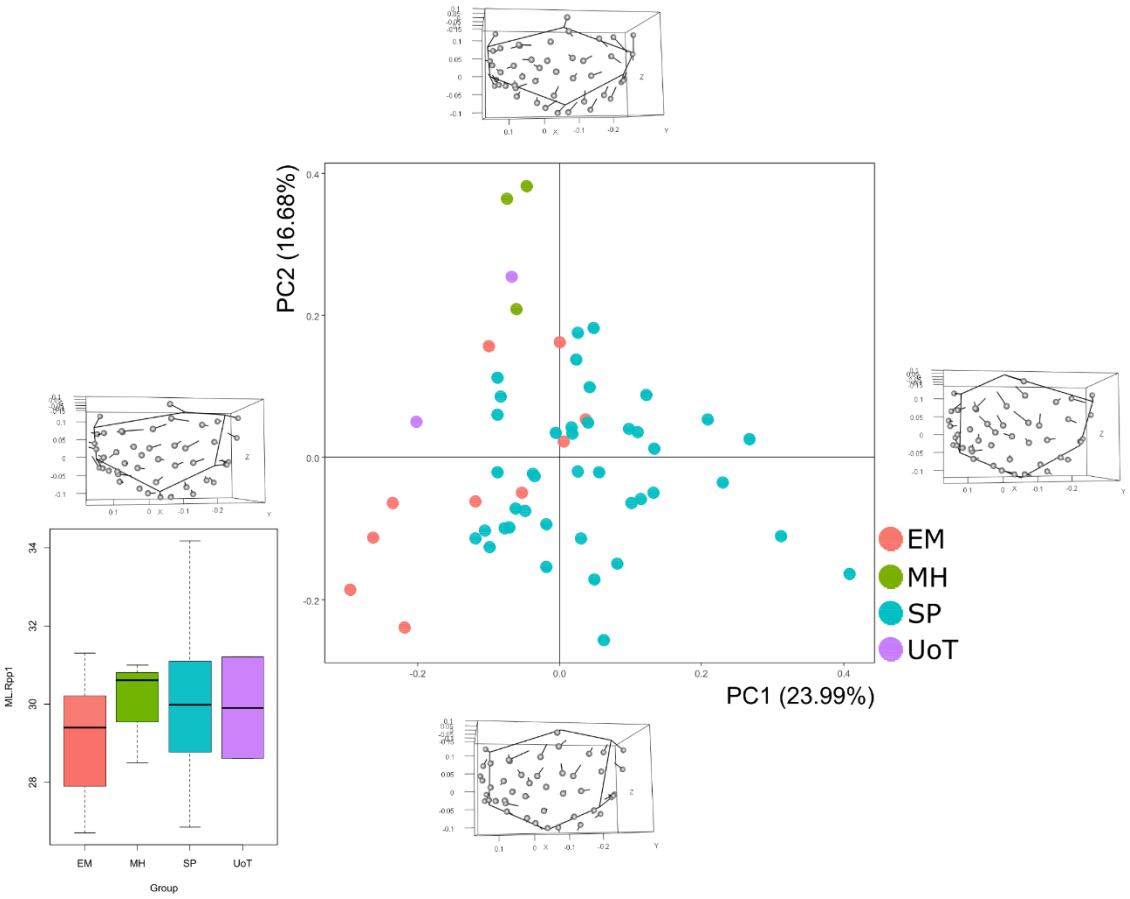

Figure 84 - Principal Component Analysis on the entire set of landmarks and shape configuration at the extremes of PC1 and PC2 for right ABP+FBP.

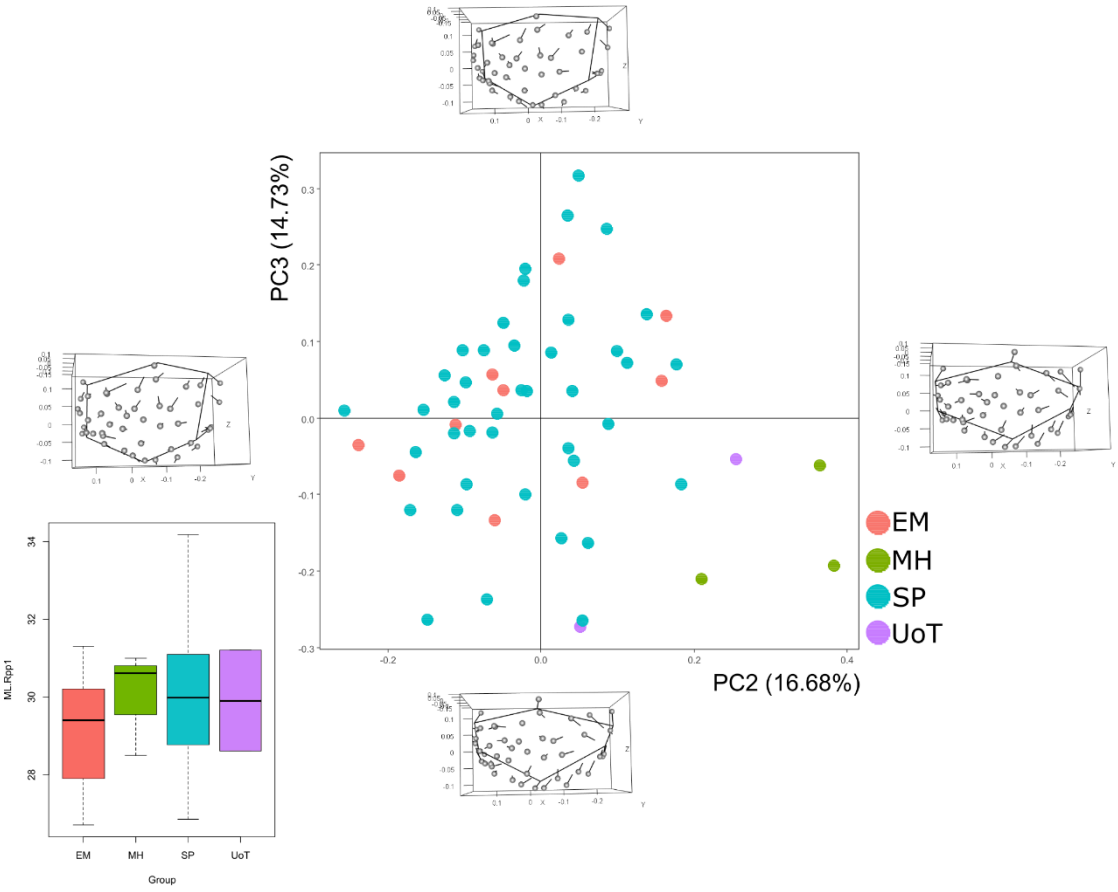

Figure 85 - Principal Component Analysis on the entire set of landmarks and shape configuration at the extremes of PC2 and PC3 for right ABP+FBP.

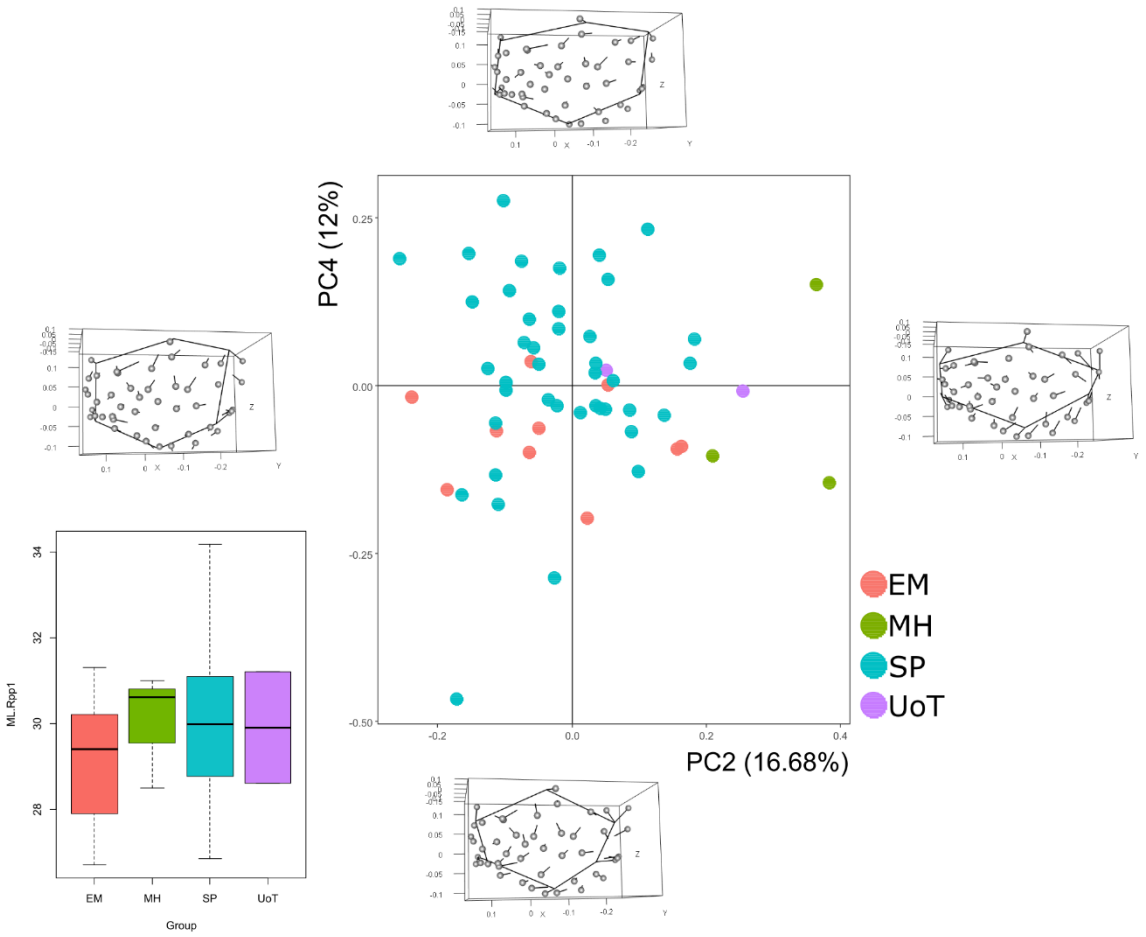

Figure 86 - Principal Component Analysis on the entire set of landmarks and shape configuration at the extremes of PC2 and PC4 for right ABP+FBP.

For the analyses of ABP+FBP of right PP1 (**Figure 83**), a total of 57 specimens were available. Here, the first four PCs were analysed, representing almost the 70% of the total variance.

Analysing shape variation along PC1, an increasing in proximo-distal direction is recorded due to relocation of fixed pseudo-landmarks: L1 and L6 are the only landmarks moving in a distal direction but towards the palmar and the dorsal surface, respectively, L2, L3 and L5 move towards the dorsal surface of the bone and also proximally, L4 moves in medial and proximal directions. About surface semi-landmarks, they move towards the centre of the enthesis from both dorsal and palmar entheseal outlines. Contrary to PC1, a decreasing in proximo-distal way can be analysed: L1 and L4 move in opposite directions, lateral and medial respectively, L2 and L3 both move laterally while L5 and L6 both move medially. As a result, an antero-posterior shift can be seen when analysing the two different morphologies along PC2. No variation is recorded in correspondence of surface semi-landmarks. Along PC3, all fixed pseudo-landmarks relocate: L1 and L2 both move distally, L3 and L4 move proximally but in opposite directions, lateral and medial respectively, while L5 and L6 both move in a medial direction, going proximally and distally, respectively. About surface semi-landmarks, those located close to the dorsal surface shift towards the centre of the enthesis, going in proximal or distal directions according to their initial position; same considerations can be made for those lying in correspondence of the palmar side. With regard to PC4, an increasing in antero-posterior way is shown, due to repositioning of the fixed pseudo-landmarks of the dorsal and palmar outlines: both L2 and L3 move towards the lateral side of the bone, L5 moves in a palmar direction and L6 moves distally and in a lateral direction, partially.

Proceeding with the description of the analyses previously shown, partially separation between samples can be seen. The larger samples of SP and EM have partially grouped for negative values of PC1, but most of EM is distinct from SP. Concerning the small samples of UoT and MH, these specimens have a distribution for negative values of PC1 and positive ones for PC2 and result completely distinct from the large sample (**Figure 84**). A similar distribution results when PC3 is introduced: the difference is about the distribution of MH and UoT along PC3, with negative values for both PC1 and PC3. In **Figure 85** and **Figure 86**, same resulting groups have been obtained, with evident separation between the Spanish samples (SP and EM) and the Neolithic ones (MH and UoT). What emerges is that specimens from MH and UoT are characterised by small entheses, narrower than the entheseal sites of individuals from SP and EM.

4.6.1.2 ADP enthesis

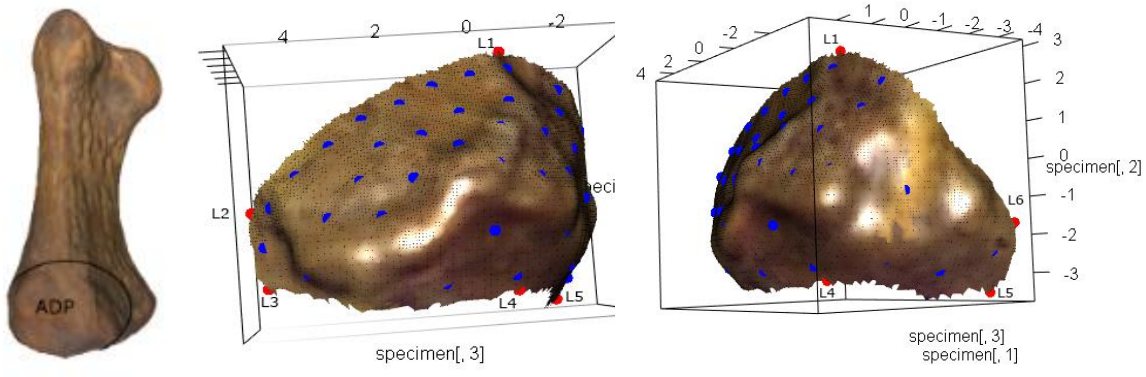

Figure 87 - On the left, the PP1 bone with delimited entheses.
On the right, the landmarks (red spots) and semi-landmarks (blue spots) on the 3D model of the surface of ADP.
For the landmarks' definitions, see Annexes (cf. A2 – 6).

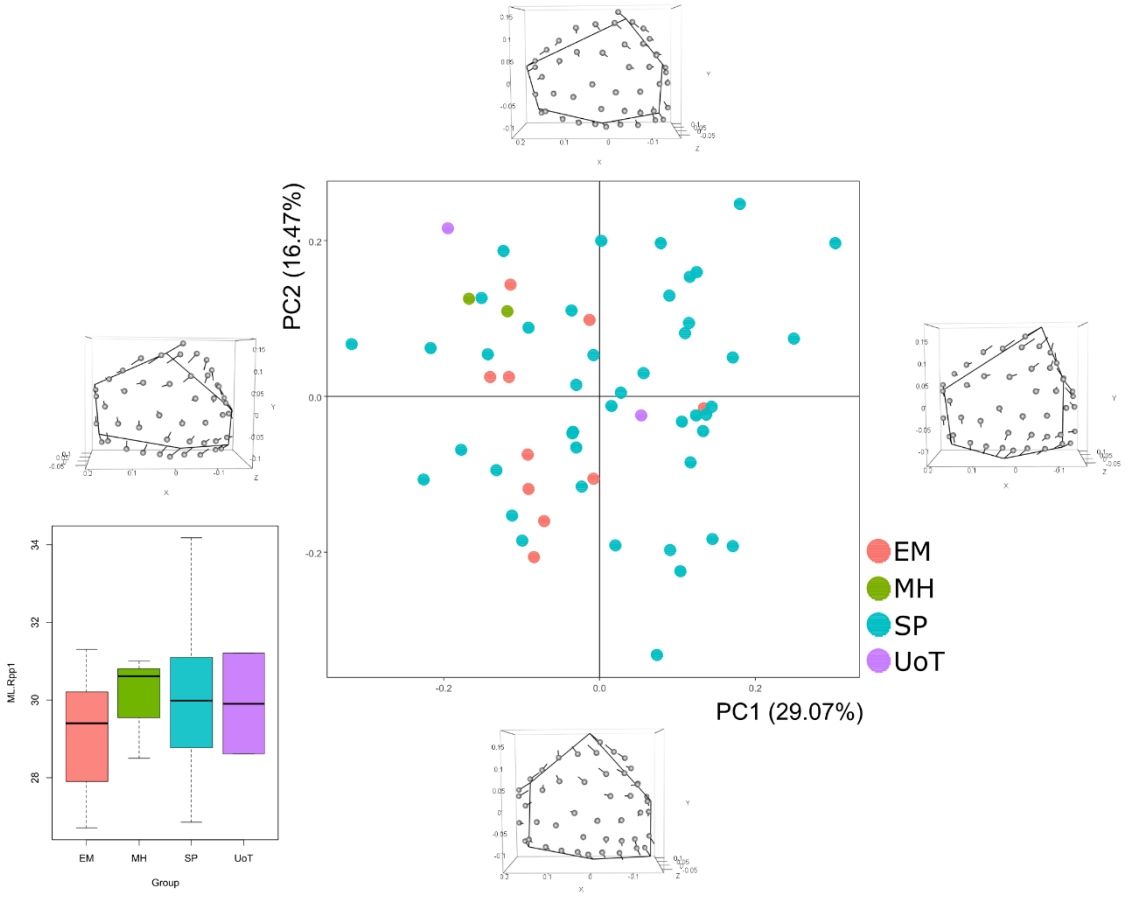

Figure 88 - Principal Component Analysis on the entire set of landmarks and shape configuration at the extremes of PC1 and PC2 for right ADP.

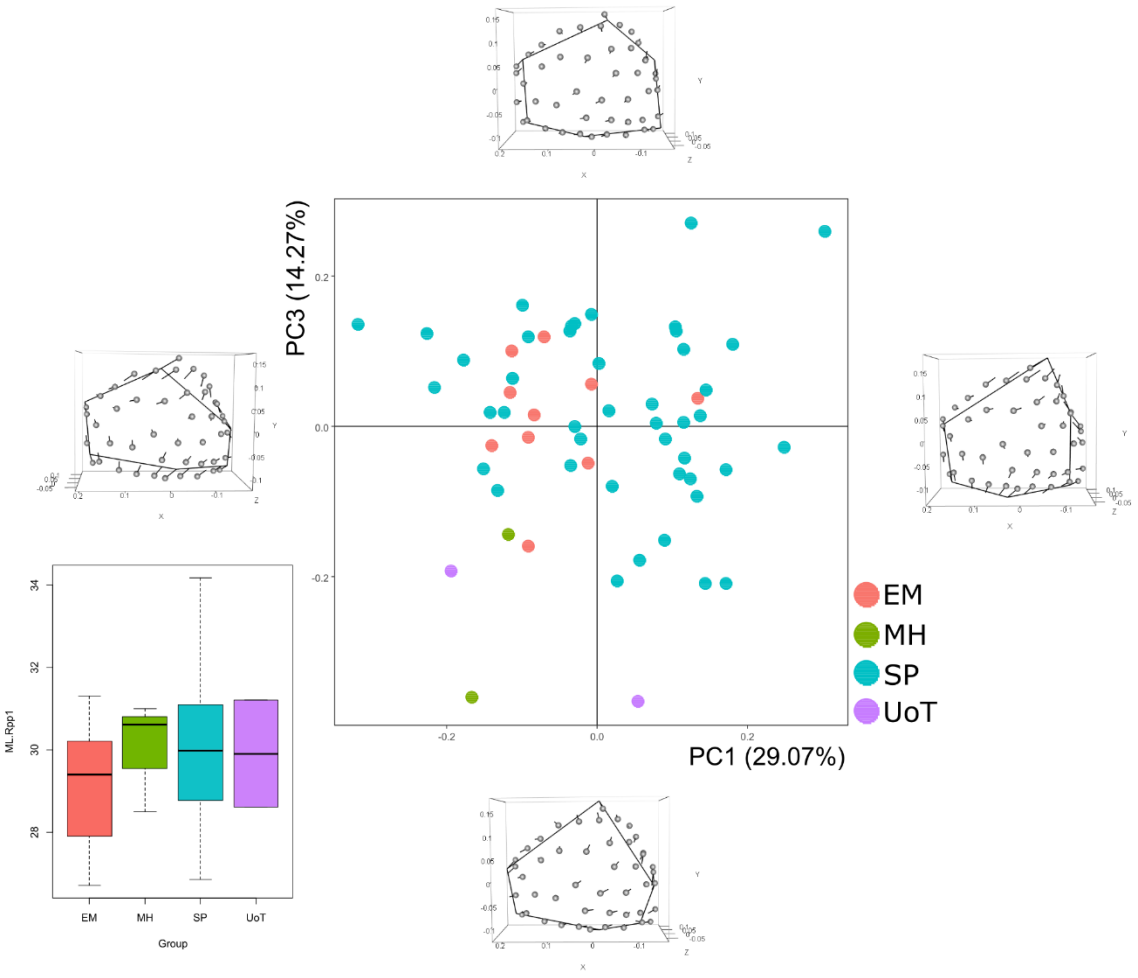

Figure 89 - Principal Component Analysis on the entire set of landmarks and shape configuration at the extremes of PC1 and PC3 for right ADP.

For the analyses of ADP of right PP1 (**Figure 87**), a total of 58 specimens were available. Here, the first three PCs were analysed, representing the 60% of the total variance.

Describing shape variation for each PC, along PC1 both fixed and surface landmarks relocate and cause an increasing in a proximo-distal way: L1 moves towards the palmar surface, going distally, L2 and L3 both move proximally, L4 moves also proximally, and both L5 and L6 move along the corresponding outlines where they lie, moving toward L4 and L1, respectively. About surface semi-landmarks, those located on the distal entheseal outline move distally and in a palmar direction, while some lying on the proximal outline move proximally: this shape variation causes an increasing of the entheseal size in a proximo-distal way and also a decreasing in an antero-posterior direction. With regard to PC2, most variation is due to fixed pseudo-landmarks, whose movements determine an increasing in size in an antero-posterior direction: L1 moves towards L6, along the distal aspect of the entheseal outline close to the palmar surface, L2 and L3 both move towards the dorsal surface of the bone, L4 partially moves towards the centre of the enthesis, and L5 moves distally. About surface semi-landmarks, those located in correspondence of the entheseal outline move towards the centre of the enthesis, determining a reduction in a proximo-distal direction. When considering PC3, a minimum reduction in entheseal shape is recorded: most of the variation is due to fixed pseudo-landmarks from L2 to L6, in particular: L2 moves in a distal direction along the entheseal outline towards L1, L3 moves along the proximal outline towards L4, L4 moves towards the dorsal surface of the bone, L5 goes in a palmar direction and L6 relocates in both distal and palmar directions. As a result, these changes cause a reduction in correspondence of the distal portion of the enthesis and an increasing in antero-posterior direction.

Proceeding with descriptions of analyses shown in **Figure 88** and **Figure 89**, no separation between groups is shown, due also to the small dimension of the samples from MH and UoT. A global distribution is shown when analysing PC1 and PC2, with specimens from the two small samples distributed for positive values for PC2 and negative ones for PC1. One exception is one specimen from UoT, with positive values of PC1 and negatives ones for PC2. Also, particular distribution is about EM, located on the left side of the graph, with one specimen falling also into the same group where the exception from UoT is. As a result, these specimens are characterised by reduced entheses in a proximo-distal way. When PC3 is introduced, different distribution for UoT and MH can be seen: these four specimens are distinct from the SP and EM and their distribution is for negative values of PC3.

4.6.2 Left PP1 - Descriptive statistics, normality tests and correlation analyses

	raw size - ABP+FBP	ERS - ABP+FBP	raw size - ADP	ERS - ADP	APWM/ML*	MLWM/ML*	ML*
N	58	57	52	52	60	60	60
Min	58,77	0,05	39,87	0,05	0,15	0,24	26,55
Max	184,60	0,14	142,90	0,14	1,95	2,05	34,17
Mean	106,55	0,10	97,07	0,09	0,23	0,33	29,51
Stand. dev	25,01	0,02	23,86	0,02	0,23	0,23	1,68

Table 40 - Summary statistics for both 3D size and linear dimensions for left PP1. Raw size is calculated in mm^2, ML is calculated in mm. **APWM/ML**: Antero-Posterior Robusticity Index. **MLWM/ML**: Medio-Lateral Robusticity Index. **ML**: Maximum Length.

	raw size - ABP+FBP	ERS - ABP+FBP	raw size - ADP	ERS - ADP	APWM/ML*	MLWM/ML*	ML*
N	58	57	52	52	60	60	60
Shapiro-Wilk W	0,96	0,98	0,98	0,96	0,17	0,21	0,96
p(normal)	0,07	0,60	0,66	0,06	1,167E-16	2,506E-16	0,05

Table 42 - Shapiro-Wilk test for each variable of left PP1.

	raw size - ABP+FBP	ERS - ABP+FBP	raw size - ADP	ERS - ADP
APWM/ML*	0,23	-0,02		0,07
MLWM/ML*		0,13		0,18
ML*		0,11		-0,12

Table 41 - Correlation tests between 3D bone sizes and linear dimensions for left PP1.

In **Tables 40 – 42**, descriptive statistics, correlation tests and normal distribution tests for all the variables used in this work are summarized.

The set of values for the entheses of left PP1 are similar, according to their comparable dimensions on the base of the bone. With regard to normality tests for each variable of left PP1, the Shapiro-Wilk's test has verified a normal distribution with a *p-value* > 0.05 for all variables except for the antero-posterior and medio-lateral RIs.

Correlation tests were performed: positive relations have been recorded between raw size and ERS of both entheses and total surface size. About relation between entheseal size (raw and ERS) and bone dimensions, ERS indexes of both entheses correlate with all linear measurements (with negative correlations between ERS of ABP+FBP and antero-posterior RI and also between ERS of ADP and maximum length), while only raw size of ABP+FBP enthesis positively correlates with antero-posterior RI.

4.6.2.1 ABP+FBP enthesis

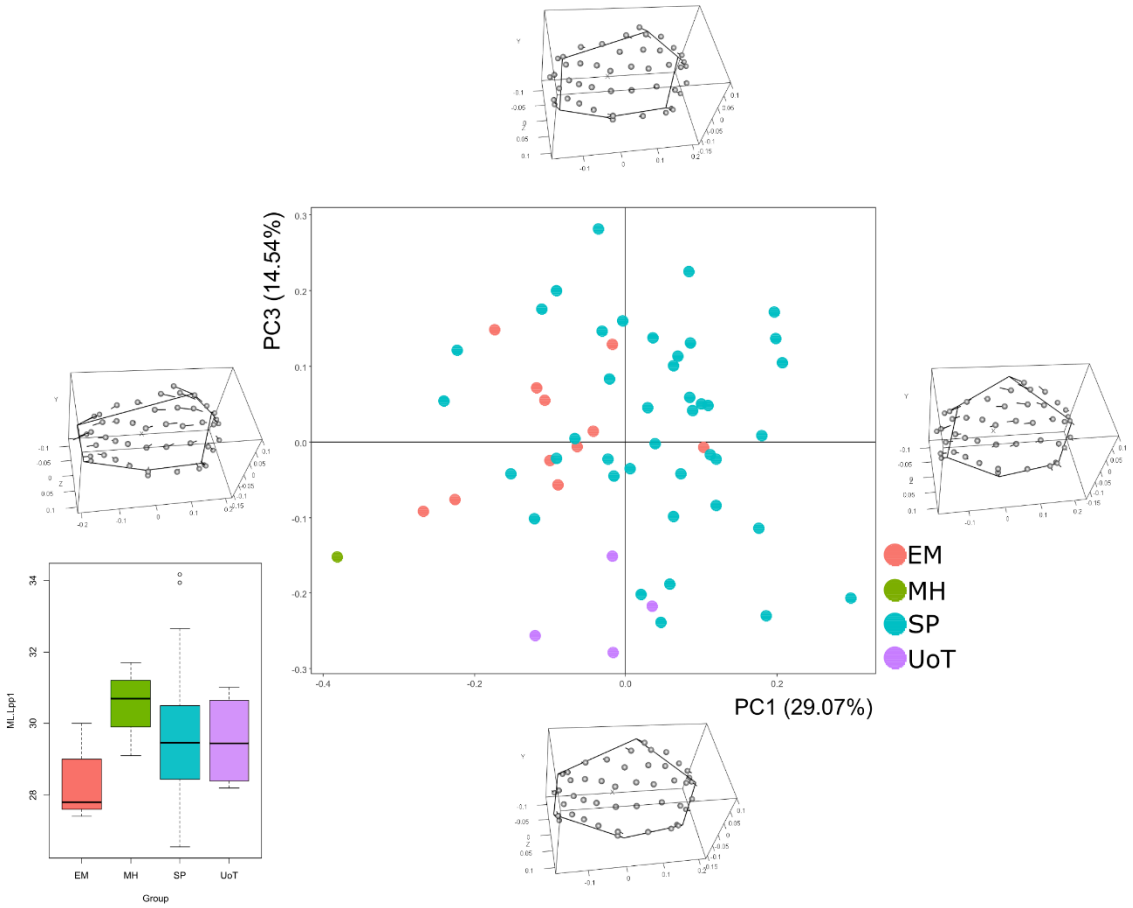

Figure 90 - Principal Component Analysis on the entire set of landmarks and shape configuration at the extremes of PC1 and PC3 for left ABP+FBP

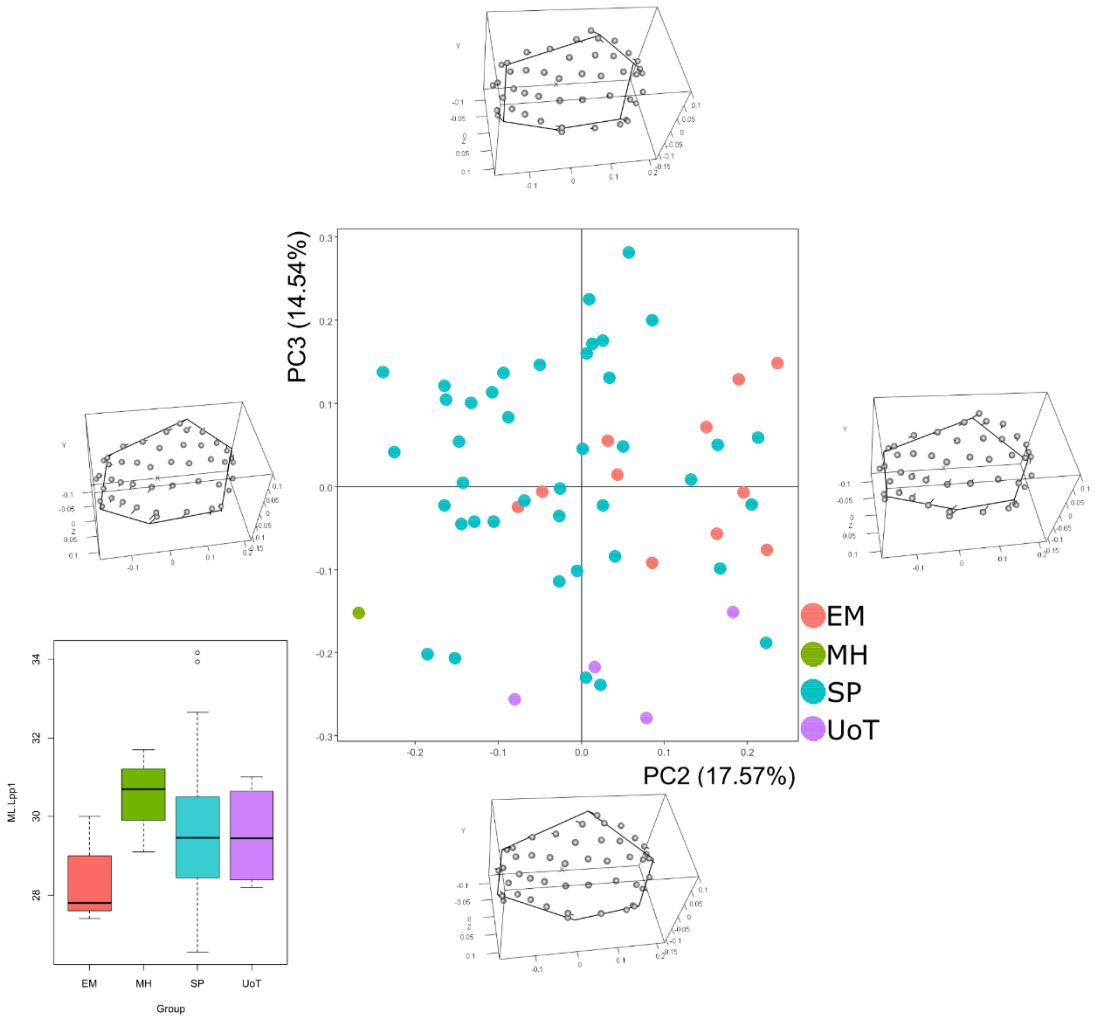

Figure 91 - Principal Component Analysis on the entire set of landmarks and shape configuration at the extremes of PC2 and PC3 for left ABP+FBP.

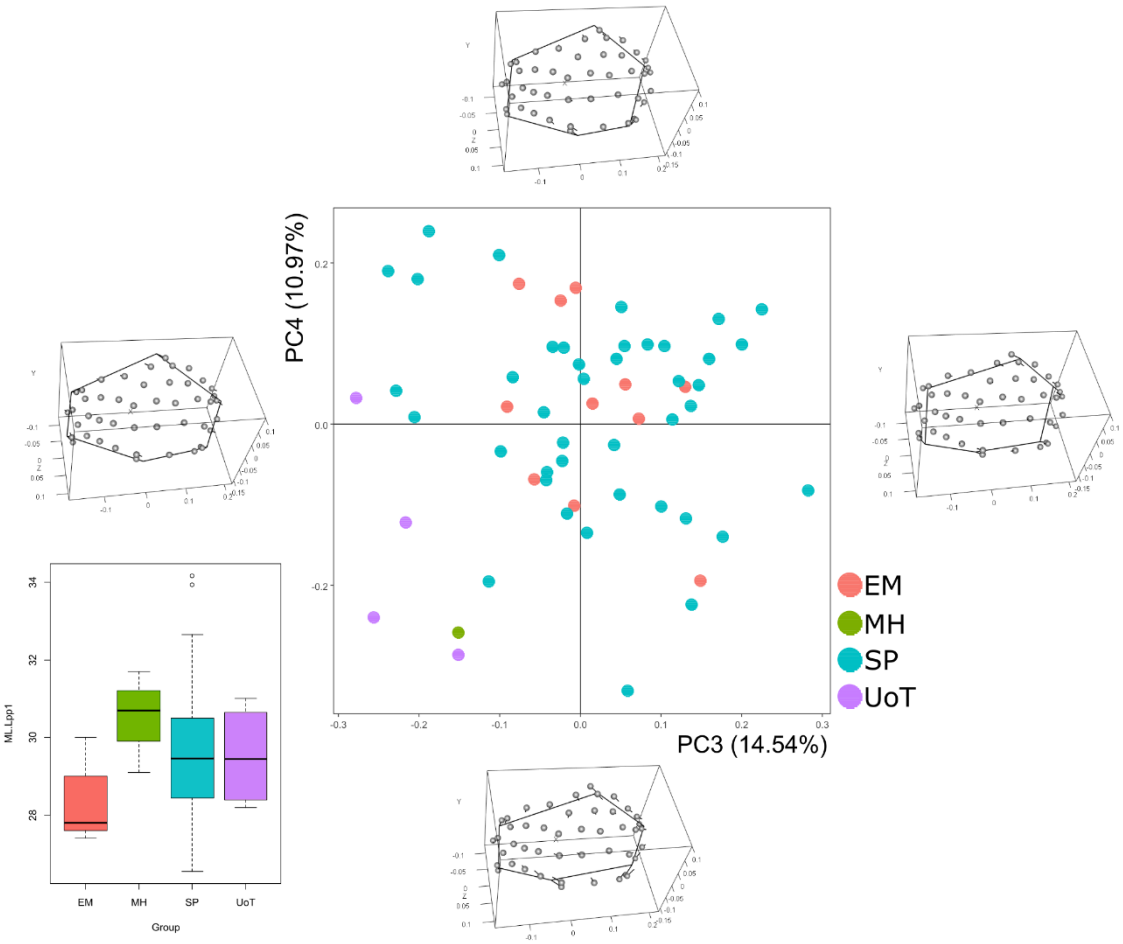

Figure 92 - Principal Component Analysis on the entire set of landmarks and shape configuration at the extremes of PC3 and PC4 for left ABP+FBP.

For the analyses of ABP+FBP of left PP1, a total of 57 specimens were available. Here, the first four PCs were analysed, representing about the 73% of the total variance.

Analysing shape variation along PC1, all fixed and surface semi-landmarks change position, causing an increasing of entheseal shape in a proximo-distal direction. About fixed pseudo-landmarks, L1 is the only landmark moving both distally and towards the dorsal surface, while L2, L3, L5 and L6 all move in a palmar direction; also, L4 moves in proximal and medial directions. About surface semi-landmarks, those located close to the dorsal and palmar outlines move towards the palmar surface, while some of them located in correspondence of the centre of the enthesis move towards the dorsal entheseal outline, made up of L2 and L3. With regard to PC2, a decreasing in a proximo-distal way is recorded, according to fixed pseudo-landmarks: both L1 and L2 move in both proximal and dorsal directions, while L3 move dorsally but in a distal direction, both L4 and L5 go towards the palmar surface, moving distally, and L6 moves in a proximal direction. About surface semi-landmarks, some of them – close to the proximal entheseal outline and located between L3 and L4 – move distally, causing an additional shape decreasing in correspondence of the dorsal entheseal aspect. Along PC3, minimum variation occurs in correspondence of fixed pseudo-landmarks: L1 and L4 move in opposite directions, palmar and dorsal respectively, while L2, L3, L5 and L6 move medially. With regard to PC4, relocation of all fixed pseudo-landmarks determines an increasing in entheseal shape in a proximo-distal direction: L1 moves both distally and dorsally, L2 and L3 both move towards the dorsal surface, going medially but also distally and proximally respectively, L4 moves opposite than L1, L5 moves proximally, going towards L4, while L6 has a minimum variation, going dorsally.

Proceeding in descriptions of PCA plots previously shown (**Figures 90 – 92**), separation between groups can be seen. Main distinction is between both UoT and MH and the Spanish samples – from SP and EM – UoT is characterised by negative values of PC3, the unique specimen from MH has negative values for both PCs, EM has a distribution for negative values of PC1, while SP is distributed all over the graph. One peculiarity is a specimen from EM, which falls into SP and, as a result, it is characterised by a larger enthesis in a proximo-distal way (**Figure 90**). A similar distribution for MH and UoT has been obtained even when considering other PCs; on the contrary, different situation is about EM, which is distributed for positive values PC2 (**Figure 91**; Annexes: cf. A4 – 20) and UoT distributed for both negative vales of PC3 and PC4 (**Figure 92**).

4.6.2.2 ADP enthesis

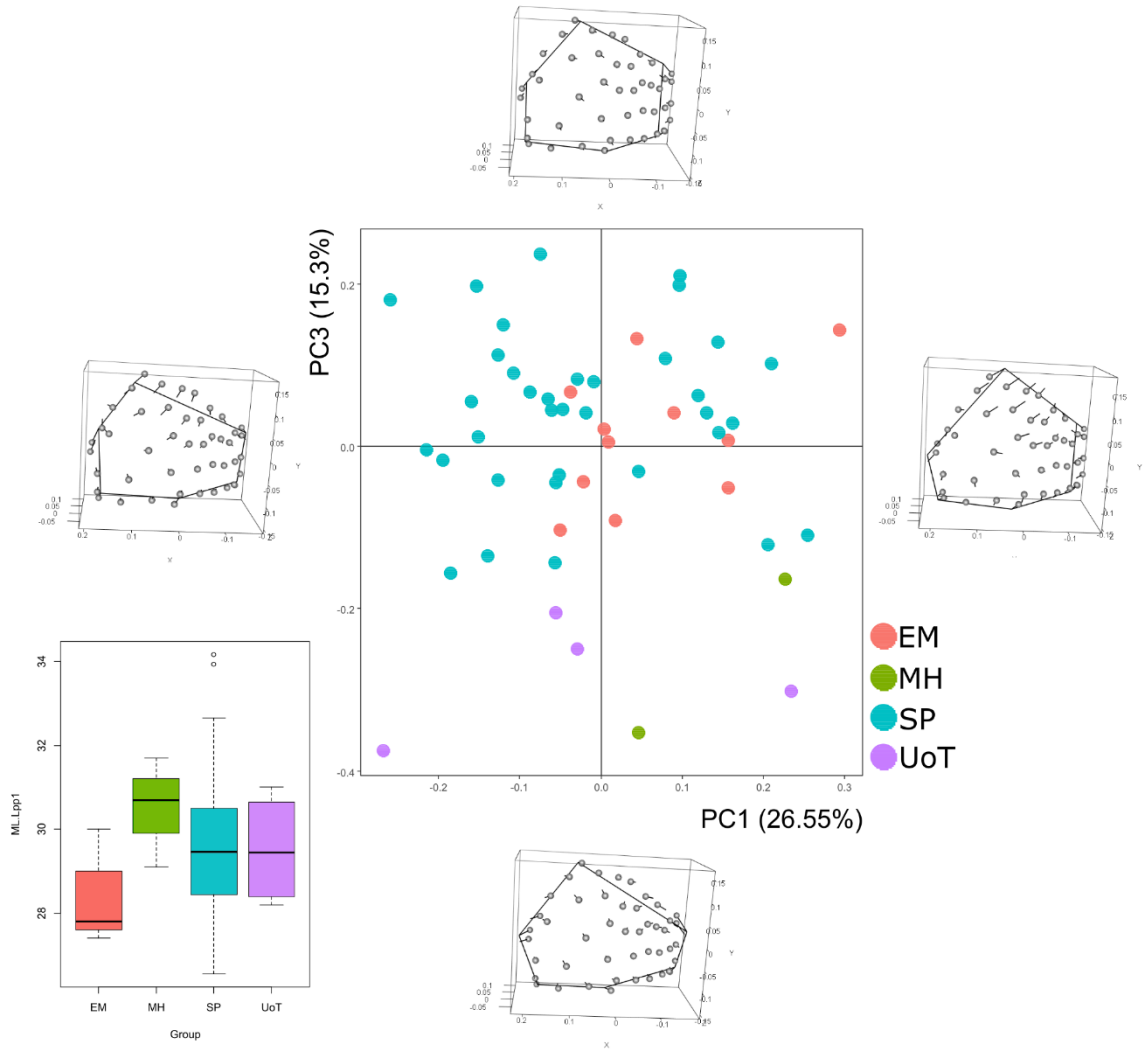

Figure 93 - Principal Component Analysis on the entire set of landmarks and shape configuration at the extremes of PC1 and PC3 for left ADP.

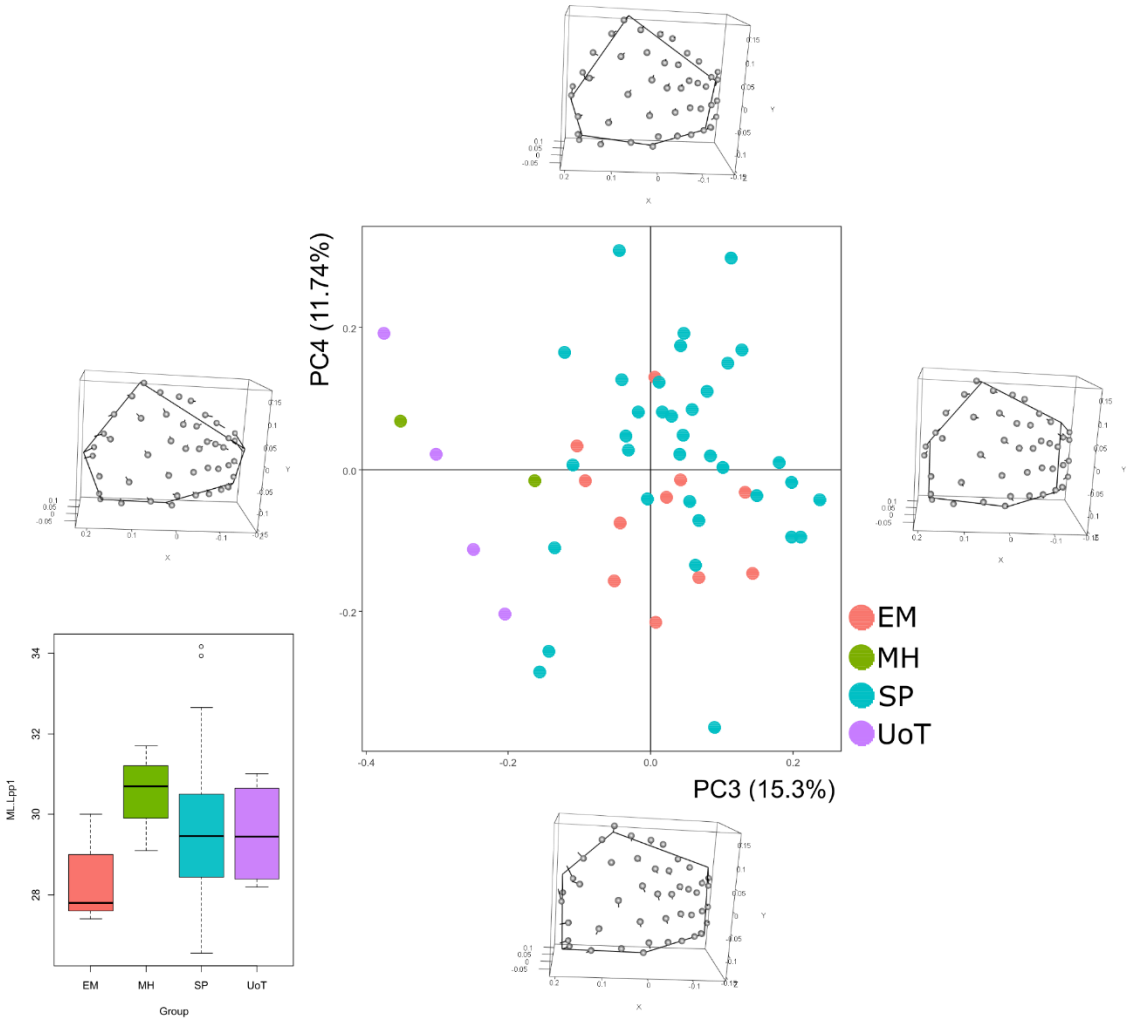

Figure 94 - Principal Component Analysis on the entire set of landmarks and shape configuration at the extremes of PC3 and PC4 for left ADP.

For the analyses of ADP of left PP1, a total of 52 specimens were available. Here, the first four PCs were analysed, representing about the 73% of the total variance.

Regarding shape variation along PC1 axis, repositioning of all fixed pseudo-landmarks causes variation in correspondence of the distal aspect of the entheseal outline, in particular due to relocation of L1, moving both distally and dorsally. About the other landmarks, L2 and L3 move along the corresponding distal and proximal entheseal outlines respectively towards the palmar surface of the bone, L4 move both proximally and laterally, L5 and L6 both move towards the proximal epiphysis. With regard to surface semi-landmarks, most variation is on the bone projection close to the dorsal surface, whose landmarks move distally. Regarding PC2, important variation is recorded in a proximo-distal way, because of decreasing in shape dimension due to landmarks L1 and L4 – moving proximally and distally, respectively. Also, variation can be seen in an antero-posterior direction, due to L2 and L3, both moving in a palmar direction. About surface semi-landmarks, those lying in correspondence of the proximal and distal aspects of the entheseal outlines – close to the dorsal surface – move towards the centre of the enthesis. Along PC3, some fixed landmarks relocate: L2 and L3 both move medially, and L5 and L6 both move medially but in distal and proximal directions, respectively: so, most evident shape variation is in antero-posterior direction, due to L2 and L6. About PC4, variation occurs in correspondence of the palmar aspect of the entheseal outline, due to relocation of L6 to a proximal position. Other fixed landmarks moving are: L1 moving distally, L2 moving both proximally and laterally, and both L3 and L5 moving in a lateral direction.

Here, distinct groups can be seen when PC3 is considered: in each case, samples of UoT and MH have a distribution for negative values of PC3 – these specimens are characterised by wider entheses in an antero-posterior direction. About the other samples, when describing **Figure 93**, EM has no particular distribution, but SP is divided into two group by the first one: part of the big medieval sample is distributed for negative values of PC1 – it is characterised by entheses whose most distal point is close to the dorsal surface – and the other part has a positive distribution for both PC1 and PC3. Similar distribution can be seen also in **Figure 94**, with MH and UoT separated by SP and EM groups; also, EM divide into two portion SP.

4.7 Analyses of 2nd proximal phalanges

4.7.1 Right PP2 – Descriptive statistics, normality tests and correlation analyses

	raw size - DI1	ERS - DI1	raw size - PI1	ERS - PI1	APWM/ML*	MLWM/ML*	ML*
N	65	61	70	65	70	70	70
Min	91,99	0,07	66,80	0,06	0,12	0,18	30,20
Max	227,69	0,13	172,67	0,11	0,20	0,29	50,30
Mean	157,05	0,11	119,18	0,08	0,16	0,24	39,65
St	33,78	0,01	31,57	0,01	0,01	0,02	3,78

Table 43 - Summary statistics for both 3D size and linear measurements of right PP2. Raw size is calculated in mm^2, ML in calculated in mm. **APWM/ML**: Antero-Posterior Robusticity Index. **MLWM/ML**: Medio-Lateral Robusticity Index. **ML**: Maximum Length.

	raw size - DI1	ERS - DI1	raw size - PI1	ERS - PI1	APWM/ML*	MLWM/ML*	ML*
N	65	61	70	65	70	70	70
Shapiro-Wilk W	0,98	0,97	0,99	0,99	0,98	0,99	0,93
p(normal)	0,53	0,14	0,73	0,65	0,21	0,65	0,00111

Table 44 - Shapiro-Wilk test for each variable of right PP2.

	raw size - DI1	ERS - DI1	raw size - PI1	ERS - PI1
APWM/ML*		0,12		
MLWM/ML*				
ML*		-0,04		0,07

Table 45 - Correlation tests between 3D bone sizes and linear dimensions for right PP2.

In **Tables 43 - 45**, descriptive statistics, correlation tests and normal distribution tests for all the variables used in this work are summarized.

The set of values for the entheses of PP2 are similar, according to their comparable dimensions on the base of the bone. With regard to normality tests for each variable of right PP2, the Shapiro-Wilk's test has verified a normal distribution with a *p-value* > 0.05 for all variable, except for maximum bone length. Correlation tests were performed: positive relations have been recorded between total surface size and both raw size and ERS of DI1 enthesis and raw size of PI1 enthesis, while a negative one has been recorded for total surface size and ERS index of PI1. About relation between entheseal size (raw and ERS) and bone dimensions, unique correlations are between ERS index of DI1 and antero-posterior RI and ML (this latter characterised by a negative one), and between ERS index of PI1 and ML.

4.7.1.1 DI1 enthesis

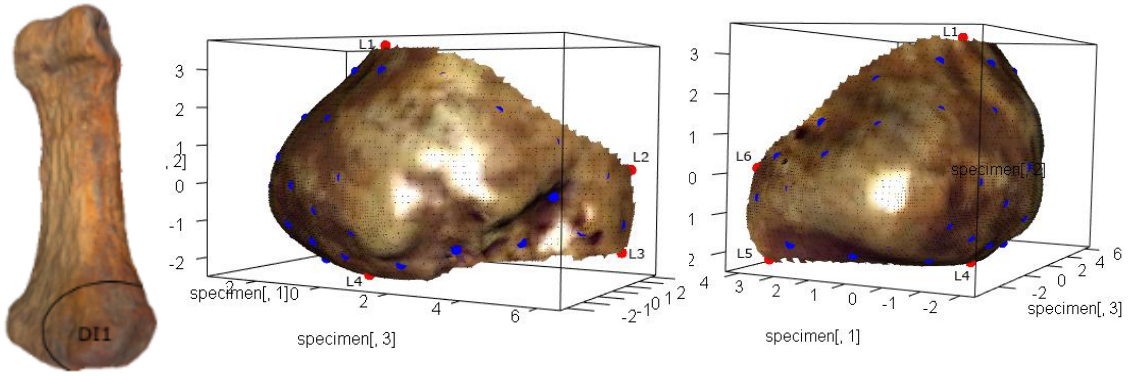

Figure 95 - On the left, the PP2 bone with delimited enthesis.
On the right, the landmarks (red spots) and semi-landmarks (blue spots) on the 3D model of the surface of DI1.
For the landmarks' definitions, see Annexes (cf. A2 – 7).

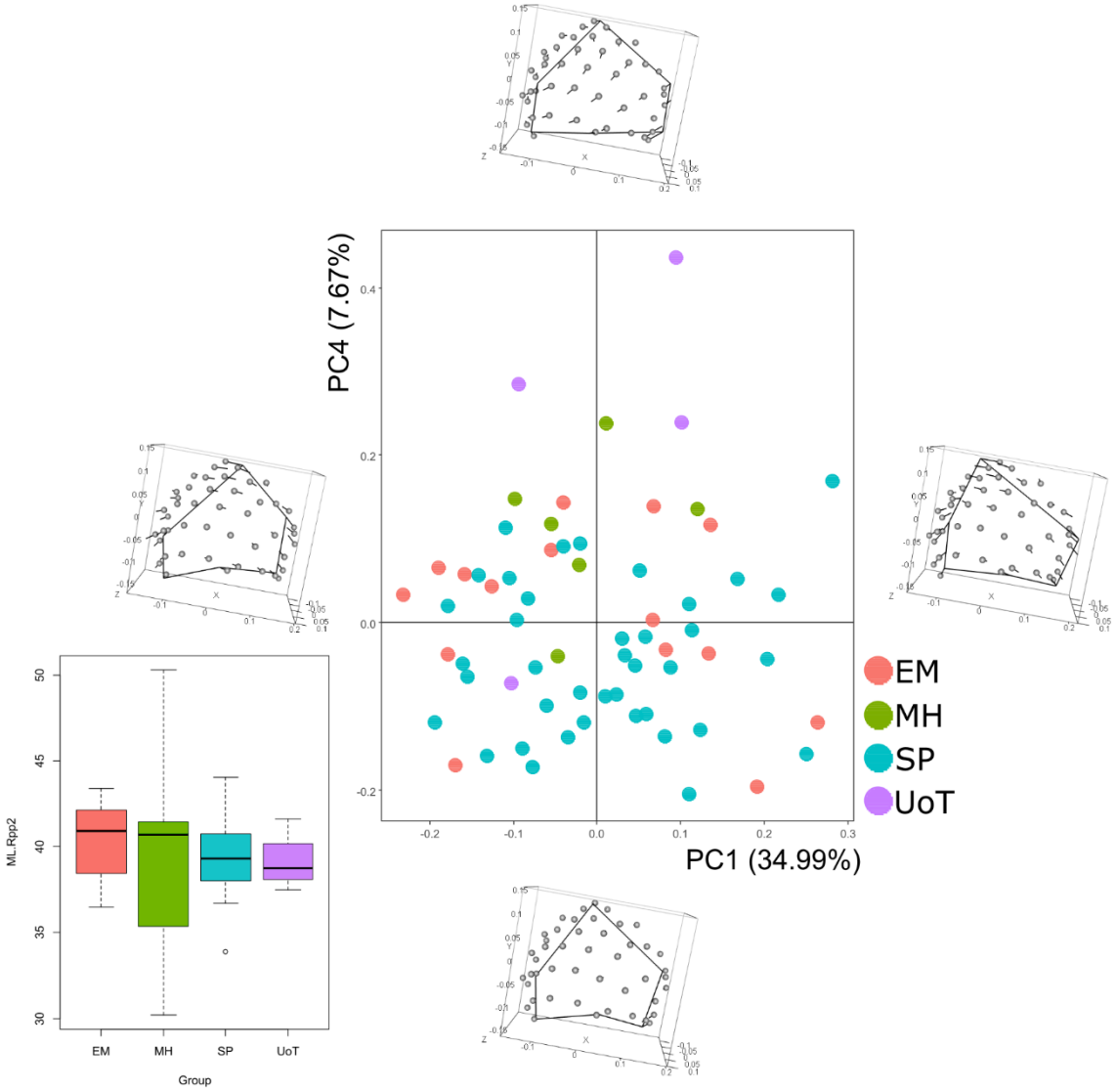

Figure 96 - Principal Component Analysis on the entire set of landmarks and shape configuration at the extremes of PC1 and PC4 for right DI1.

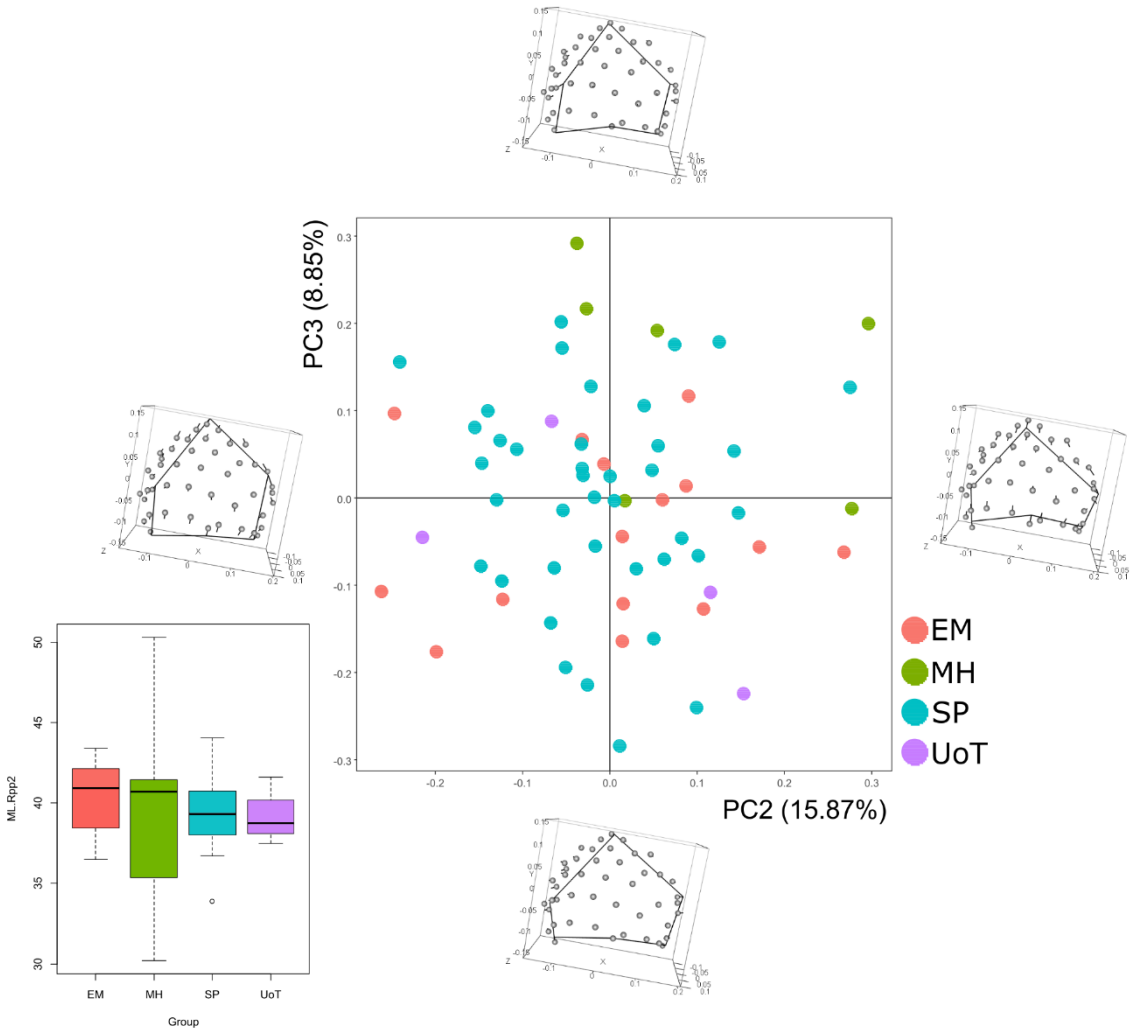

Figure 97 - Principal Component Analysis on the entire set of landmarks and shape configuration at the extremes of PC2 and PC3 for right DI1.

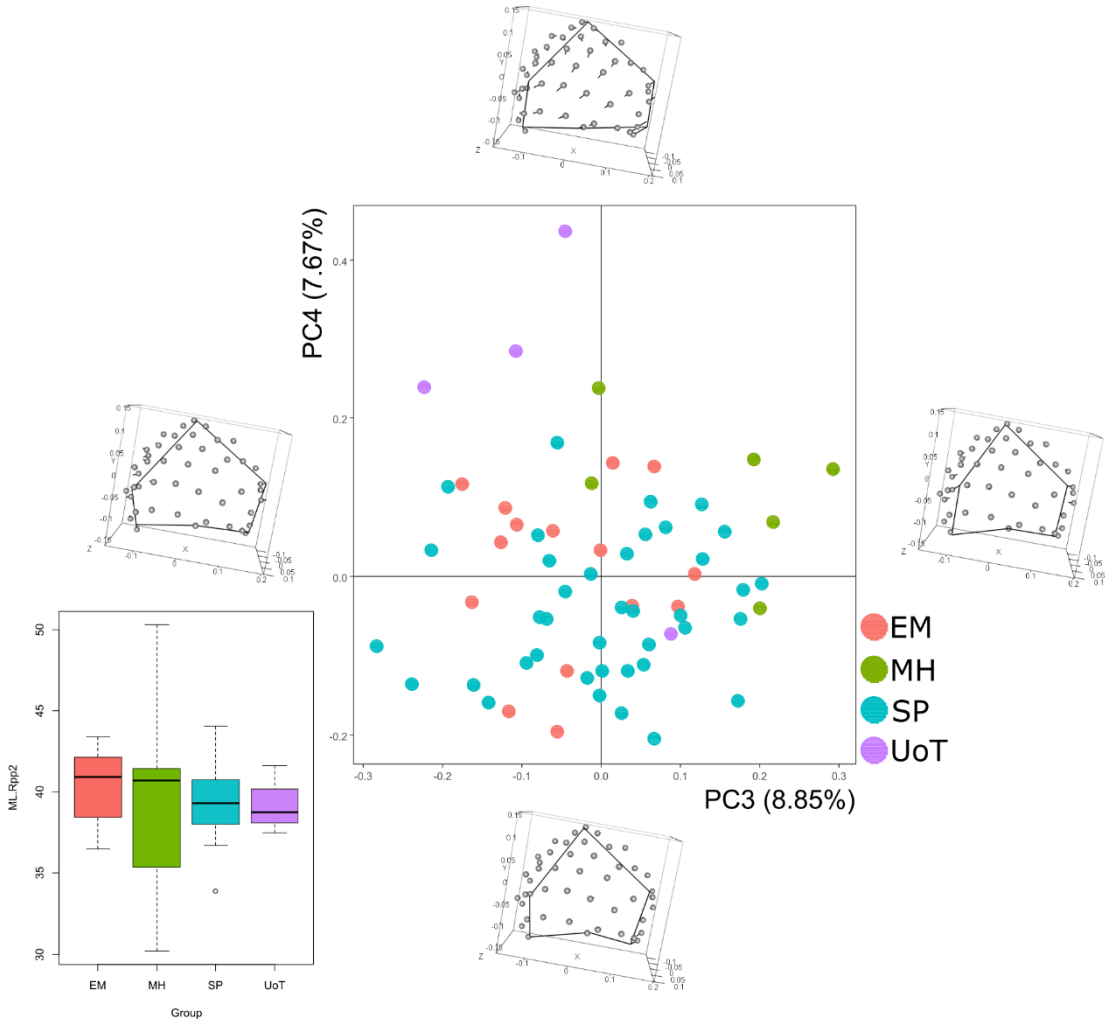

Figure 98 - Principal Component Analysis on the entire set of landmarks and shape configuration at the extremes of PC3 and PC4 for right DI1.

For the analyses of DI1 of right PP2 (**Figure 95**), a total of 64 specimens were available. Here, the first four PCs were analysed, representing about the 70% of the total variance.

Analysing shape variation along PC1, this is due to relocation of all kind of landmarks, but major variation is in correspondence of L1 and the dorsal aspect of the entheseal outline and surface semi-landmarks located on the palmar portion of the enthesis: L1 moves in a palmar direction, together with some surface semi-landmarks located on the central part of the enthesis, both L2 and L3 move dorsally, towards the proximal epiphysis, while L4, L5 and L6 partially move in a dorsal direction. About the other surface landmarks, those located close to the dorsal and palmar aspects of the entheseal outline go in a dorsal direction. Along PC2, relocation of fixed pseudo-landmarks causes a decreasing in a proximo-distal direction and an increasing in antero-posterior way: L1 and L4 move in opposite directions, going proximally and distally, respectively, L2 and L6 move both proximally and medially, and L3 and L6 move both proximally and distally. No particular variation is due to surface semi-landmarks, except for some of them located in correspondence of the proximal aspect of the entheseal outline, which move distally and determine a shift on this part of the outline. With regard to PC3, a decreasing in antero-posterior direction is recorded due to relocation of fixed pseudo-landmarks on dorsal and palmar sides of the enthesis, where most of the variation is visible: these are L2, L3, L5 and L6, all moving medially – and L6 also relocating proximally. About PC4, minimum variation is recorded on fixed landmarks L3 and L4, which move medially and laterally, respectively.

In these shape spaces, similar distribution can be seen in **Figure 96** and **Figure 98**, where UoT is distinct from the remaining samples, with a distribution for positive values of PC4, and MH and EM are separated between them along x-axis. Also, a split is recorded for EM in **Figure 96** and **Figure 97**, due to the different entheseal morphologies on PC1 and PC2 shown on the two graphs.

4.7.1.2 PI1 enthesis

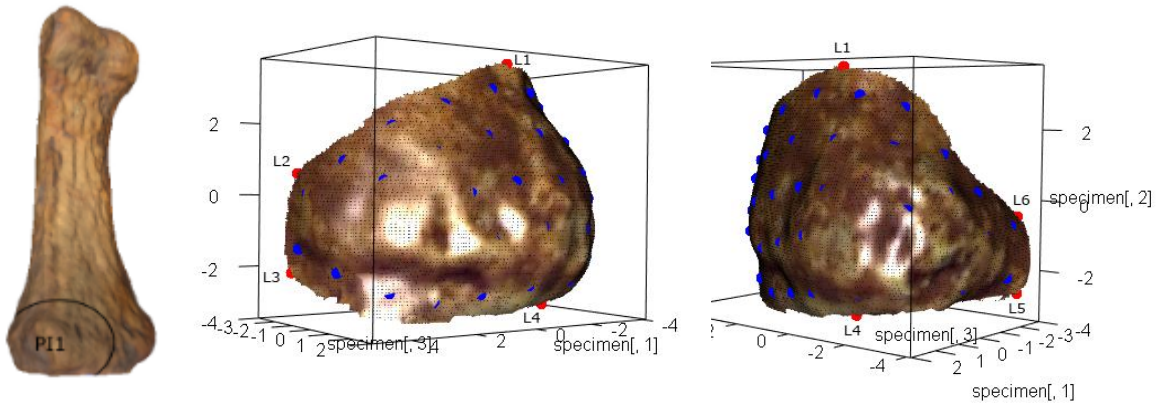

Figure 99 - On the left, the PP2 bone with delimited entheses.
On the right, the landmarks (red spots) and semi-landmarks (blue spots) on the 3D model of the surface of PI1.
For the landmarks' definitions, see Annexes (cf. A2 – 7).

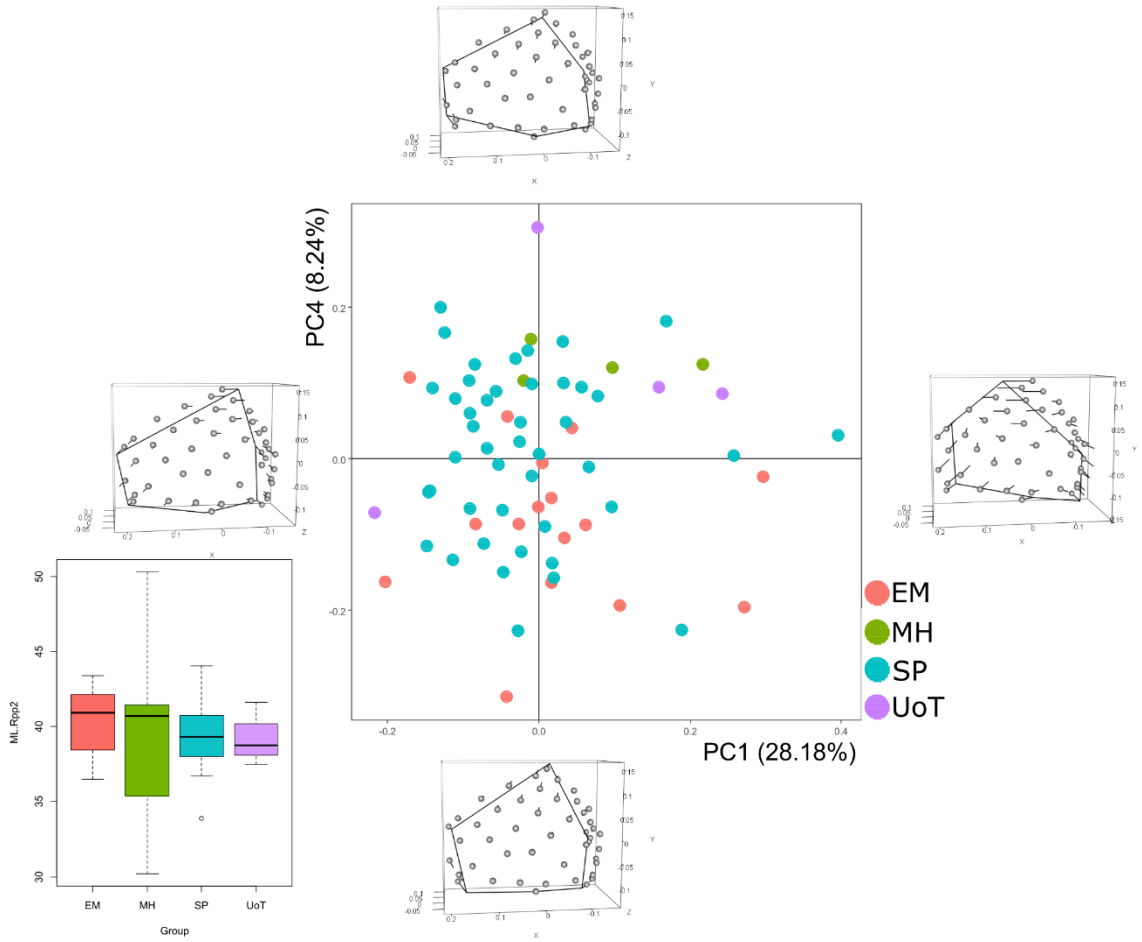

Figure 100 - Principal Component Analysis on the entire set of landmarks and shape configuration at the extremes of PC1 and PC4 for right PI1.

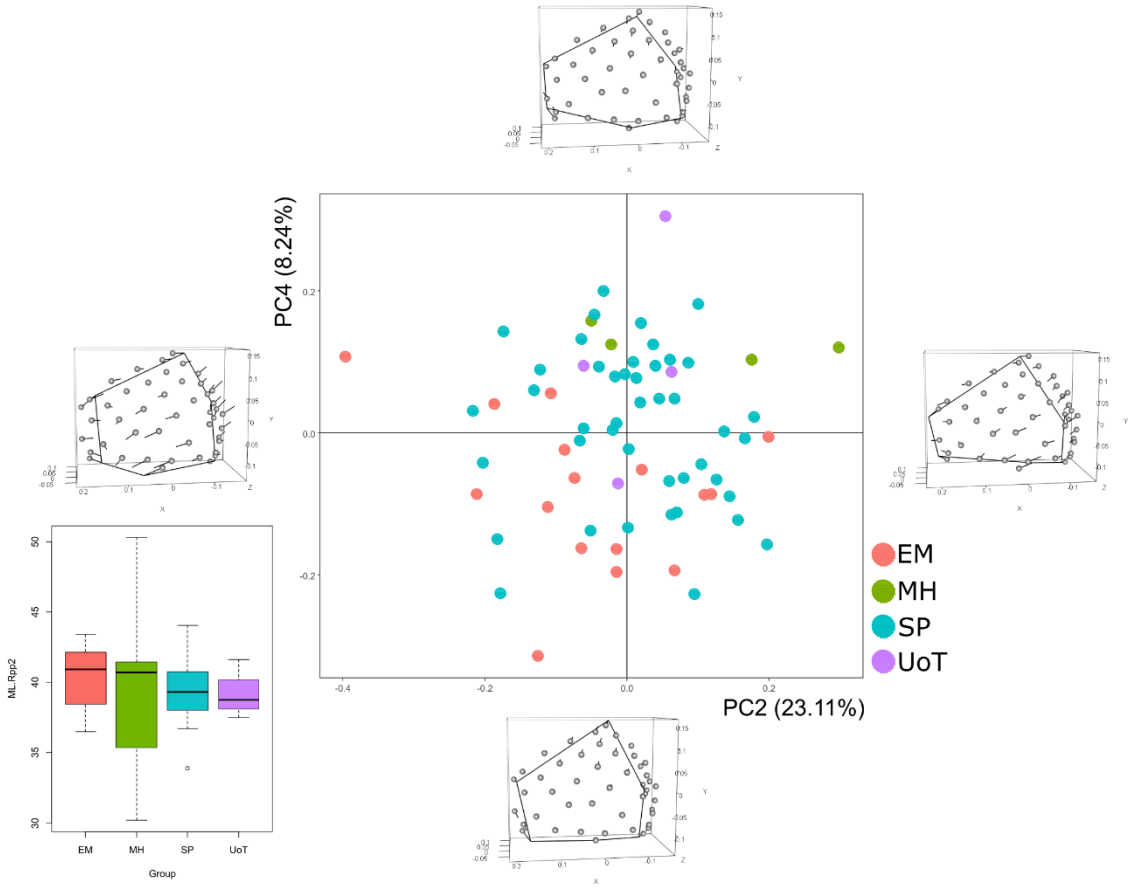

Figure 101 - Principal Component Analysis on the entire set of landmarks and shape configuration at the extremes of PC2 and PC4 for right PI1.

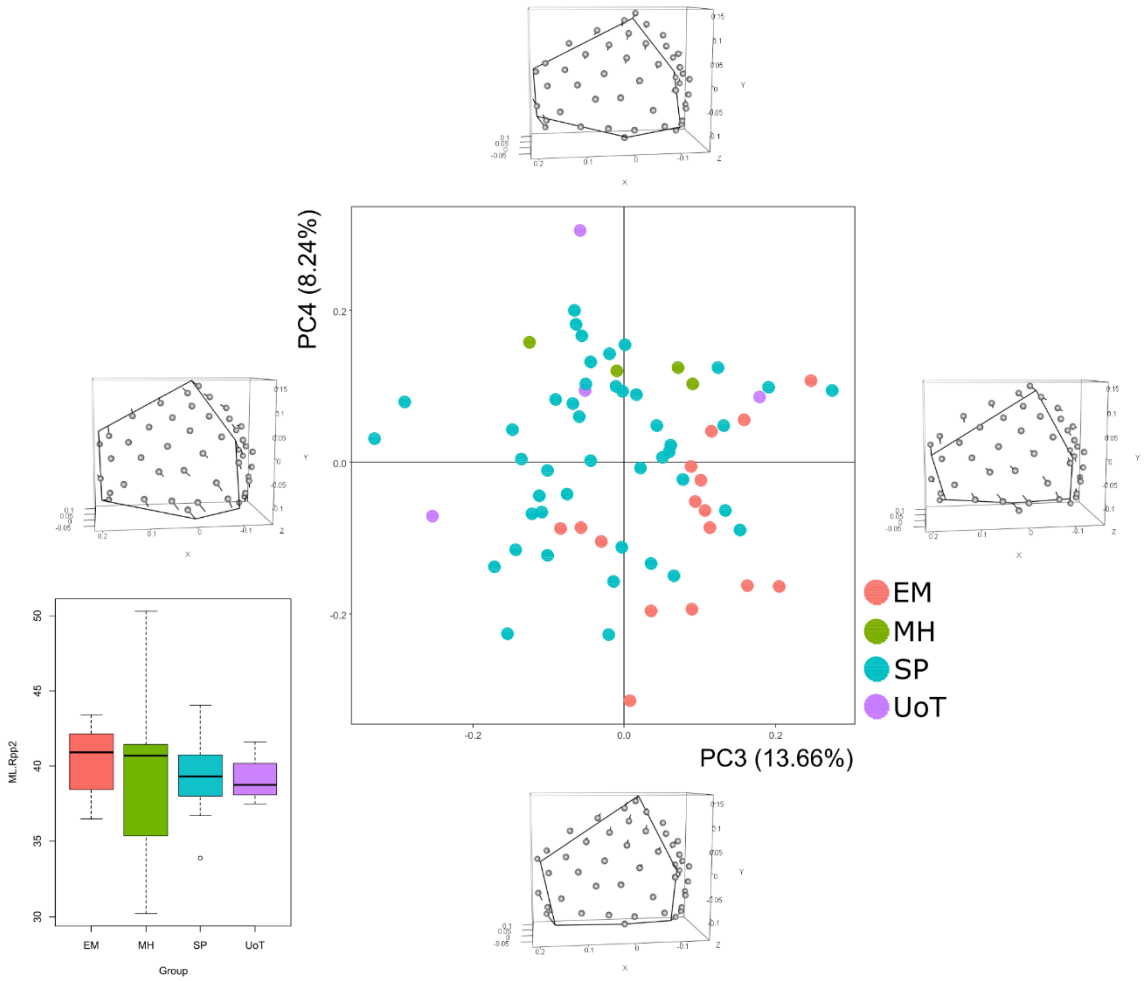

Figure 102 - Principal Component Analysis on the entire set of landmarks and shape configuration at the extremes of PC3 and PC4 for right PI1.

For the analyses of PI1 of right PP2 (**Figure 99**), a total of 68 specimens were available. Here, the first four PCs were analysed, representing about the 75% of the total variance.

Proceeding with descriptions of entheseal morpho-spaces, along PC1 variation is about both fixed and surface landmarks: L1 is the only landmark moving dorsally which determine the most important shape variation, while landmarks from L2 to L6 all move in a palmar direction – with L2 and L3 going distally and L5 and L6 moving proximally. About surface semi-landmarks, some located on the palmar and dorsal entheseal outlines move in a palmar direction, proximally and distally, respectively, while others located close to L1 move towards the dorsal surface. Regarding PC2, shape entheseal variation occurs in both proximo-distal and antero-posterior directions, corresponding to an increasing and a reduction of the entheseal shape. Concerning fixed pseudo-landmarks, L1 and L4 move in opposite directions, dorsal and palmar, respectively, L2 and L3 both move in a lateral direction, while L6 moves towards the proximal end of the bone; L5 could not be considered in this case because of minimum variation to a lateral position. About surface ones, those located on the palmar and proximal aspects of the entheseal outline move toward the centre of the enthesis, while some on the dorsal aspect of the outline continue going dorsally. With regard to PC3, most evident variation is in correspondence of both distal and proximal aspects of the outline of the enthesis, due to relocation of both fixed and surface landmarks, towards the centre of the enthesis – as a result, an entheseal reduction in a proximo-distal way and a increasing in antero-posterior direction can be seen. About fixed pseudo-landmarks, L1 moves dorsally and in a medio-palmar direction, L2 and L6 both move in a proximal direction, L3 and L5 both move medially and L4 moves opposite than L1, going both distally and dorsally. About PC4, fixed pseudo-landmarks with an important role in shape variation are L1 (going laterally), L3 and L5 (both going distally) and L4 (moving to a medial direction); with regard to surface semi-landmarks, those located on the most distal portion of the entheseal surface move towards the centre of the enthesis, both proximally and laterally.

Following, plots shown before are discussed, all considering PC4 axis and showing similar distributions for MH and SP (**Figures 100 – 102**). Concerning MH, it is always distributed for positive values of PC4, while EM changes disposition according to different PCs: in **Figure 102**, its main distribution is on the right part of the plot, resulting completely distinct MH: they are so characterised by sharper distal extremities and more flattened proximal entheseal portions than other samples.

4.7.2 Left PP2 – Descriptive statistics, normality tests and correlation analyses

	raw size - DI1	ERS - DI1	raw size - PI1	ERS - PI1	APWM/ML*	MLWM/ML*	ML*
N	60	60	61	61	68	68	68
Min	60,40	0,06	64,77	0,06	0,13	0,19	33,47
Max	243,72	0,15	174,50	0,12	0,22	0,28	45,80
Mean	158,43	0,12	117,28	0,09	0,17	0,24	39,38
Stand. dev	30,76	0,02	22,02	0,01	0,02	0,02	2,32

Table 46 - Summary statistics for both 3D size and linear measurements of left PP2. Raw size is calculated in mm^2, ML in calculated in mm. **APWM/ML**: Antero-Posterior Robusticity Index. **MLWM/ML**: Medio-Lateral Robusticity Index. **ML**: Maximum Length.

	raw size - DI1	ERS - DI1	raw size - PI1	ERS - PI1	APWM/ML*	MLWM/ML*	ML*
N	60	60	61	61	68	68	68
Shapiro-Wilk W	0,9631	0,9631	0,983	0,9835	0,9424	0,9787	0,9738
p(normal)	0,0669	0,06662	0,5553	0,5811	0,003505	0,2944	0,1619

Table 47 - Shapiro-Wilk test for each variable of left PP2.

	raw size - DI1	ERS - DI1	raw size - PI1	ERS - PI1
APWM/ML*	0,10	0,16	0,03	-0,01
MLWM/ML*			0,17	0,01
ML*		-0,02		0,11

Table 48 - Correlation tests between 3D bone sizes and linear dimensions for left PP2.

In **Tables 46 – 48**, descriptive statistics, correlation tests and normal distribution tests for all the variables used in this work are summarized.

The set of values for the entheses of PP2 are similar, according to their comparable dimensions on the base of the bone. With regard to normality tests for each variable of left PP2, the Shapiro-Wilk's test has verified a normal distribution with a *p-value* > 0.05 for all variable, except for antero-posterior RI.

Correlation tests were performed: positive relations have been recorded between total surface size and both raw size and ERS of each enthesis. About relation between entheseal size (raw and ERS) and bone dimensions, antero-posterior Robusticity Index correlates with all 3D bone sizes (with negative correlation recorded for ERS of PI1 enthesis); also, ERS index of DI1 enthesis negatively correlates with bone length, raw size of PI1 correlates to medio-lateral RI and ERS index of PI1 enthesis correlates with all linear dimensions.

4.7.2.1 DI1 enthesis

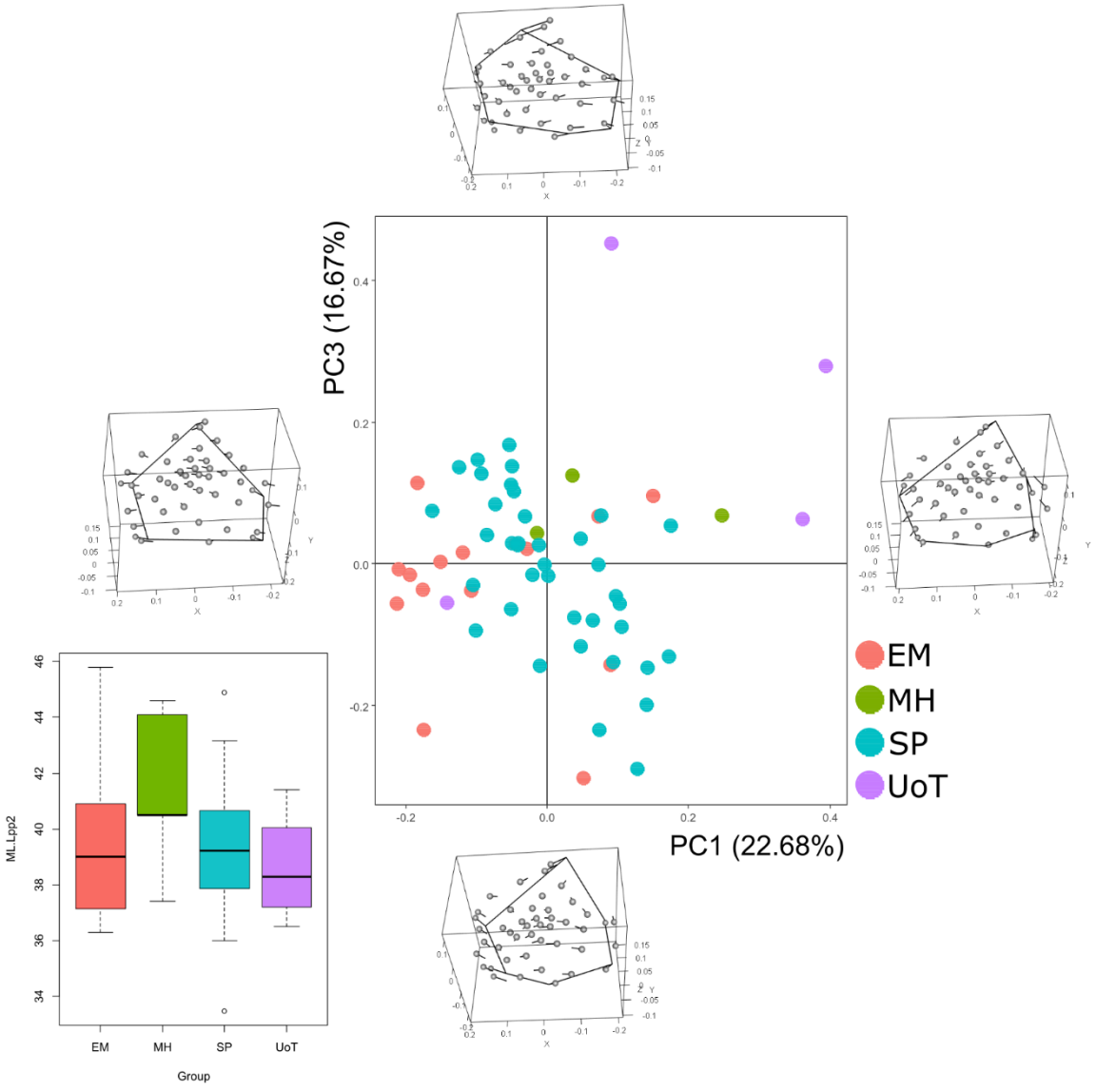

Figure 103 - Principal Component Analysis on the entire set of landmarks and shape configuration at the extremes of PC1 and PC3 for left DI1.

For the analyses of DI1 of left PP2, a total of 60 specimens were available. Here, the first four PCs were analysed, representing about the 70% of the total variance.

Regarding PC1, shape variation occurs in correspondence of both fixed and surface landmarks. About pseudo-landmarks, they all move in a dorsal direction, except for L1 - shifting towards the palmar surface. Concerning surface ones, distinctions can be made: those located on the central portion of the enthesis move in a palmar direction, while those located close to both dorsal and palmar aspect of the entheseal outline move dorsally. About shape variation along PC2, a decreasing in proximo-distal direction can be recorded: L1 moves both proximally and laterally, L2, L5 and L6 move in medial and proximal directions, while L3 move also medially but towards the distal extremity. No variation is shown for L4. About semi-landmarks, main surface variation is in correspondence of the dorsal portion of the enthesis towards the centre of the enthesis. Even when considering PC3, repositioning of both fixed and surface landmarks determines morphological entheseal changes. In this case, the shift of L1 to a more palmar and distal position causes an increasing of the enthesis in a proximo-distal way, while relocation of other landmarks is crucial for an increasing in antero-posterior direction: in particular, L2 and L3 both move to a lateral and distal direction, while L5 and L6 both move laterally and proximally. With regard to PC4, L1 and L6 both move medially, L2 and L3 both move also medially, with L2 going to a distal direction, L4 relocates laterally and L5 moves to dorsal and proximal directions: as result, a partial increasing in proximo-distal way can be seen along this component.

Proceeding with analysis and description of plot in **Figure 103**, only PC1 and PC3 shown separation between groups: SP has a global distribution, specimens from MH are spread for positive values of both PCs while EM is distributed for negative values of PC1 – with two specimens falling into SP and other two falling into MH. About the small sample of UoT, three specimens are far from the rest, distributed on the 1st quarter of the graph, while one individual falls into the EM group. This is related to the different entheseal morphologies among the specimens: these three samples are characterised by wider entheses in a proximo-distal direction with L1 as main tip. Similar distribution can be seen also when PC2 and PC4 are introduced in relation to PC3, with UoT with a partial identical grouping than the graph here described; for this reason, these graphs are not included here but can be found in the Annexes (cf. A4 – 21, A4 – 22).

4.7.2.2 PI1 enthesis

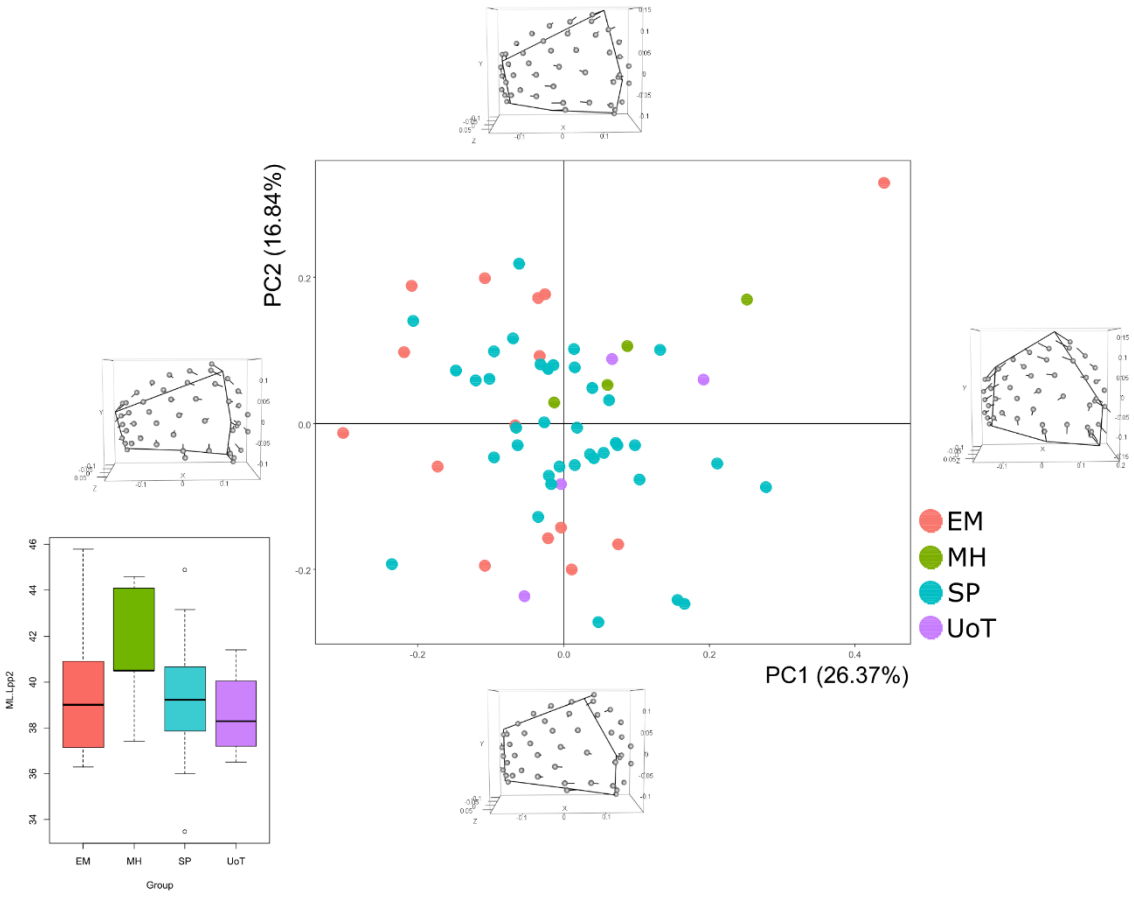

Figure 104 - Principal Component Analysis on the entire set of landmarks and shape configuration at the extremes of PC1 and PC2 for left PI1.

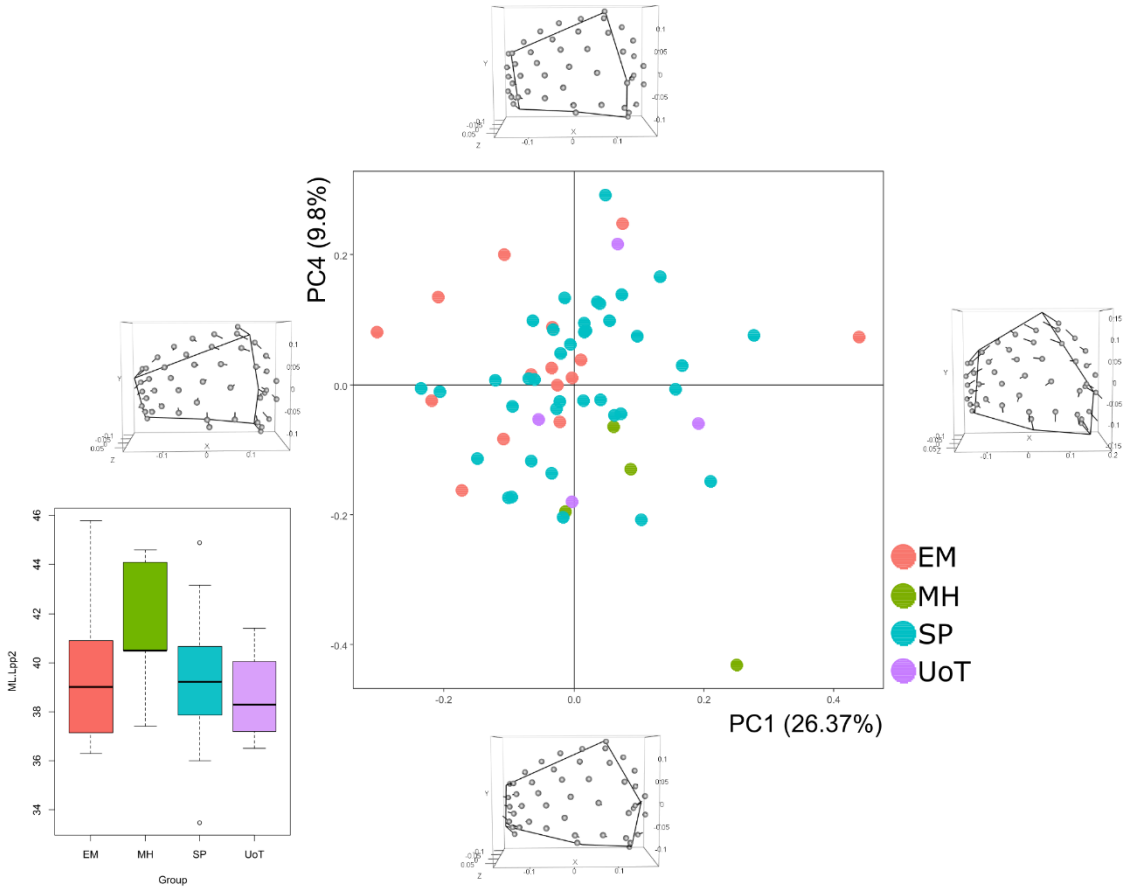

Figure 105 - Principal Component Analysis on the entire set of landmarks and shape configuration at the extremes of PC1 and PC4 for left PI1.

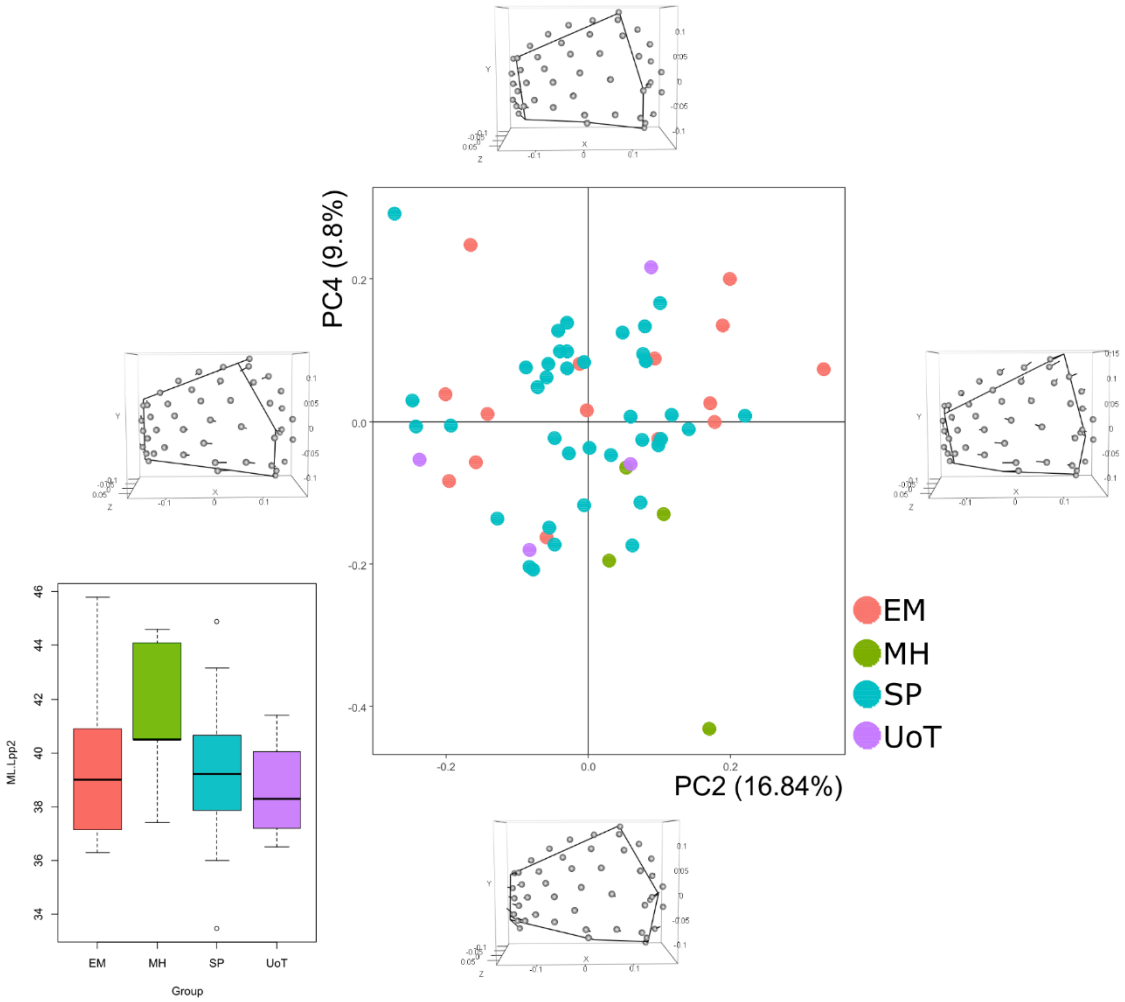

Figure 106 - Principal Component Analysis on the entire set of landmarks and shape configuration at the extremes of PC2 and PC4 for left PI1.

For the analyses of PI1 of left PP2, a total of 61 specimens were available. Here, the first four PCs were analysed, representing about the 67% of the total variance.

Describing shape variation along PC1, L1 is the unique fixed pseudo-landmarks going to a palmar direction, together with some of surface semi-landmarks lying close to the distal aspect of the entheseal outline; with regard to the other landmarks, L2, L3 and L4 all move to proximal and dorsal directions, L5 moves medially and L6 moves towards the dorsal surface, distally. Concerning surface semi-landmarks, major variation occurs in correspondence of the palmar aspect of the entheseal outline, with surface points moving towards the centre of the enthesis. Regarding PC2, shift of L1 to a most dorsal position – together with some surface semi-landmarks – cause an increasing in antero-posterior way ad a minimum decreasing in proximo-distal direction in correspondence of the palmar entheseal outline. About PC3, a reduction in length of both palmar and dorsal aspects of the entheseal outline can be seen caused by repositioning of L2 and L6, moving proximally and dorsally. Concerning other landmarks, L1 moves to a medial direction, L3 and L4 both moves laterally – this latter also relocates distally – and L5 partially moves towards the dorsal surface. No particular variation is recorded in correspondence of surface semi-landmarks. With regard to PC4, a decreasing in antero-posterior direction is visible, due to a lateral relocation of L2, L3 and L6; also, L5 moves in both proximal and – partially – dorsal directions.

In **Figures 104 – 106**, separation between MH and EM is recorded, with SP and UoT groups homogenously distributed all over the graph. With regard to the two distinct archaeological collections, in **Figure 104**, MH has a distribution for positive values of both PC1 and PC2, while EM is divided into two groups, separated by SP, for different values of PC2. Also, a specimen from EM is distinct from its own group for positive values of both PCs. Similar distribution is seen for PC1 and PC2 related to PC3 – whose plots have been added in the Annexes (cf. A4 – 23, A4 – 24) – and for PC1 and PC4; this latter (**Figure 105**) differs from the first one for a different spread of MH, distributed for negative values of both PC1 and PC4. Also, in **Figure 106** same distribution as **Figure 105** is shown.

4.8 Analyses of 3rd proximal phalanges

4.8.1 Right PP3 – Descriptive statistics, normality tests and correlation analyses

	raw size - DI2	ERS - DI2	raw size - DI3	ERS - DI3	APWM/ML*	MLWM/ML*	ML*
N	53	49	58	53	57	57	57
Min	91,56	0,07	67,02	0,06	0,13	0,19	36,09
Max	233,49	0,12	210,20	0,11	0,22	0,28	47,80
Mean	159,53	0,10	131,64	0,08	0,17	0,23	42,73
Stand. dev	34,61	0,01	27,91	0,01	0,02	0,02	2,41

Table 49 - Summary statistics for both 3D size and linear measurements of right PP3. Raw size is calculated in mm2, ML in calculated in mm. APWM/ML: Antero-Posterior Robusticity Index. MLWM/ML: Medio-Lateral Robusticity Index. ML: Maximum Length.

	raw size - DI2	ERS - DI2	raw size - DI3	ERS - DI3	APWM/ML*	MLWM/ML*	ML*
N	53	49	58	53	57	57	57
Shapiro-Wilk W	0,98	0,98	0,99	0,98	0,96	0,98	0,97
p(normal)	0,38	0,58	0,88	0,41	0,08	0,59	0,27

Table 50 - Shapiro-Wilk test for each variable of right PP3.

	raw size - DI2	ERS - DI2	raw size - DI3	ERS - DI3
APWM/ML*		0,25		0,15
MLWM/ML*		0,15		
ML*		0,20		0,13

Table 51 - Correlation tests between 3D bone sizes and linear dimensions for right PP3.

In **Tables 49 – 51**, descriptive statistics, correlation tests and normal distribution tests for all the variables used in this work are summarized.

The set of values for the entheses of PP3 are similar, according to their comparable dimensions on the base of the bone. With regard to normality tests for each variable of right PP3, the Shapiro-Wilk's test has verified a normal distribution with a *p-value* > 0.05 for all variable. Correlation tests were performed: positive relations have been recorded between total surface size and both raw size and ERS of each enthesis. About relation between entheseal size (raw and ERS) and bone dimensions, ERS index of DI2 enthesis correlates with all linear measurements and other correlation is between ERS of DI3 enthesis and antero-posterior RI and bone length.

4.8.1.1 DI2 enthesis

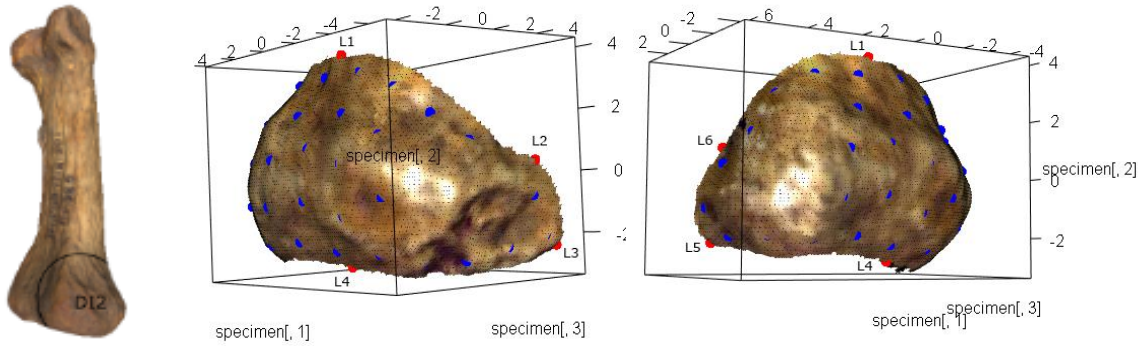

Figure 107 - On the left, the PP3 bone with delimited DI2 enthesis.
On the right, the landmarks (red spots) and semi-landmarks (blue spots) on the 3D model of the surface of DI2.
For the landmarks' definitions, see Annexes (cf. A2 – 8).

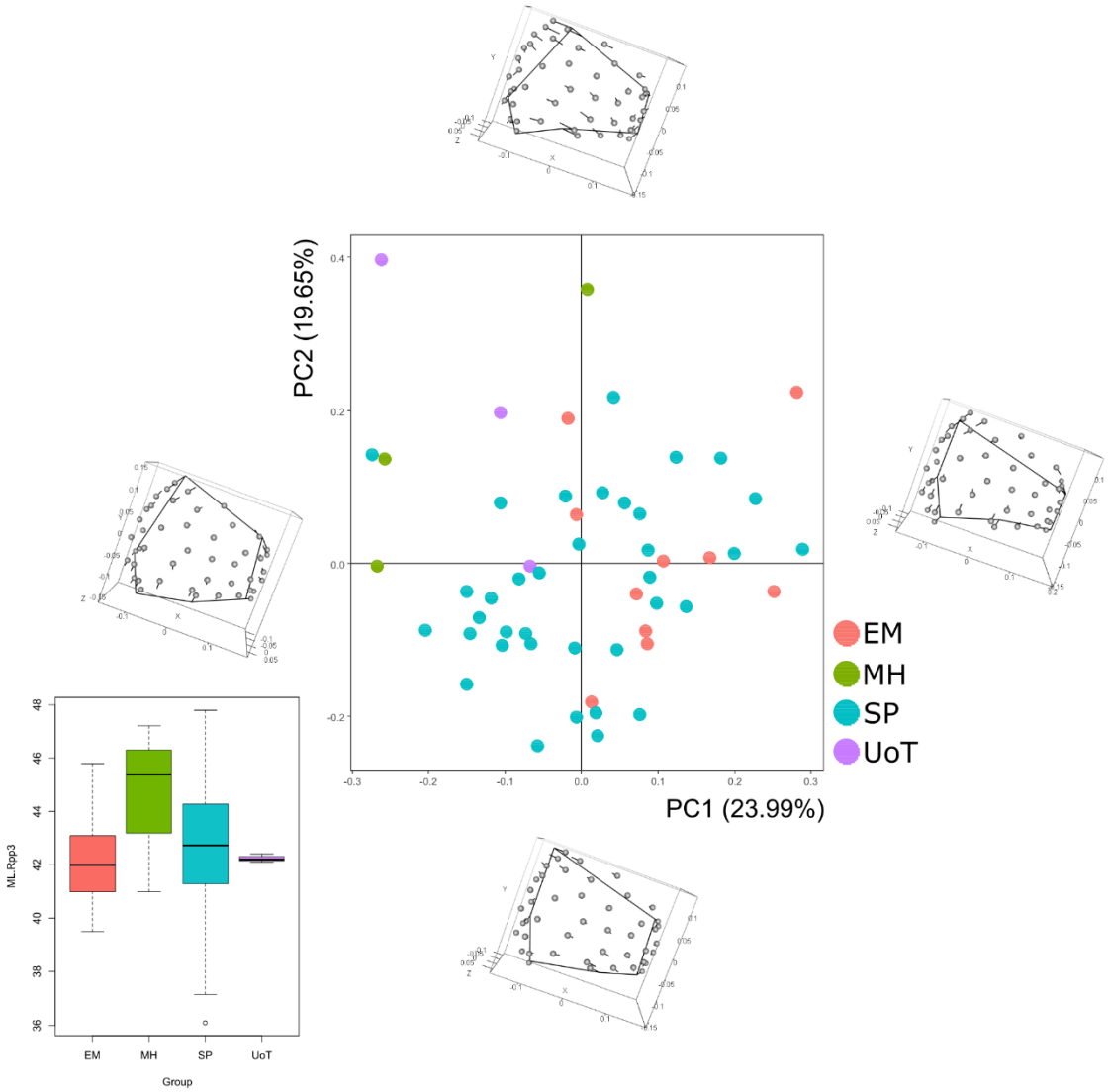

Figure 108 - Principal Component Analysis on the entire set of landmarks and shape configuration at the extremes of PC1 and PC2 for right DI2.

For the analyses of DI2 of right PP3 (**Figure 107**), a total of 52 specimens were available. Here, the first two PCs were analysed, representing almost the 45% of the total variance.

Therefore, only shape variation along PC1 and PC2 are described. About PC1, both fixed pseudo-landmarks and surface semi-landmarks relocate and cause a reduction in correspondence of the dorsal aspect of the entheseal outline in a proximo-distal way: L1 moves in a palmar direction, along the distal outline towards L6, L2 moves both medially and proximally, L3 moves both proximally and dorsally, L4 move towards the distal extremity, while L5 and L6 move both distally – with L6 also going in a medial direction. About surface semi-landmarks, those located on the distal tip move to a proximal direction, those lying on the proximal entheseal outline move to a distal one, and others on the dorsal side continue going dorsally. Regarding PC2, shape variation is due in particular to a shift of L1 from a palmar to a most dorsal position and to surface semi-landmarks lying close to the palmar surface – which move dorsally. With regard to the other fixed points, both L2 and L3 move towards the dorsal surface, L4 moves to a palmar direction, and L6 moves proximally. No variation is about L5. In this case, variation is described as a decreasing in shape morphology on the palmar portion of the enthesis.

In all cases and all graphs, the same distribution is visible: for this reason, only the first two PCs have been introduced and described. In **Figure 108**, partial separation between groups can be seen, with SP distributed all over the area – except for 2nd quarter of the plot – and EM mixed with SP only for positive PC1. At the same time, MH and UoT have a distribution for negative and positive values of PC1 and PC2, respectively; they are distinct from the EM and SP and are characterised by entheses with wider dorsal portion than these latter.

4.8.1.2 DI3 enthesis

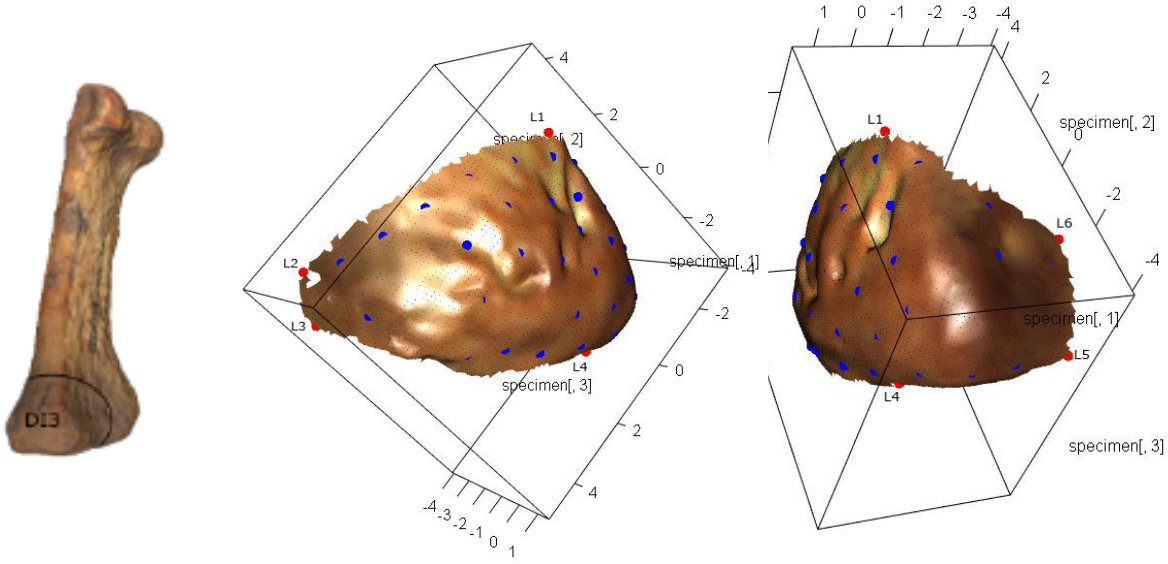

Figure 109 - On the left, PP3 bone with delimited DI3 enthesis.
On the right, the landmarks (red spots) and semi-landmarks (blue spots) on the 3D model of the surface of DI3.
For the landmarks' definitions, see Annexes (cf. A2 – 8).

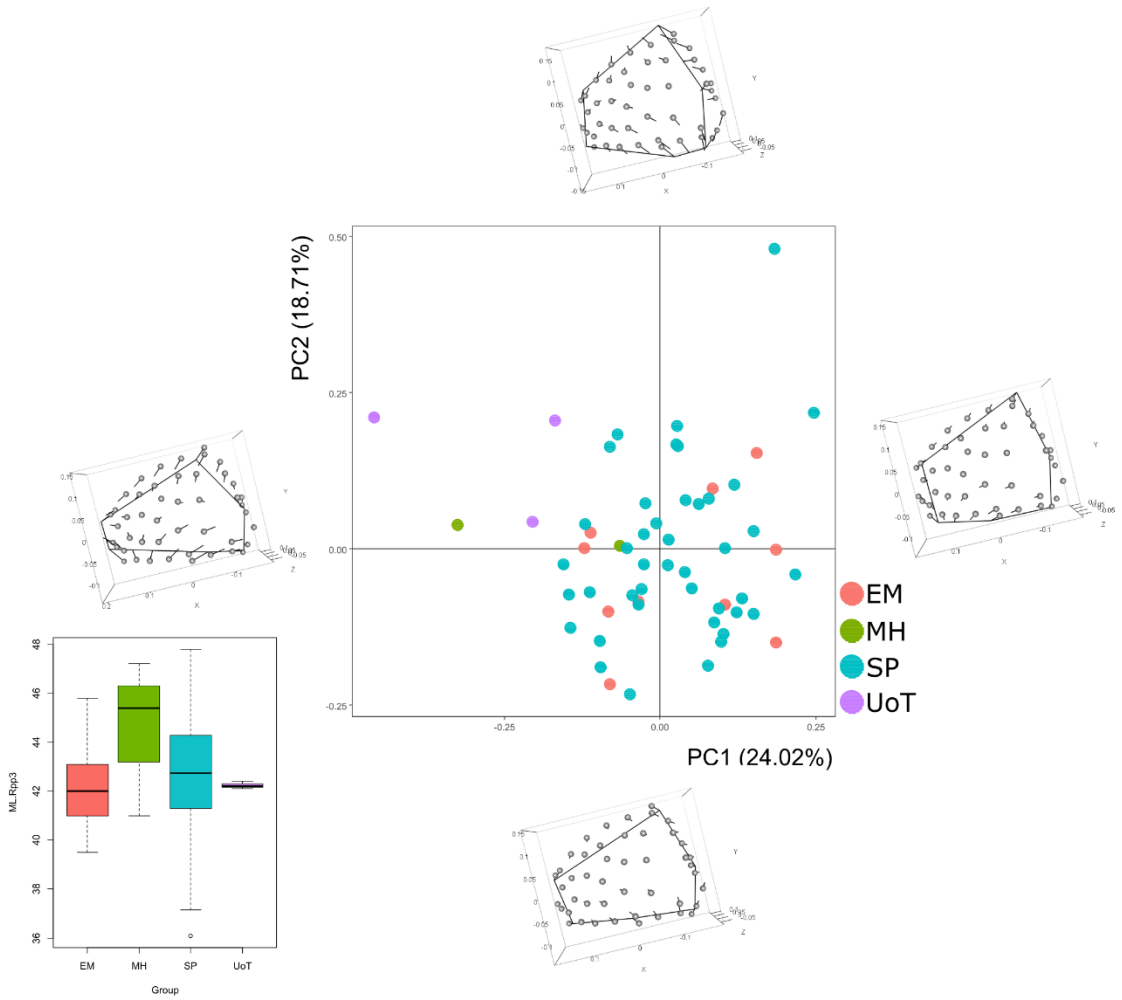

Figure 110 - Principal Component Analysis on the entire set of landmarks and shape configuration at the extremes of PC1 and PC2 for right DI3.

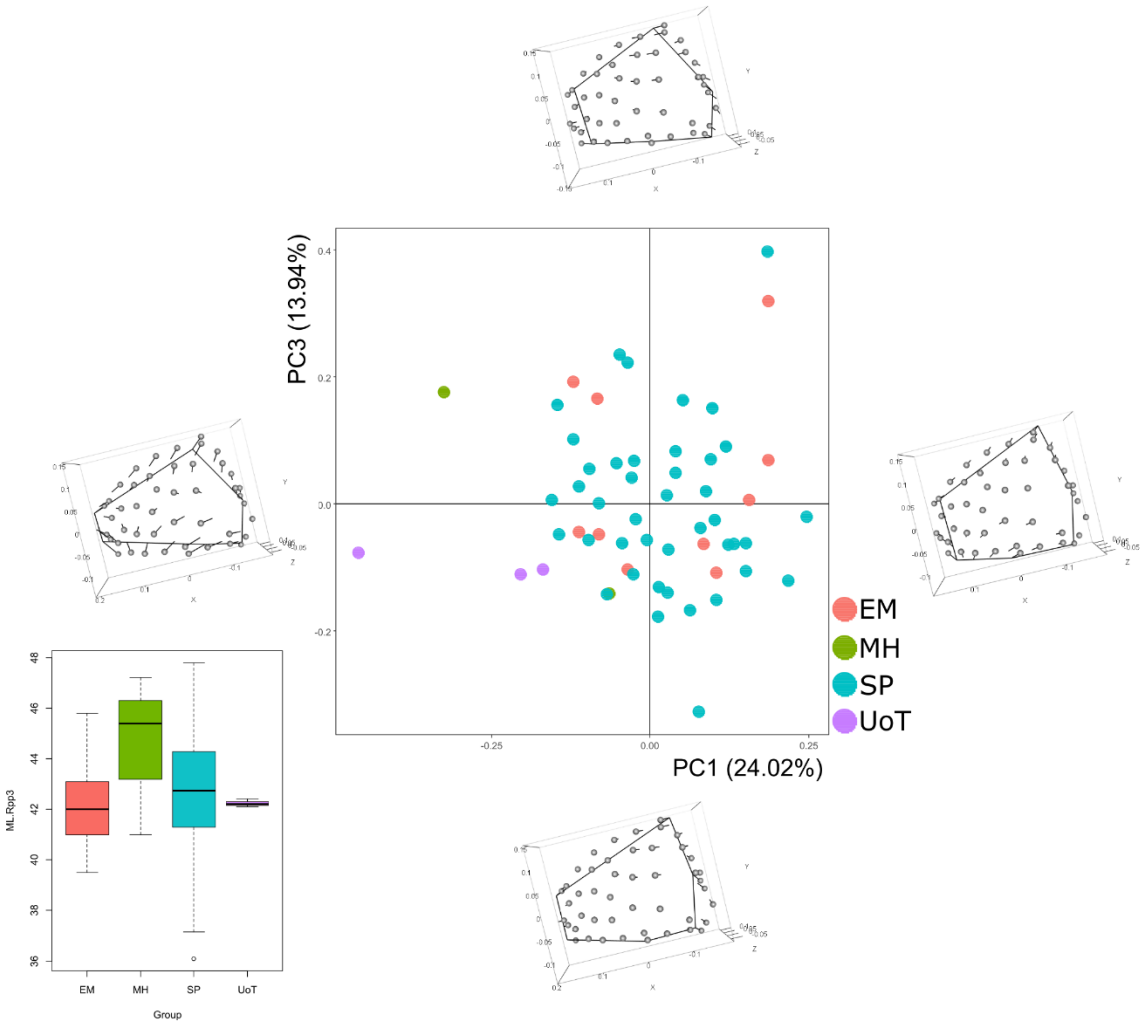

Figure 111 - Principal Component Analysis on the entire set of landmarks and shape configuration at the extremes of PC1 and PC3 for right DI3.

For the analyses of DI3 of right PP3 (**Figure 109**), a total of 57 specimens were available. Here, the first four PCs were analysed, representing almost the 67% of the total variance.

Analysing shape variation along PC1, different morphologies are shown, characterised by an increasing and a decreasing in proximo-distal and antero-posterior directions, respectively. This is due to both fixed and surface landmarks relocation: L1 moves towards the distal epiphysis, together with the surface semi-landmarks lying on the distal aspect of the entheseal outline, L2 moves towards L1, L3 and L4 both move proximally to palmar and dorsal positions, respectively, L5 is not affected by any shift, and L6 partially moves also distally. About surface landmarks on the proximal outline, they continue going to proximal direction, causing the before mentioned proximo-distal increasing. Regarding PC2, an increasing in correspondence of the palmar side of the enthesis is recorded, due to relocation of surface semi-landmarks moving from a dorsal to a palmar position: about fixed pseudo-landmarks, most variation is on L1 moving dorsally and distally, L4 moving to both proximal and palmar directions, L5 moving proximally but dorsally, and L6 partially moves only dorsally. Along PC3, the unique significant shape variation is about a shift on L1 to a most dorsal position, together with the surface semi-landmarks on the palmar outline between L6 and L1; also, L5 and L6 move to both proximal and palmar directions. With regard to PC4, a minimum increasing in proximo-distal way is recorded, due to L2, L3, L5 and L6 movements to a medial position.

Resulting analyses are shown in **Figure 110** and **Figure 111**, where a different distribution for UoT is recorded; this group is distributed for positive values of PC2 and negative ones for PC1, along with the two specimens from MH. Therefore, they are distinct SP and EM. Similar distribution for the small sample constituted by MH and UoT is evident when PC4 is introduced: for this reason, plot analysing PC1 and PC4 is not included here, but in the Annexes (cf. A4 – 25). As resulting description, specimens from UoT and MH are characterised by small entheses in a proximo-distal way. In **Figure 111**, different distribution for the UoT is recorded: it is distributed for negative values of both PCs, characterised by morphological reduced entheses in proximo-distal direction.

4.8.2 Left PP3 - Descriptive statistics, normality tests and correlation analyses

	raw size - DI2	ERS - DI2	raw size - DI3	ERS - DI3	APWM/ML*	MLWM/ML*	ML*
N	57	56	60	59	63	63	63
Min	80,15	0,07	67,66	0,05	0,12	0,17	36,60
Max	270,26	0,13	189,84	0,11	0,22	0,26	47,40
Mean	152,93	0,10	127,82	0,08	0,16	0,22	42,82
Stand. dev	36,21	0,01	26,57	0,01	0,02	0,02	2,34

Table 52 - Summary statistics for both 3D size and linear measurements of left PP3. Raw size is calculated in mm^2, ML in calculated in mm. **APWM/ML**: Antero-Posterior Robusticity Index. **MLWM/ML**: Medio-Lateral Robusticity Index. **ML**: Maximum Length.

	raw size - DI2	ERS - DI2	raw size - DI3	ERS - DI3	APWM/ML*	MLWM/ML*	ML*
N	57	56	60	59	63	63	63
Shapiro-Wilk W	0,98	0,99	0,99	0,96	0,92	0,98	0,99
p(normal)	0,41	0,87	0,93	0,07	0,0004855	0,48	0,76

Table 53 - Shapiro-Wilk test for each variable of left PP3.

	raw size - DI2	ERS - DI2	raw size - DI3	ERS - DI3
APWM/ML*				
MLWM/ML*				
ML*				0,097

Table 54 - Correlation tests between 3D bone sizes and linear dimensions for left PP3.

In **Tables 52 - 54**, descriptive statistics, correlation tests and normal distribution tests for all the variables used in this work are summarized.

The set of values for the entheses of PP3 are similar, even if values of DI2 are higher than DI3 ones, according to their comparable dimensions on the base of the bone. With regard to normality tests for each variable of left PP3, the Shapiro-Wilk's test has verified a normal distribution with a *p-value* > 0.05 for all variable, except for antero-posterior Robusticity Index. Correlation tests were performed: positive relations have been recorded between total surface size and both raw size and ERS of each enthesis. About relation between entheseal size (raw and ERS) and bone dimensions, only correlation between ERS index of DI3 and maximum bone length is recorded.

4.8.2.1 DI2 enthesis

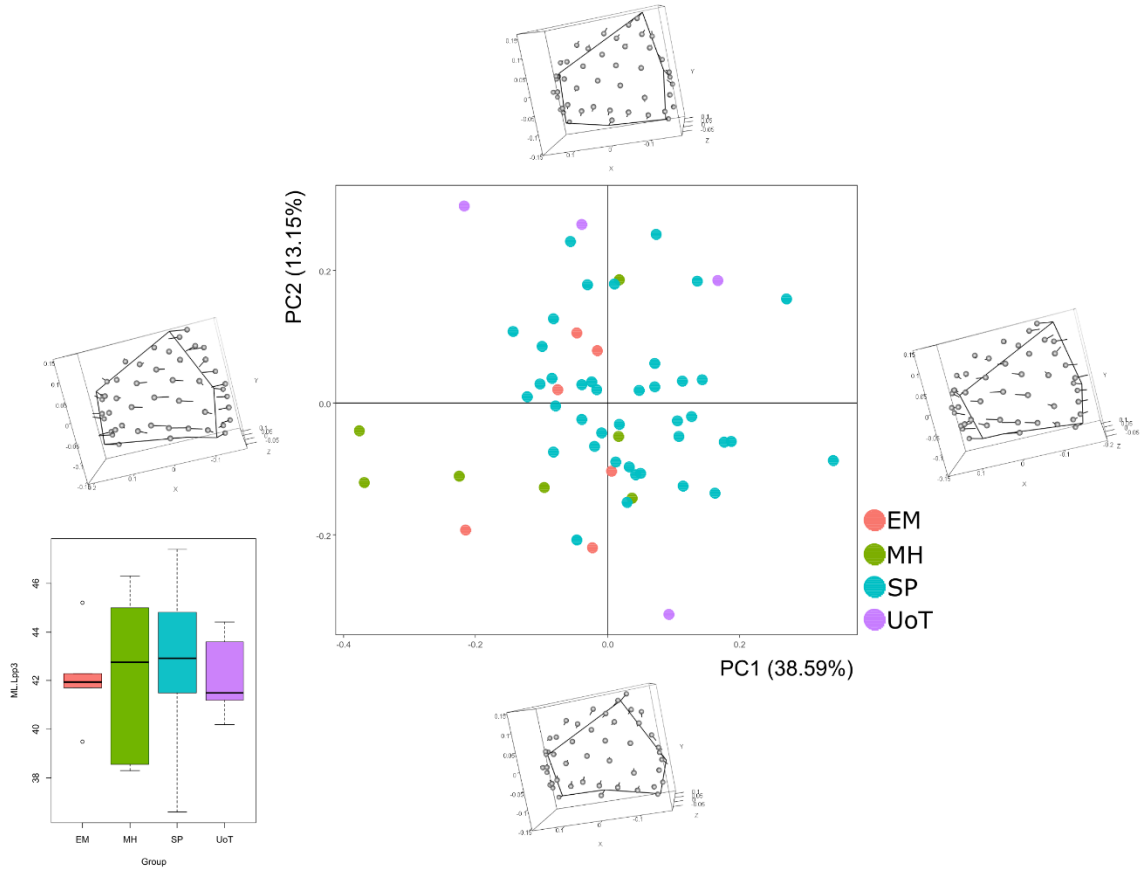

Figure 112 - Principal Component Analysis on the entire set of landmarks and shape configuration at the extremes of PC1 and PC2 for left DI2.

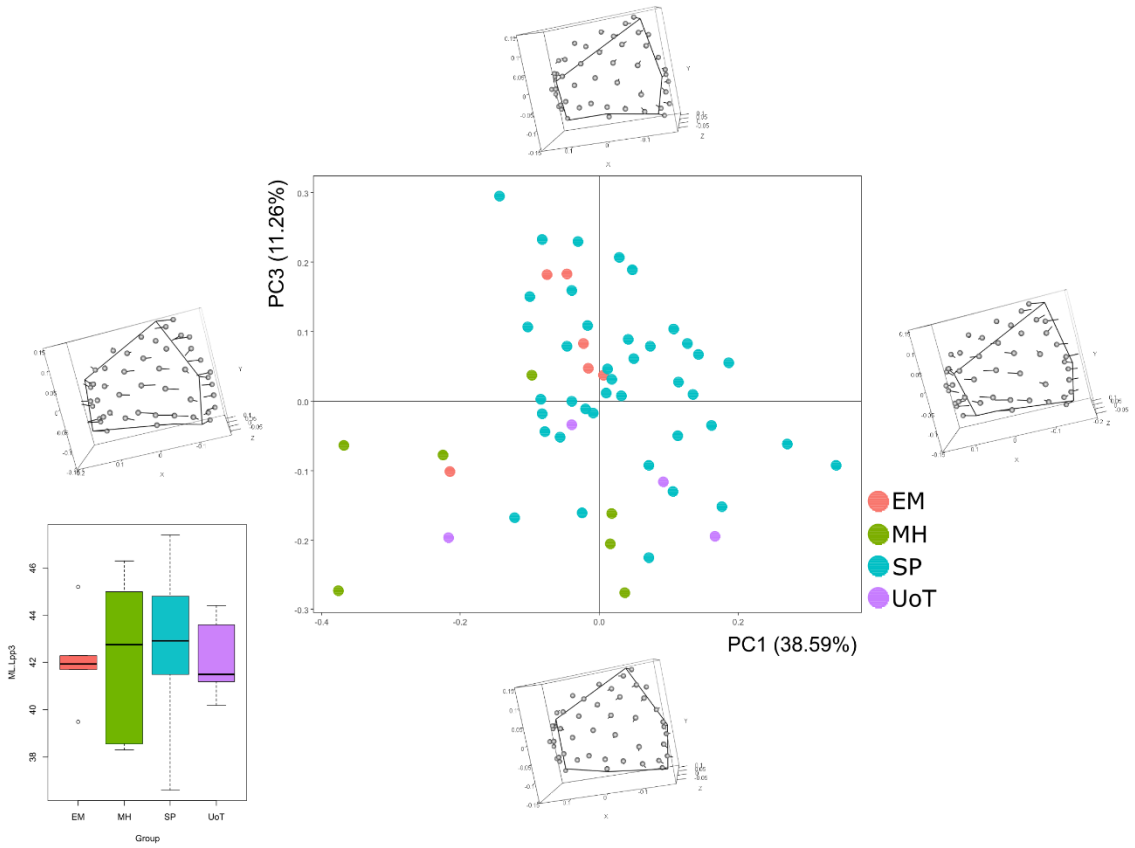

Figure 113 - Principal Component Analysis on the entire set of landmarks and shape configuration at the extremes of PC1 and PC3 for left DI2.

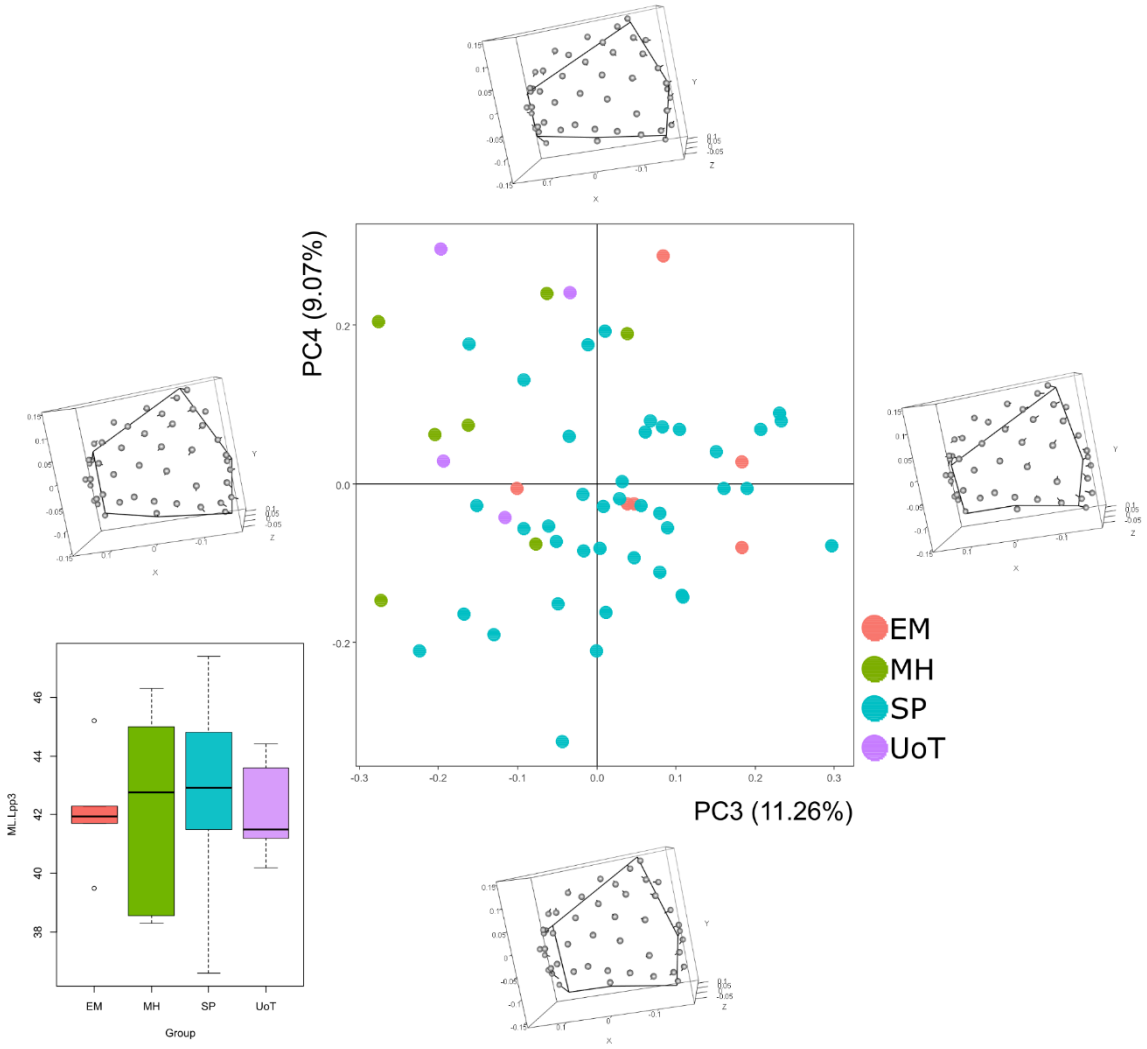

Figure 114 - Principal Component Analysis on the entire set of landmarks and shape configuration at the extremes of PC3 and PC4 for left DI2.

For the analyses of DI2 of left PP3, a total of 57 specimens were available. Here, the first four PCs were analysed, representing almost the 63% of the total variance.

Along PC1, shape variation is related to a shift of the entheseal morphology to a most palmar position, due to relocation of both fixed and surface landmarks: L1 to L3 move to a palmar direction – with L2 moving also proximally – L4 goes dorsally, and both L5 and L6 move to a medial position. About surface semi-landmarks, those located in correspondence of the palmar surface and on the dorsal aspect of the entheseal outline move to a palmar direction, while those located on the centre of the enthesis move dorsally. Also, when considering PC2, a shift to a most palmar position is recorded but an increasing in a proximo-distal way can be observed: major variation is on L1, moving distally to a palmar surface, L4 moving proximally and dorsally, while L5 and L6 move along each corresponding entheseal outlines, towards L1 and L4, respectively. A minimum variation is verified for relocation of L2 and L3, going to palmar and lateral directions, respectively. About PC3, a proximo-distal reduction occurs in correspondence of the dorsal entheseal outline, particularly due to L1 – moving to palmar and proximal directions – and L2 – going both proximally and dorsally. With regard to PC4, a minimum decreasing in proximo-distal direction can be seen along with an increasing in antero-posterior way, due to partial repositioning of L1 (moving proximally), L2 (moving proximally and laterally), L3, L5 and L6 (going towards a distal direction).

Proceeding with descriptions of analyses shown before, separation between MH and UoT from the remaining sample is recorded: in particular, in **Figure 112**, specimens from MH have a distribution for negative values for both PC1 and PC2, while UoT is in the positive part of PC2 axis. This means that specimens of MH are characterised by wider entheses in a proximo-distal way, while those belonging to SP have a morphology most pointed towards the palmar surface. Along PC3 (**Figure 113**), a shift of UoT is recorded, with a distribution of negative values of both PC1 and PC3; also, EM moves to positive side of PC3 axis. With regard to PC4, distribution is similar to graphs previously shown, but grouping between UoT and MH is evident, resulting also distinct from EM and SP: in this case, specimens of MH are characterised by partially wider entheses, distributed for positive values of both PC3 and PC4 (**Figure 114**).

4.8.2.2 DI3 enthesis

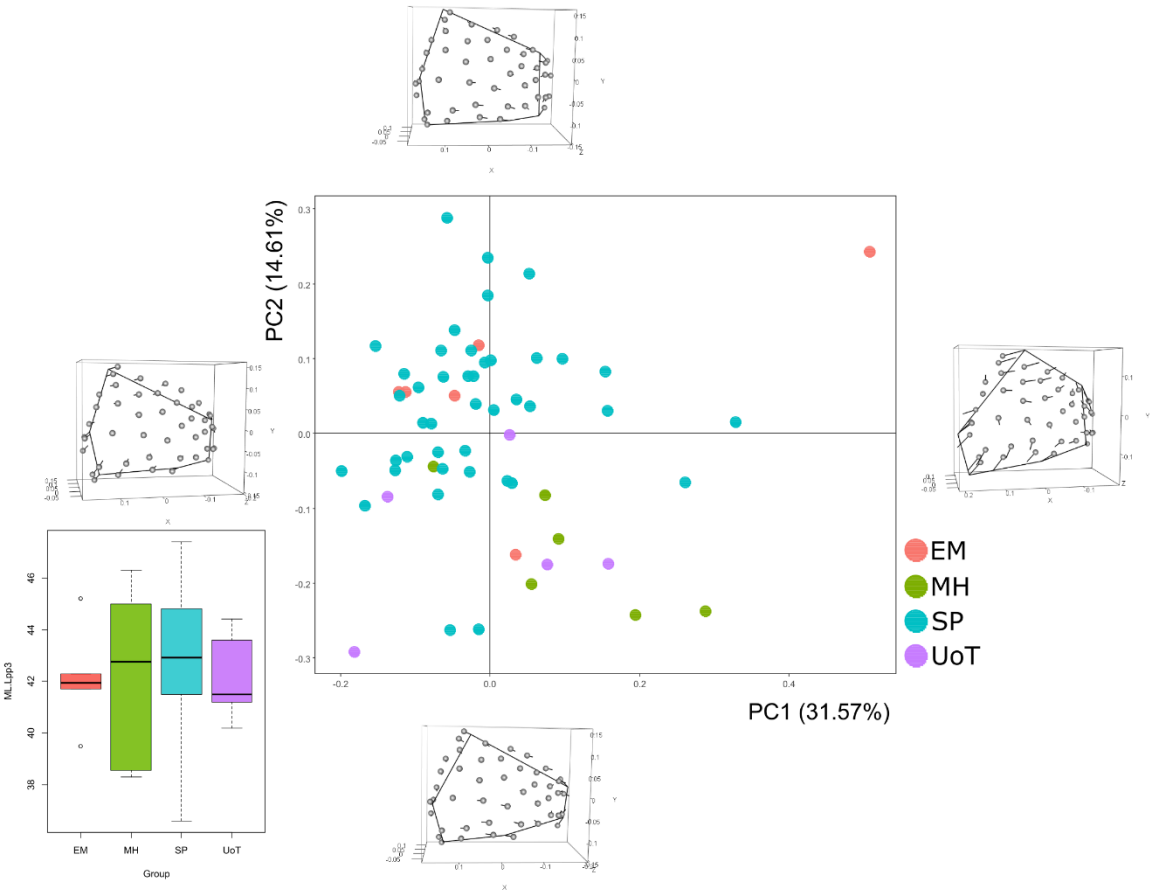

Figure 115 - Principal Component Analysis on the entire set of landmarks and shape configuration at the extremes of PC1 and PC2 for left DI3.

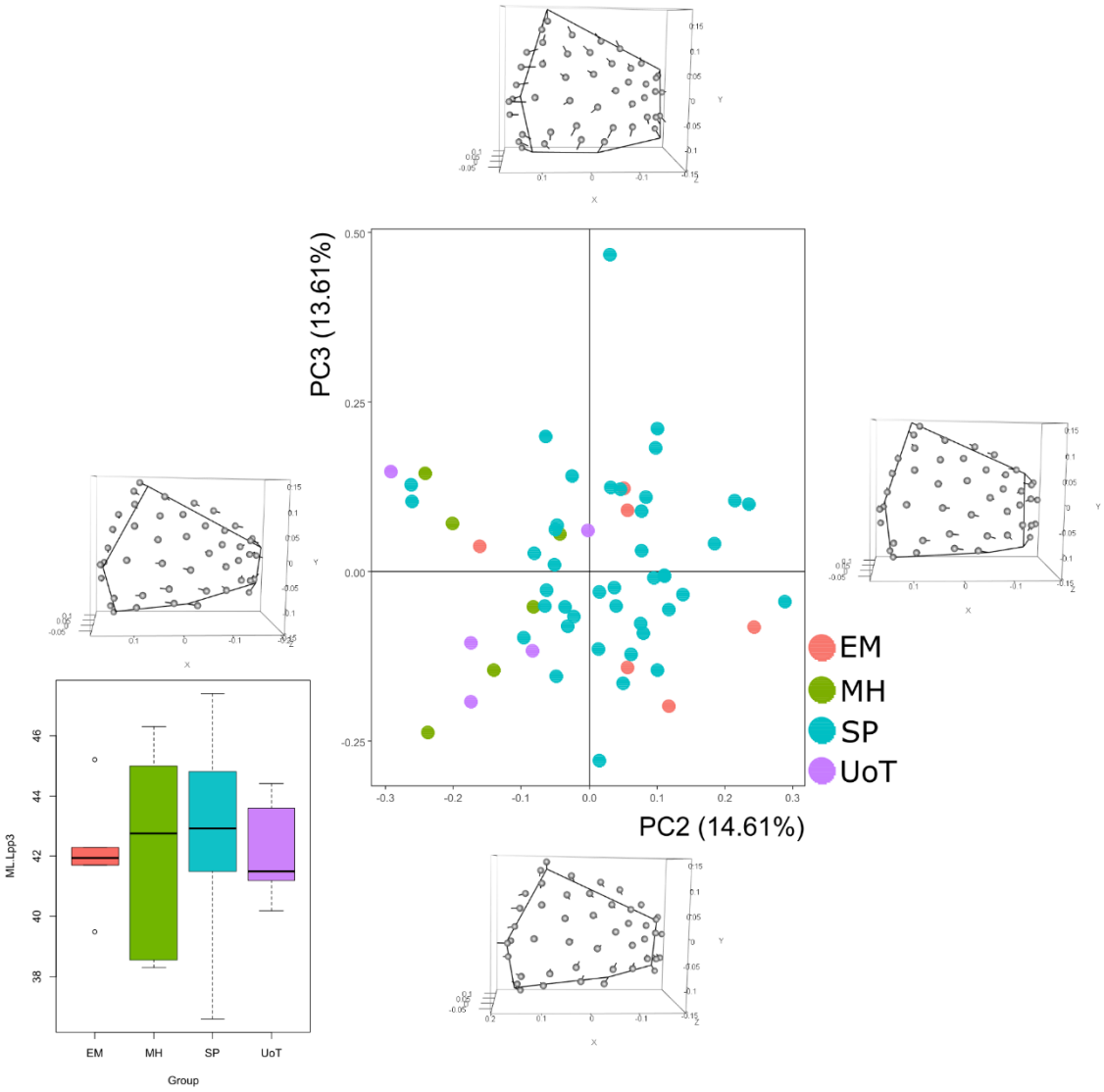

Figure 116 - Principal Component Analysis on the entire set of landmarks and shape configuration at the extremes of PC2 and PC3 for left DI3

For the analyses of DI3 of left PP3, a total of 59 specimens were available. Here, the first four PCs were analysed, representing almost the 70% of the total variance.

Starting from shape analyses along PC1, a significant shift of the entheseal morphology can be seen from a palmar to a most dorsal direction. Both fixed and surface landmark are interested in this relocation; about fixed ones, L1 moves towards the dorsal surface, L2 to L4 move to a palmar direction, while L5 and L6 move along the corresponding entheseal outlines to a palmar direction too, towards L4 and L1, respectively. About surface semi-landmarks, some of them lying in correspondence of the palmar surface move to a proximal direction, while others located on the centre of the enthesis move dorsally. With regard to PC2, an increasing in correspondence of the dorsal aspect of the entheseal outline – between L2 and L3 – is recorded, determining an increasing of the enthesis on that side. About fixed pseudo-landmarks which relocate, L1 move to a most distal position, L4 moves both proximally and dorsally, while L5 and L6 move in opposite directions, proximally and distally respectively. About surface ones, those located along the distal aspect of the entheseal outline relocate to a most distal position, while those located on the proximal one move proximally. Same kind of considerations can be done for shape variation along PC3: in this case, the increasing is cause by relocation of L1 to a most distal position and relocation of L5 towards the proximal epiphysis. Also, L4 moves to both palmar and proximal directions and some surface semi-landmarks lying on the palmar aspect of the enthesis move to the dorsal surface of the bone. With regard to PC4, a decreasing in correspondence of the dorsal aspect of the enthesis is caused by relocation of L1 – going medially – and L2 – moving proximally. About other fixed pseudo-landmarks, L3 and L4 move in opposite directions – going medially and laterally, respectively – and L6 going towards the proximal extremity.

In **Figure 115**, separation between samples is recorded. MH and UoT are distributed for positive and negative values of PC1 and PC2, respectively; they are characterised by more reduced entheses than the SP and EM. Similar distribution and distinction can be seen also in **Figure 116**, where MH and UoT are distributed for negative values of PC2 and are also distinct from EM – except for one specimen of El Mirador which falls into the Neolithic sample. When PC2 and PC4 are considered, similar resulting visualization is obtained: for this reason, this plot is included in the Annexes (cf. A4 – 26).

4.9 Analyses of 4th phalangeal bones

4.9.1 Right PP4 – Descriptive statistics, normality tests and correlation analyses

	raw size - DI4	ERS - DI4	raw size - PI2	ERS - PI2	APWM/ML*	MLWM/ML*	ML*
N	62	57	57	55	63	63	63
Min	72,75	0,07	57,54	0,04	0,13	0,17	32,86
Max	185,53	0,12	164,54	0,12	0,20	0,31	44,90
Mean	120,75	0,09	114,46	0,09	0,16	0,22	39,79
Stand. dev	25,05	0,01	24,81	0,01	0,01	0,02	2,68

Table 55 - Summary statistics for both 3D size and linear measurements of right PP4. Raw size is calculated in mm^2, ML in calculated in mm. **APWM/ML**: Antero-Posterior Robusticity Index. **MLWM/ML**: Medio-Lateral Robusticity Index. **ML**: Maximum Length.

	raw size - DI4	ERS - DI4	raw size - PI2	ERS - PI2	APWM/ML*	MLWM/ML*	ML*
N	62	57	57	55	63	63	63
Shapiro-Wilk W	0,98	0,98	0,99	0,94	0,97	0,97	0,98
p(normal)	0,39	0,37	0,90	0,007352	0,17	0,16	0,57

Table 56 - Shapiro-Wilk test for each variable of right PP4.

	raw size - DI4	ERS - DI4	raw size - PI2	ERS - PI2
APWM/ML*				0,08
MLWM/ML*		0,09	0,24	-0,08
ML*		-0,03		0,01

Table 57 - Correlation tests between 3D bone sizes and linear dimensions for right PP4.

In **Tables 55 – 57**, descriptive statistics, correlation tests and normal distribution tests for all the variables used in this work are summarized.

The set of values for the entheses of PP4 are similar, according to their comparable dimensions on the base of the bone. With regard to normality tests for each variable of right PP4, the Shapiro-Wilk's test has verified a normal distribution with a *p-value* > 0.05 for all variable, except for ERS index of PI2. Correlation tests were performed: positive relations have been recorded between total surface size and both raw size and ERS of each enthesis. About relation between entheseal size (raw and ERS) and bone dimensions, ERS of PI2 enthesis correlates with all linear dimensions, while ERS index of DI4 correlates with maximum bone length and medio-lateral RI, positive and negative, respectively; also, raw size of PI2 enthesis has a correlation with medio-lateral RI.

4.9.1.1 DI4 enthesis

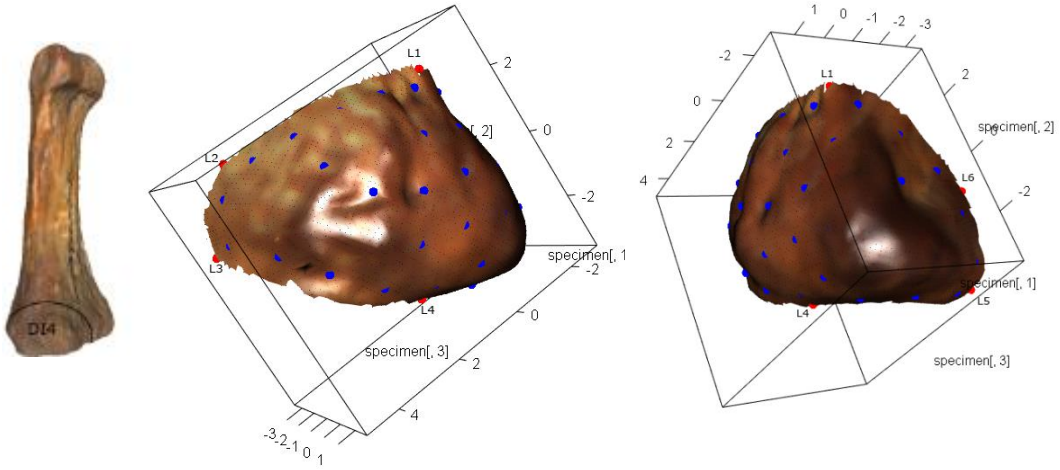

Figure 117 - On the left, the PP4 bone with delimited DI4 enthesis.
On the right, the landmarks (red spots) and semi-landmarks (blue spots) on the 3D model of the surface of DI4.
For the landmarks' definitions, see Annexes (cf. A2 – 9).

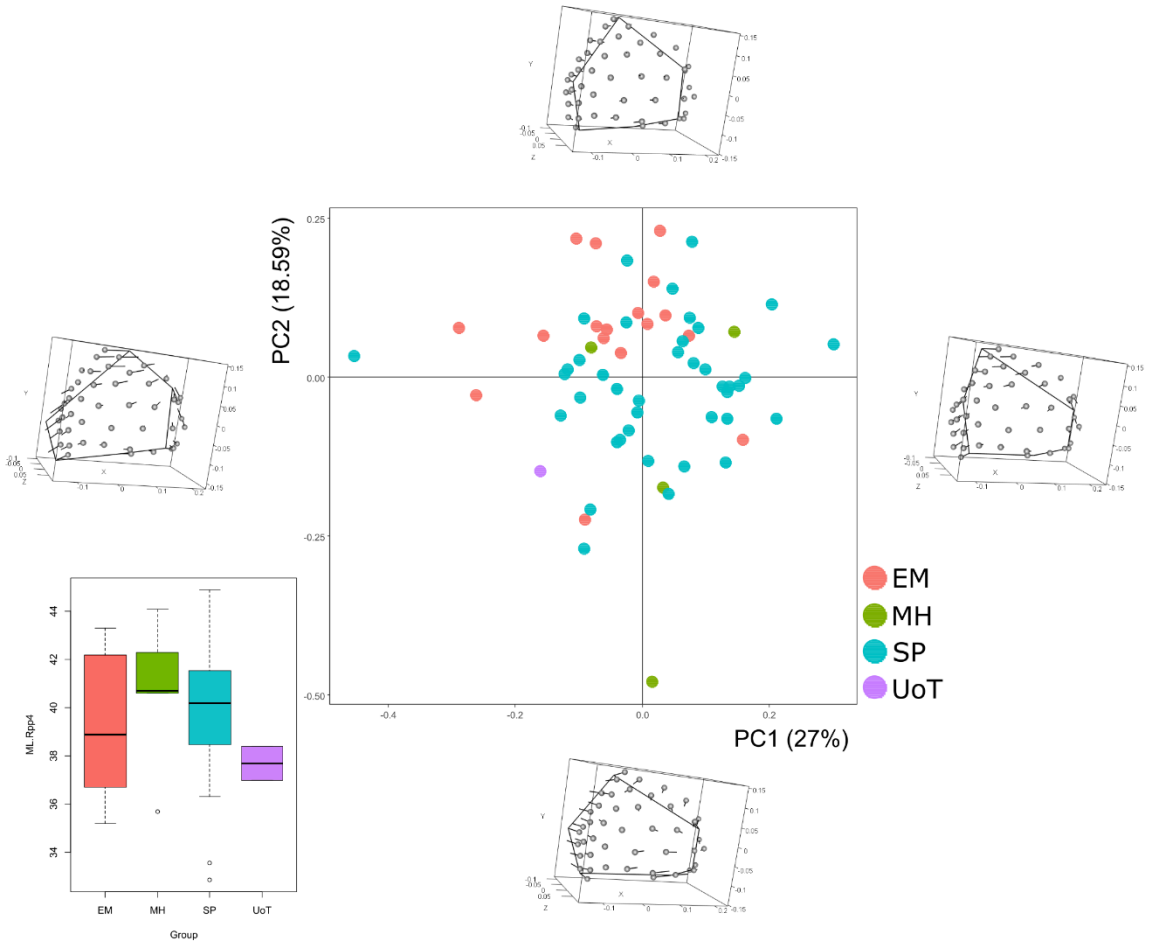

Figure 118 - Principal Component Analysis on the entire set of landmarks and shape configuration at the extremes of PC1 and PC2 for right DI4.

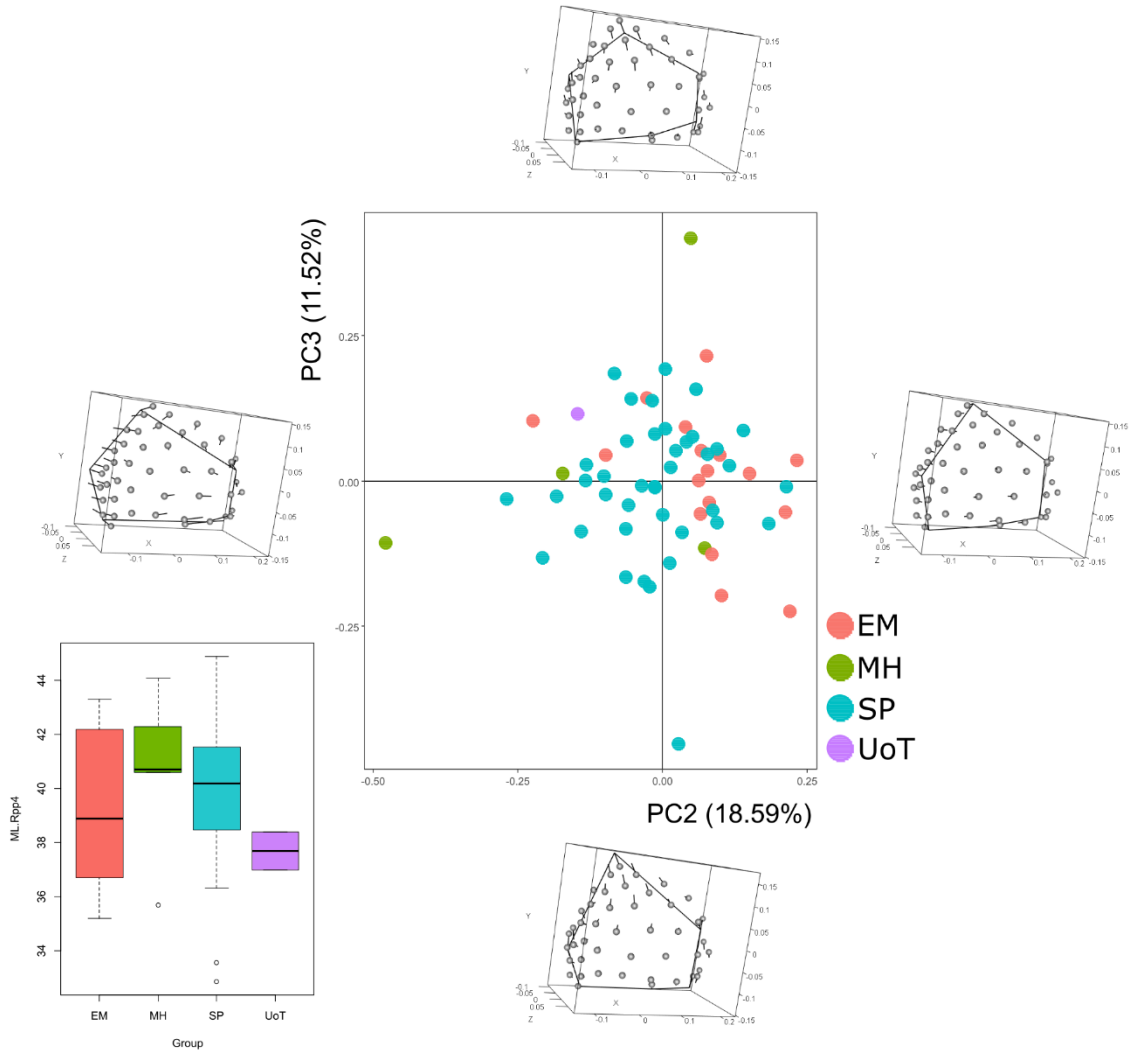

Figure 119 - Principal Component Analysis on the entire set of landmarks and shape configuration at the extremes of PC2 and PC3 for right DI4.

For the analyses of DI4 of right PP4 (**Figure 117**), a total of 62 specimens were available. Here, the first four PCs were analysed, representing almost the 68% of the total variance.

Shape variation along PC1 can be seen as a resulting shift from a palmar to a most dorsal direction, due to both fixed and surface landmarks: L1, along with some surface semi-landmarks, moves towards the dorsal surface of the bone, L2 and L3 both move along each corresponding outline, going distally, L4 goes towards a palmar direction, and L5 and L6 both move to a palmar direction too but move also proximally. About surface semi-landmarks relocating, those located close to the dorsal surface of the bone and others located on the palmar aspect of the entheseal outline move towards the palmar surface. With regard to PC2, an increasing in correspondence of the palmar portion in a proximo-distal way is recorded; all kind of landmarks relocate and cause these changes: L1 and L2 both move to a palmar direction, L3 moves to both palmar and proximal directions, L4 move towards the dorsal surface, while L5 and L6 both move laterally. About surface semi-landmarks, those located on the dorsal aspect of the entheseal outline move to a palmar direction, while some points lying near the palmar surface proceed in a dorsal way, towards the centre of the enthesis. Regarding PC3, a decreasing of entheseal morphology in proximo-distal direction can be seen, caused by relocation of L1 and surrounding surface landmarks to a most proximal position, even if L2 moves distally; furthermore, L4 moves medially and both L5 and L6 move to lateral and distal positions. About PC4, major variation is in antero-posterior direction, caused by relocation of L2 and L6 – both moving proximally but to dorsal and palmar directions, respectively – and L4, going dorsally.

In the shape space shown in **Figure 118**, partial separation between EM and SP can be observed, with EM distributed for positive values of PC2 (except for two specimens with negative values of the same component which fall into SP). Concerning the two small samples MH and UoT, the totality of five specimens is spread all over the graph, with no peculiar distinction. About EM, specimens are characterised by wider entheses in proximo-distal direction, with the distal tip to a most dorsal position. Similar distribution for this group is shown in **Figure 119** – with three specimens falling into SP for negative values of PC2; about specimens from MH, two specimens can be considered as outliers – one with positive values for both PCs, the second with negative values for both PCs – and are characterised by similar entheseal morphologies. Similar distribution can be seen also when PC2 and PC4 are considered; for this reason, this plot is not described here and can be found in the Annexes (cf. A4 – 27).

4.9.1.2 PI2 enthesis

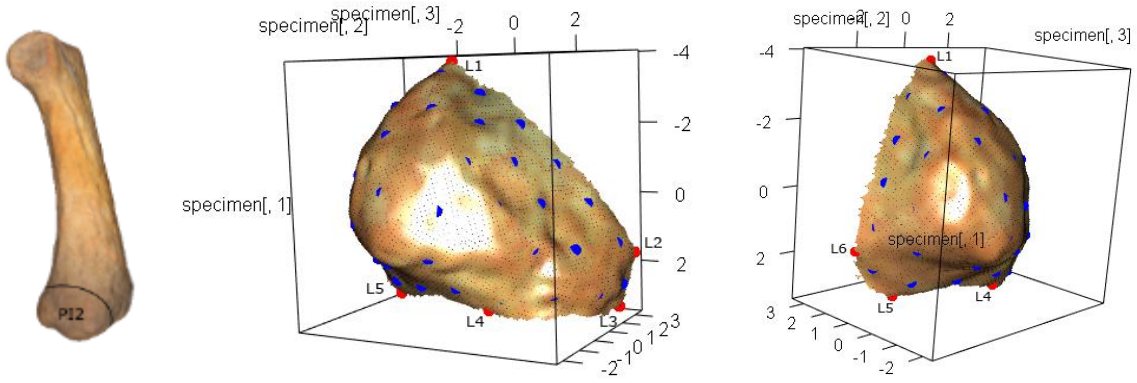

Figure 120 - On the left, the PP4 bone with PI2 delimited enthesis.
On the right, the landmarks (red spots) and semi-landmarks (blue spots) on the 3D model of the surface of PI2.
For the landmarks' definitions, see Annexes (cf. A2 – 9).

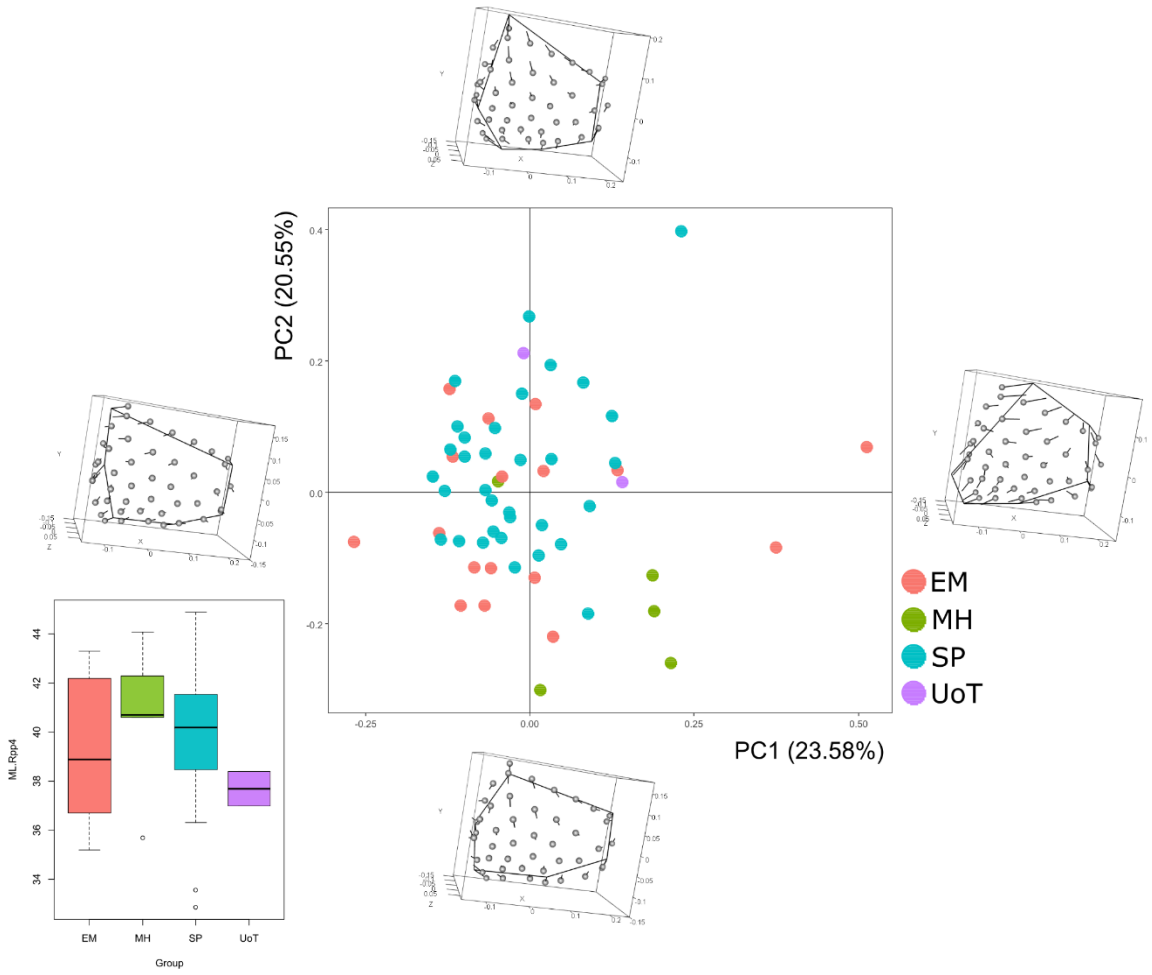

Figure 121 - Principal Component Analysis on the entire set of landmarks and shape configuration at the extremes of PC1 and PC2 for right PI2.

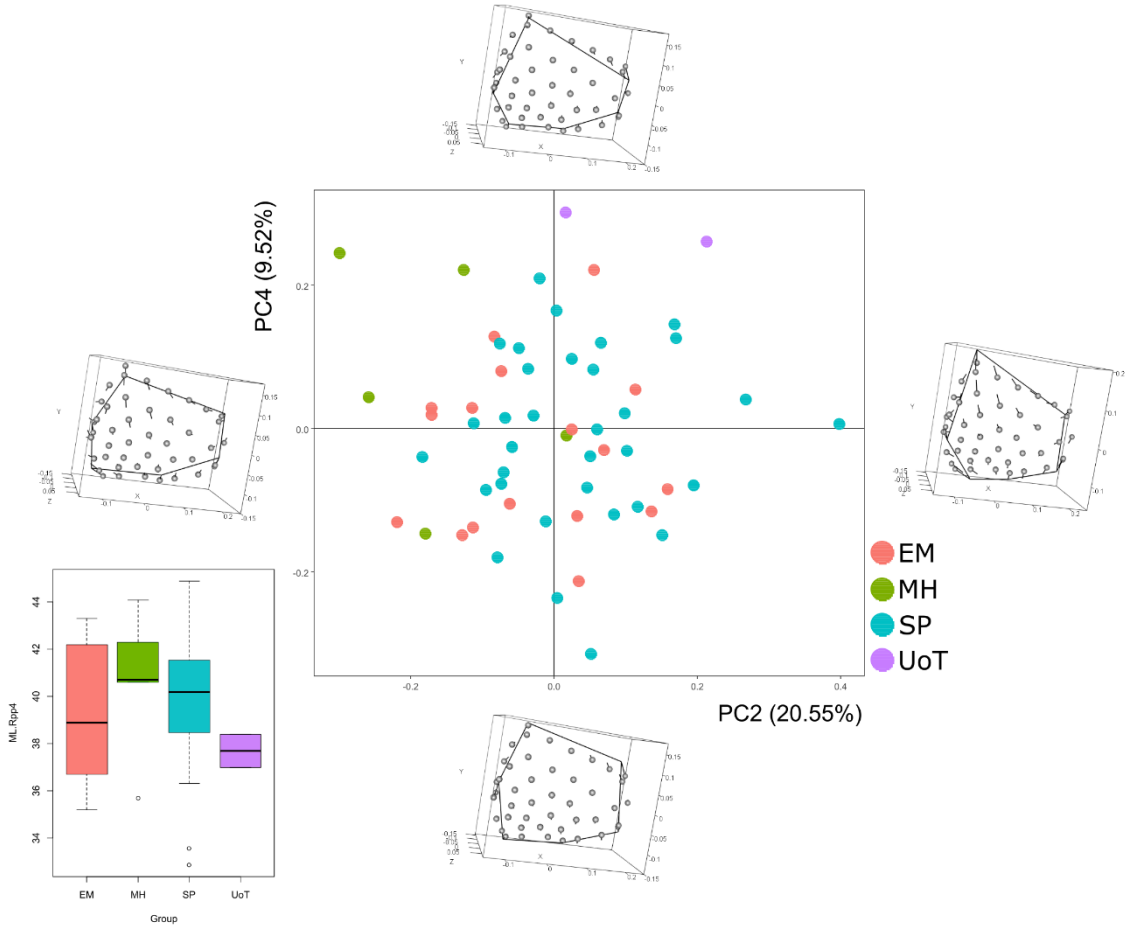

Figure 122 - Principal Component Analysis on the entire set of landmarks and shape configuration at the extremes of PC2 and PC4 for right PI2.

For the analyses of PI2 of right PP4 (**Figure 120**), a total of 57 specimens were available. Here, the first four PCs were analysed, representing almost the 75% of the total variance.

Proceeding with descriptions of shape variation, along PC1 both fixed and surface landmarks relocate from a palmar to a most dorsal position, in particular: L1, along with surrounding surface semi-landmarks on the distal outline, moves to the dorsal surface, L2 and L3 both move to palmar and distal directions, and L4, L5 and L6 also move towards the palmar surface. About surface semi-landmarks located on the palmar and dorsal aspects of the entheseal outline, all relocate to the palmar surface, with proximal and distally directions, respectively. With regard to PC2, an increasing on proximo-distal direction is recorded, due to distal relocation of the landmarks lying on the distal aspect of the entheseal outline; also, a minimum increasing in correspondence of the dorsal outline can be seen. About fixed pseudo-landmarks, L1 and L4 move to opposite directions, going distally and laterally and proximally and medially, respectively, L2 and L3 both goes towards the palmar surface – with L3 also moving proximally – L5 relocates both proximally and dorsally, while L6 only move towards the proximal extremity. With regard to PC3, minimum variation can be seen in correspondence of landmarks L2 and L3 – both moving medially and in part distally – and L1 and L4 – moving in opposite directions, going towards dorsal and palmar surfaces, respectively. Regarding PC4, unique variations are in correspondence of L2 and L6, both moving to a proximal direction, and L5 partially moving medially.

In the shape space shown in **Figure 121**, distinction between MH and the rest of the sample can be seen, distributed for positive and negative values of PC1 and PC2, respectively. These specimens are therefore characterised by reduced entheses in proximo-distal direction along PC2 and the distal point – where L1 is – directed to a most palmar direction. Also, two specimens belonging to EM have a distribution for high values of PC1. With regard to description of the shape space in **Figure 122**, same kind of distribution can be seen, with MH distributed for negative and positive values of PC2 and PC4, respectively, and UoT with positive values of both PCs; their entheses are therefore characterised by reduced dimensions in correspondence of the dorsal aspect of the outline and general reduction in proximo-distal way. For MH, two exceptions can be seen, because falling inside SP and EM distributions.

4.9.2 Left PP4 – Descriptive statistics, normality tests and correlation analyses

	raw size - DI4	ERS - DI4	raw size - PI2	ERS - PI2	APWM/ML*	MLWM/ML*	ML*
N	53	52	55	54	66	66	66
Min	78,56	0,07	61,63	0,06	0,13	0,19	33,97
Max	192,83	0,13	188,20	0,12	0,19	0,27	44,90
Mean	119,77	0,09	110,72	0,08	0,16	0,22	39,96
Stand. dev	25,28	0,01	23,76	0,01	0,01	0,02	2,24

Table 58 - Summary statistics for both 3D size and linear measurements of left PP4. Raw size is calculated in mm2, ML in calculated in mm. **APWM/ML**: Antero-Posterior Robusticity Index. **MLWM/ML**: Medio-Lateral Robusticity Index. **ML**: Maximum Length.

	raw size - DI4	ERS - DI4	raw size - PI2	ERS - PI2	APWM/ML*	MLWM/ML*	ML*
N	53	52	55	54	66	66	66
Shapiro-Wilk W	0,94	0,95	0,97	0,98	0,99	0,99	0,98
p(normal)	0,01449	0,02102	0,22	0,67	0,87	0,78	0,41

Table 59 - Shapiro-Wilk test for each variable of left PP4.

	raw size - DI4	ERS - DI4	raw size - PI2	ERS - PI2
APWM/ML*		-0,03		
MLWM/ML*		-0,02		0,23
ML*		0,03		0,01

Table 60 - Correlation tests between 3D bone sizes and linear dimensions for left PP4.

In **Tables 58 – 60**, descriptive statistics, correlation tests and normal distribution tests for all the variables used in this work are summarized.

The set of values for the entheses of PP4 are similar, according to their comparable dimensions on the base of the bone. With regard to normality tests for each variable of left PP4, the Shapiro-Wilk's test has verified a normal distribution with a *p-value* > 0.05 for all variable, except for both raw size and ERS index of DI4 enthesis. Correlation tests were performed: positive relations have been recorded between total surface size and both raw size and ERS of each enthesis. About relation between entheseal size (raw and ERS) and bone dimensions, correlation is recorded for ERS index of DI4 enthesis and all linear dimensions (with negative values for RIs); also, ERS index of PI2 enthesis highly correlates with bone length.

4.9.2.1 DI4 enthesis

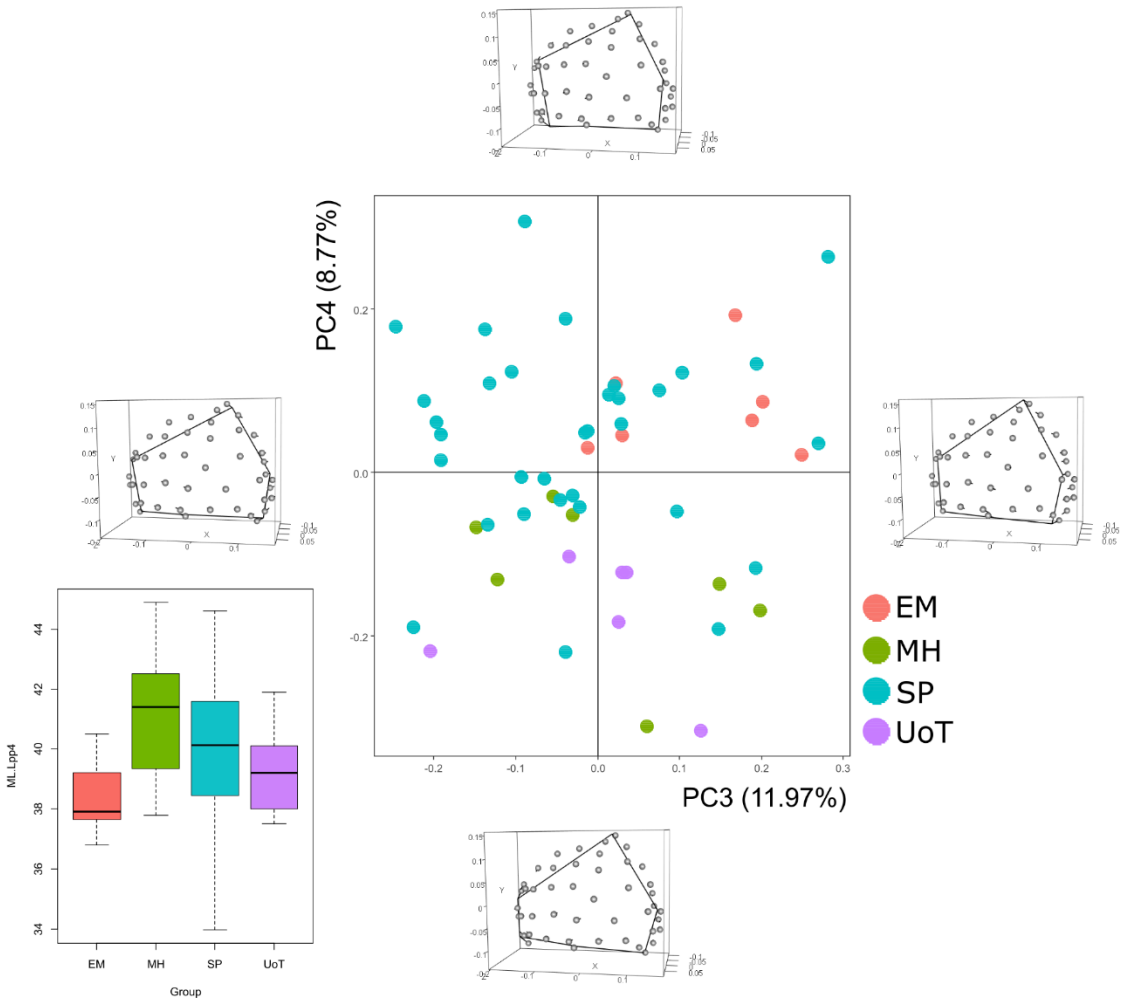

Figure 123 - Principal Component Analysis on the entire set of landmarks and shape configuration at the extremes of PC3 and PC4 for left DI4.

For the analyses of DI4 of left PP4, a total of 53 specimens were available. Here, the first four PCs were analysed, representing almost the 64% of the total variance.

Analysing shape variation along PC1, a shift from a dorsal to a palmar position can be shown in correspondence of the most distal portion, due to L1 and surrounding semi-landmarks. About other landmarks, L2 and L3 both move to proximal and dorsal directions, L4 moves dorsally along the outline towards L3, while L5 and L6 both relocate dorsally and in a distal way. With regard to surface semi-landmarks, those lying in correspondence of the dorsal aspect of the entheseal outline move proximally and dorsally, as L2 and L3. Along PC2, the morphological variation occurs in a proximo-distal direction due to minimum relocation of L1, L2, L4 and L5– L1 moves distally, L2 and L5 move medially and L4 moves laterally. Even along PC3, a partial increasing in proximo-distal direction is visible but a minimum shift from a dorsal to palmar direction is also recorded. These changes are due to minimum repositions of five fixed landmarks: L1 moves to distal and palmar directions, L2 and L3 go also to palmar direction (and L3 also moving proximally), L4 moves proximally and L6 goes to a lateral way. About surface semi-landmarks, they are not affected by repositioning. With regard to PC4, most important shape variation occurs on the palmar side of the enthesis, with L5 moving to proximal and dorsal directions and L6 moving distally and also laterally; these changes can be seen and described as an increasing on the palmar aspect of the entheseal outline, between landmarks L5 and L6.

Separation between MH and UoT groups and EM and SP groups is visible for each PCs; here, in **Figure 123**, only plot considering PC3 and PC4 is described because of complete distinction between EM from the other groups – MH and UoT have a distribution for negative values of PC4 while EM is distributed for positive values of both PCs. No particular distribution is about SP, but its major spreading is for positive values of PC4. As final consideration, specimens from EM are characterised by increased entheses in proximo-distal direction on the corresponding palmar outline. Similar distributions can be seen when other PCs are considered; they are not shown here but are introduced in the Annexes (cf. A4 – 28, A4 – 29).

4.9.2.2 PI2 enthesis

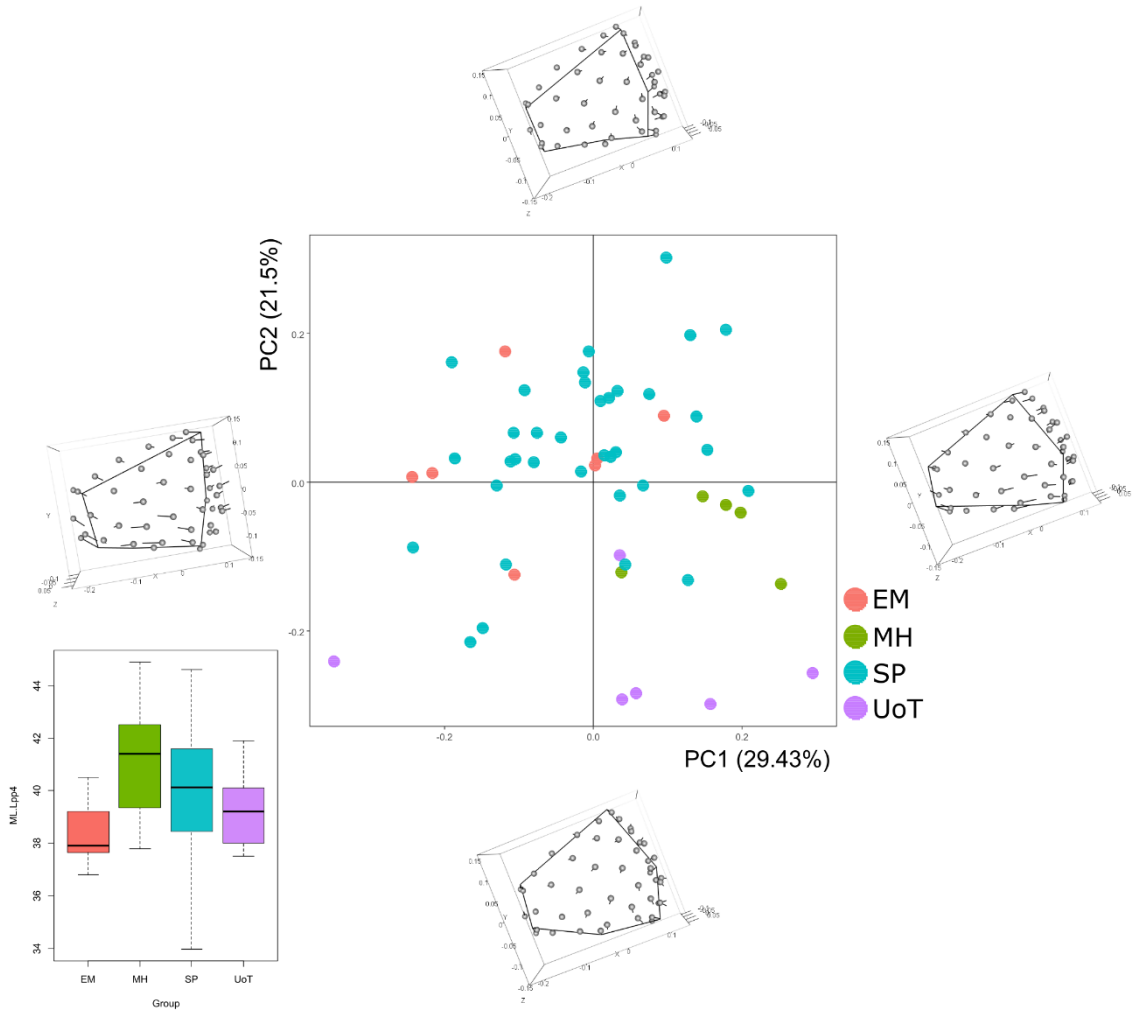

Figure 124 - Principal Component Analysis on the entire set of landmarks and shape configuration at the extremes of PC1 and PC2 for left PI2.

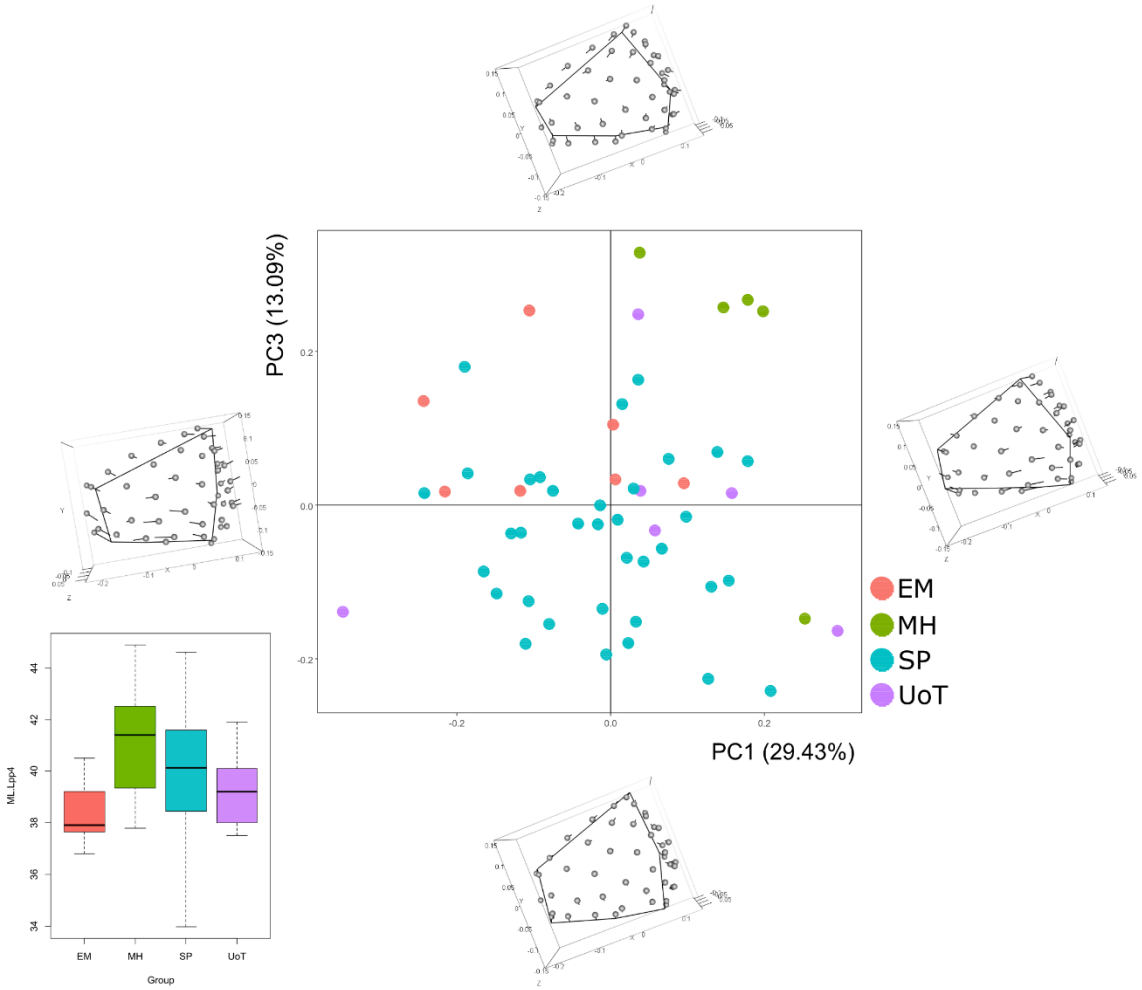

Figure 125 - Principal Component Analysis on the entire set of landmarks and shape configuration at the extremes of PC1 and PC3 for left PI2.

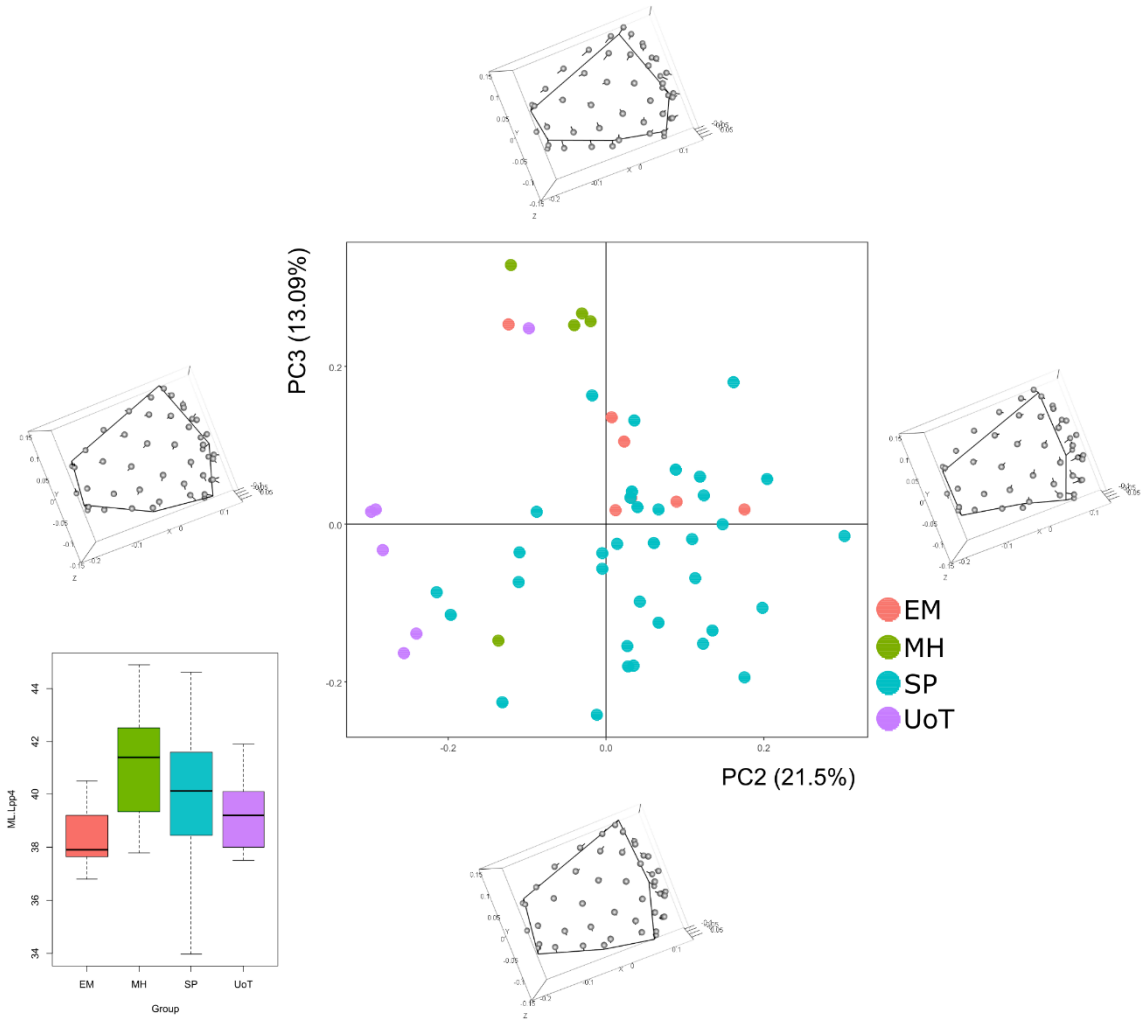

Figure 126 - Principal Component Analysis on the entire set of landmarks and shape configuration at the extremes of PC2 and PC3 for left PI2.

For the analyses of PI2 of left PP4, a total of 53 specimens were available. Here, the first four PCs were analysed, representing almost the 75% of the total variance.

Proceeding with description of morpho spaces to analyse shape variation, along PC1 all landmarks – both fixed and surface ones – relocates, causing a shift of the enthesis towards a dorsal direction: L1, L2 and L3 move dorsally – with L2 and L3 also going medially – while L4 move to a palmar direction, L5 and L6 go towards the lateral side of the enthesis. About surface semi-landmarks, those located on the dorsal and palmar aspects of the entheseal outline relocate to a dorsal direction, while others lying close to the central portion of the enthesis move towards a palmar direction. Regarding PC2, a decreasing in proximo-distal direction can be seen, caused by minimum relocation of each fixed pseudo-landmark: L1 moves proximally towards L6, L4 goes to a distal direction, while L2, L3, L5 and L6 all move both medially and dorsally. About surface semi-landmarks, they move to a lateral position, causing a partial increasing of the entheseal surface. When PC3 is introduced, a reduction in proximo-distal direction and an increasing in antero-posterior way can be seen at the same time; in this case, L1 and L2 both move proximally, towards the dorsal surface, L3 and L4 both move distally, while L5 and L6 move medially but towards proximal and distal direction, respectively. With regard to surface semi-landmarks, some located on the proximal aspect of the entheseal outline move to a distal direction, some located on the palmar aspect of the outline move towards the palmar direction, and others lying on the distal entheseal outline move along the outline between L1 and L2, going dorsally. Along PC4, the major shape variation occurs in a proximo-distal way in correspondence of the dorsal aspect of the entheseal outline; this variation is due to L1 moving dorsally, L2 and L3 both moving to a palmar direction but distally and proximally, respectively, and L5 and L6 both moving in a palmar direction.

Distinct groups can be seen in the graphs previously shown: in **Figure 124**, specimens from MH and UoT are distributed for negative and positive values for PC2 and PC1, respectively, and are distinct from EM. The main difference is related to the dorsal side of the enthesis, which is reduced in proximo-distal way for MH and UoT specimens. One specimen from Un. of Turin can be considered as an outlier of its own group because its negative values for both PCs. Similar distribution is about PC1 and PC4, so it is described in the Annexes (cf. A4 – 30). In **Figure 125**, same kind of separation can be seen but, in this case, MH has positive values for both PC1 and PC3 and EM is distributed for only negative PC1. Furthermore, when PC2 and PC3 are considered, clear separation between each group is shown: EM is in the 1st quarter of the plot (with positive values of both PCs), MH has positive values of PC3 and negatives' for PC2, while UoT has negative values for both PCs. In **Figure 126**, separation between UoT and MH with the rest of the sample is recorded – they lie on the negative side of PC2 but are distributed for negative and positive values of PC3, respectively.

4.10 Analyses of 5th phalangeal bones

4.10.1 Right PP5 – Descriptive statistics, normality tests and correlation analyses

	raw size - PI3	ERS - PI3	raw size - ADM+FDM	ERS - ADM+FDM	APWM/ML*	MLWM/ML*	ML*
N	61	59	65	61	70	70	70
Min	49,90	0,06	67,57	0,08	0,13	0,03	26,90
Max	138,28	0,12	179,16	0,14	0,20	0,30	40,94
Mean	90,25	0,09	108,08	0,11	0,17	0,25	32,34
Stand. dev	22,00	0,01	26,11	0,01	0,02	0,04	2,42

Table 61 - Summary statistics for both 3D size and linear measurements of right PP5. Raw size is calculated in mm^2, ML in calculated in mm. **APWM/ML**: Antero-Posterior Robusticity Index. **MLWM/ML**: Medio-Lateral Robusticity Index. **ML**: Maximum Length.

	raw size - PI3	ERS - PI3	raw size - ADM+FDM	ERS - ADM+FDM	APWM/ML*	MLWM/ML*	ML*
N	61	59	65	61	70	70	70
Shapiro-Wilk W	0,97	0,98	0,95	0,98	0,99	0,75	0,96
p(normal)	0,22	0,57	0,01148	0,35	0,70	1,27E-09	0,0173

Table 62 - Shapiro-Wilk test for each variable of right PP5.

	raw size - PI3	ERS - PI3	raw size - ADM+FDM	ERS - ADM+FDM
APWM/ML*			0,19	0,08
MLWM/ML*				0,22
ML*		0,05		0,20

Table 63 - Correlation tests between 3D bone sizes and linear dimensions for right PP5.

In **Tables 61 – 63**, descriptive statistics, correlation tests and normal distribution tests for all the variables used in this work are summarized.

The set of values for the entheses of PP5 are similar, according to their comparable dimensions on the base of the bone. With regard to normality tests for each variable of right PP5, the Shapiro-Wilk's test has verified a normal distribution with a *p-value* > 0.05 for all variable, except for raw size of ADM+FDM enthesis. Correlation tests were performed: positive relations have been recorded between total surface size and both raw size and ERS of each enthesis. About relation between entheseal size (raw and ERS) and bone dimensions, ERS of ADM+FDM enthesis correlates with all linear dimensions, while ERS index of PI3 correlates with maximum bone length; also, raw size of ADM+FDM enthesis has a low correlation with antero-posterior RI.

4.10.1.1 ADM+FDM enthesis

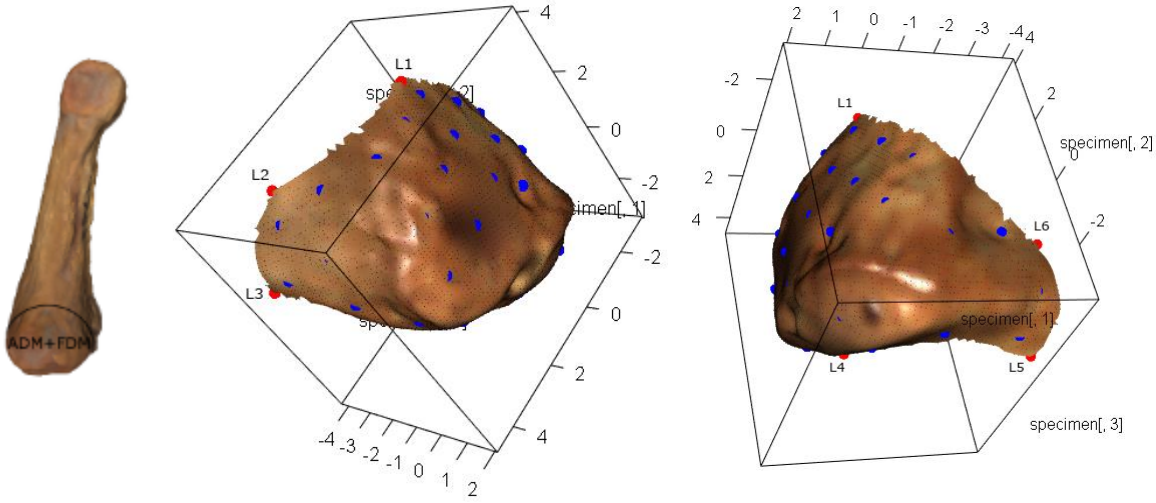

Figure 127 - On the left, the PP5 bone with ADM+FDM delimited enthesis.
On the right, the landmarks (red spots) and semi-landmarks (blue spots) on the 3D model of the surface of ADM+FDM.
For the landmarks' definitions, see Annexes (cf. A2 – 10).

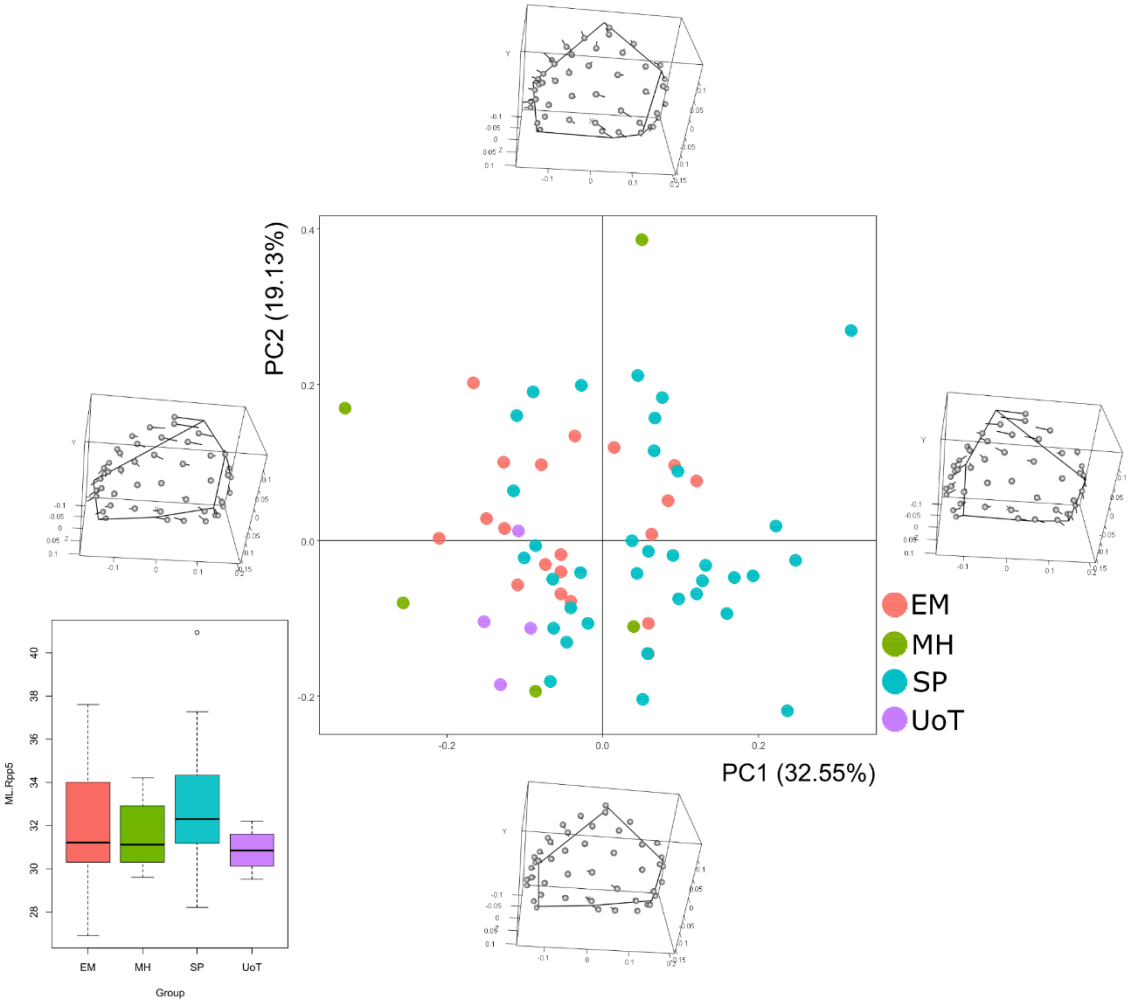

Figure 128 - Principal Component Analysis on the entire set of landmarks and shape configuration at the extremes of PC1 and PC2 for right ADM+FDM.

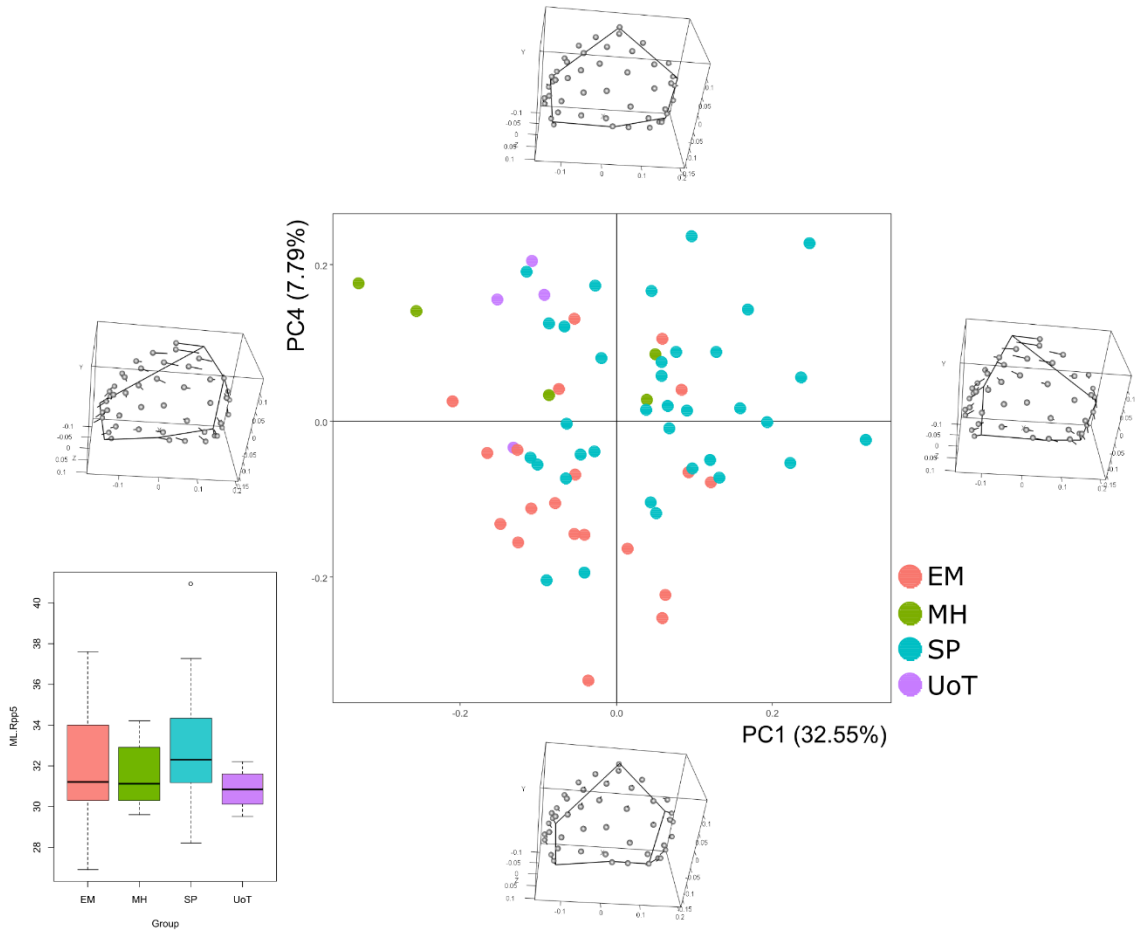

Figure 129 - Principal Component Analysis on the entire set of landmarks and shape configuration at the extremes of PC1 and PC4 for right ADM+FDM.

For the analyses of ADM+FDM of right PP5 (**Figure 127**), a total of 64 specimens were available. Here, the first four PCs were analysed, representing almost the 75% of the total variance.

Analysing shape variation along each PC, regarding PC1 both fixed and surface landmarks relocate, determining an increasing in antero-posterior way and a shift of L1 – along with surrounding surface semi-landmarks – moving from a palmar to a most dorsal position; L2, L3 and L4 both move to distal and palmar directions, while L5 and L6 both move to proximal and palmar directions. About other surface semi-landmarks, some of them located on the dorsal aspect of the entheseal outline move distally, towards the palmar surface, while others located on the proximal and palmar outlines move towards the proximal epiphysis. Along PC2, an increasing in proximo-distal direction in correspondence of the dorsal and palmar outlines is evident: this change is due to repositioning of L1 to a distal position, L4 to a palmar direction, and L5 and L6 moving dorsally along the corresponding outline towards L4 and L1, respectively. Major variation can be seen in correspondence of surface semi-landmarks close to the dorsal surface which relocate to a most distal position. With regard to PC3, a resulting increasing in correspondence of the palmar entheseal outline is recorded, caused by relocation of L1 and L5 to a distal position and L6 to a proximal one; also, a partial decreasing in antero-posterior direction can be seen, due to L2 and L3, along with surrounding surface semi-landmarks, moving medially. About PC4, the major differences between minimum and maximum morpho-spaces concerns the relocation of L2 and L3 – both moving distally, along the outlines towards L1 and L4 – and L5 and L6 moving to medial and distal-palmar directions, respectively.

In shape spaces previously shown, different distributions concerning MH and UoT are evident. In **Figure 128**, specimens from MH have a wide distribution around the entire sample. About specimen from UoT, they have a distribution for negative values of both PC1 and PC2: this means that they are characterised by reduced entheses in a proximo-distal direction and a most dorsal position of the landmarks located distally. Similar distribution can be seen when PC1 and PC3 are considered (Annexes, A4 – 31). A different situation can be described in **Figure 129**, where MH and UoT are distributed for positive and negative values of PC4 and PC1, respectively (except for two specimens from MH, with positive values of PC1). A peculiarity is EM, whose specimens are for the most spread for negative values of PC4 – so they are characterised by larger entheses in a proximo-distal direction.

4.10.1.2 PI3 enthesis

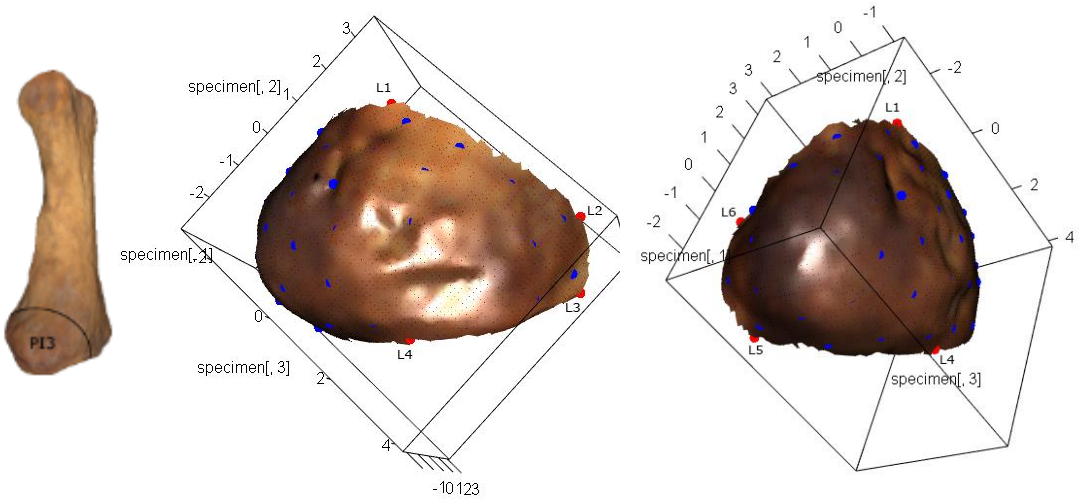

Figure 130 - On the left, the PP5 bone with delimited PI3 enthesis.
On the right, the landmarks (red spots) and semi-landmarks (blue spots) on the 3D model of the surface of PI3.
For the landmarks' definitions, see Annexes (cf. A2 – 10).

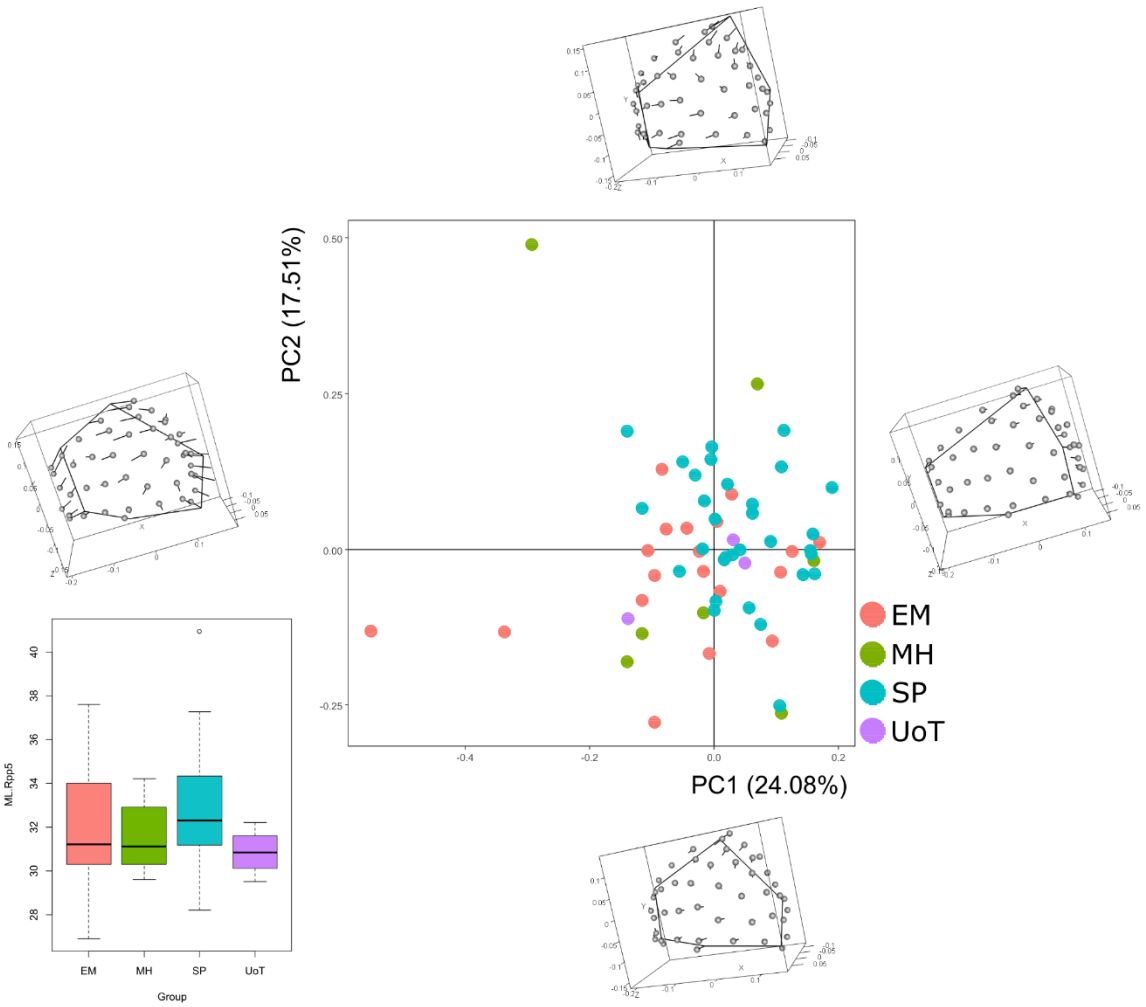

Figure 131 - Principal Component Analysis on the entire set of landmarks and shape configuration at the extremes of PC1 and PC2 for right PI3.

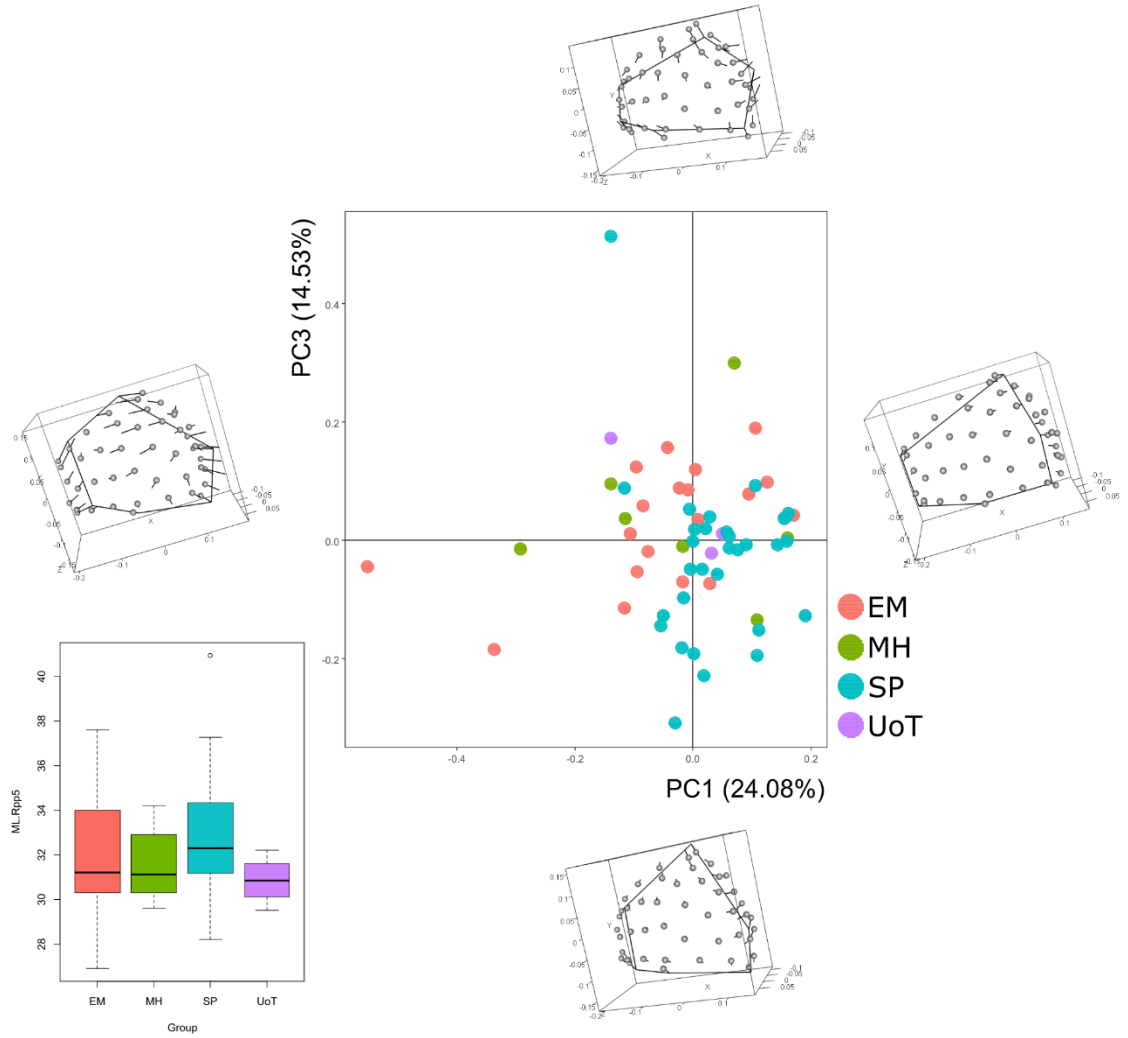

Figure 132 - Principal Component Analysis on the entire set of landmarks and shape configuration at the extremes of PC1 and PC3 for right PI3.

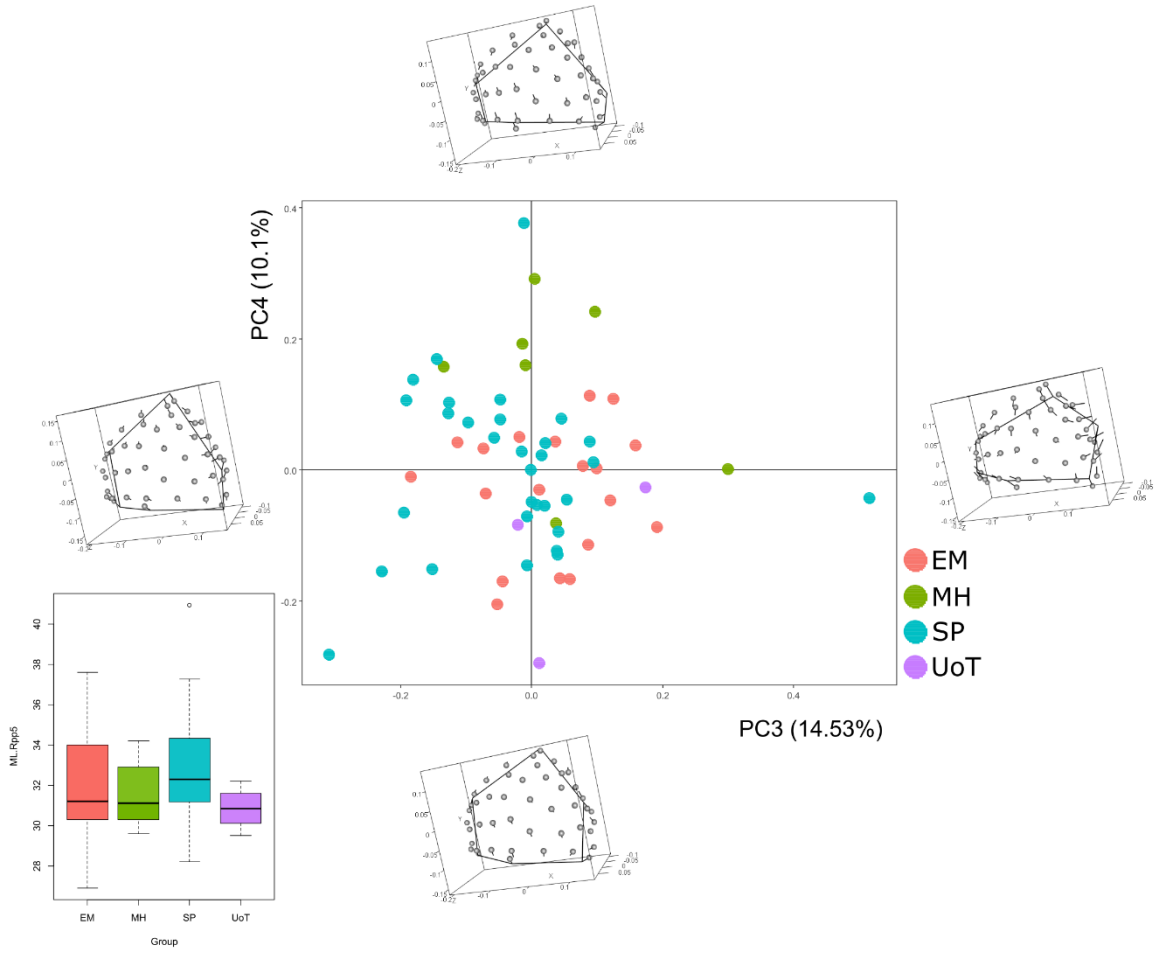

Figure 133 - Principal Component Analysis on the entire set of landmarks and shape configuration at the extremes of PC3 and PC4 for right PI3.

For the analyses of PI3 of right PP5 (**Figure 130**), a total of 60 specimens were available. Here, the first four PCs were analysed, representing almost the 67% of the total variance.

Proceeding with analyses and description of shape variation, along PC1 both L1 and surrounding surface semi-landmarks relocate, causing a shift of the entheseal distal portion to a dorsal direction; with regard to other landmarks, all move towards the palmar surface, with L5 and L6 also going proximally and medially. About surface semi-landmarks, those lying on the palmar and dorsal aspects of the entheseal outline proceed to palmar surface, while others lying on the centre of the enthesis go both dorsally and distally. With regard to PC2, an increasing in proximo-distal direction in recorded, along with a shift from palmar to a most dorsal position of the distal tip where L1 is; about other fixed landmarks, L5 and L6 also relocate, moving to a medial and proximal directions, partially. No important variation is about surface semi-landmarks – some of them close to L1 move distally towards the dorsal surface while others lying on the proximal and palmar entheseal outline continue moving proximally. Regarding PC3, an important decreasing in proximo-distal direction can be seen, along with an increasing in correspondence of the entheseal surface to a medial direction: these variations are due to L1, moving both proximally and dorsally, along the outline towards L2, L2 moving distally, while L3 and L5 moving distally and medially, and L4 moving distally but towards a palmar direction. About surface semi-landmarks, those lying on the dorsal entheseal portion move to a most dorsal and distal position, causing changes on surface entheseal morphology. With regard to PC4, even in this case an increasing in a proximo-distal way can be seen, due to minimum relocation of five fixed pseudo-landmarks: L1 moves laterally and proximally, L2 and L3 both move to a medial direction but proximally and medially, respectively, L4 partially moves to a distal direction, while L6 relocates to a most proximal position, moving along the entheseal outline towards L5. About surface semi-landmarks, some of them lying in correspondence of the dorsal aspect of the outline move to the same direction of both L2 and L3 – medially, towards the dorsal surface.

Proceeding in descriptions of shape spaces previously shown, MH has a distribution for negative values of PC2 – it has characterised by entheses with L1 directed to the palmar surface. About EM, specimens are distributed in each part of the graph, except for the quarter with positive values for both PCs – where most of SP lies, with one specimen from MH (**Figure 131**). Different distribution can be seen in **Figure 132**, because of distribution of each sample: EM is distributed in all graphic area – the exception is the area with positive values of PC1 and negative ones for PC3, where only SP specimens are. The real distinction is among SP and EM – the latter with specimens with reduced entheses than SP. In **Figure 133**, MH is for the most distributed for positive values of PC4, with entheseal area reduced in proximo-distal direction. A similar distribution is visible for PC2 and PC4 (Annexes, cf. A4 – 32).

4.10.2 Left PP5 – Descriptive statistics, normality tests and correlation analyses

	raw size - PI3	ERS - PI3	raw size - ADM+FDM	ERS - ADM+FDM	APWM/ML*	MLWM/ML*	ML*
N	58	57	56	55	62	62	62
Min	32,88	0,05	61,35	0,09	0,13	0,19	27,80
Max	139,41	0,14	148,24	0,13	0,21	0,31	35,87
Mean	89,67	0,09	106,22	0,11	0,17	0,24	32,13
Stand. dev	19,95	0,02	19,78	0,01	0,02	0,03	1,81

Table 64 - Summary statistics for both 3D size and linear measurements of left PP5. Raw size is calculated in mm2, ML in calculated in mm. **APWM/ML**: Antero-Posterior Robusticity Index. **MLWM/ML**: Medio-Lateral Robusticity Index. **ML**: Maximum Length.

	raw size - PI3	ERS - PI3	raw size - ADM+FDM	ERS - ADM+FDM	APWM/ML*	MLWM/ML*	ML*
N	58	57	56	55	62	62	62
Shapiro-Wilk W	0,97	0,94	0,97	0,99	0,99	0,99	0,98
p(normal)	0,20	0,01044	0,18	0,74	0,89	0,73	0,61

Table 65 - Shapiro-Wilk test for each variable of left PP5.

	raw size - PI3	ERS - PI3	raw size - ADM+FDM	ERS - ADM+FDM
APWM/ML*		0,24		0,17
MLWM/ML*		0,16		0,20
ML*		0,01		0,11

Table 66 - Correlation tests between 3D bone sizes and linear dimensions for left PP5.

In **Tables 64 – 66**, descriptive statistics, correlation tests and normal distribution tests for all the variables used in this work are summarized.

The set of values for the entheses of PP5 are similar, according to their comparable dimensions on the base of the bone. With regard to normality tests for each variable of left PP5, the Shapiro-Wilk's test has verified a normal distribution with a *p-value* > 0.05 for all variable, except for ERS index of PI3 enthesis. Correlation tests were performed: positive relations have been recorded between total surface size and both raw size and ERS of each enthesis. About relation between entheseal size (raw and ERS) and bone dimensions, ERS indexes of both ADM+FDM and PI3 entheses positively correlate with all bone linear measurements.

4.10.2.1 ADM+FDM enthesis

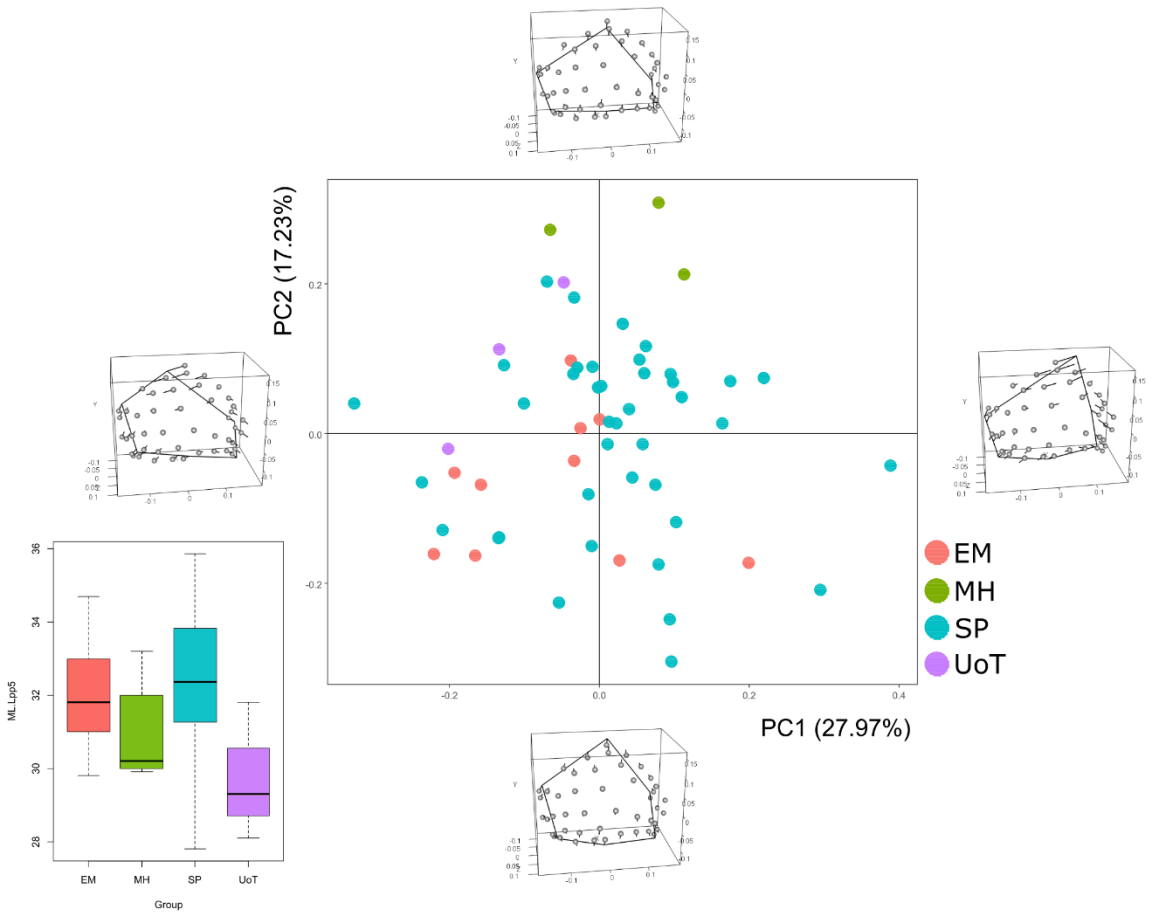

Figure 134 - Principal Component Analysis on the entire set of landmarks and shape configuration at the extremes of PC1 and PC2 for left ADM+FDM.

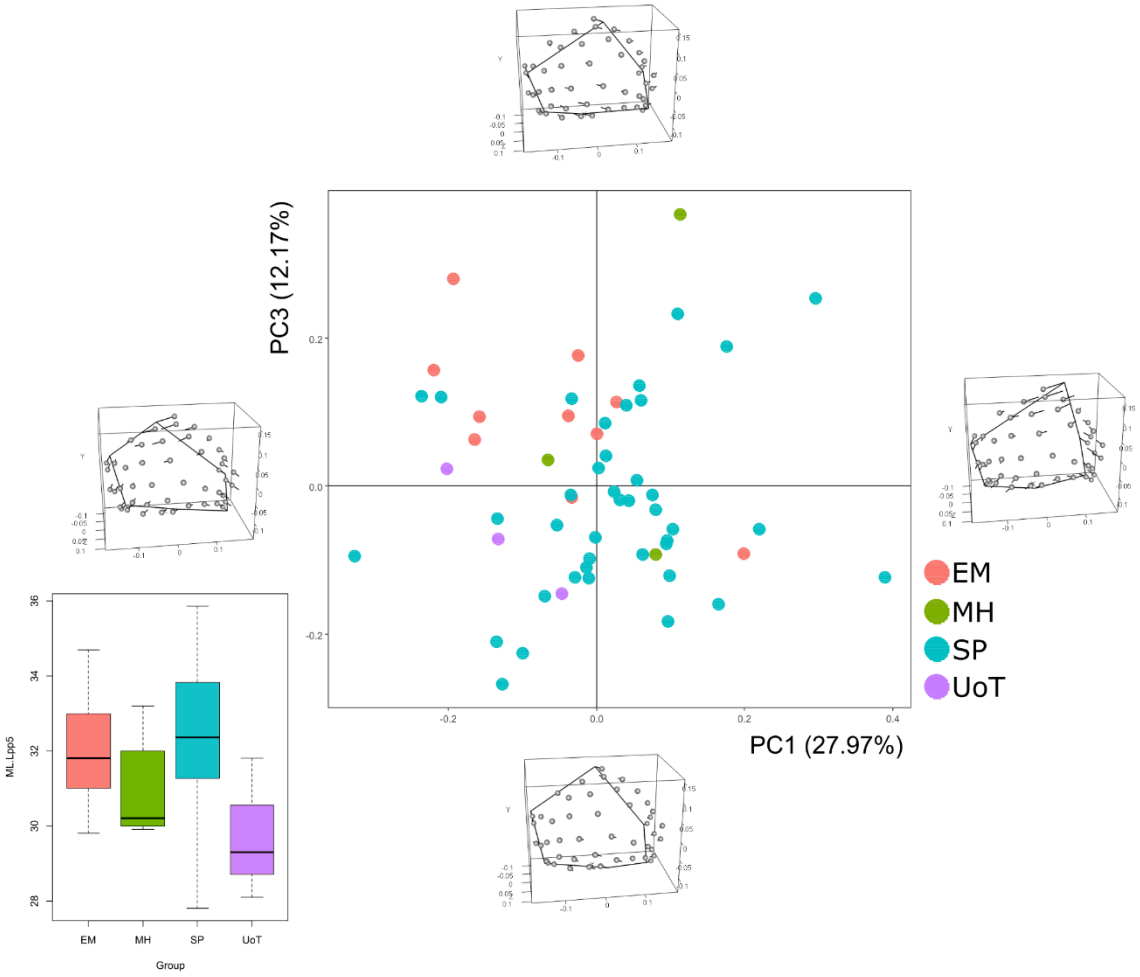

Figure 135 - Principal Component Analysis on the entire set of landmarks and shape configuration at the extremes of PC1 and PC3 for left ADM+FDM.

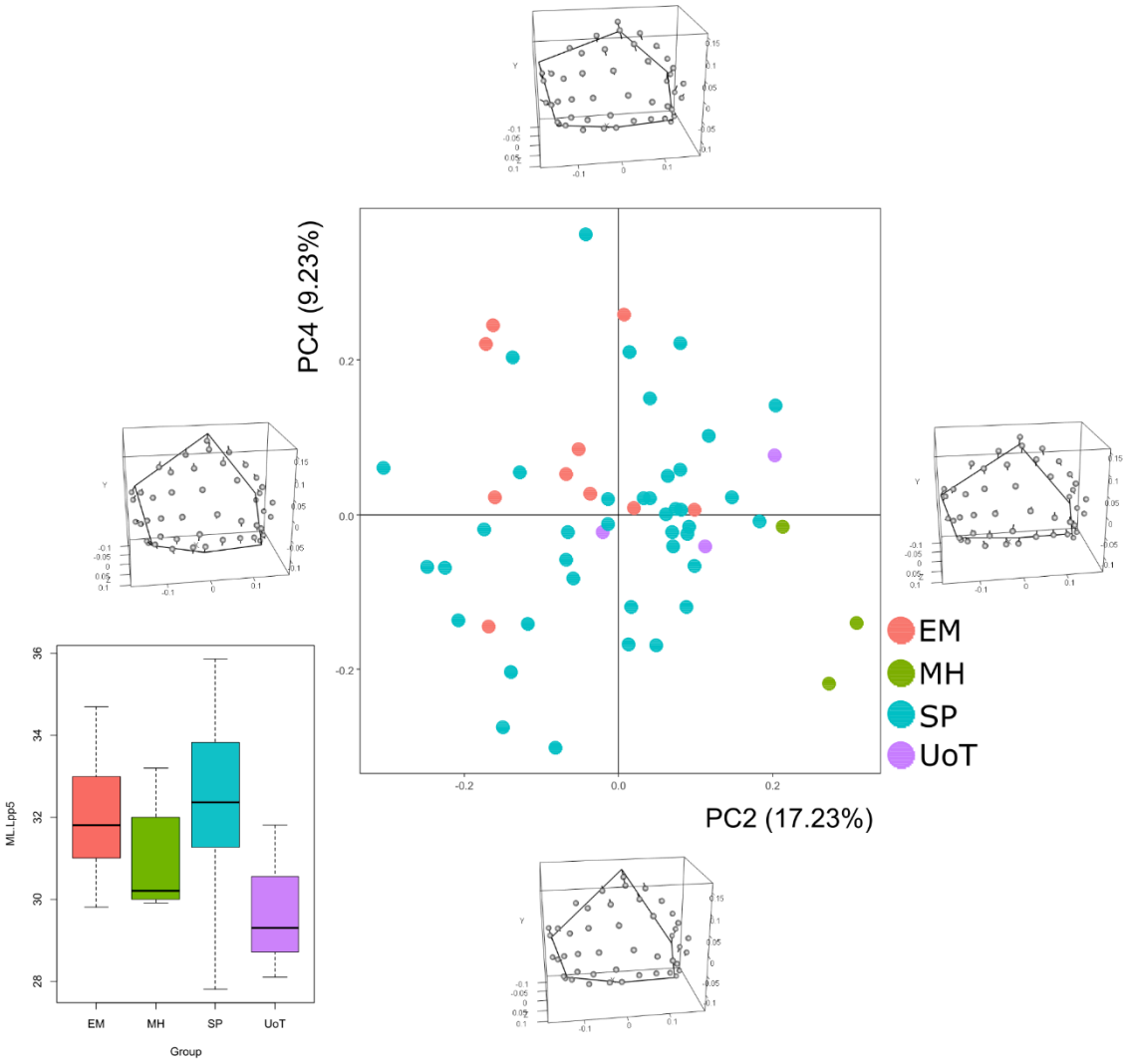

Figure 136 - Principal Component Analysis on the entire set of landmarks and shape configuration at the extremes of PC2 and PC4 for left ADM+FDM.

For the analyses of ADM+FDM of left PP5, a total of 56 specimens were available. Here, the first four PCs were analysed, representing almost the 67% of the total variance.

Analysing shape differences along PC1, relocation of fixed landmark L1 and surrounding surface semi-landmarks to a most dorsal position determine a shift of the distal portion of the entheses towards the dorsal bone surface, causing also a proximo-distal increasing in correspondence of the dorsal portion. About other landmarks, from L2 to L6 all move towards the palmar surface, with L2 and L3 both moving distally, and L4 to L6 moving proximally. With regard to the other surface semi-landmarks, those located from dorsal to palmar entheseal portion move to a palmar direction. Regarding PC2, a decreasing in proximo-distal direction is recorded, due to repositioning of landmarks of the distal outline to a proximal position: in particular, L1 moves proximally, L2 and L6 move proximally but also laterally, L3 and L5 move only to a medial direction, and L4 goes distally. About surface semi-landmarks, minimum variation is recorded: generally, they follow the direction of the closest fixed pseudo-landmark. Regarding PC3, variation is in correspondence of the palmar aspect of the entheseal outline, caused by a proximal relocation of L6 and a dorsal shift of L1; also, L2 and L3 move both dorsally, L4 moves to a palmar direction and L5 moves along the proximal outline towards L4. No important variation occurs for surface semi-landmarks. With regard to PC4, an increasing in correspondence of the palmar and dorsal sides of the entheses and a decreasing due to a proximal relocation of L1 are recorded: L2 and L6 both move to a distal direction and surface semi-landmarks surrounding L1 also move proximally.

In shape spaces previously shown, separation between samples is evident. In **Figure 134**, MH has the highest values for PC2, and is distinct by UoT, SP, and EM. At the same time, major distribution for EM is for negative values of both PC1 and PC2: the main consideration is about the different morphologies between entheses along each axis and MH specimens are characterised by more reduced entheses than EM or SP. In **Figure 135**, different distributions are evident: most of SP is all spread for positive values of PC1 and negatives' for PC2, while EM has positive and negative values for PC3 and PC1, respectively – one exception is one specimen falling into SP group. Specimens from UoT are also distinct from the two archaeological collections – spread for negative values of both PCs, and one specimen with positive values for PC3. Similar distributions can be seen when PC4 is considered (**Figure 136**; Annexes, cf. A4 – 33).

4.10.2.2 PI3 enthesis

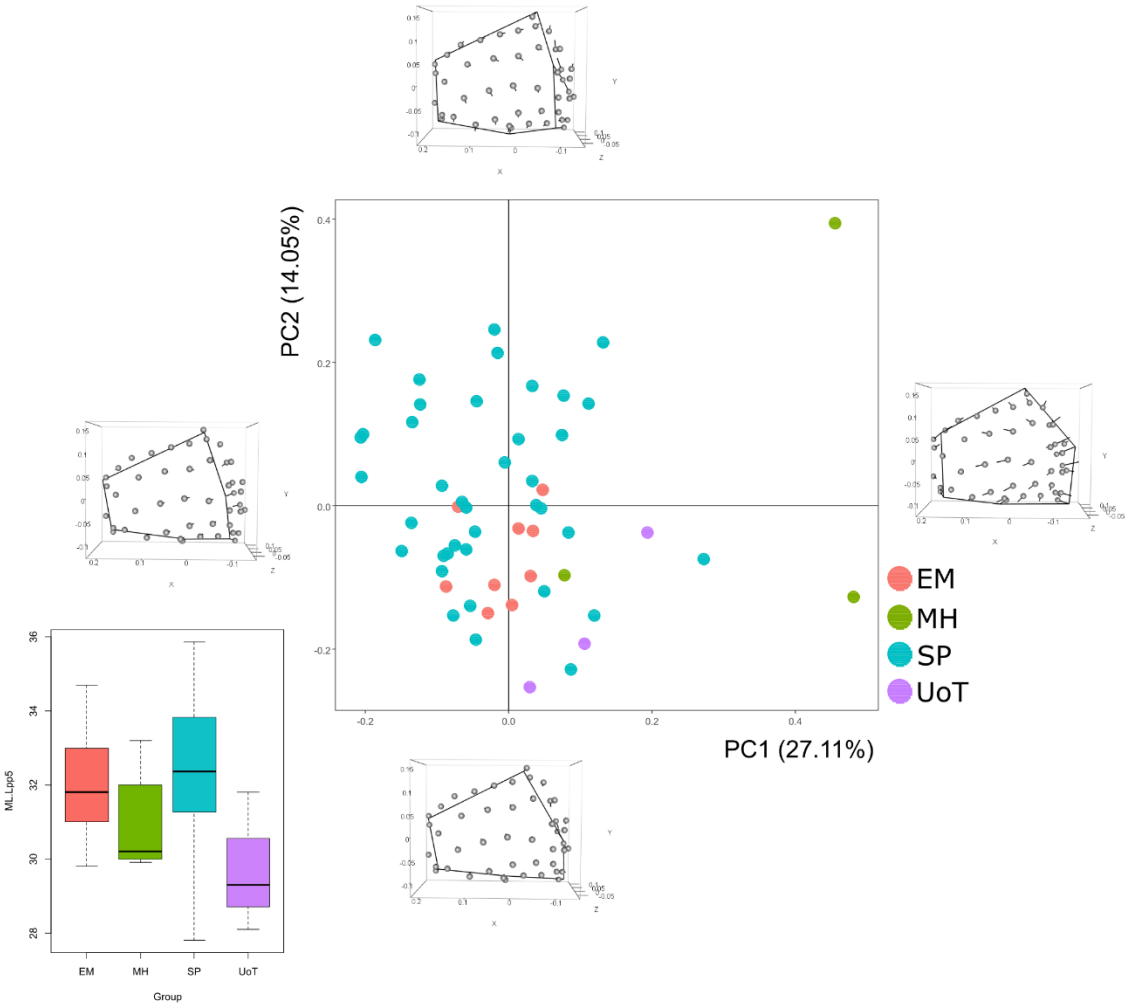

Figure 137 - Principal Component Analysis on the entire set of landmarks and shape configuration at the extremes of PC1 and PC2 for left PI3.

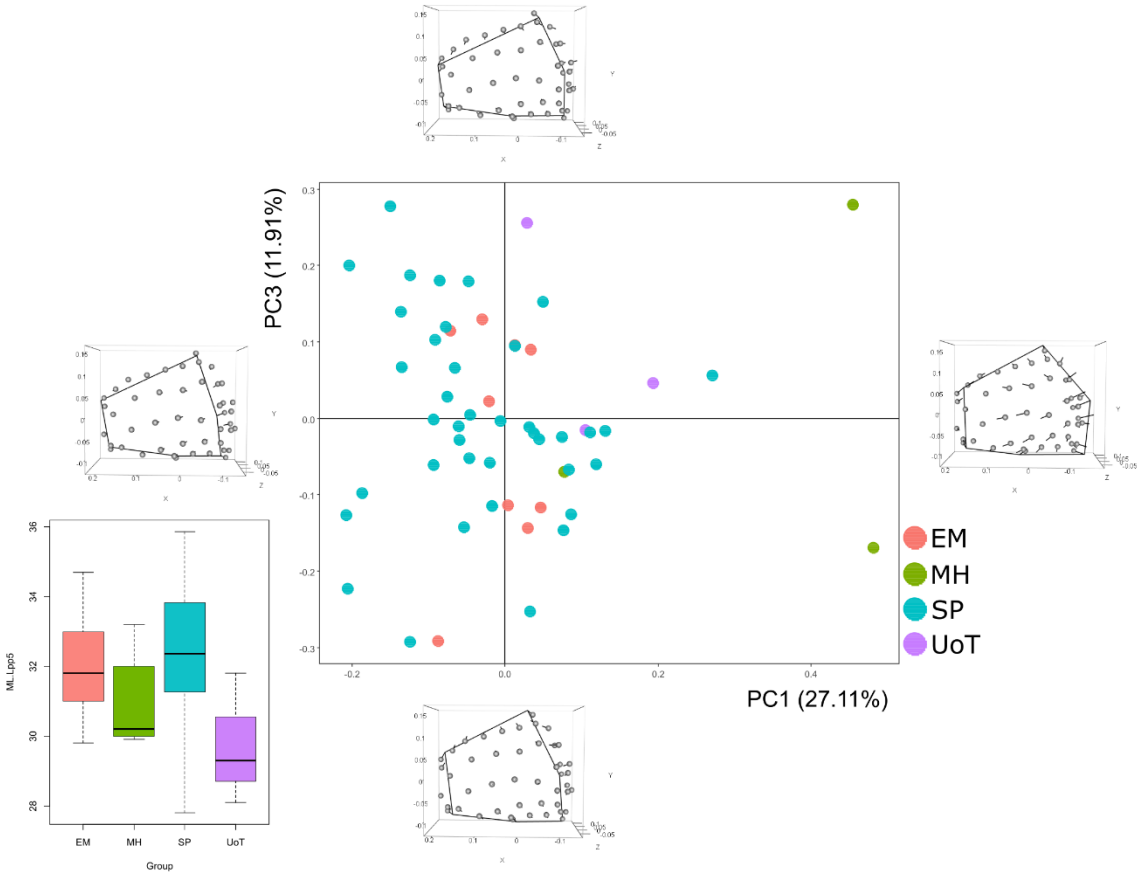

Figure 138 - Principal Component Analysis on the entire set of landmarks and shape configuration at the extremes of PC1 and PC3 for left PI3.

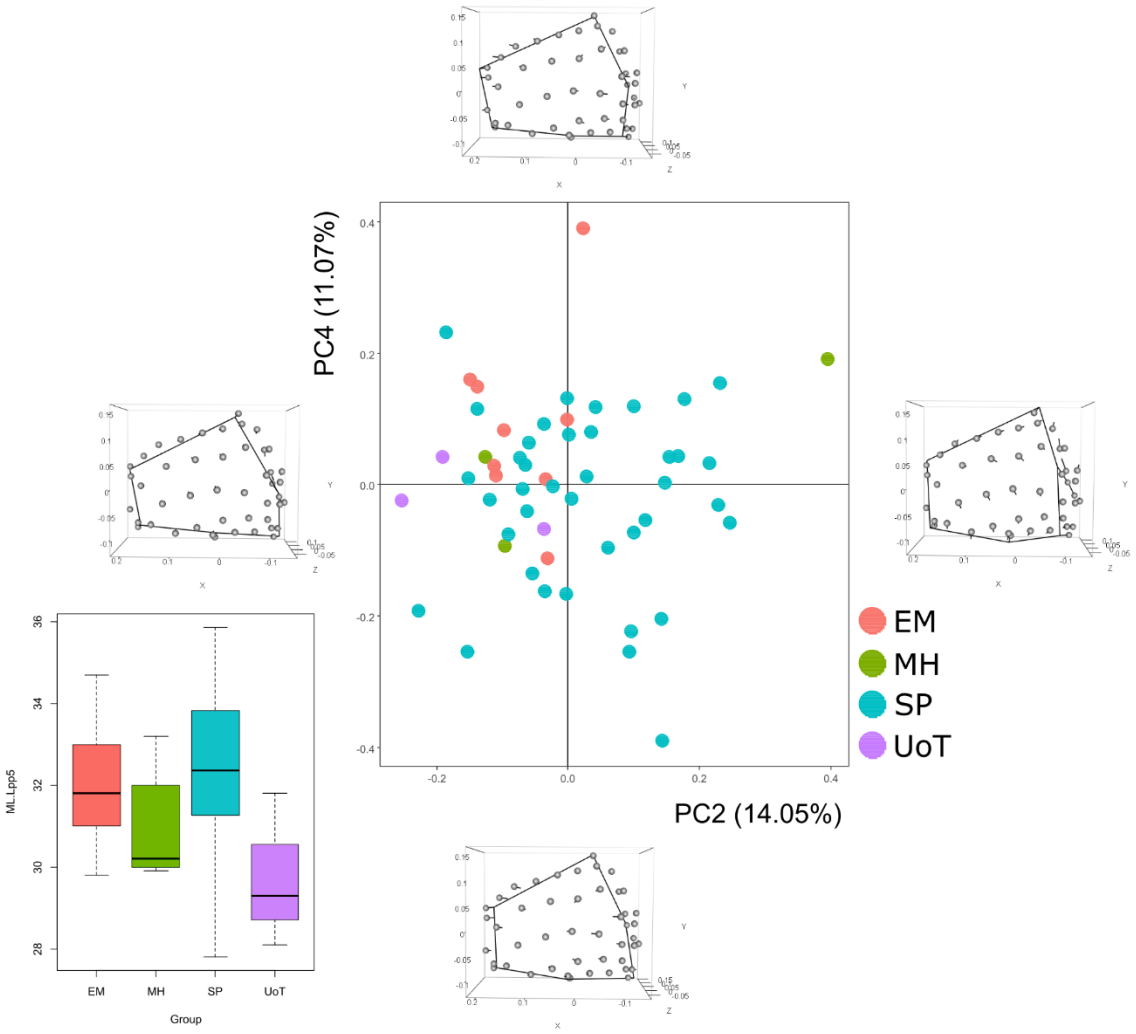

Figure 139 - Principal Component Analysis on the entire set of landmarks and shape configuration at the extremes of PC2 and PC4 for left PI3.

For the analyses of PI3 of left PP5, a total of 54 specimens were available. Here, the first four PCs were analysed, representing almost the 65% of the total variance.

Analysing shape variation along PC1, an increasing of the palmar entheseal outline is recorded, due to relocation of L5 and L6, moving both to palmar and lateral directions, and a partial movement of L3, going only laterally. About surface semi-landmarks, some of them lying close to the palmar surface continue proceeding to the palmar direction. Even with regard to PC2, main variation is on the palmar aspect of the entheseal outline, due to L6 moving distally, along the outline towards L1, and L4 moving to a lateral direction; also, L3 moves towards the dorsal bone surface, causing an increasing on the proximal entheseal outline. About surface semi-landmarks, those lying on the palmar portion move distally, supporting the distal shift of the entheseal area. Regarding PC3, a decreasing in proximo-distal direction is recorded, with main reduction in correspondence of the distal aspect of the entheseal outline caused by both surface and fixed landmarks: L1 moves to proximal and palmar directions, L2 and L3 move proximally and distally, respectively, while surface semi-landmarks on the distal outline moving also proximally. With regard to PC4, two minimum variations on both palmar and dorsal sides of the entheses can be seen: L2 moves towards the dorsal surface, while L3, L5 and L6 relocate in a most lateral position.

Proceeding with descriptions of analyses in figures previously shown, in **Figure 137** different distribution for each group can be seen: two specimens of MH are distributed for high values of PC1, including the largest entheses of the entire sample; UoT and EM are distinct from SP and between them, dispersed for negative values of PC2, but with similar entheseal morphologies. When considering PC1 and PC3 – as in **Figure 138** – samples' distribution is different: two specimens of MH are distributed for high values of PC1, but UoT and EM relocate along PC3 – similar dispersion can be seen when PC4 is considered (Annexes, cf. A4 - 34). In **Figure 139**, all small samples are distributed for negative values of PC2 and, on the positive side of PC2 axis only specimens of SP are present: two exceptions are one specimen EM (with high values for PC4) and one from MH (with high values of PC2), characterised by minimum morphological changes on the outline.

Chapter 5

Discussion

The main focus of this research concerned the morphometric analyses of insertion sites of metacarpals and phalanges in order to reconstruct multivariate activity patterns of ancient populations through the analyses of bones' entheseal surfaces.
First, descriptive statistics were carried out to test the correlation between entheseal size (both raw and ERS) and linear measurements – as bone length and bone robusticity. The set of multivariate analyses were performed to investigate the statistical correlation between all variables before cited and to understand if genetics or biomechanics determine entheseal changes. Furthermore, geometric morphometric analyses were conducted on hand muscular insertions to investigate entheseal shape variation and to obtain information about possible correlation between Shape and Size.

5.1 Considerations on the sample linear dimensions

The descriptive statistics carried out between entheseal and linear measurements made separation between origin and insertion sites possible. From a macroscopic point of view, these two different entheseal sites are characterised by different dimensions and morphologies, related to the different nature of each entheseal group: muscular origin sites have larger insertion areas and insert along the metacarpal shafts, while muscular insertion sites can be distinguished thanks to both small entheseal areas and the position of the attachment near the bone's proximal epiphysis – one exception is OP enthesis which inserts on the lateral side of the bone, near the distal head of MC1 and proceeding along the bone's midshaft. This kind of distinction is also visible when raw size and ERS indexes of both types of muscular attachments are considered: origin insertion sites, characterised by larger surface areas, present high resulting values, while low values have been recorded for small insertion ones. In addition, positive relation between entheseal raw size of each enthesis and the corresponding total bone area is visible, showing that the entheseal dimension is related to the surface area of the bone it belongs.

In the context of univariate statistics, correlation analyses between both entheseal measurements (both raw size and ERS indexes) and linear dimensions (maximum length, antero-posterior and medio-lateral robusticity indexes) were performed to investigate the possible influence of genetic and systemic factors or biomechanical stress on the entheses. As it was described in the methodological section, bone length is not subjected to the influence of bone remodelling and does not change during adulthood (Gilsanz, Ratib, 2005; Rauch, 2005; Krishan, Sharma, 2007; Charmode *et al.*, 2019); on the contrary, bone robusticity at midshaft is regulated by biomechanical stress and is subjected to muscular forces which determine changes on the bone surface. In other words, if bones of different dimensions are exposed to a well-defined amount of muscular stress, the final response due to bone remodelling will be related to corresponding surface dimension of the bone; related to this case, the introduction of ERS index helps to remove genetic influences. In a most general situation, usually both stress and genetic factors tend to modify bone surface, and the same amount

of stress could also produce a different amount of remodelling across specimens, due to inter-individual hormonal variability (Rauch, 2005; Karakostis, 2015).

5.1.1 General considerations on laterality

Analyses on laterality at individual level were not conducted: only general considerations about possible and different use of right and left sides for each bone were depicted. Regarding dissimilarities between samples, right and left differences seem to be associated to powerful and precision grasping patterns, based on the correlation analyses performed on entheseal (raw size and ERS) measurements. Unfortunately, the archaeological material comes from collective burials and it is not possible to assemble bones to reconstruct single and correct individuals; this does not allow to obtain information about laterality and, therefore, bilateral asymmetry for each individual was not evaluated.

5.1.2 Considerations about muscles and related activity patterns

For an initial discussion of the whole sample, distinction between each bone have been done. Moreover, geographical and chronological contexts are not considered for the moment, because of the complex nature of the collective burials the skeletal elements belong.

In right and left MC1 bones (cf. **Table 9**, **Table 12**) ,different correlations were recorded, because of both genetic and biomechanical factors which influence the bones' surfaces; as a whole, in left MC1 a major genetic effect can be described for OP enthesis, while biomechanical factors have probably modified the morphologies of entheses of right MC1. Such an assertion can be done because of the different values of correlation between entheseal raw size and ERS and bone linear measurements, which allow to observe a biomechanical or genetic influence.
In right and left MC2 (cf. **Table 15**, **Table 18**), most significative correlations are in left metacarpals: here, raw size and ERS of the muscles inserted along the diaphysis correlate with both antero-posterior and medio-lateral Robusticity Indexes, highlighting a biomechanical influence which is not evident in right MC2. In both right and left MC3 (cf. **Table 21**,**Table 24**), physical stress loading seems to be more important than genetics, because of the highest values of correlation between Robusticity Indexes and muscle sites inserted on the metacarpal shaft. The two RIs are calculated starting from the antero-posterior and medio-lateral widths at midshaft: therefore, if major variation occurs in correspondence of the bone midshaft, this variation can be observed also in Robusticity Indexes. In both right and left MC4 (cf. **Table 27**, **Table 30**), highest values of correlation are recorded between raw sizes and medio-lateral and antero-posterior RIs, respectively, along with small values between ERS indexes and the same RIs. Also, in right MC5, raw size of ODM enthesis correlates with medio-lateral RI, showing biomechanical influences on this enthesis; regarding left

MC5, both genetics and muscular loadings seems to have modified bony surfaces' morphologies, as seen from correlations with both maximum length and RIs (cf. **Table 33**, **Table 36**).

In phalangeal bones, a general situation can be described: in all cases, correlation with Robusticity Indexes is recorded, highlighting a most evident muscular activity influencing the bones, even if in some cases, correlation with bone length is recorded (cf. **Table 41**, **Table 45**, **Table 48**, **Table 51**, **Table 53**, **Table 57**, **Table 60**, **Table 63**, **Table 66**). See **Figure 140** for a graphic representation of these results.

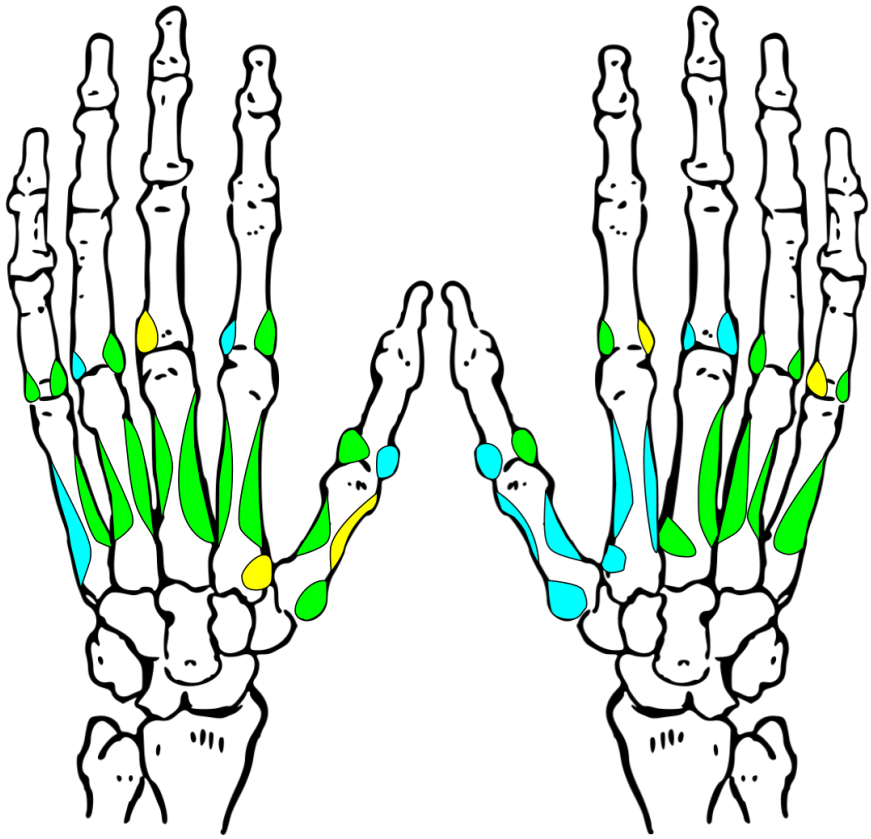

Figure 140 - Graphic representation of the correlations of each entheses with biomechanical stress and genetics. **Green:** Biomechanical influence; **Yellow:** genetics influence; **Light Blue:** both biomechanical and genetic influence.

In most of cases of the current work, correlation was found between entheseal sizes and both antero-posterior and medio-lateral Robusticity Indexes: this may be related to the fact that bone widths and entheseal surfaces are subjected to remodelling when affected by physical activities, contrary to bone length which is not influenced by muscle loadings (Rauch, 2005; Karakostis, 2015). Therefore, increasing in bone widths at midshaft may be related to a higher robusticity of the bone and, consequently, also entheseal surfaces increase in size. According to these considerations, for high values of correlations with hand RIs, the corresponding muscles are those frequently used in manual physical activities. It is important to consider that the modification of bone surfaces and widths do not depend on a single muscle, but is related to several muscular actions, according to the type of forces which affects bone surface – abduction, adduction, flexion, extension. Moreover, all kind of muscles act simultaneously in performing activities, so entheseal morphological aspects are related to a mix of muscular actions.

With regard to raw size, correlation is recorded with the following muscles: ABL, OP, DI1, DI2+PI1, DI3+PI2, DI4, ODM, ABP+FBP, ADP, PI1, PI2, ADM+FDM. These muscles can be distinguished into two groups on the base of the actions they perform: ABL, OP, ABP and ADM muscles make abduction and opposition and insert along the 1st and 5th fingers, while ODM, ADM, ADP and FDM muscles perform adduction, flexion and opposition movements, inserting also on the 1st and the 5th fingers. Dorsal and palmar interosseous intrinsic muscles are important in performing abduction of the 2nd and 4th fingers, abduction and adduction of 3rd finger, flexion of the 2nd, 3rd and 4th phalanges and adduction and flexion of metacarpal-phalangeal joints of the 2nd, 4^{th,} and 5th fingers. Those muscles lying on the 1st and 2nd fingers are usually involved in *precision grips* activities, while the 5th finger is usually used in *powerful grasping*, in particular its opposition movement has a very important role in manipulation of cylindrical objects in power grips (which is reflected on the robusticity of MC5 which also reflects its skill in loading sustaining) (Key *et al.*, 2019).
With regard to ERS, correlation is recorded with the following muscles: DI1, OP, ABL, ECRL, DI2+PI1, ECRB, DI3+ADP, DI4+PI3, ADP, PI2, ADM+FDM. Correlation is evident between ERS indexes and muscles performing both precision and powerful activities but, in this case, other muscles are recognisable such as ECRL, ECRB and ADP – where ECRL and ECRB both perform extension and abduction movements of the wrist, while ADP adducts the thumb. The MC4 bone does not correlate with ERS indexes and ODM enthesis – this latter lying on MC5 diaphysis – does not have correlation with entheseal indexes, although its important role in objects holding. Also, the existent correlation with ECRL and ECRB muscles, which simultaneously act in closing the hand into a fist, causes to think to power grasping activities which can be seen only when Robusticity Indexes are considered, because of their relation to manual performing activities.
When correlations between ERS indexes and right and left groups are evaluated, different patterns emerge: for right bones, higher values of correlation are recorded with DI1, OP, ECRL, ECRB, DI3+ADP entheses, all belonging from the 1st to the 3rd fingers, performing abduction/extension and

opposition movements (except for ADP which adducts the thumb), while for left hand bones correlation is recorded with ABL, ADP, ADM+FMD and DIs and PIs, related to powerful grasping patterns. Similar results emerged from EMG works conducted to evaluate muscle recruitments during hard hammer percussion (Marzke *et al.*, 1998). The thumb and the 5th finger emerged to be important in flaking activities and this can also be compliant to results obtained in this work, that correlation exists between the 1st, the 2nd and the 5th fingers and activities performed by ancient human groups analysed here are related to precision grips. An important consideration can be made for ADM+FDM muscles, characteristic of forceful power grasping in muscle recruitments; in particular, ADM muscle seems to be active after strike in the dominant hand percussion and before strike in a non-dominant situation. For the entire sample, a possible explanation can be related to the use of the right hand as predominant for manual activities, while the left side as non-dominant. According to these general considerations about activity patterns related to subsistence strategies previously cited, a dominant use of right hand for precision grips could be described because of the presence of correlation between those muscles characteristic of precision activities and correlated high robusticity; about left-hand side, highest values of correlation agree with muscles performing powerful grasping.

5.1.3 Considerations about collections' activity patterns

Up to now, the entire sample has been discussed as a whole: following, subdivision of each subsample has been done, according to chronology, origin, and possibly different working activities.

About prehistoric and proto-historic samples coming from University of Turin, *Musée de l'Homme* and El Mirador, information about subsistence strategies comes from archaeological and historical sources (see *"3.2 – The anthropological collections"* for major details) and:

- about the Predynastic and Dynastic samples sampled from University of Turin's anthropological collections, main activities are agriculture, farming and more specialised crafts such as jewels manufactory, stone palettes, metallurgy (Bard, 2015);
- about Neolithic samples from the *Musée de l'Homme*, main subsistence strategies are related to agriculture and farming, hunter-gathering activities and clay handling;
- about El Mirador (dated to Bronze age and Chalcolithic), even in this case the main subsistence economies are about agricultural and livestock practises and farming (Vergès *et al.*, 2016).

In prehistoric and proto-historic samples, also flaking activities can be taken into consideration because of its importance during the considered periods.
A different situation must be remembered for San Pablo's sample as reference collection, belonging to Late Medieval and characterised by different activities than the prehistoric and proto-historic

groups, as previously descripted (Estepa-Diez, Baruque, 1984; Montenegro-Duque, 1987; Stuard, 1989; Gerli, 2003).

Contrary to other studies which analyse single but complete skeletal individuals, here it was not possible to make analyses on muscle recruitments for each individual, because of the nature of the burials of the samples introduced (collective burials).

In his work, conducted on right individuals of the same San Pablo collection here analysed, A. Karakostis (Karakostis, 2015) obtained strong correlations among entheses ABP, ADP, PI1 (PP2), ADP (MC3), ECU, ADM+FDM and ODM, with lower values for OP and FPL, and midshaft robusticity. Furthermore, they belong to the 1st, the 2nd, and the 5th fingers – as obtained for the entire sample analysed in this work – while the significant intercorrelation recorded for DIs and PIs at the base of proximal phalanges can be related to their function of both positioning of fingers and cooperation in performing power and precision activities (Karakostis, 2015; Karakostis, Lorenzo, 2016; Karakostis *et al.*, 2018). Moreover, the intercorrelation between DIs and PIs could be related to their muscular functions in correspondence of the hand palm; also, Marzke and colleagues (Marzke *et al.*, 1998) described movements like adduction and flexion as fundamental for patterns of manual activities involving precision actions related, for example, to stone knapping. In A. Karakostis work, this correlation is coherent with these sentences, in particular for correlation between muscles acting on the wrist and the 1st, the 2nd and the 5th fingers (Karakostis, 2015; Karakostis *et al.*, 2018). These results are also in agreement with those obtained in the present study, even if the selected osteological material comes from several collections from different chronological periods and not complete individuals were considered, analysing each bone as a group.

Analysing each collection separately, the Predynastic/Dynastic sample is characterised by entheses smaller in size than the remaining sample, according to corresponding bones' dimensions – regarding bone size, the prehistoric and proto-historic samples from *Musée de l'Homme* and El Mirador are between UoT and San Pablo collections. With particular attention to UoT, in most cases this group is separated by El Mirador and San Pablo's, with particular attention for MC1 (right and left), MC2 (right and left), MC3 (right and left), MC4 (right and left), MC5 (only right), PP1 (only left), PP3 (only right) and PP4 (only left). The Neolithic specimens from *Musée de l'Homme* are between UoT and EM, while the SP group seems to include the other samples – this could be related to both the dimension of the sample and to the variety of activities performed during Late Medieval. Therefore, it is possible to affirm that the Predynastic and Dynastic individuals from UoT seem to perform different activities compared to proto-historic and medieval populations, while Neolithic individuals have intermediate traits between UoT and both EM and SP. Unfortunately, the Principal Component Analyses conducted on linear measurements (entheseal raw sizes and ERS indexes) for each bone did not allow to obtain peculiar visualisations useful to distinguish each group – basically, along the axis of maximum variation, specimens from UoT and MH have most negative values than EM and SP. To conclude, the most ancient populations here analysed (those belonging to University of Turin and *Musée de l'Homme*) used to perform different kind of manual activities compared to individuals

from El Mirador and San Pablo, although similar subsistence strategies recorded, for example, during Neolithic and Bronze Age – agricultural and farming activities and hunter-gathering.
When differences between groups are not evident but a total or partial overlapping between samples is recorded, this is probably related to the absence of peculiar manual activities for the corresponding bones – as it happens from MC5 (only left), PP1 (only right), PP2 (right and left), PP3 (only left), PP4 (only right), PP5 (right and left).

5.2 Geometric morphometric analyses: considerations about entheses

Geometric morphometric analyses were performed. Several analyses have been conducted and were shown in the previous 'Results' chapter. These analyses concerned the investigation of shape variation for each enthesis and were plotted in tangent space along each PC axis. Even if several PCA plots were described for each entheseal specimen, only some of them were considered because they showed separation between groups – those not considered were inserted in the Annexes.
Focusing on the two archaeological collections, with particular interest to the GMM analyses performed, differences between entheses are probably correlated to different activity patterns associated to ancient subsistence strategies (related to agriculture, farming, flaking activities and/or clay handling). Distinctions between groups are evident in **Figure 16**, **Figure 22**, **Figure 23**, **Figure 25**, **Figure 29**, **Figure 30**, **Figure 39**, **Figure 40**, **Figure 42**, **Figure 45**, **Figure 54**, **Figure 57**, **Figure 59**, **Figure 60**, **Figure 66**, **Figure 73**, **Figure 77**; these visualisations also confirm that differences are evident between Neolithic collections from *Musée de l'Homme* and both San Pablo and El Mirador ones – in most cases, these latter seem to be characterised by larger entheseal shapes than the Neolithic group. Therefore, since a most intense muscular activity seems to influence entheseal morphologies (Karakostis, 2015), then it is possible to suppose that different kind of activities could be performed between each population, even if similar subsistence economies were conducted.
An important consideration is about the absence of correlation between Shape and Size in the whole sample: for each enthesis and its corresponding landmark configuration, all negative and near-zero values were obtained, except for left OP enthesis – characterised by a positive but near-zero correlation. Similar results have been obtained by A. Karakostis in his work, that the overall size of right OP enthesis (PC1) seems to be the only one which showed this kind of correlation (Karakostis, 2015); furthermore, the main characteristic change is in correspondence of the proximal portion of the enthesis, which expands toward the base of the bone along the diaphysis. Also, the author affirmed that this proximally oriented expansion seems to be correlated with entheseal size, growing along with the size of the enthesis. (Karakostis, 2015).
It is possible to affirm that the main characteristic of OP concerns its morphology, which modify in accordance with the entheseal change due to muscular activity, whose expansion along the midshaft can also be an indicator of entheseal development (Karakostis, 2015). The lack of correlation between Shape and Size for all the entheses, could be related to the fact that entheseal modification

does not cause shape change on the human hand entheses (Karakostis *et al.*, 2018). A difference between the previous work considered and the research here conducted is about the correlation between Shape and Size of OP enthesis: if A. Karakostis's results concerned OP of right MC1, in the current work correlation has been obtained only for OP of left MC1. A possible explanation about the different correlations obtained for the two studies performed could be due to the samples analysed, coming from several collections, so different populations. The whole sample introduced here could be characterised by a most intense muscular activity influencing more left OP enthesis, even if correlation analyses show different results. In the GMM analyses, distinctions between groups for left OP are not evident; this could be related to a major but different use of OP muscle among the Neolithic group from *Musée de l'Homme* and the rest of the sample, also related to different kind of manual activity.

Summarising and connecting information about the correlation analyses with RIs and precision or powerful grasping activities, the GMM analyses conducted on each single metacarpal bone agree with the previously data about correlation with ERS indexes; this situation is evident in particular for entheses ECRL (both right and left), DI2+PI1 (only left), ECRB (both right and left), DI3+APD (both right and left) and DI4+PI3 (only right), in accordance with both precision and powerful manual grasping activities for right and left sides, respectively.
When phalanges are considered, correlations with ERS indexes are evident for ADP (only left), DI1 (both right and left), PI2 (only left) and ADM+FDM and PI3 (only left) entheses but plots shown in 'Results' chapter do not have particular groups or distributions: in some cases, separation between groups of the archaeological collections were obtained; unfortunately, it was not possible to assign each phalange to the corresponding metacarpal and to the corresponding individual, so complete information about each single individual is not available.
For each enthesis, it is possible to observe that shape variation occurs along the entheseal outline in correspondence of the fixed pseudo-landmarks specifically defined for this work. From a general point of view, variations in size and in proportion are recorded along the principal components PC1 and PC2, respectively; obviously, surface and entheseal variations depend on both biomechanical stresses affecting the bone and the several muscular movements which allow human body to move (Karakostis, 2015).

A. Karakostis and colleagues obtained distinction between powerful and precision grips in human hand entheses and defined different activity patterns in accordance with each kind of grasping – bricklayer, stonemason, butcher, carpenter and other mansions are typical of continuous and sustained high grip forces, while precision activities are related to mansions like tailor, baker, shoe-maker […] and other kind of jobs characterised by less strenuous and mechanised activities (Karakostis *et al.*, 2017). Their results did not show inter-population variation along with association of these patterns with sex, body mass, hand bone length and pathology. In some cases, raw size of

3D entheses seems to correlate with both body size and hand bone length (Nolte & Wilczak, 2013; Karakostis, Lorenzo, 2016), indicating a significant relation and association with body weight and length. Previous works have also demonstrated the influence of age and pathological conditions along with biomechanical stress in entheseal changes (Foster *et al.*, 2012; Milella *et al.*, 2012; Nolte, Wilczak, 2013). Obviously, other factors – such as nutrition and genetic and systemic factors – can influence the bone morphology (Rauch, 2005; Foster *ei al.*, 2012). The two different entheseal patterns here recognised and described are also coherent with those obtained by A. Karakostis in his work previously cited, who analysed the part of the material here introduced belonging to San Pablo collection – he only analysed the right individuals (Karakostis, 2015; Karakostis, Lorenzo, 2016). His analysis showed that populations of different chronologies and cultures can be related, according to the same kind of activity patterns. Even if activity patterns of precision and grips and powerful grasping are common in all the osteological collections here studied, entheseal morphological differences can be seen between each group. For collections from University of Turin and *Musée de l'Homme*, entheses resulted to be smaller in dimension than the rest of the sample coming from San Pablo and El Mirador; this could be due to manual physical activities performed with different intensity according to different subsistence strategies during ages. The fact that several entheses – in particular, right ABL, OP, DI1, ECRL, ECRB, DI3+ADP, DI4, ODM, DI4+PI3 and left ABL, DI1, ECRL, DI2+PI1, ECRB, DI2, DI3+ADP, ADP, ADM+FDM – show evident morphological differences could be related to more specialised crafts developed after Neolithic age; hypothetically, the idea that during medieval periods more specialised and precision activities – tailor, shoemaker, silk-man, baker, and so on – were performed, could have supported a major increasing of entheseal development than activities performed during prehistoric and proto-historic changes (Estepa-Diez, Baruque, 1984; Montenegro-Duque, 1987; Stuard, 1989; Gerli, 2003; Bard, 2015; Karakostis, 2015; Karakostis, Lorenzo, 2016; Vergès *et al.*, 2016; Karakostis *et al.*, 2017).

Moreover, other analyses conducted by the same A. Karakostis about the presence of association between entheseal shape morphology and calcified fibrocartilage, showed that entheseal surfaces with additional bony projections are related to frequent and /or intense biomechanical work, suggesting that bone elevation could be considered '[…] as a potential indicator of increased biomechanical stress' (Karakostis *et al*., 2019).

The presence of sexual dimorphism was not evaluated for the entire archaeological sample because distinction between men and women was not possible. For the specimens from Late Medieval San Pablo, A. Karakostis investigated the hypothesis of sexual dimorphism in human hand entheses (Karakostis *et al.*, 2013; Karakostis, 2015; Karakostis, Lorenzo, 2016). His results concerned highly dimorphic entheses of proximal phalanges, with high values of sexual dimorphism for antero-posterior and medio-lateral widths in correspondence of the base; along the midshaft, it seems that most of physical stress is here applied, causing an increasing of the surface size of the selected

entheseal area due to muscular contraction (Larsen, 1997). Different values of sexual dimorphism could be due to different amount of physical strength applied on the origin and insertion areas: in particular, it seems that the muscular origin sites are less affected by surface modification caused by muscular contraction than the insertion ones (Martini *et al.*, 2012). As a result, low values of dimorphism could be due to a minimum movement, so to low levels of muscular stress which entheseal area is affected to. For the collection of San Pablo, distinction between men and women has not been evidenced with the geometric morphometric approach used to carry out this research, even if sexual dimorphism is evident from a morphological point of view – as seen from A. Karakostis previous analyses – with male characterised by more extended entheses than female individuals (Karakostis, 2015). To corroborate these results, the *Opponens Pollicis* enthesis for both right and left MC1 were chosen to evaluate possible intra-population differences in the unique enthesis which showed different correlation between Size and Shape (negative and positive ones, respectively, even if both had near-zero values). No differences emerged from this analysis between male and female specimens from San Pablo and all the individuals were homogenously spread on the graph – for this general visualization, the graph was not introduced in this research.

Chapter 6

Conclusions and Future Perspectives

The entire set of analyses has provided information about the Research Questions exposed in the introductive chapter – and shown below – regarding the degree of shape variation of human hand entheses and the differences between groups of different areas and chronologies:

Which is the degree of shape variation of the entheseal surfaces of hand bones of individuals coming from populations of different historical periods? How do the different human groups correlate? Are there differences in 3D entheseal shape and size from a diachronic point of view?

The whole sample has been subdivided into four groups, according to the corresponding collection: Predynastic and Dynastic individuals from University of Turin, Neolithic populations from *Musée de l'Homme* (Paris, France), protohistoric human group from *El Mirador* cave (Atapuerca, Burgos, Spain), and the medieval sample from San Pablo cemetery (Burgos, Spain).
In this research, primary importance has been given to hand bones, whose relevance grew more and more in anthropological and biomechanical studies during the years, although their small dimensions and not-easy identification. Their manipulative functions can be generally summarised as precision grips and powerful grasping activities, as described here; all the final considerations have been made in accordance with subsistence economies of the sampled populations, related to agriculture and farming activities, clay-handling and more-specialised crafts for the medieval individuals (Estepa-Diez, Baruque, 1984; Montenegro-Duque, 1987; Stuard, 1989; Gerli, 2003; Bard, 2015; Karakostis, 2015; Karakostis, Lorenzo, 2016; Vergès *et al.*, 2016).

A total of more of 500 osteological elements have been sampled, including metacarpals and proximal phalanges from 1st to 5th fingers; later, all the entheses to investigate have been selected and delimited, and each specific reference landmark protocol have been applied on the corresponding enthesis, in order to conduct the expected analyses.

Within the scope of statistical analyses, both uni- and multivariate ones were performed to understand if a major genetic or biomechanical influence is evident, concerning the morphological variation on the bones' surface; for these analyses, linear measurements such as maximum bone length, robusticity indexes and entheseal raw size and corresponding ERS indexes were considered and applied on the bones of the whole sample.
These analyses showed different degrees of correlation between entheses, in particular when ERS indexes are taken into account because of their relation to bone robusticity. In most of cases, the correlation obtained may be related to several muscles' activity, all influencing the morphology of the affected skeletal elements. The resulting correlation analyses allowed to obtain information about the activity patterns concerning precision and powerful grasping and, specifically, a possible dominant use of the right hand for precision grips; regarding left-hand bones, the results agree with the description of powerful patterns. Moreover, distinction between samples according to different

kind of activities were obtained: more ancient groups – such as specimens belonging to University of Turin and *Musée de l'Homme* collections – seem to perform different kind of activities than the medieval and proto-historic populations from San Pablo and El Mirador, even though the subsistence economies used to be comparable.

Within the scope of GMM analyses, each enthesis – or rather, each 3D entheseal surface – has been analysed individually. The presence of correlation between Shape and Size has been investigated, in relation to the description of activity patterns of the ancient populations previously described. The unique correlation has been obtained for left *Opponens Pollicis* enthesis – in accordance with A. Karakostis research, even if his result concerned only the right enthesis (Karakostis, 2015; Karakostis, Lorenzo, 2016).

The doctoral research conducted and described in this dissertation has allowed to support the relation between muscular insertion sites and physical activity, which determines changes in bone morphology during lifelong remodelling processes from a macroscopic point of view – although correlation between Shape and Size was not recorded. The development of new methodologies could let researchers to better investigate this kind of aspects and to obtain more information about activity patterns of human groups. For example, analyses of modifications of bone surfaces could be conducted (not of the outlines', as in this case): the idea concerns the creation of specific landmark protocols considering entheses as topographic surfaces to be investigated. Other types of analyses could take into consideration CT images of individuals with known age and sex (i.d. hospitalised patients) to create complete datasets with all the useful information about working activities performed; even in this case, obviously, the methodology should be created specifically for the sample under study, according to the analyses that are going to conduct. Also, a perfect dataset could come from human groups buried in cemeteries dated on last decades, because both biological information and pathological conditions and specific data about working activities could allow most complete analyses as possible.

Unfortunately, in the present research, several aspects could not be evaluated because of the incompleteness of the archaeological collections. First, sexual dimorphism was not investigated because complete individuals were not present and distinction between men and women was not possible; consequently, distinctive sexual activity patterns were not investigated. For the same reason, laterality and individual bilateral asymmetry were not taken into account, because all the analyses were performed for hand bones, each one considered as single groups. Regarding the effect of age, this was not analysed because all individuals introduced in the research were adult, so age-group entheseal variation was not evaluated.

Focusing on the prehistoric collections from *Musée de l'Homme*, the difficulty in obtaining information on the several sites introduced and on the osteological material – because of the absence of bibliographic material – let the reconstruction of the general context of each site hard to do.
For this reason, major attention should be applied on the field, during excavation activities, with regard to hand bones, characterised by small dimensions and peculiar morphologies (with particular reference to carpals); about metacarpals and phalanges, their vulnerability should let archaeologists and anthropologists to make attention with their recovery.
The analysis of a complete skeleton or a whole population would let a 360-degrees analyses, analysing both biological profiles and lifelong working activities, also considering (if present) all the bones of the human skeleton, from which to draw all the main information to reconstruct biological profiles of the individuals of a population.

Furthermore, new methodologies and future applications on fossil human remains (i.d. both 3D materials and CT images) will lead the way to future analyses, allowing the researchers to obtain a wider framework about human evolution and manual physical activities.

References

Adams, D. C., & Otárola-Castillo, E. (2013). Geomorph: An r package for the collection and analysis of geometric morphometric shape data. *Methods in Ecology and Evolution*, *4*(4), 393–399. https://doi.org/10.1111/2041-210X.12035

Bard, K. A. (2015). *An Introduction to the Archaeology of Ancient Egypt* (2nd ed.). Blackwell, Wiley.

Bardo, A., Borel, A., Meunier, H., Guéry, J. P., & Pouydebat, E. (2016). Behavioral and functional strategies during tool use tasks in bonobos. *American Journal of Physical Anthropology*, *161*(1), 125–140. https://doi.org/10.1002/ajpa.23015

Bardo, A., Cornette, R., Borel, A., & Pouydebat, E. (2017). Manual function and performance in humans, gorillas, and orangutans during the same tool use task. *American Journal of Physical Anthropology*, *164*(4), 821–836. https://doi.org/10.1002/ajpa.23323

Bardua, C., Felice, R. N., Watanabe, A., Fabre, A.-C., & Goswami, A. (2019). A Practical Guide to Sliding and Surface Semilandmarks in Morphometric Analyses. *Integrative Organismal Biology*, *1*(1). https://doi.org/10.1093/iob/obz016

Baye (de), J. (1874). Sur les grottes de la vallée de petit-Morin (Marne). *Bulletins de La Société d'anthropologie de Paris*, *9*(1), 225–244. https://doi.org/10.3406/bmsap.1874.3574

Benjamin, M, Evans, E. J., & Copp, L. (1986). The histology of tendon attachments to bone in man. *Journal of Anatomy*, *149*, 89–100. Retrieved from http://www.ncbi.nlm.nih.gov/pubmed/3693113%0Ahttp://www.pubmedcentral.nih.gov/articlerender.fcgi?artid=PMC1261636

Benjamin, M, Kumai, T., Milz, S., Boszczyk, B. M., Boszczyk, a a, & Ralphs, J. R. (2002). The skeletal attachment of tendons--tendon "entheses". *Comparative Biochemistry and Physiology. Part A, Molecular & Integrative Physiology*, *133*(4), 931–945. https://doi.org/10.1016/S1095-6433(02)00138-1

Benjamin, M, Toumi, H., Ralphs, J. R., Bydder, G., Best, T. M., & Milz, S. (2006). Where tendons and ligaments meet bone: Attachment sites ('entheses') in relation to exercise and/or mechanical

load. *Journal of Anatomy*, *208*(4), 471–490. https://doi.org/10.1111/j.1469-7580.2006.00540.x

Benjamin, Michael. (2000). Anatomy and biochemistry of entheses - Abstract. *Ann. Rheum. Dis*, *59*. Retrieved from www.annrheumdis.com

Boano, R., Grilletto, R., & Rabino Massa, E. (2013). I reperti umani antichi nei musei: ricerca, conservazione e comunicazione. Le esperienze del Museo di Antropologia ed Etnografia dell'Università di Torino. *Journal of History of Medicine*, *25*(1), 251–265.

Bookstein, F. L. (1991). *Morphometric tools for landmark data - Geometry and biology*. Cambridge University Press (CUP). https://doi.org/10.1016/s0889-5406(05)81803-7

Bucchi, A., Manzanares, M., Luengo, J., Bucchi, C., & Lorenzo, C. (2019). Muscle strength and human entheseal size in human thumbs: Testing the relationship with a cadaveric model. *The Journal of the International Union for Prehistoric and Protohistoric Sciences*, *2*(September), 38–42.

Bush, M. E., Lovwoy, C. O., & Johanson, D. C. (1982). *Hominid Carpal, Metacarpal, and Phalangeal Bones Recovered From the Hadar Formation: 1974-1 977 Collections*. *AMERICAN JOURNAL OF PHYSICAL ANTHROPOLOGY* (Vol. 57).

Cáceres, I., Lozano, M., & Saladié, P. (2007). Evidence for Bronze Age cannibalism in El Mirador Cave (Sierra de Atapuerca, Burgos, Spain). *American Journal of Physical Anthropology*, *133*(3), 899–917. https://doi.org/10.1002/ajpa.20610

Cashmore, L. A., & Zakrzewski, S. R. (2013). Assessment of musculoskeletal stress marker development in the hand. *International Journal of Osteoarchaeology*, *23*(3), 334–347. https://doi.org/10.1002/oa.1254

Charmode, S., Kadlimatti, H., & Pujari, D. (2019). Correlation of Human Height with Hand Dimensions: A Study in Young Population of Central India. *International Journal of Human Anatomy*, *1*(3), 36–44. https://doi.org/10.14302/issn.2577-2279.ijha-19-2609

Cignoni, P., Callieri, M., Corsini, M., Dellepiane, M., Ganovelli, F., Ranzuglia, G. (2008). MeshLab: an Open-Source Mesh Processing Tool. *Sixth Eurographics Italian Chapter Conference*, 129–136. https://doi.org/10.2312/LocalChapterEvents/ItalChap/ItalianChapConf2008/129-136

Dastugue, J. (1973). Les crânes trépanés de la vallée du Petit-Morin. *Bulletins et Mémoires de La*

Société d'anthropologie de Paris, *10*(3), 249–263. https://doi.org/10.3406/bmsap.1973.2071

Derevenski, J. R. S., Words, K. E. Y., & Sofaer Derevenski, J. R. (2000). Sex differences in activity-related osseous change in the spine and the gendered division of labor at Ensay and Wharram Percy, UK. *American Journal of Physical Anthropology*, *111*(3), 333–354. https://doi.org/10.1002/(SICI)1096-8644(200003)111:3<333::AID-AJPA4>3.0.CO;2-K

Djukic, K., Milovanovic, P., Hahn, M., Busse, B., Amling, M., & Djuric, M. (2015). Bone microarchitecture at muscle attachment sites: The relationship between macroscopic scores of entheses and their cortical and trabecular microstructural design. *American Journal of Physical Anthropology*, *157*(1), 81–93. https://doi.org/10.1002/ajpa.22691

Estepa-Diez C, Valdeon-Baruque JV. (1984). Burgos en ela Edad Media. Burgos: Junta de Castilla y Leon

Foster, A., Buckley, H., & Tayles, N. (2014). Using Enthesis Robusticity to Infer Activity in the Past: A Review. *Journal of Archaeological Method and Theory*, *21*(3), 511–533. https://doi.org/10.1007/s10816-012-9156-1

Galletta, L., Stephens, N. B., Bardo, A., Kivell, T. L., & Marchi, D. (2019). Three-dimensional geometric morphometric analysis of the first metacarpal distal articular surface in humans, great apes and fossil hominins. *Journal of Human Evolution*, *132*, 119–136. https://doi.org/10.1016/j.jhevol.2019.04.008

Garrido Varas, C. E., & Thompson, T. J. U. U. (2011). Metric dimensions of the proximal phalanges of the human hand and their relationship to side, position, and asymmetry. *HOMO- Journal of Comparative Human Biology*, *62*(2), 126–143. https://doi.org/10.1016/j.jchb.2010.07.005

Gaskin, C. M., Khan, S. L., Bertozzi, J. C., & Buch, P. M. (2011). *Skeletal Development of the Hand and Wrist. A Radiographic Atlas and Digital Bone Age Companion*. Oxford University Press.

Gerli M.E. (2003). *Medieval Iberia: An Enclyclopedia*. New York: Routledge.

Gilsanz, V., & Ratib, O. (2005). *Hand Bone Age. A Digital Atlas of Skeletal Maturity*. Springer.

Gray, H. (1918). *Anatomy of the Human Body* (20th ed.).

Hammer, Ø., Harper, D. A. T., & Ryan, P. D. (2001). PAST: Paleontological Statistics Software

Package for Education and Data Analysis. *Palaeontologia Electronica*, *4*(1), 1–9.

Hardy M., (1880), Note sur la grotte sépulcrale de Campniac, près Périgueux. *Catalogue de la bibliothèque*, Archives départementales de la Dordogne, Texte imprimé: 104–107.

Hawkey, D. E., Merbs, C. F., Hawkey, D. E., & Merbs, C. F. (1995). Activity-induced musculoskeletal stress markers (MSM) and subsistence strategy changes among ancient Hudson Bay Eskimos. *International Journal of Osteoarchaeology*, *5*(4), 324–338. https://doi.org/10.1002/oa.1390050403

Henderson, C., Mariotti, V., Pany-Kucera, D., Perréard-Lopreno, G., Villotte, S., & Wilczak, C. (2010). *Scoring entheseal changes: proposal of a new standardised method for fibrocartilaginous entheses*. *Poster presented at the …*. Retrieved from http://www.uc.pt/en/cia/msm/

Henderson, C. Y., Mariotti, V., Pany-Kucera, D., Villotte, S., & Wilczak, C. (2016). The New 'Coimbra Method': A Biologically Appropriate Method for Recording Specific Features of Fibrocartilaginous Entheseal Changes. *International Journal of Osteoarchaeology*, *26*, 925–932. https://doi.org/10.1002/oa.2477

Henderson, C. Y., Wilczak, C., & Mariotti, V. (2017). Commentary: An Update to the new Coimbra Method for Recording Entheseal Changes. *International Journal of Osteoarchaeology*, *27*(3), 521–522. https://doi.org/10.1002/oa.2548

Henderson, C Y. (2013). Technical note: Quantifying size and shape of entheses. *Anthropological Science*, *121*(1), 63–73. https://doi.org/10.1537/ase.121017

Henderson, C Y, Mariotti, V., Santos, F., Villotte, S., & Wilczak, C. A. (2017). La nouvelle méthode Coimbra : changement au niveau des enthèses et influence de l'âge au décès. *Bulletins et Memoires de La Societe d'Anthropologie de Paris*, *29*(3–4), 140–149. https://doi.org/10.1007/s13219-017-0185-x

Henderson, Charlotte Y, Mariotti, V., Pany-Kucera, D., Lopreno, G. P., Villotte, S., & Wilczak, C. (2012). *The effect of age on entheseal changes at some fibrocartilaginous entheses*. Retrieved from https://www.uc.pt/en/cia/msm/Vienna2010.pdf

Hora, M., Farka, K., Sládek, V., Hora, M., Farkašová, K., & Rocek, T. R. (2016). Impact of grinding technology on bilateral asymmetry in muscle activity of the upper limb. *Journal of*

Archaeological Science, *72*, 142–156. https://doi.org/10.1016/j.jas.2016.07.001

Jurmain, R., & Villotte, S. (2010). Terminology. Entheses in medical literature and physical anthropology: a brief review. *Workshop in Musculoskeletal Stress Markers (MSM): Limitations and Achievements in the Reconstruction of Past Activity Patterns. University of Coimbra.*, (Villotte 2006), 5 p.

Jurmain, Robert, Cardoso, F. A., Henderson, C., & Villotte, S. S. (2012). Bioarchaeology's Holy Grail: The Reconstruction of Activity. *A Companion to Paleopathology*, (November 2014), 531–552. https://doi.org/10.1002/9781444345940.ch29

Karakostis, F. A., Zorba, E., & Moraitis, K. (2015). Sexual Dimorphism of Proximal Hand Phalanges. *International Journal of Osteoarchaeology*, *25*(5), 733–742. https://doi.org/10.1002/oa.2340

Karakostis, Fotios Alexandros. (2015). *Morphometric analysis of entheseal surfaces in modern human metacarpals, proximal hand phalanges and the pollical distal phalanx*, International Master Thesis in Quaternary and Prehistory.

Karakostis, Fotios Alexandros, Hotz, G., Scherf, H., Wahl, J., & Harvati, K. (2017). Occupational manual activity is reflected on the patterns among hand entheses. *American Journal of Physical Anthropology*, *164*(1), 30–40. https://doi.org/10.1002/ajpa.23253

Karakostis, F. A., Hotz, G., Tourloukis, V., & Harvati, K. (2018). *Evidence for precision grasping in Neandertal daily activities*. *Sci. Adv* (Vol. 4). Retrieved from http://advances.sciencemag.org/

Karakostis, Fotios Alexandros, Hotz, G., Scherf, H., Wahl, J., & Harvati, K. (2018). A repeatable geometric morphometric approach to the analysis of hand entheseal three-dimensional form. *American Journal of Physical Anthropology*, *166*(October 2017), 246–260. https://doi.org/10.1002/ajpa.23421

Karakostis, Fotios Alexandros, Jeffery, N., & Harvati, K. (2019). Experimental proof that multivariate patterns among muscle attachments (entheses) can reflect repetitive muscle use. *Scientific Reports*, *9*(1). https://doi.org/10.1038/s41598-019-53021-8

Karakostis, Fotios Alexandros, & Lorenzo, C. (2016). Morphometric patterns among the 3D surface areas of human hand entheses. *American Journal of Physical Anthropology*, *160*(4), 694–707.

https://doi.org/10.1002/ajpa.22999

Karakostis, Fotios Alexandros, Wallace, I. J., Konow, N., & Harvati, K. (2019). Experimental evidence that physical activity affects the multivariate associations among muscle attachments (entheses). *Journal of Experimental Biology*, *22*(23). https://doi.org/10.1242/jeb.213058

Kendall, D. G. (1984). SHAPE MANIFOLDS , PROCRUSTEAN METRICS , AND COMPLEX PROJECTIVE SPACES. *Bulletin of the London Mathematical Society*, *16*(2), 81–121.

Key, A. J. M., Dunmore, C. J., & Marzke, M. W. (2019). The unexpected importance of the fifth digit during stone tool production. *Scientific Reports*, *9*(1). https://doi.org/10.1038/s41598-019-53332-w

Krishan, K., & Sharma, A. (2007). Estimation of stature from dimensions of hands and feet in a North Indian population. *Journal of Forensic and Legal Medicine*, *14*(6), 327–332. https://doi.org/10.1016/j.jcfm.2006.10.008

Kubicka, A. M., Lubiatowski, P. P., Długosz, J. D., Romanowski, L., Piontek, J. (2016). Directional asymmetry of upper limbs in a medieval population from Poland: A combination of linear and geometric morphometrics. *American Journal of Human Biology*, *28*(6), 817–824. https://doi.org/10.1002/ajhb.22873

Kubicka, A. M., Nowaczewska, W., Balzeau, A., & Piontek, J. (2018). Bilateral asymmetry of the humerus in Neandertals, Australian aborigines and medieval humans, 167 American Journal of Physical Anthropology § Wiley-Blackwell. https://doi.org/10.1002/ajpa.23601

La Cava, G. (1959). Enthesitis - Traumatic Disease or Insertions. *Journal of the American Medical Association*, *169*(3), 254.

Larroque, J.-M., & Riquet, R. (1966). Documents anthropologiques inédits sur la civilisation de la Seine-Oise-Marne. *Bulletins et Mémoires de La Société d'anthropologie de Paris*, *9*(1), 29–43. https://doi.org/10.3406/bmsap.1966.1345

Larsen, C. S. (1997). *Bioarchaeology: interpreting behavior from the human skeleton*. *Choice Reviews Online*. Cambridge University Press (CUP). https://doi.org/10.5860/choice.35-6311

Macintosh, A. A., Pinhasi, R., & Stock, J. T. (2014). Divergence in male and female manipulative behaviors with the intensification of metallurgy in central Europe. *PLoS ONE*, *9*(11).

https://doi.org/10.1371/journal.pone.0112116

Maki, J., & Trinkaus, E. (2011). Opponens Pollicis Mechanical Effectiveness in Neandertals and Early Modern Humans. *PaleoAnthropology*, 62−71. https://doi.org/doi:10.4207/PA.2011.ART43

Manzon, V. S. (2011). *Analisi dei marcatori scheletrici di stress occupazione (MOS) in una popolazione etrusca della Pianura Padana: Spina, VI-III a.C.*, Università degli Studi di Ferrara

Mariotti, V., Facchini, F., & Belcastro, M. G. (2004). Enthesopathies-Proposal of a Standardized Scoring Method and Applications. *Coll. Antropol*, *28*(1), 145–159.

Mariotti, V., Facchini, F., & Belcastro, M. G. (2007). The study of entheses: proposal of a standardised scoring method for twenty-three entheses of the postcranial skeleton. *Collegium Antropologicum*, *31*(1), 291–313.

Marquer, P. (1954). Les ossements humains de Pinterville (Eure). *Bulletins et Mémoires de La Société d'anthropologie de Paris*, *5*(3), 209–235. https://doi.org/10.3406/bmsap.1954.2639

Martini, Frederic H., Nath, Judi D., Bartholomew, E. F. (2012). *Fundamentals of Anatomy & Physiology* (9th ed.). Pearson.

Marzke, M. W., Toth, N., Schick, K., Reece, S., Steinberg, B., Hunt, K., … An, A. K.-N. (1998). EMG Study of Hand Muscle Recruitment During Hard Hammer Percussion Manufacture of Oldowan Tools. *Am J Phys Anthropol*, *332*(November 1997), 315–332.

Masali, M., & Chiarelli, B. (1972). Demographic Data on the Remains of Ancient Egyptians. *Journal of Human Evolution*, *1*, 161–169.

Milella, M., Alves Cardoso, F., Assis, S., Perréard Lopreno, G., & Speith, N. (2015). Exploring the relationship between entheseal changes and physical activity: A multivariate study. *American Journal of Physical Anthropology*, *156*(2), 215–223. https://doi.org/10.1002/ajpa.22640

Milella, M., Belcastro, M. G., Zollikofer, C. P. E. E., Mariotti, V., Giovanna Belcastro, M., Zollikofer, C. P. E. E., & Mariotti, V. (2012). The effect of age, sex, and physical activity on entheseal morphology in a contemporary Italian skeletal collection. *American Journal of Physical Anthropology*, *148*(3), 379–388. https://doi.org/10.1002/ajpa.22060

Mitteroecker, P., & Gunz, P. (2009). Advances in Geometric morphometrics. *Evolutionary Biology*, *36*(2), 235–247. https://doi.org/10.1007/s11692-009-9055-x

Mitteroecker, P., Gunz, P., Bernhard, M., Schaefer, K., & Bookstein, F. L. (2004). Comparison of cranial ontogenetic trajectories among great apes and humans. *Journal of Human Evolution*, *46*(6), 679–698. https://doi.org/10.1016/j.jhevol.2004.03.006

Molnar, P. (2006). Tracing prehistoric activities: Musculoskeletal Stress Marker Analysis of a Stone-Age Population on the Island of Gotland in the Baltic Sea. *American Journal of Physical Anthropology*, *129*(1), 12–23. https://doi.org/10.1002/ajpa.20234

Montenegro-Duque A. (1987). Historia de Burgos: Edad Media, Volu- men 2, Parte 2. Burgos: Caja de Ahorros Municipal de Burgos

Morley, J., Bucchi, A., Lorenzo, C., & Püschel, T. A. (2020). Characterizing the body morphology of the first metacarpal in the Homininae using 3D geometric morphometrics. *BioRxiv*, *2020*(May), 2020.04.30.070326. https://doi.org/10.1101/2020.04.30.070326

Noldner, L. K., & Edgar, H. J. H. H. (2013). 3D representation and analysis of enthesis morphology. *American Journal of Physical Anthropology*, *152*(3), 417–424. https://doi.org/10.1002/ajpa.22367

Nolte, M., & Wilczak, C. (2013). Three-dimensional Surface Area of the Distal Biceps Enthesis, Relationship to Body Size, Sex, Age and Secular Changes in a 20th Century American Sample. *International Journal of Osteoarchaeology*, *23*(2), 163–174. https://doi.org/10.1002/oa.2292

Pawar PK, Dadhich A. (2012). Study of correlation between human height and hand length in residents of Mumbai. J Int Med Res 3:2072–2075

Rauch, F. (2005). Bone Growth in Lenght and Width: The Yin and Yang of Bone Stability. *J. Musculoskelet. Neutonal. Interact*, *5*(3), 194–201.

Rodríguez, P. M. (2015). Caracterización zooarqueológica de las cuevas redil en la Prehistoria de la Meseta Norte : el caso de El Mirador (Sierra de Atapuerca , Burgos).

Roland, M. (1911). Découverte d'une Grotte néolithique à Courjeonnet, près Villevenard (Marne). *Bulletin de La Société Préhistorique de France*, *8*(11), 669–676. https://doi.org/10.3406/bspf.1911.6335

Ruff, C. B., & Runestad, A. (1992). *Primate Limb Bone Structural Adaptations*. *Annu. Rev. Anthropol* (Vol. 21). Retrieved from www.annualreviews.org

Santana-Cabrera, J., Velasco-Vázquez, J., & Rodríguez-Rodríguez, A. (2015). Entheseal changes and sexual division of labor in a North-African population: The case of the pre-Hispanic period of the Gran Canaria Island (11th-15th c. CE). *HOMO- Journal of Comparative Human Biology*, *66*(2), 118–138. https://doi.org/10.1016/j.jchb.2014.10.005

Sládek, V. V., Berner, M., Sosna, D., & Sailer, R. (2007). Human Manipulative Behavior in the Central European Late Eneolithic and Early Bronze Age: Humeral Bilateral Asymmetry. *American Journal of Physical Anthropology*, *133*(1), 669–681. https://doi.org/10.1002/ajpa

Slice, D. E., & Slice. (2005). *Modern Morphometrics in Physical Anthropology*. *Kluwer Academic/Plenum Publishers* (Vol. 43). https://doi.org/10.1007/0-387-27614-9

Standring, S. (2008). *Gray's Anatomy. The Anatomical Basis of Clinical Practice*. (Susan Standring, Ed.), *Gray's Anatomy* (4th Editio, Vol. 57). Churchill Livingston, Elsevier. https://doi.org/10.1016/B978-0-443-06684-9.50095-0

Stuard SM. (1989). *Women in Medieval Society.* Pensylvania: The University of Pensylvania Press

Torre, C., Giacobini, G., & Sicuro, A. (1980). The Skull and Vertebral Column Pathology of Ancient Egyptians . A Study of the Marro Collection Giacobini. *Journal of Human Evolution*, *9*, 41–44.

Vergès, J. M., Allué, E., Fontanals, M., Morales, J. I., Martín, P., Carrancho, Á., … Rodríguez, A. (2016). El Mirador cave (Sierra de Atapuerca, Burgos, Spain): A whole perspective. *Quaternary International*, *414*, 236–243. https://doi.org/10.1016/j.quaint.2016.01.044

Villotte, S., & Knüsel, C. J. (2013). Understanding Entheseal Changes: Definition and Life Course Changes. *International Journal of Osteoarchaeology*, *23*(2), 135–146. https://doi.org/10.1002/oa.2289

Villotte, Sébastien, Churchill, S. E., Dutour, O. J., & Henry-Gambier, D. (2010). Subsistence activities and the sexual division of labor in the European Upper Paleolithic and Mesolithic: Evidence from upper limb enthesopathies. *Journal of Human Evolution*, *59*(1), 35–43. https://doi.org/10.1016/j.jhevol.2010.02.001

Wallace, I. J., Winchester, J. M., Su, A., Boyer, D. M., & Konow, N. (2017). Physical activity alters limb bone structure but not entheseal morphology. *Journal of Human Evolution*, *107*, 14–18. https://doi.org/10.1016/j.jhevol.2017.02.001

White, T. D., Black, M. T., & Folkens, P. A. (2012). *Human Osteology - Third Edition*. *Elsevier, Academic Press* (Third Edit). Elsevier. https://doi.org/10.1007/s13398-014-0173-7.2

Williams-Hatala, E. M., Hatala, K. G., Hiles, S., & Rabey, K. N. (2016). Morphology of muscle attachment sites in the modern human hand does not reflect muscle architecture. *Scientific Reports*, *6*(June), 1–8. https://doi.org/10.1038/srep28353

Zumwalt, A. (2006). The effect of endurance exercise on the morphology of muscle attachment sites. *The Journal of Experimental Biology*, *209*(Pt 3), 444–454. https://doi.org/10.1242/jeb.02028

ACKNOWLEDGEMENTS

Several people I really need to thank for their help and support during these years.

First of all, I am grateful to Dr. J. Arnaud, for her valuable guide, trust and really important support during the final steps of my PhD.

I would like to really thank my supervisor, Prof. M. Arzarello, for her support during all these years and for giving me the opportunity to work with her research group in University of Ferrara.

I am also grateful to all people who gave me the opportunity to introduce all the osteological materials in this research: special thanks to Prof. R. Boano and Dr. G. Mangiapane (for giving me the opportunity to study the osteological materials from University of Turin collections), Prof. D. Grimaud-Hervé (for giving me the chance to study the Neolithic collections of *Musée de l'Homme*), and Prof. C. Lorenzo e J.M. Vergès (for giving me the change to study the osteological materials from San Pablo cemetery and from El Mirador). Special thanks also to all people who supported me during the sampling of the materials at University of Turin, *Musée de l'Homme* and IPHES.

I am really grateful to Sara and Gabbro for their help and support during my most anxious periods. Thanks also to Petra, Pirro and Attila.
I thank Claudio, dear friend and confidant, your support and friendship have been really important during the first months of my PhD.
I am very grateful to Iván, special friend and partner of adventures; thanks for the *champagne*, for hosting me in Paris and Ferrara, for your company at the base of Eiffel Tower, for your friendship and support during the last year. Thanks for everything, you are a special guy, thanks to be my friend.
Thanks to Sandro, partner of tricks and bus trips.
Thanks to all people I have known and met in Paris and Tarragona: Iván, Pamela, Chiara, Antonia, thank to all of you for all the breaks during long working days.
I am grateful to Roberto, Riccardo G., Federica, Valentina, Franz, Dario, Maurizio, thanks for your company and opinions, and for your support during my most stressed periods.
Very thanks to Riccardo F., even if you are young, you are a great counsellor.
Very thanks to Fabiola, for your fundamental presence during the first Covid-19 quarantine.
I am grateful to Chiara, special Friend, you are always present in every moment of my life.
Thanks to Luigi, called 'Gigio', cousin, friend, trusty help in supervision of CV tests.
Thank to Luca 'Snow', partner of movie series and pizzas.

Thanks to Soraia, always present in my mind and life, thanks for your company in the long, lonely nights in Ferrara.
I am very grateful to my awesome family: nothing to say, just thank you.
And, finally, I thank you, Bern, for your constant support, for your patience, for your trust and presence in my life. Thank you.

Tantissime sono le persone che devo assolutamente ringraziare e che mi hanno accompagnata durante questi anni.

Il primo ringraziamento va alla Dott.ssa J. Arnaud, per il suo aiuto e il suo sostegno, importante guida e fondamentale supporto, soprattutto durante gli ultimi step del mio dottorato. Questo lavoro esiste anche grazie a te, che mi hai dato fiducia anche quando io non sapevo dove trovarla: dunque, cara Julie, grazie davvero per tutto.

Un secondo ringraziamento va alla Prof.ssa M. Arzarello, per il suo supporto durante tutti questi anni e per avermi concesso l'opportunità di lavorare con il suo gruppo di ricerca presso UniFe.

Un importante ringraziamento va a tutti coloro che mi hanno permesso di studiare il materiale osteologico introdotto in questa ricerca: ringrazio la Prof.ssa R. Boano e il Dott. G. Mangiapane (per la gentile concessione del campione del Museo di Antropologia ed Etnografia (Università degli Studi di Torino), ringrazio la Prof.ssa D. Grimaud-Hervé e le responsabili delle collezioni del *Musée de l'Homme* (per la gentile concessione del campione archeologico proveniente dalle collezioni del *Musée de l'Homme*), ringrazio il Prof. C. Lorenzo Merino e il Dott. J.M. Vergès (per la gentile concessione del materiale osteologico proveniente dai siti di San Pablo e El Mirador).
Un ringraziamento speciale va anche a tutti coloro che mi hanno sostenuta durante il lavoro di campionamento presso le varie istituzioni (Università di Torino, *Musée de l'Homme*, IPHES); grazie soprattutto per le sessioni di confronto scientifico e dibattito accademico.

Proseguendo coi ringraziamenti, tantissime sono le persone mi sono state accanto e mi hanno aiutata a superare più facilmente i periodi di difficoltà.
Mille grazie Sara e Gabbro, per avermi aiutata a superare il periodo ansiogeno precedente la partenza per Parigi, per avermi diverse volte ospitata, per le battute sul mio stato di ansia che, in realtà, sono state utilissime per superarla. Grazie anche alle coccole di Petra e Pirro e alle sveglie di Attila.

Grazie Claudio, grande amico e carissimo confidente, il tuo supporto e la tua amicizia sono stati importanti soprattutto durante i primi mesi del dottorato, quando non sapevo bene cosa fare e come farlo.

Grazie infinite Iván, il *chico* spagnolo, amico speciale e compagno di avventure; grazie per lo *champagne*, per l'ospitalità a Parigi e a Ferrara, per la compagnia sotto la Tour Eiffel aspettando le 18h, per le passeggiate e il cinema alle 9h del mattino, per il sostegno morale e psicologico durante questo ultimo anno, per le conversazioni simil-spagnole, per lo sport… grazie veramente per tutto, sei una persona speciale, grazie per essere entrato nella mia vita, per caso.

Grazie Sandro, compagno di battute e di viaggi in bus e ottimo ascoltatore, grazie per la tua presenza che ricorda casa.

Ringrazio tutti coloro che ho conosciuto per la prima volta ed incontrato nuovamente tra Parigi e Tarragona: Iván, Pamela, Chiara, Antonia, grazie per le chiacchere e le pause nelle lunghe giornate di lavoro.

Ringrazio tutti i compagni di scavo, conosciuti per caso, adesso amici: Roberto, Riccardo G., Federica, Valentina, Franz, Dario, Maurizio, grazie per i consigli, le opinioni e soprattutto per il supporto nei periodi di maggior stress.

Un ringraziamento particolare va a Riccardo F.: ci conosciamo da poco, ma sei riuscito a farti voler bene in pochissimo tempo; nonostante la tua giovane età, sei un super consigliere, un super tranquillante e un ottimo compagno di videochiamate notturne.

Ringrazio Fabiola 'dell'interno 8': la tua presenza nella mia vita è stata fondamentale in quest'ultimo anno. Grazie per le risate, per le tinte, e soprattutto per i pacchi dal 'centro-sud'.

Ringrazio Chiara, Amica per eccellenza, ascoltatrice perfetta di vocali dalla durata indefinita; un immenso grazie perché sei stata e sei sempre presente, a qualsiasi ora di qualsiasi giorno, qualunque sia l'emergenza.

Un ringraziamento speciale va a Luigi detto 'Gigio', cugino, amico, continuo revisore di CV su Canva e fidato aiuto nella revisione di testi.

Ringrazio Luca 'Snow', collega e sostenitore di maratone di film, compagno di recensioni e, soprattutto, cacciatore e scopritore di buone pizze palermitane.

Ringrazio Soraia, onnipresente e costante 'correttore automatico' di grafiche brutte, compagna notturna di conversazioni anglo-ferraresi.

Ringrazio la mia meravigliosa famiglia: decisamente poco da dire, soltanto grazie.

Ed infine ringrazio Bern, per il sostegno costante, per la pazienza, per gli scambi di opinioni, per la continua presenza nella mia vita. Semplicemente grazie.

Annexes

Muscles	Abbr.	Origin	Insertion	Function
Opponens Pollicis	OP	Trapezium	Diaphysis of MC1 - radial side	Abduction, rotation and flection of the thumb
Abductor Pollicis Longus	ABL	Ulna and radius	Base of MC1 - radial side	Abduction of the hand
Abductor Pollicis Brevis	ABP	*Flexor retinaculum*, scaphoid, trapezium	Base of PP1 - radial side	Abduction of the thumb
Adductor Pollicis	ADP	Oblique head: Capitate, MC2 (diaphysis), MC3 (base, palmar side) Transverse head: MC3 (Diaphysis)	Base of PP1 (ulnar side)	Adduction of the thumb
Extensor Pollicis Brevis	EPB	Dorsal surface of radius	Base of PP1 (dorsal surface)	Extension of the thumb
Flexor Pollicis Brevis	FPB	*Flexor retinaculum*, trapezium	Base of PP1 (radial side)	Flexion of the 1st metacarpo-phalangeal joint
Flexor Pollicis Longus	FPL	Radius, interossea antebrachii membrane	Base of MC1 (palmar surface)	Flexion of DP1
Extensor Pollicis Longus	EPL	Dorsale surface of ulna and interossea antibrachii membrane	Base of DP1	Extension and abduction of the thumb
Extensor Carpi Radialis Longus	ECRL	Lateral supracondylar crest of the humerus, lateral intermuscular septum	Base of MC2 - towards articular surface with trapezium	Extension and abduction of the wrist
Flexor Carpi Radialis	FCR	Medial epicondyle of the humerus	Base of MC2 (radial side)	Flexion and abduction of the wrist
Extensor Carpi Radialis Brevis	ECRB	Lateral epicondyle of the humerus	Base of MC3 - towards articular surface of capitate-MC2	Extension and abduction of the wrist
Opponens Digiti Minimi	ODM	Hook of the hamate, *flexor retinaculum*	Diaphysis of MC5 (ulnar side)	Movement of MC5 in a palmar direction (opposition)
Flexor Carpi Ulnaris	FCU	Humeral head: medial epicondyle of the humerus Ulnar head: olecranon	Pisiform, hook of the hamate, base of MC5	Flexion of the wrist and adduction of the hand
Extensor Digiti Minimi	EDM	Lateral epicondyle of the humerus	Base of PP5 (dorsal surface)	Extension of the wrist and 5th finger
Abductor Digiti Minimi	ADM	Pisiform	Base of PP5 (ulnar side)	Flexion and abduction of the 5th finger and extension of the joints of the 5th finger
Flexor Digiti Minimi	FDM	*Flexor retinaculum*, hook of the hamate	Base of PP5	Flexion of the metacarpo-phalangeal joint of the 5th finger
Extensor Carpi Ulnaris	ECU	Humeral head: lateral epicondyle of the humerus Ulnar head: diaphysis of the ulna	MC5 - medial tubercle on the nonarticular surface	Extension of the wrist and adduction of the hand
1st Dorsal Interosseous	DI1	Diaphysis of MC1 and MC2	Base of PP2 (radiale side)	Abduction of the 2nd and 4th fingers, abduction and adduction of the 3rd finger, flexion of the PP2, PP3 and PP4
2nd Dorsal Interosseous	DI2	Diaphysis of MC2 and MC3	Base of PP3 (radial side)	
3rd Dorsal Interosseous	DI3	Diaphysis of MC3 and MC4	Base of PP3 (ulnar side)	
4th Dorsal Interosseous	DI4	Diaphysis of MC4 and MC5	Base of PP4 (ulnar side)	
1st Palmar Interosseous	PI1	Diaphysis of MC2 (ulnar side)	Base of PP2 (ulnar side)	Adduction and flexion of the metacarpo-phalangeal joints of the 2nd, the 4th and the 5th finger
2nd Palmar Interosseous	PI2	Diaphysis of MC4 (radial side)	Base of PP4 (radial side)	
3rd Palmar Interosseous	PI3	Diaphysis of MC5 (radial side)	Base of PP5 (radial side)	

ABL.MC1

Landmark	Type	Description
L1	3	The point of the distal aspect of the entheseal outline that is closest to the dorsal surface of the bone
L2	3	The point of the proximal aspect of the entheseal outline that is closest to the dorsal surface of the bone
L3	2	The maximum point of the curve on the proximal aspect of the entheseal outline, between L2 and L4
L4	3	The point of the proximal aspect of the entheseal outline that is closest to the palmar surface of the bone
L5	3	The point of the distal aspect of the entheseal outline that is closest to the palmar surface of the bone
L6	2	The maximum point of the curve on the distal aspect of the entheseal outline, between L5 and L1

50 equidistant surface semi-landmarks automatically disposed

DI1.MC1

Landmark	Type	Description
L1	3	The point of the distal aspect of the entheseal outline that is closest to the dorsal surface of the bone
L2	3	The point of the distal aspect of the entheseal outline that is closest to the palmar surface of the bone
L3	3	The point of the proximal aspect of the entheseal outline that is closest to the palmar surface of the bone
L4	3	The point of the proximal aspect of the entheseal outline that is closest to the dorsal surface of the bone

50 equidistant surface semi-landmarks automatically disposed

OP.MC1

Landmark	Type	Description
L1	3	The point of the distal aspect of the entheseal outline that is closest to the palmar surface of the bone
L2	2	The maximum point of the curve between L1 and L3, near the metacarpal head
L3	3	The point of the distal aspect of the entheseal outline that is closest to the dorsal surface of the bone
L4	2	The inflection point of the curve between L3 and L5 that is closest to the dorsal surface of the bone
L5	2	The most proximal point of the enthesis
L6	3	The inflection point of the curve between L5 and L1 that is closest to the palmar surface of the bone

50 equidistant surface semi-landmarks automatically disposed

ECRL.MC2

Landmark	Type	Description
L1	3	The point of the distal aspect of the entheseal outline that is closest to the palmar surface of the bone
L2	2	The most distal point of the enthesis
L3	3	The point of the distal aspect of the entheseal outline that is closest to the dorsal surface of the bone
L4	3	The point of the proximal aspect of the entheseal outline that is closest to the dorsal surface of the bone
L5	2	The most proximal point of the enthesis
L6	3	The point of the proximal aspect of the entheseal outline that is closest to the palmar surface of the bone

40 equidistant surface semi-landmarks automatically disposed

DI1.MC2

Landmark	Type	Description
L1	3	The point of the distal aspect of the entheseal outline that is closest to the dorsal surface of the bone
L2	3	The point of the distal aspect of the entheseal outline that is closest to the palmar surface of the bone
L3	3	The point of the proximal aspect of the entheseal outline that is closest to the palmar surface of the bone
L4	3	The point of the proximal aspect of the entheseal outline that is closest to the dorsal surface of the bone

50 equidistant surface semi-landmarks automatically disposed

DI2+PI1.MC2

Landmark	Type	Description
L1	2	The most distal point of the enthesis
L2	2	The highest point of the curve between L1 and L3
L3	2	The most proximal point of the entheseal outline that is closest to the metacarpal base
L4	2	The highest point of the curve between L3 and L5
L5	3	The point of the proximal aspect of the entheseal outline that is closest to the palmar surface of the bone (between L4 and L6)
L6	3	The point of the distal aspect of the entheseal outline that is closest to the palmar surface of the bone (between L5 and L1)

50 equidistant surface semi-landmarks automatically disposed

ECRB.MC3

Landmark	Type	Description
L1	2	The most distal point of the enthesis
L2	3	The point of the entheseal outline that is closest to the dorsal surface of the bone
L3	2	The most proximal point of the enthesis
L4	3	The point of the entheseal outline that is closest to palmar surface of the bone

40 equidistant surface semi-landmarks automatically disposed

DI2.MC3

Landmark	Type	Description
L1	2	The most distal point of the enthesis
L2	3	The point of the proximal aspect of the entheseal outline that is closest to the dorsal surface of the bone
L3	2	The highest point of the curve between L2 and L4, at the proximal aspect of the entheseal outline, closest to the styloid process of the metacarpal base
L4	3	The point of the proximal aspect of the entheseal outline that is closest to palmar surface of the bone
L5	3	The point of the distal aspect of the entheseal outline that is closest to palmar surface of the bone

50 equidistant surface semi-landmarks automatically disposed

DI3+ADP.MC3

Landmark	Type	Description
L1	3	The point of the distal aspect of the entheseal outline that is closest to the dorsal surface of the bone
L2	3	The point of the distal aspect of the entheseal outline that is closest to the palmar surface of the bone
L3	2	The lowest point of the curve of the entheseal outline between L2 and L4, towards the palmar surface of the bone
L4	2	The most palmar point of the enthesis
L5	2	The most proximal point of the enthesis
L6	2	The lowest point of the curve of the entheseal outline between L4 and L5, where proximal epiphysis and midshaft (towards the palmar surface) separate
L7	3	The point of the proximal aspect of the entheseal outline that is closest to the dorsal surface of the bone

50 equidistant surface semi-landmarks automatically disposed

	Landmark	Type	Description
	L1	3	The point of the distal aspect of the entheseal outline that is closest to the dorsal surface of the bone
	L2	3	The point of the proximal aspect of the entheseal outline that is closest to the dorsal surface of the bone
DI3+PI2.MC4	L3	2	The maximum point of the curve between L2 and L4, at the proximal aspect of the entheseal outline
	L4	3	The point of the proximal aspect of the entheseal outline that is closest to palmar surface of the bone
	L5	3	The point of the distal aspect of the entheseal outline that is closest to palmar surface of the bone

50 equidistant surface semi-landmarks automatically disposed

	Landmark	Type	Description
	L1	3	The point of the distal aspect of the entheseal outline that is closest to the palmar surface of the bone
	L2	3	The point of the proximal aspect of the entheseal outline that is closest to the palmar surface of the bone
DI4.MC4	L3	2	The maximum point of the curve between L2 and L4, at the proximal aspect of the entheseal outline
	L4	3	The point of the proximal aspect of the entheseal outline that is closest to dorsal surface of the bone
	L5	3	The point of the distal aspect of the entheseal outline that is closest to dorsal surface of the bone

50 equidistant surface semi-landmarks automatically disposed

	Landmark	Type	Description
DI4+PI3.MC5	L1	3	The point of the distal aspect of the entheseal outline that is closest to the dorsal surface of the bone
	L2	3	The point of the proximal aspect of the entheseal outline that is closest to the dorsal surface of the bone
	L3	2	The highest point of the curve on the proximal aspect of the entheseal outline, between L2 and L4
	L4	3	The point of the proximal aspect of the entheseal outline that is closest to palmar surface of the bone
	L5	3	The point of the distal aspect of the entheseal outline that is closest to palmar surface of the bone

50 equidistant surface semi-landmarks automatically disposed

	Landmark	Type	Description
ODM.MC5	L1	3	The point of the distal aspect of the entheseal outline that is closest to the dorsal surface of the bone
	L2	3	The point of the distal aspect of the entheseal outline that is closest to the palmar surface of the bone
	L3	3	The point of the proximal aspect of the entheseal outline that is closest to the palmar surface of the bone
	L4	2	The maximum point of the curve on the proximal aspect of the entheseal outline between L3 and L5
	L5	3	The point of the proximal aspect of the entheseal outline that is closest to dorsal surface of the bone

50 equidistant surface semi-landmarks automatically disposed

	Landmark	Type	Description
ABP+FBP.PP1 ADP.PP1	L1	2	The most distal point of the enthesis
	L2	3	The point of the distal aspect of the entheseal outline that is closest to the dorsal surface of the bone
	L3	3	The point of the proximal aspect of the entheseal outline that is closest to the dorsal surface of the bone
	L4	2	The maximum inflection point of the curve between L3 and L5
	L5	3	The point of the proximal aspect of the entheseal outline that is closest to palmar surface of the bone
	L6	3	The point of the distal aspect of the entheseal outline that is closest to palmar surface of the bone

40 equidistant surface semi-landmarks automatically disposed

	Landmark	Type	Description
DI1.PP2 PI1.PP2	L1	2	The most distal point of the enthesis
	L2	3	The point of the distal aspect of the entheseal outline that is closest to the dorsal surface of the bone
	L3	3	The point of the proximal aspect of the entheseal outline that is closest to the dorsal surface of the bone
	L4	2	The maximum inflection point of the curve between L3 and L5
	L5	3	The point of the proximal aspect of the entheseal outline that is closest to the palmar surface of the bone
	L6	3	The point of the distal aspect of the entheseal outline that is closest to the palmar surface of the bone

40 equidistant surface semi-landmarks automatically disposed

DI2.PP3
DI3.PP3

Landmark	Type	Description
L1	2	The most distal point of the enthesis
L2	3	The point of the distal aspect of the entheseal outline that is closest to the dorsal surface of the bone
L3	3	The point of the proximal aspect of the entheseal outline that is closest to the dorsal surface of the bone
L4	2	The maximum inflection point of the curve between L3 and L5
L5	3	The point of the proximal aspect of the entheseal outline that is closest to the palmar surface of the bone
L6	3	The point of the distal aspect of the entheseal outline that is closest to the palmar surface of the bone

40 equidistant surface semi-landmarks automatically disposed

DI4.PP4
PI2.PP4

Landmark	Type	Description
L1	2	The most distal point of the enthesis
L2	3	The point of the distal aspect of the entheseal outline that is closest to the dorsal surface of the bone
L3	3	The point of the proximal aspect of the entheseal outline that is closest to the dorsal surface of the bone
L4	2	The maximum inflection point of the curve between L3 and L5
L5	3	The point of the proximal aspect of the entheseal outline that is closest to the palmar surface of the bone
L6	3	The point of the distal aspect of the entheseal outline that is closest to the palmar surface of the bone

40 equidistant surface semi-landmarks automatically disposed

	Landmark	Type	Description
ADM+FDM.PP5 PI3.PP5	L1	2	The most distal point of the enthesis
	L2	3	The point of the distal aspect of the entheseal outline that is closest to the dorsal surface of the bone
	L3	3	The point of the proximal aspect of the entheseal outline that is closest to the dorsal surface of the bone
	L4	2	The maximum inflection point of the curve between L3 and L5
	L5	3	The point of the proximal aspect of the entheseal outline that is closest to the palmar surface of the bone
	L6	3	The point of the distal aspect of the entheseal outline that is closest to the palmar surface of the bone

40 equidistant surface semi-landmarks automatically disposed

Function	Description	Details
read.ply	To read and import '.ply' files. It can be used for digitizing landmark coordinates	The function reads 3D surface data, ASCII format only
digit.fixed	Interactive function to digitize 3D landmarks.	The function digitizes fixed 3D landmarks
buildtemplate	Interactive function to build a template for the digitization across speciments of 3D surface sliding landmarks.	The function constructs a template of surface sliding semilandmarks. In this case, the fixed pseudo-landmarks have been previously digitized with *digit.fixed* function. It chooses automatically surface semilandmarks from the mesh at equal distance, using the nearest-neighbor algorithm previously outlined in Gunz et al. (2005) and Mitteroecker and Gunz (2009)
plotspec	To plot 3D specimen along with its landmarks	The function plots 3D speciments along with their digitized fixed landmarks and semilandmarks "surface sliders" and "curve sliders". If speciment is a 3D surface, mesh is plotted
digitsurface	Interactive function to digitize 3D landmarks on a surface lacking known landmarks	The function digitizes fixed 3D landmarks and places surface sliding semilandmarks using the previously created template. The function finds surface semilandmarks following the algorithme outlined in Gunz et al. (2005) and Mitteroecker and Gunz (2009). *digitsurface* finds the same number of surface semilandmarks as the template previously fixed and saved as 'template.txt'
list.files	To produce a character vector of the names of files or directories in the named directory	
readmulti.nts	To read multiple '.nts' files, each containing landmark coordinates for a single specimen	The function reads a character vector of filenames for a set of '.nts' file, each containing 2D or 3D landmark coordinates for a single specimen
plotAllSpecimens	To plot landmark coordinates for a set of specimens	The function creates a plot of the landmark coordinates for all specimens. This is useful for examining patterns of variation in Procrustes shape variables, after a GPA has been performed
gpagen	General function to perform Procrustes analysis of 2- or 3D landmark data that can include both fixed landmarks and sliding semilandmarks	The function performs a GPA on 2- or 3D landmark coordinates. The analysis can be performed on fixed landmark points, semilandmarks on curves, semilandmarks on surfaces, or any other combination
gm.prcomp	To perform principal component analysis (PCA) on Procrustes shape coordinates	
autoplot (ggplot2)	This function use ggplot2 to draw a particular plot for an object of a particular class in a single command	
mshape	Estimate the mean shape for a set of aligned specimens	The function estimates the average landmark coordinates for a set of aligned specimens
PlotRefToTarget	Function plots shape differences between a reference and a target specimen	The function generates a plot of the shape differences of a target specimen relative to a reference specimen. The option mag allows the user to indicates the degree of magnification to be used when displaying the shape difference. The function will plot either two- or three-dimensional data.

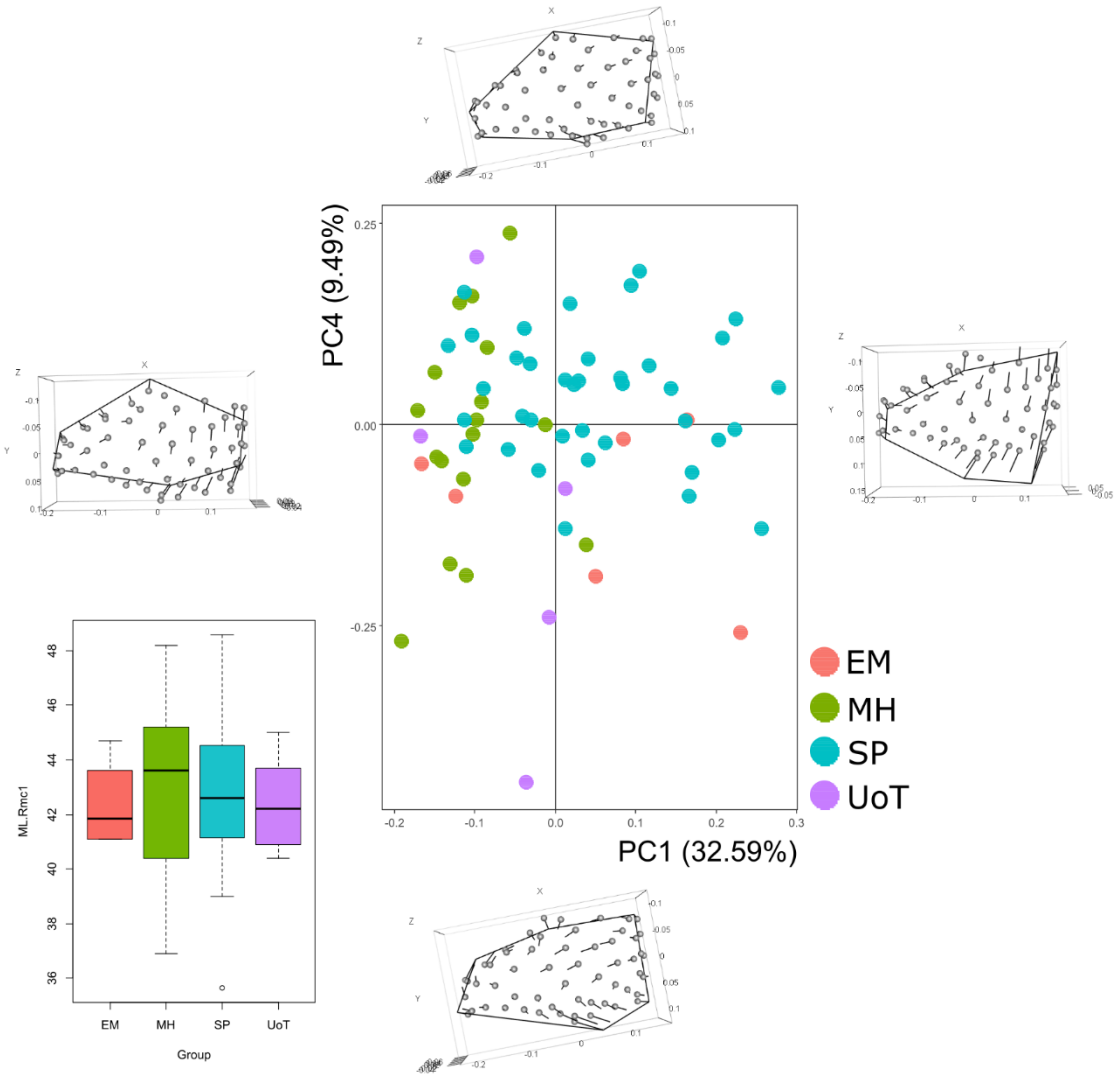
PC4 (9.49%)
PC1 (32.59%)
0.25
0.00
-0.25
-0.2
-0.1
0.0
0.1
0.2
0.3
EM
MH
SP
UoT
ML.Rmc1
36
38
40
42
44
46
48
EM
MH
SP
UoT
Group

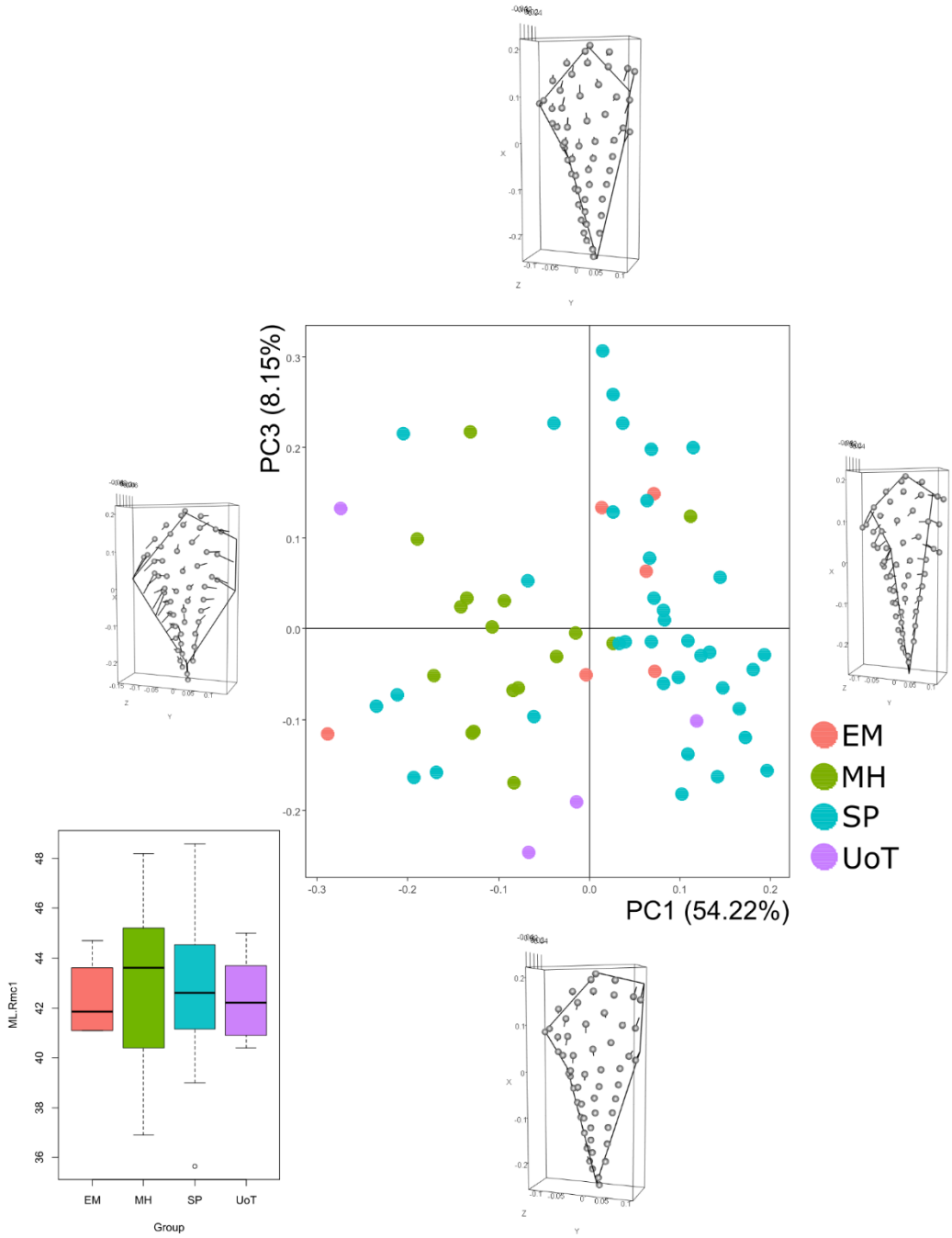
PC3 (8.15%)
PC1 (54.22%)
EM
MH
SP
UoT
ML.Rmc1
Group
EM
MH
SP
UoT

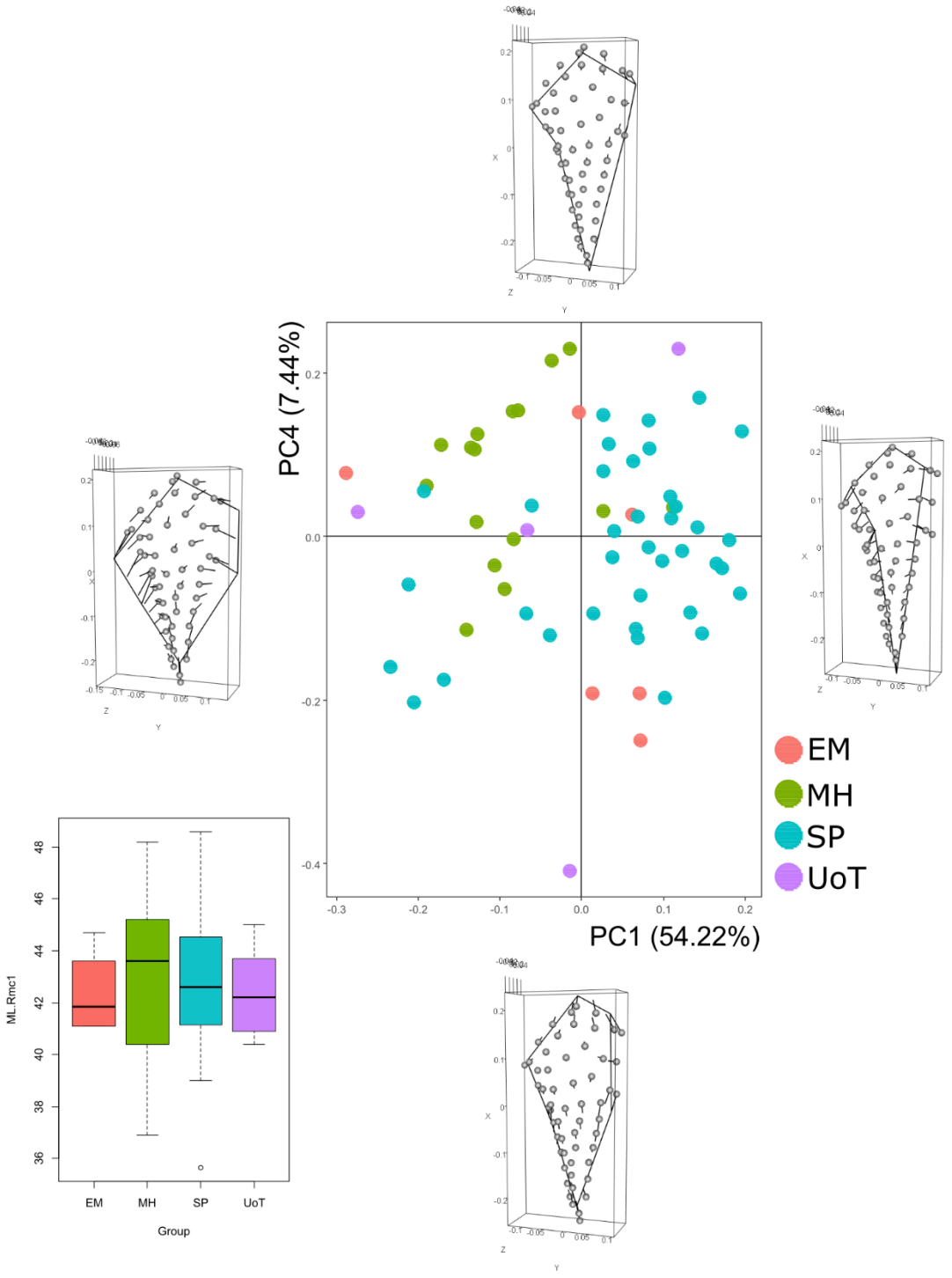
PC4 (7.44%)
PC1 (54.22%)
EM
MH
SP
UoT
MLRmc1
Group

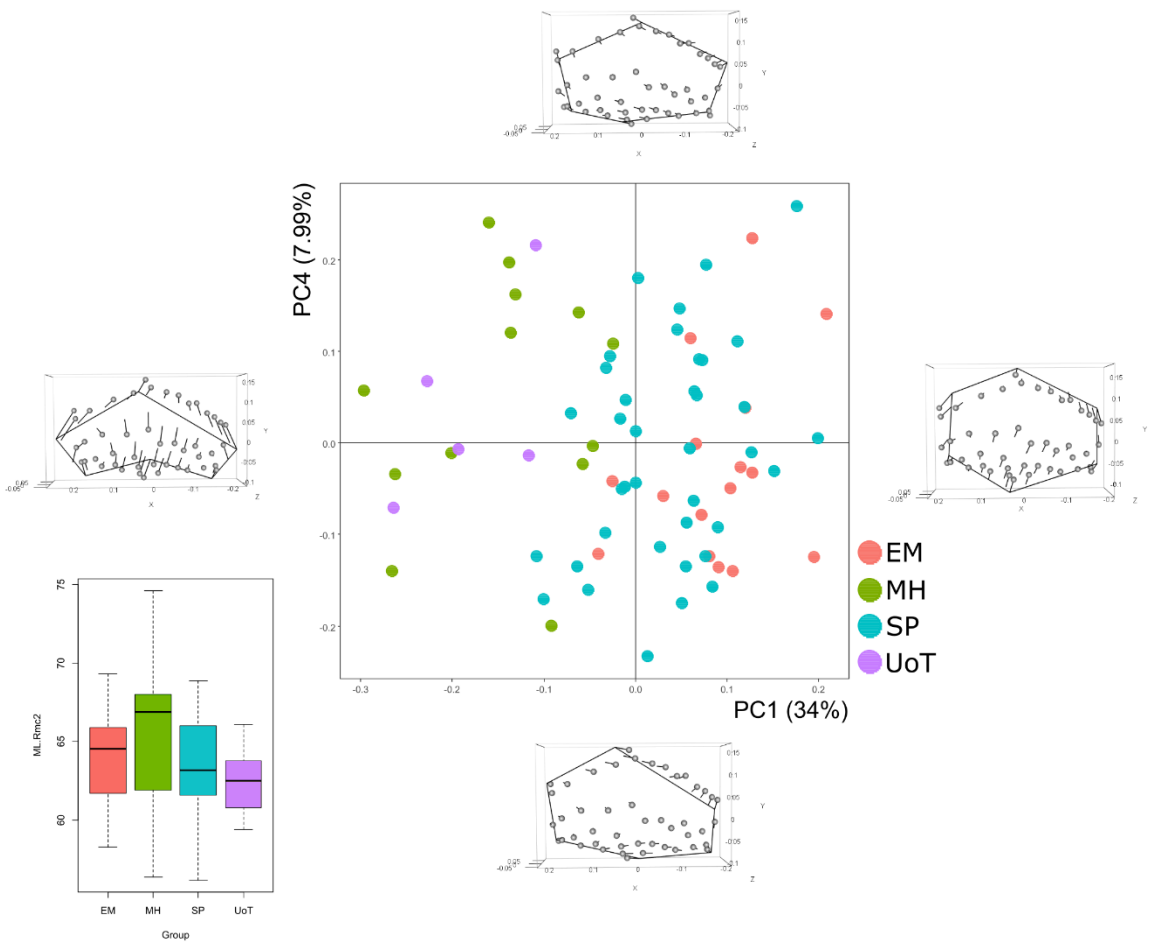
PC4 (7.99%)
PC1 (34%)
EM
MH
SP
UoT
ML.Rmc2
Group
EM
MH
SP
UoT

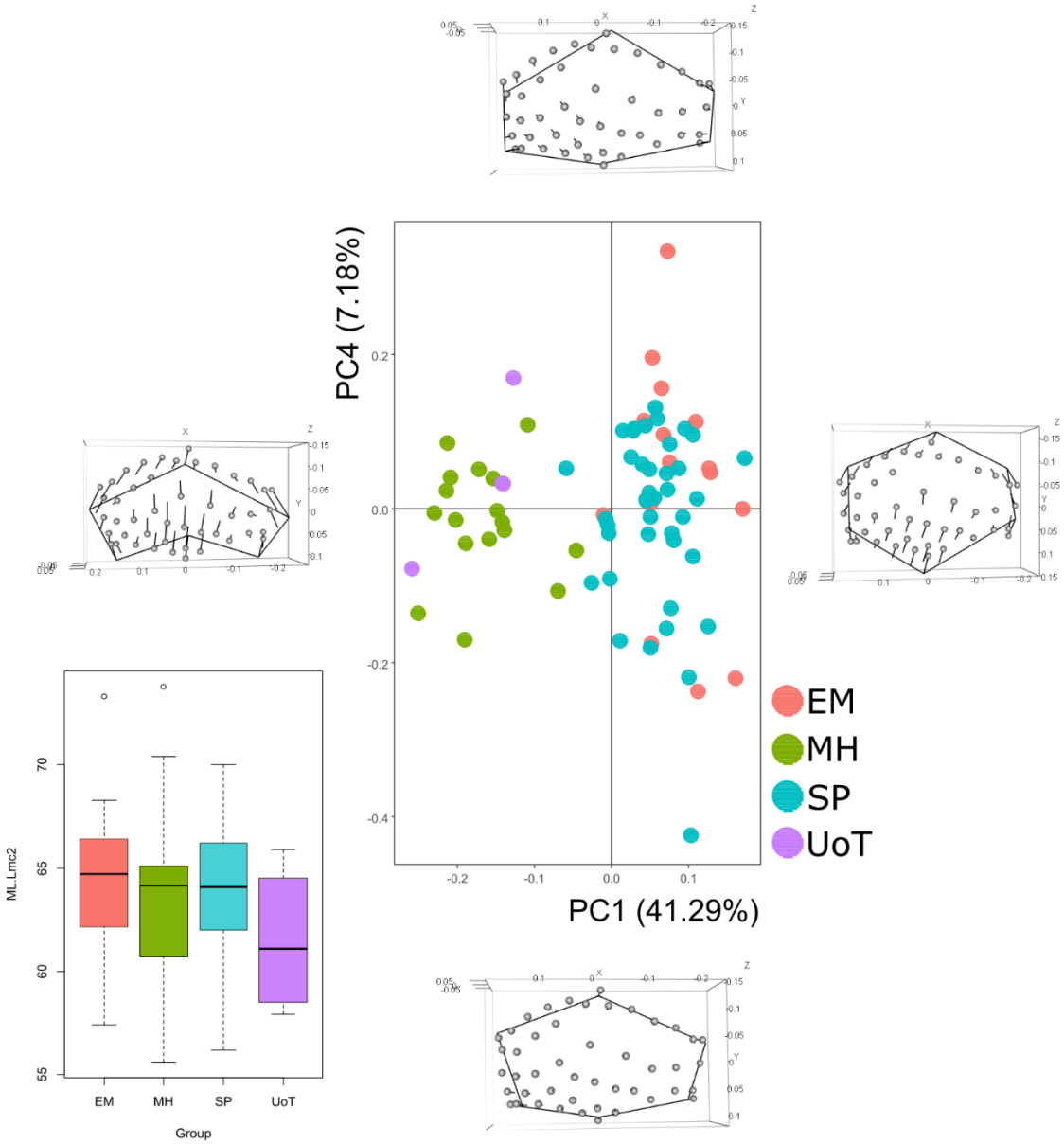
PC4 (7.18%)
PC1 (41.29%)
EM
MH
SP
UoT
ML.Lmc2
Group
EM
MH
SP
UoT

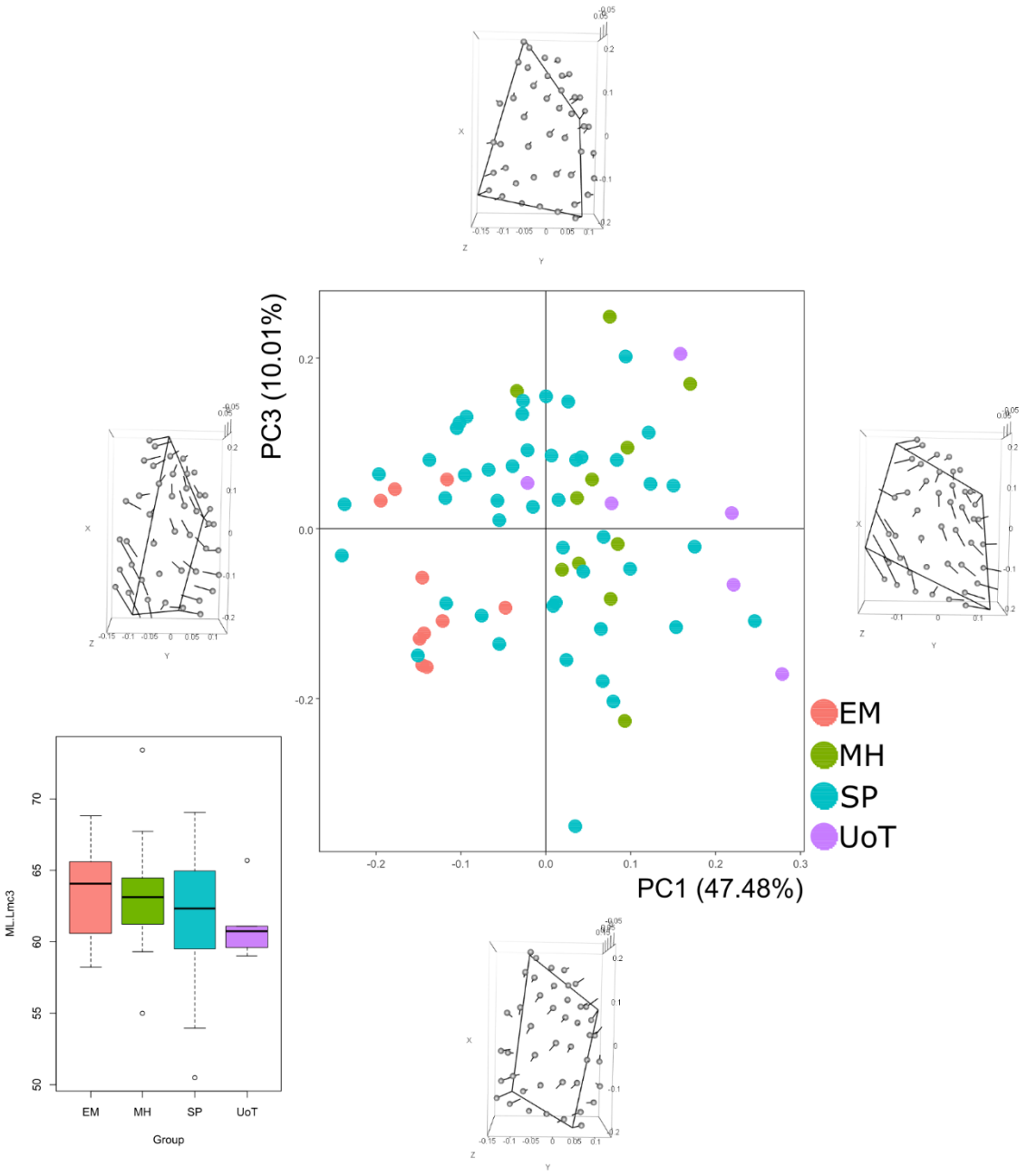
PC3 (10.01%)
PC1 (47.48%)
EM
MH
SP
UoT
ML.Lmc3
Group
EM
MH
SP
UoT

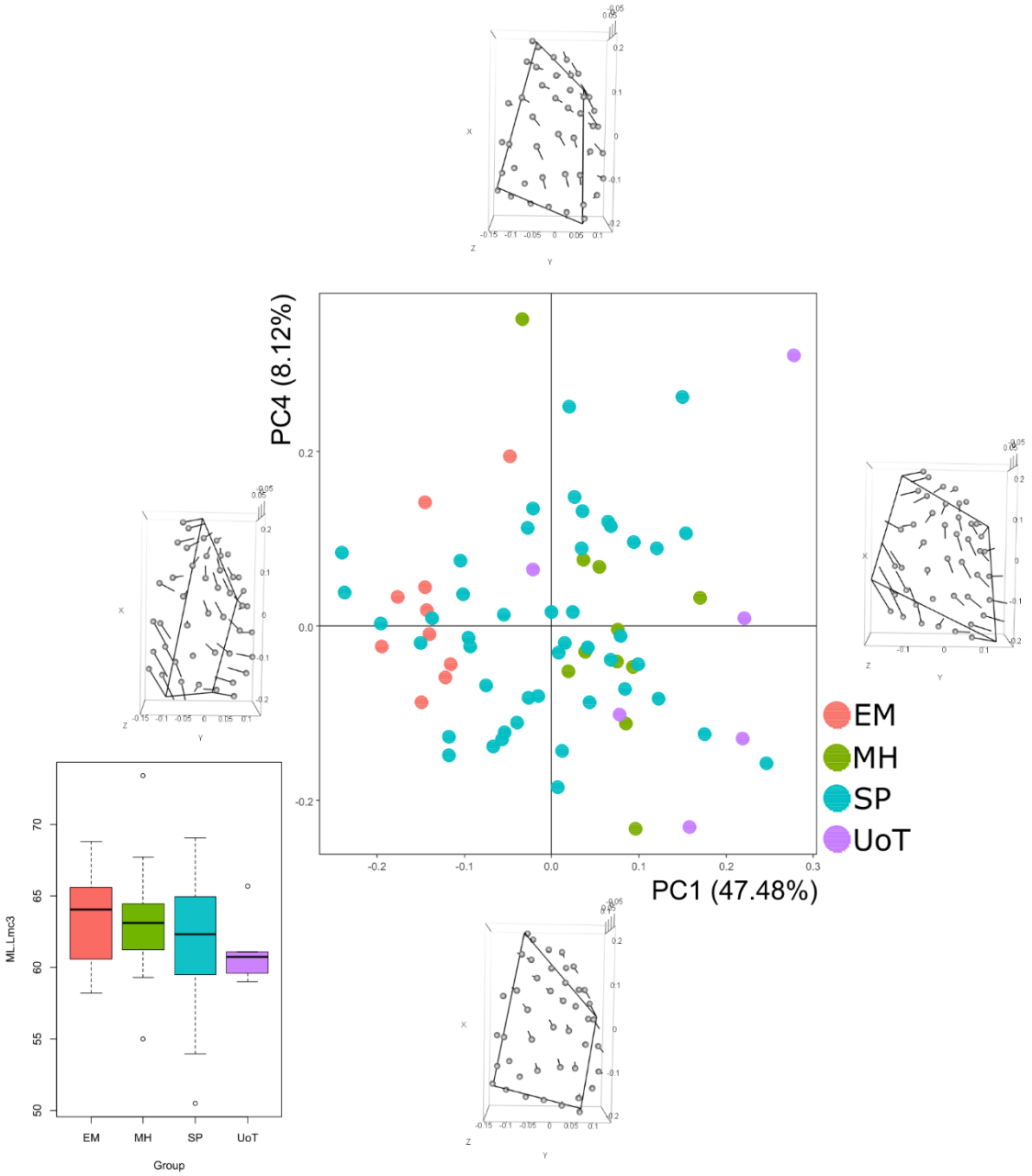
PC4 (8.12%)
PC1 (47.48%)
EM
MH
SP
UoT
ML.Lmc3
Group
EM
MH
SP
UoT

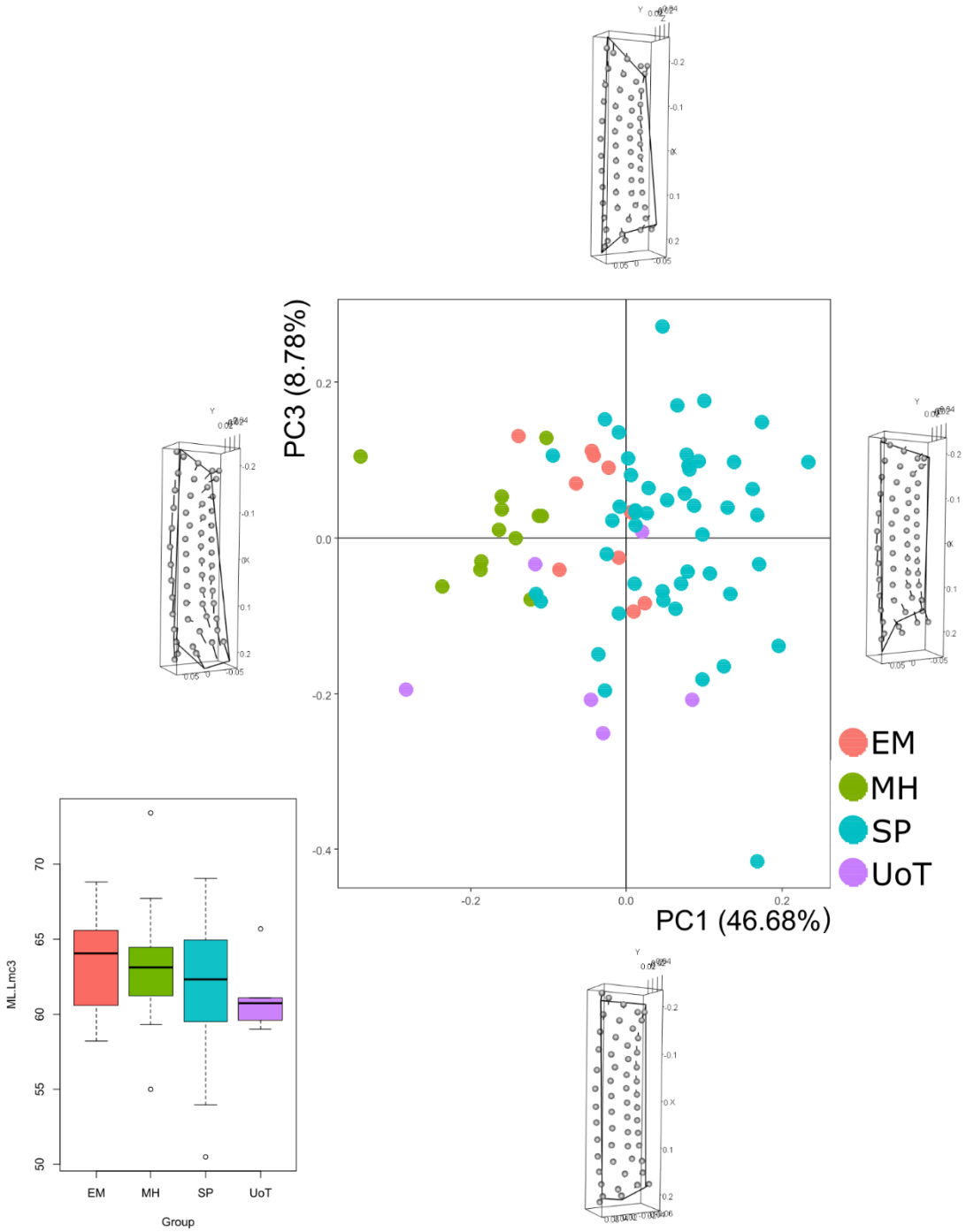
PC3 (8.78%)
PC1 (46.68%)
EM
MH
SP
UoT
ML.Lmc3
Group
EM
MH
SP
UoT

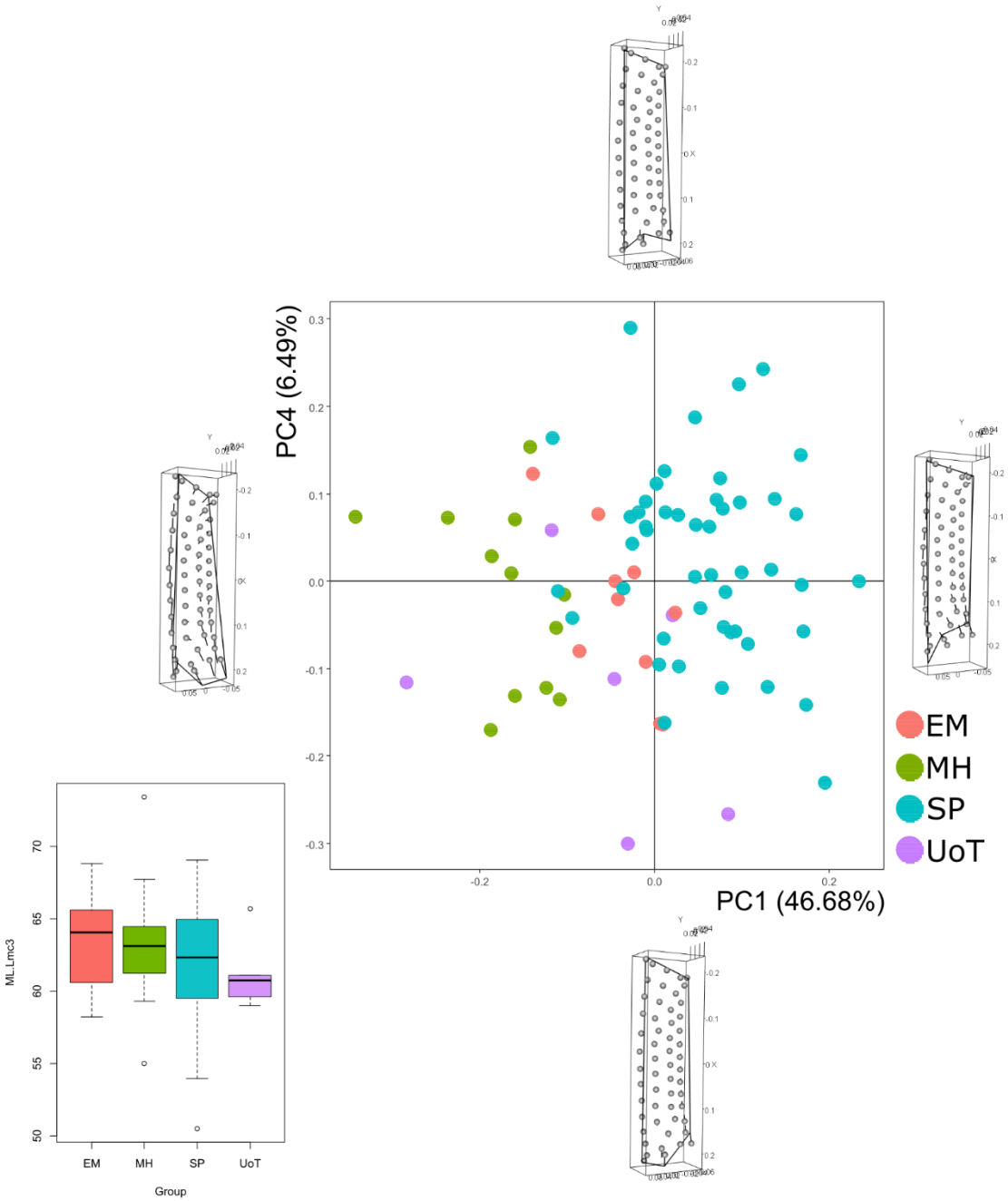
PC4 (6.49%)
PC1 (46.68%)
EM
MH
SP
UoT
ML.Lmc3
Group
EM
MH
SP
UoT

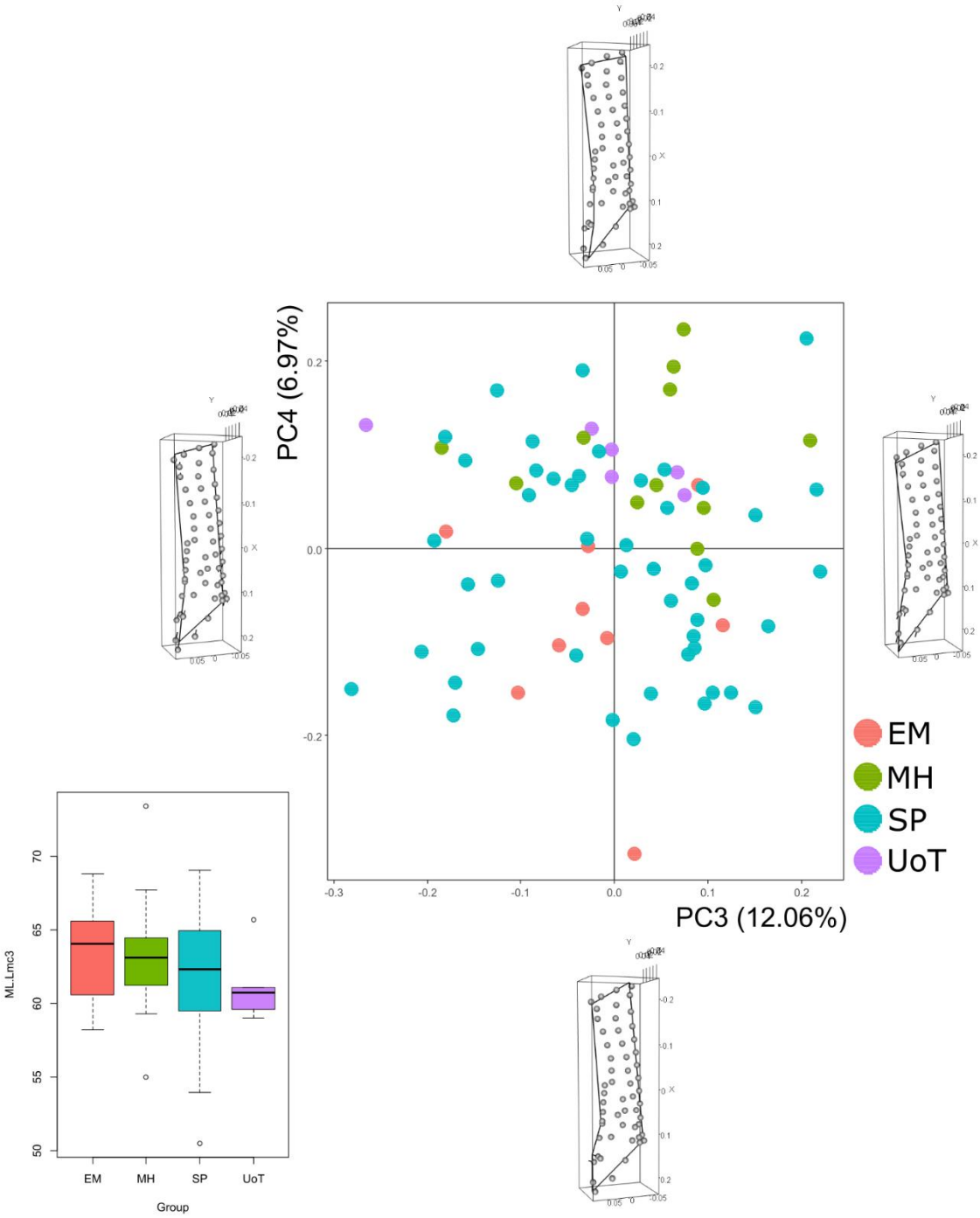
PC4 (6.97%)
PC3 (12.06%)
EM
MH
SP
UoT
ML.Lmc3
Group

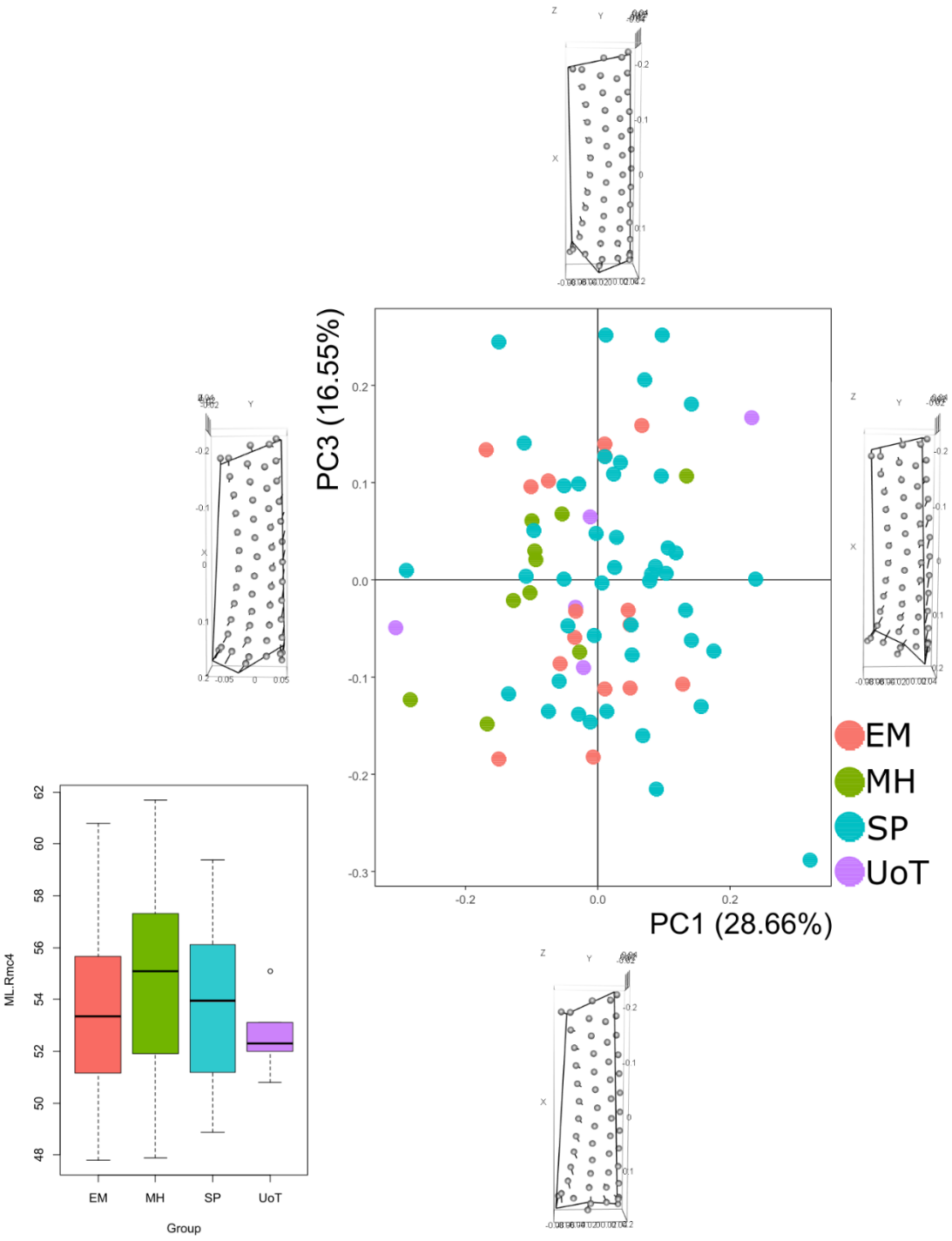
PC3 (16.55%)
PC1 (28.66%)
EM
MH
SP
UoT
MLRmc4
Group
EM
MH
SP
UoT

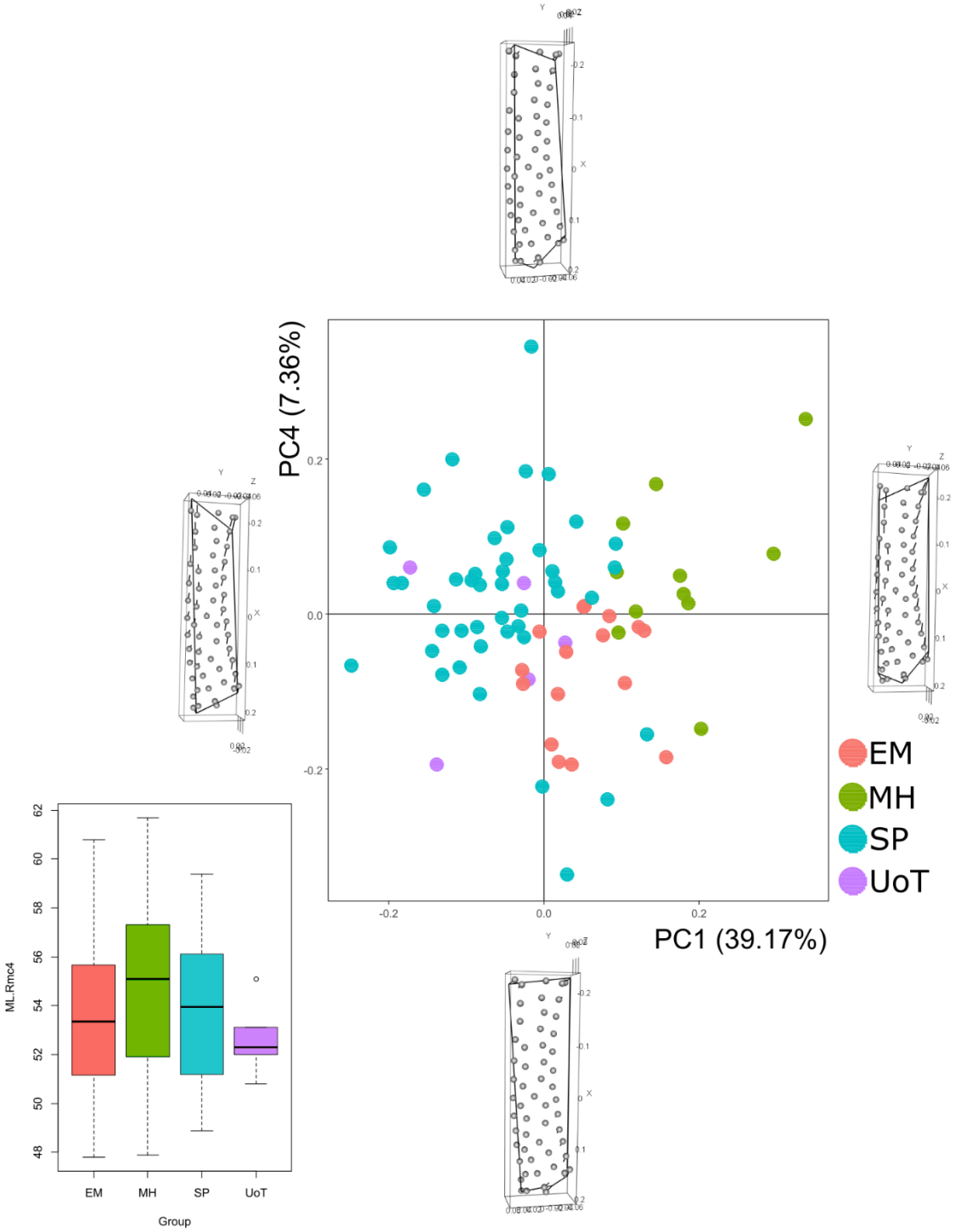
PC4 (7.36%)
PC1 (39.17%)
EM
MH
SP
UoT
MLRmc4
Group
EM
MH
SP
UoT

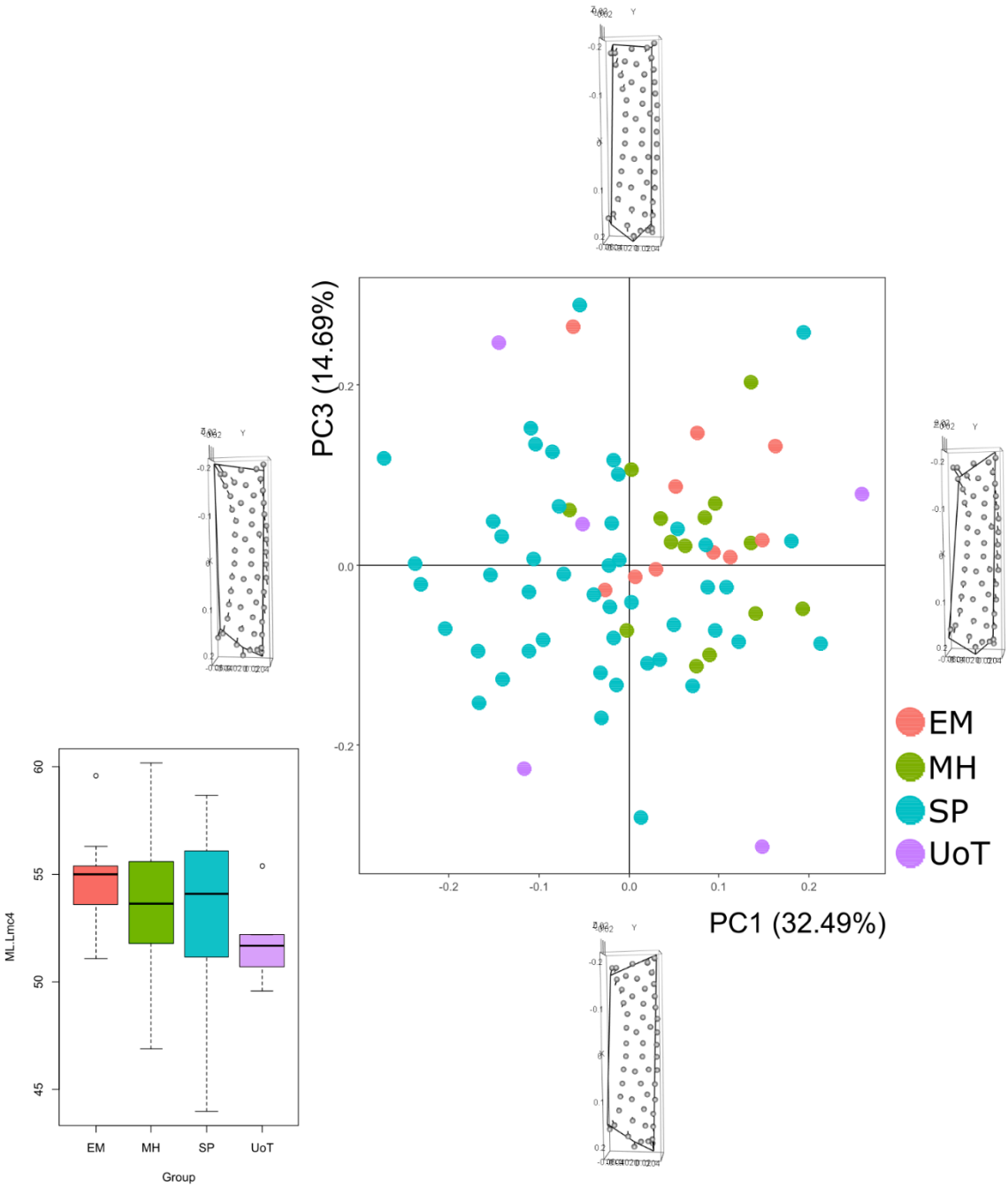
PC3 (14.69%)
PC1 (32.49%)
EM
MH
SP
UoT
ML.Lmc4
Group
EM
MH
SP
UoT

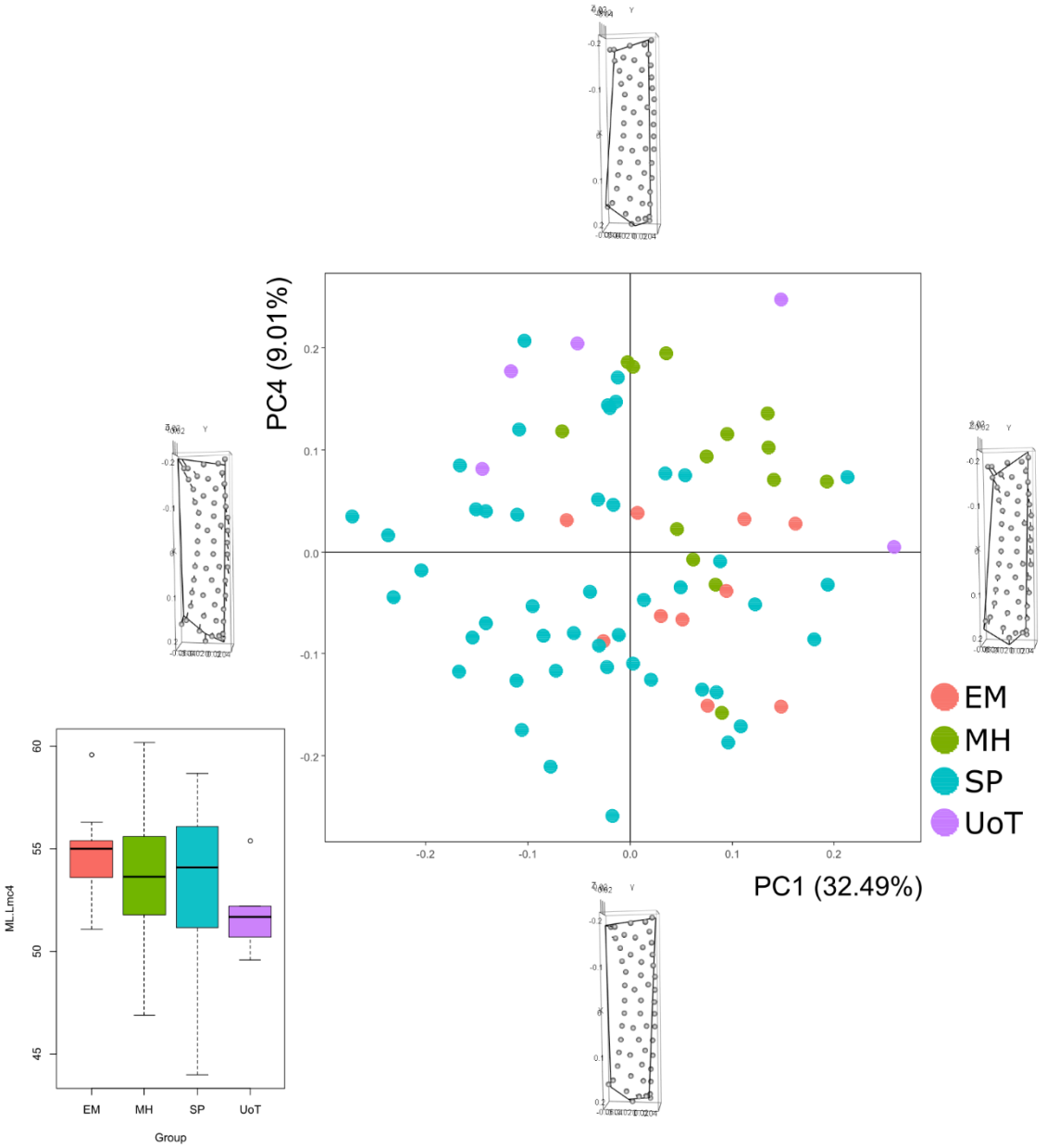
PC4 (9.01%)
PC1 (32.49%)
EM
MH
SP
UoT
ML_Lmc4
Group

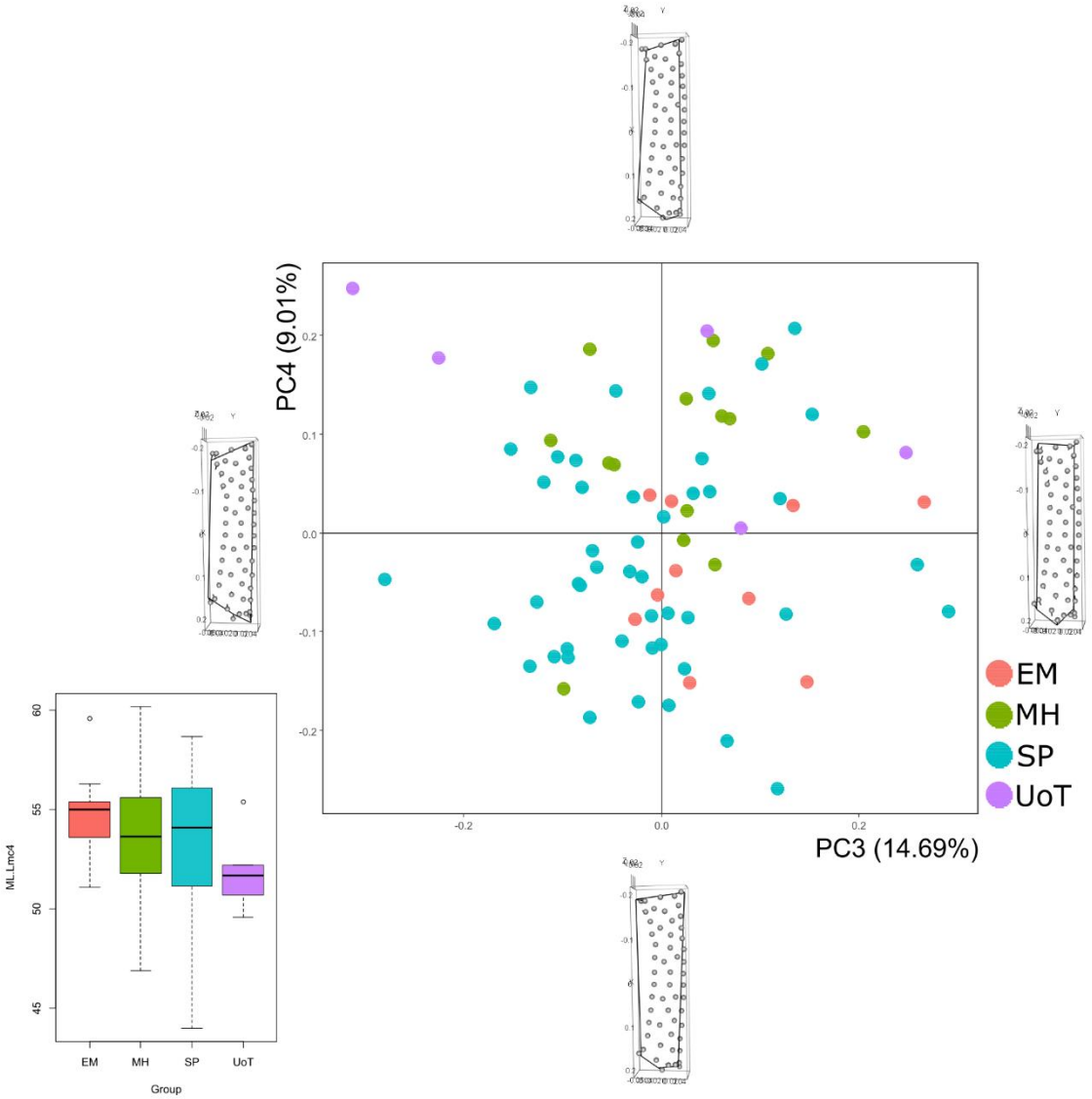
PC4 (9.01%)
PC3 (14.69%)
EM
MH
SP
UoT
MLLmc4
Group
EM
MH
SP
UoT

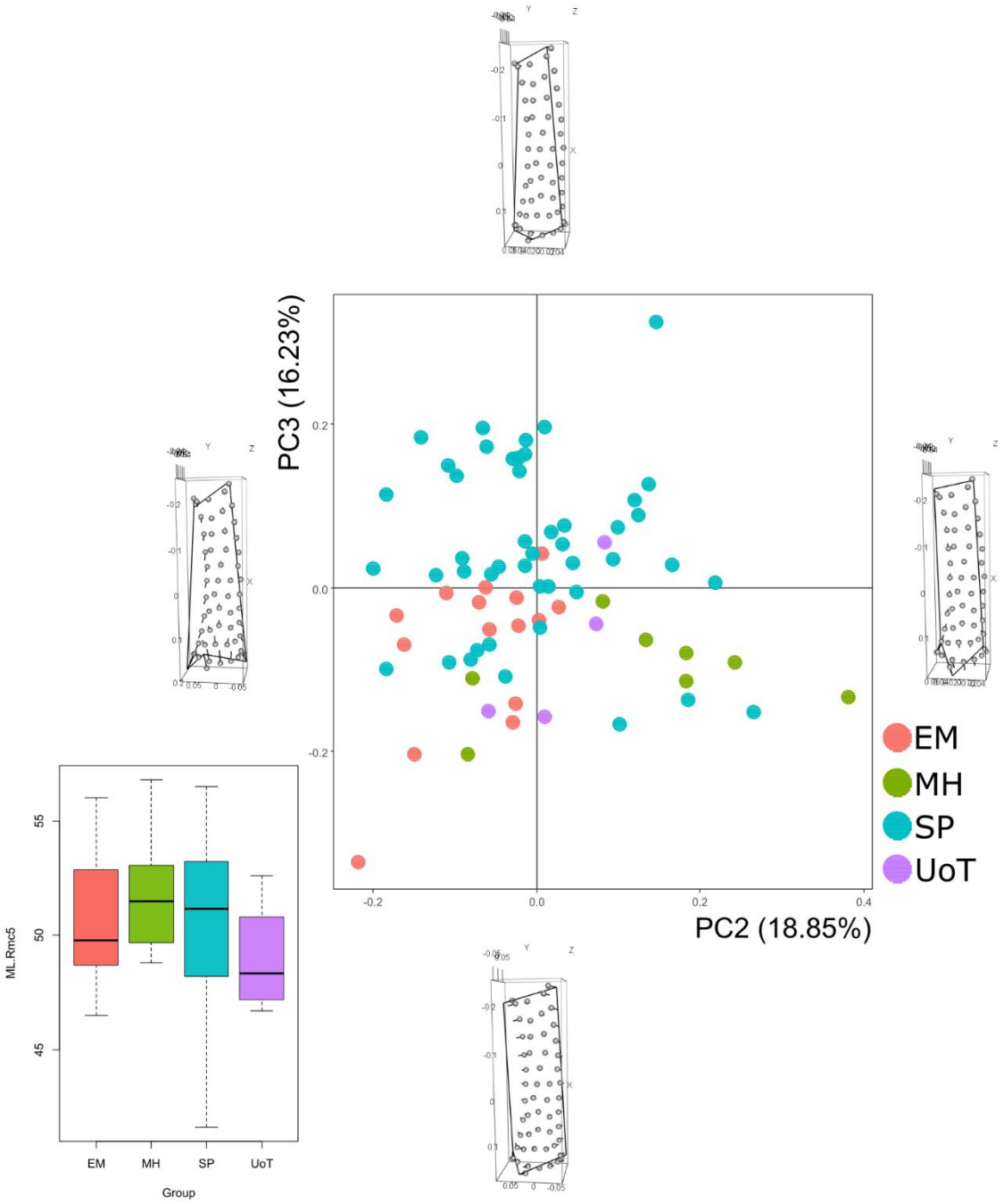
PC3 (16.23%)
PC2 (18.85%)
EM
MH
SP
UoT
ML.Rmc5
Group
EM
MH
SP
UoT

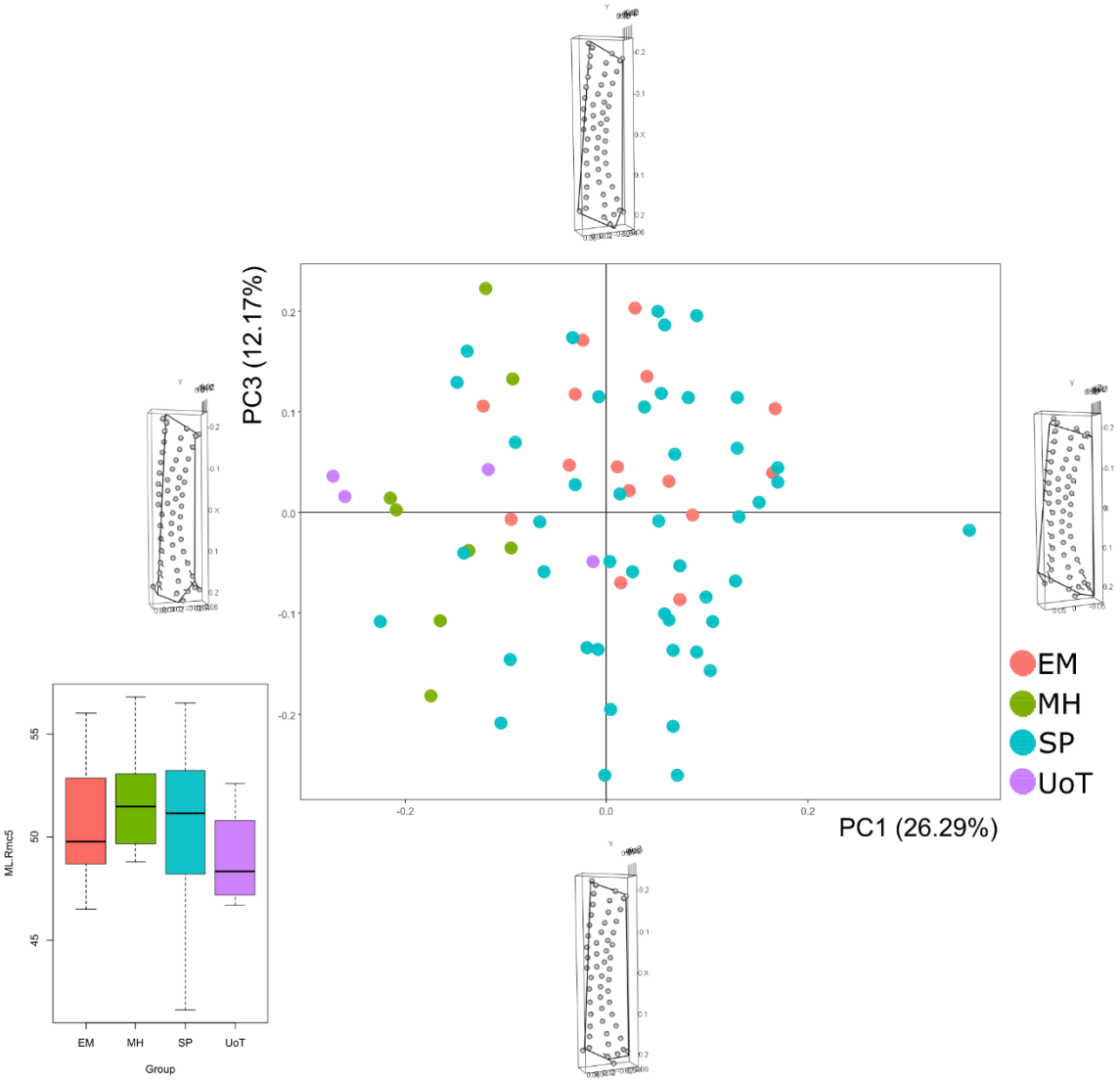
PC3 (12.17%)
PC1 (26.29%)
EM
MH
SP
UoT
MLRmc5
Group
EM
MH
SP
UoT

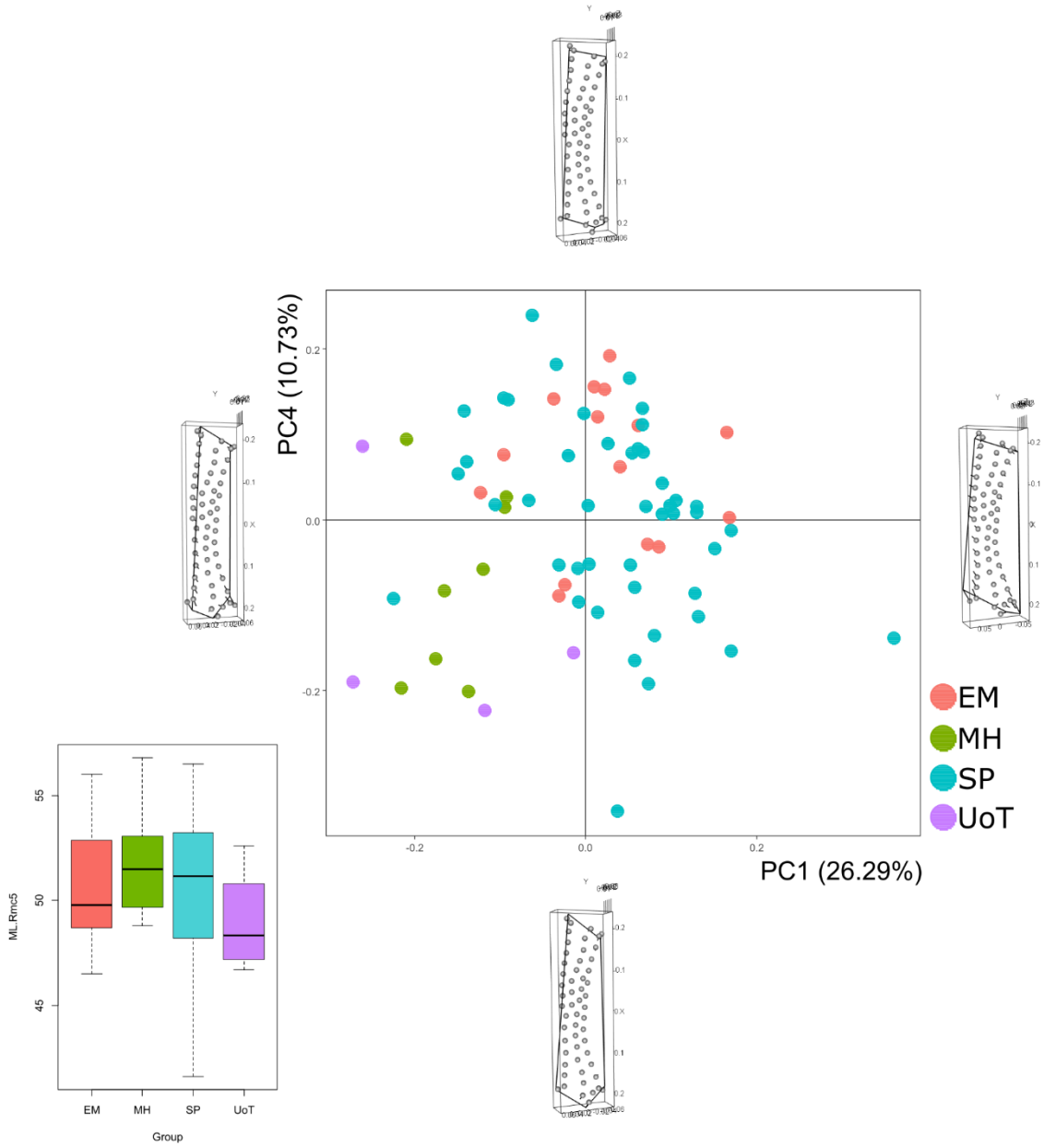
PC4 (10.73%)
PC1 (26.29%)
EM
MH
SP
UoT
ML.Rmc5
Group
EM
MH
SP
UoT

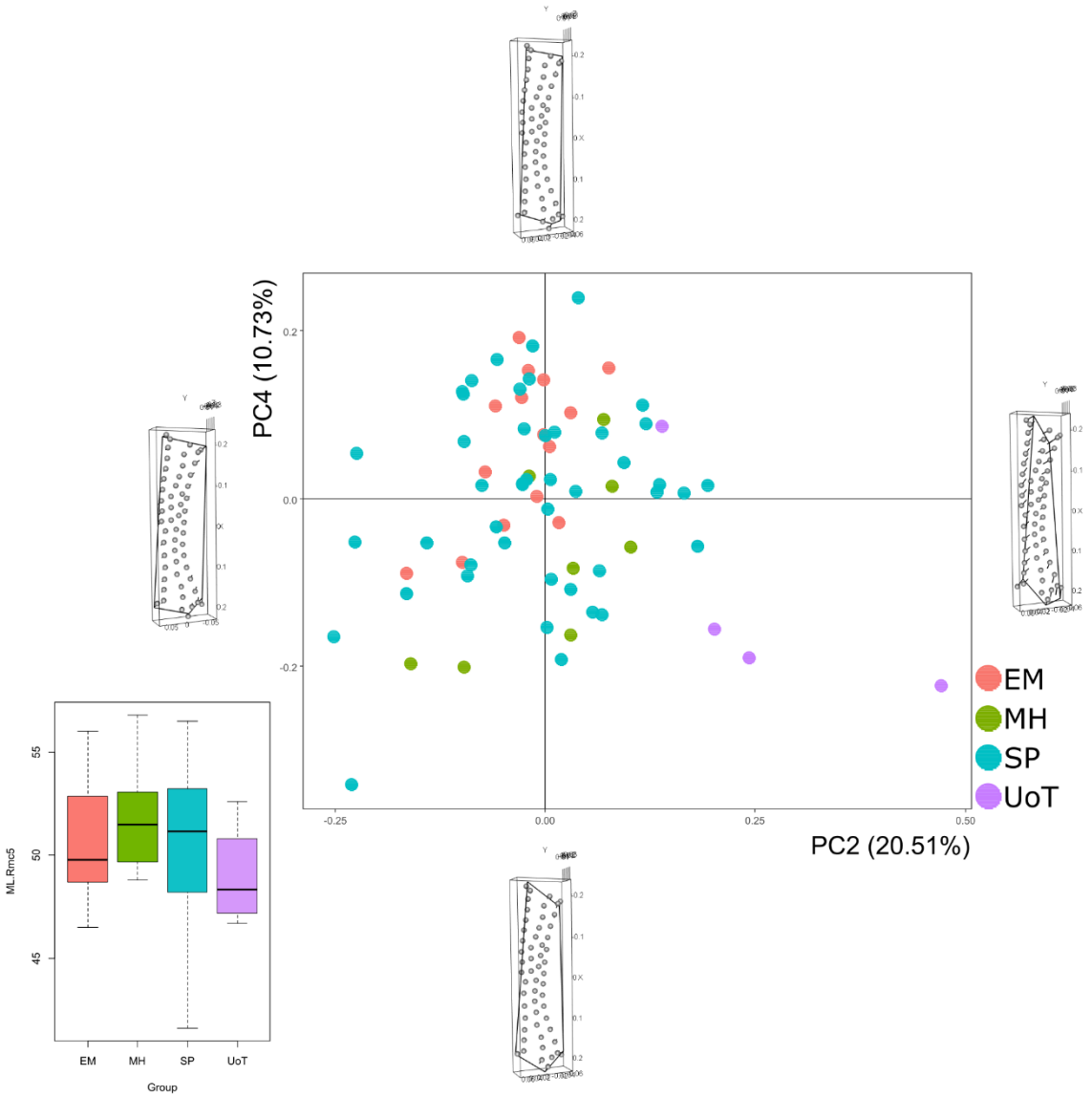
PC4 (10.73%)
PC2 (20.51%)
0.2
0.0
-0.2
-0.25
0.00
0.25
0.50
EM
MH
SP
UoT
MLRmc5
55
50
45
EM
MH
SP
UoT
Group

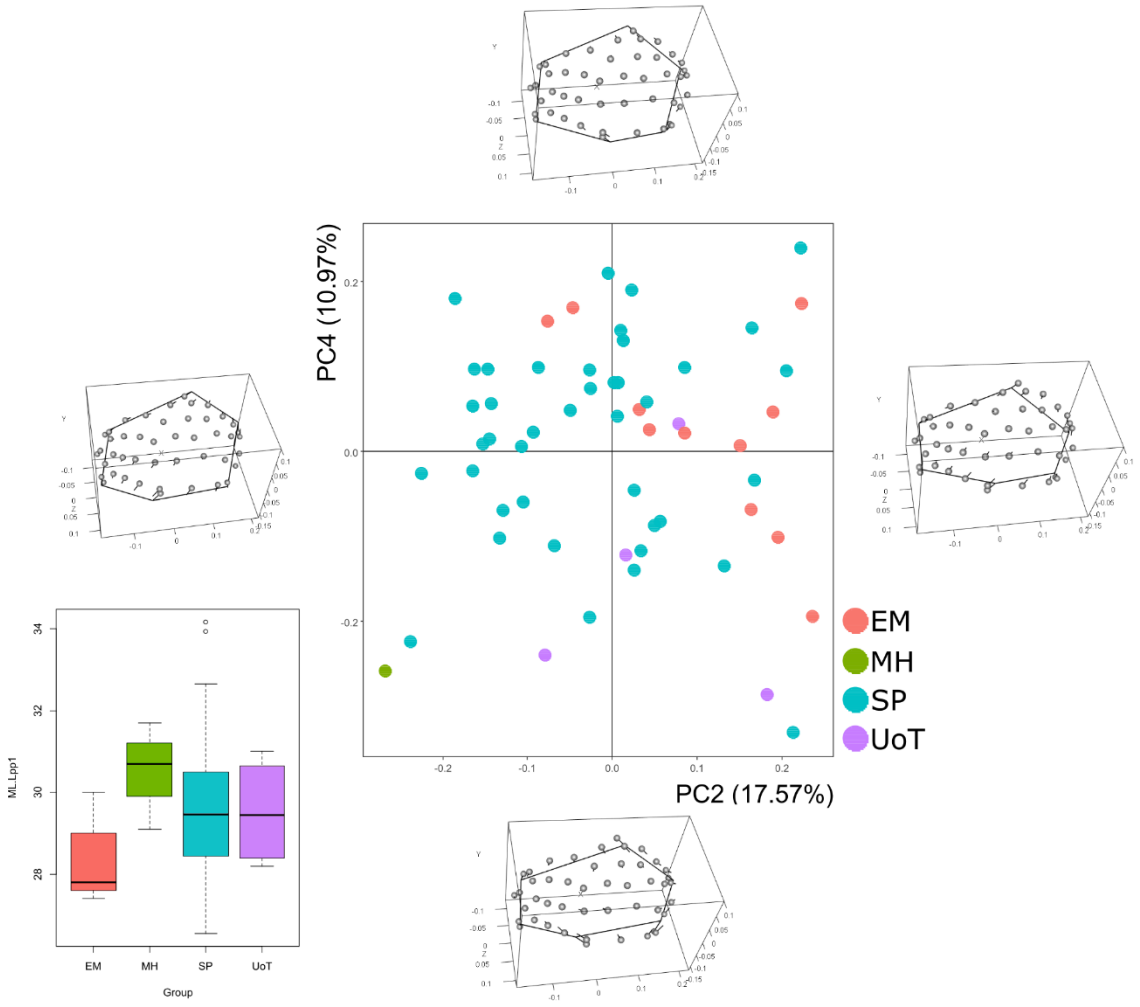
PC4 (10.97%)
PC2 (17.57%)
EM
MH
SP
UoT
ML.Lpp1
Group

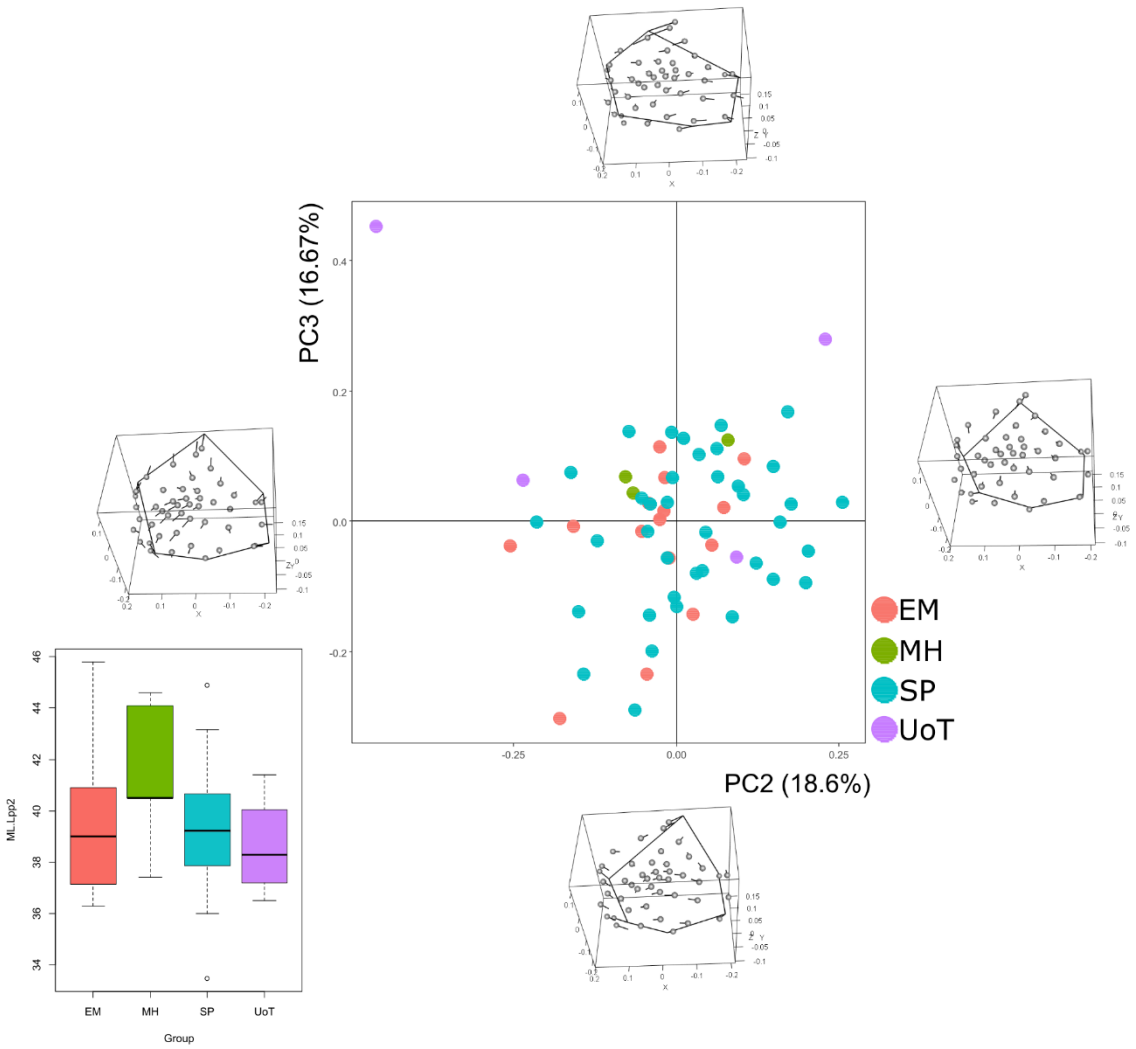
PC3 (16.67%)
PC2 (18.6%)
EM
MH
SP
UoT
ML.Lpp2
Group

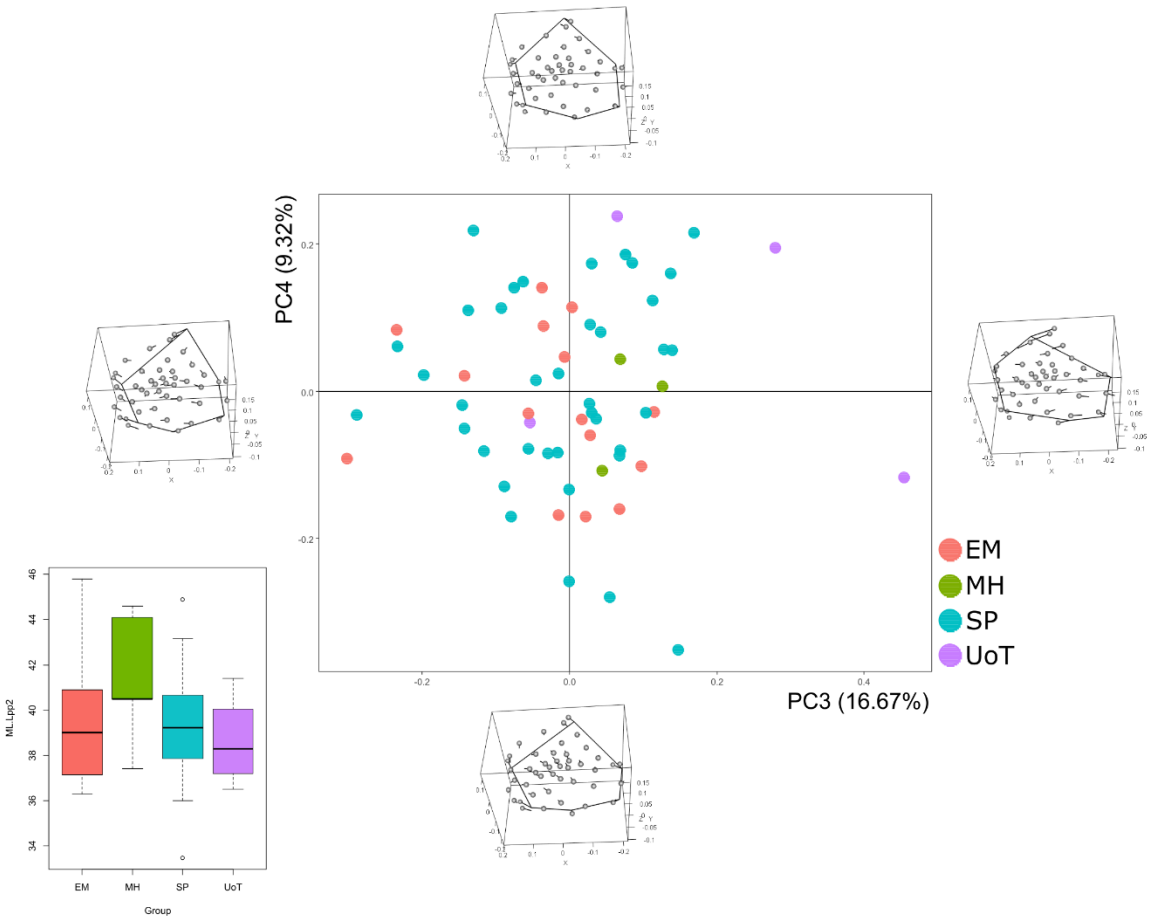
PC4 (9.32%)
PC3 (16.67%)
EM
MH
SP
UoT
ML.Lpp2
Group

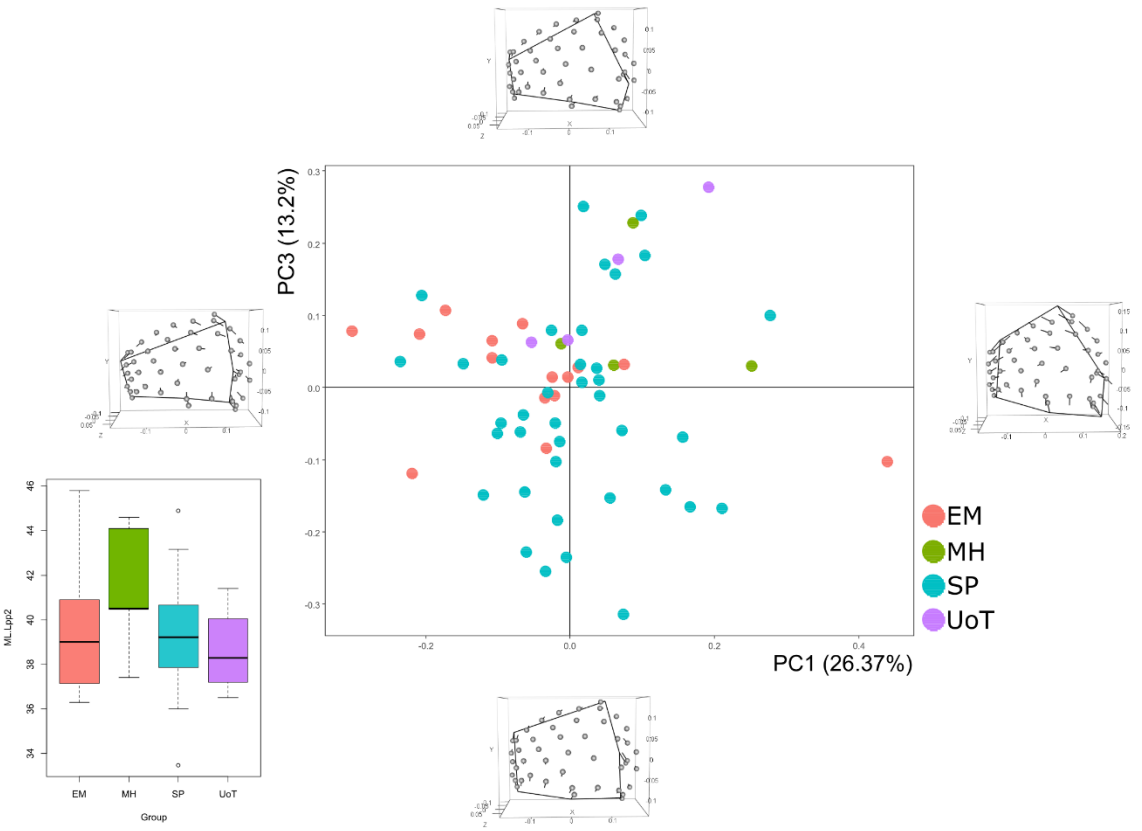
PC3 (13.2%)
PC1 (26.37%)
EM
MH
SP
UoT
MLLpp2
Group

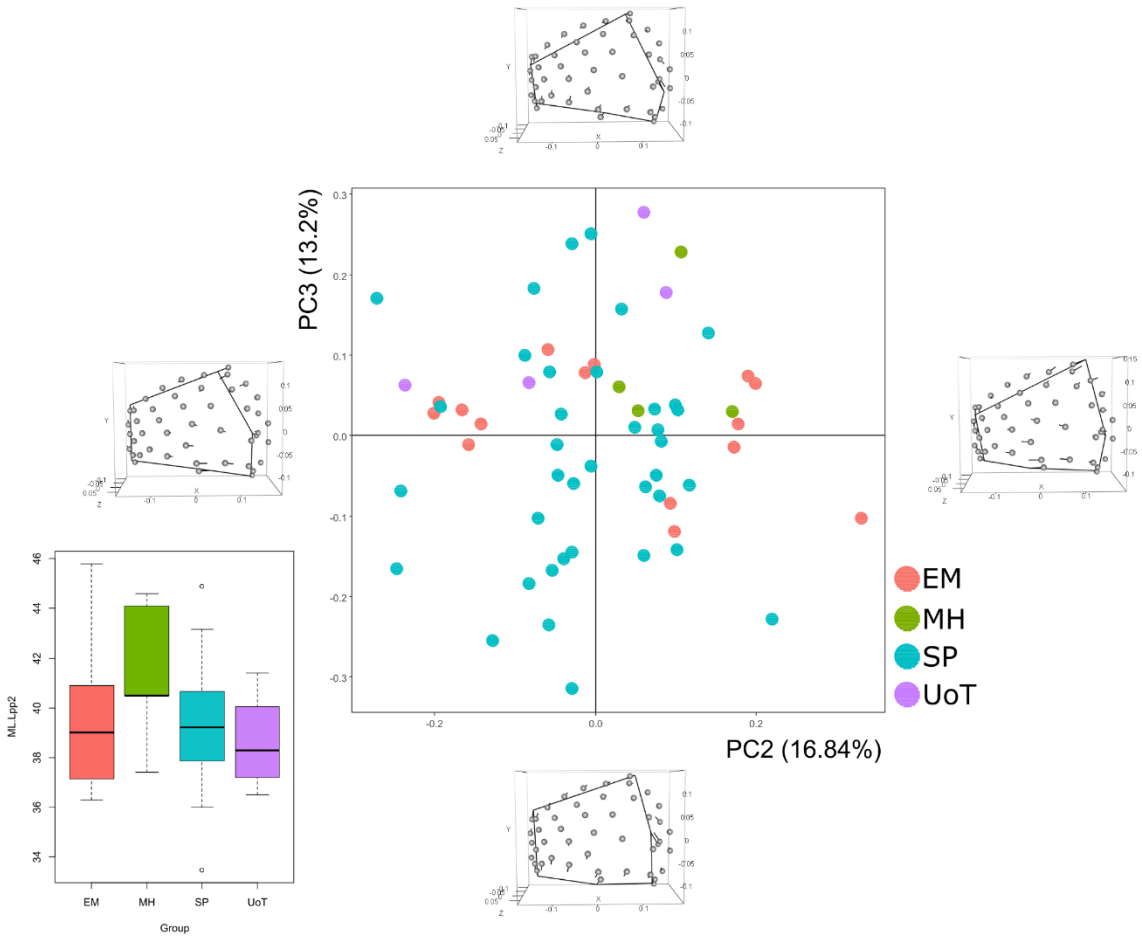
PC3 (13.2%)
PC2 (16.84%)
EM
MH
SP
UoT
ML.Lpp2
Group

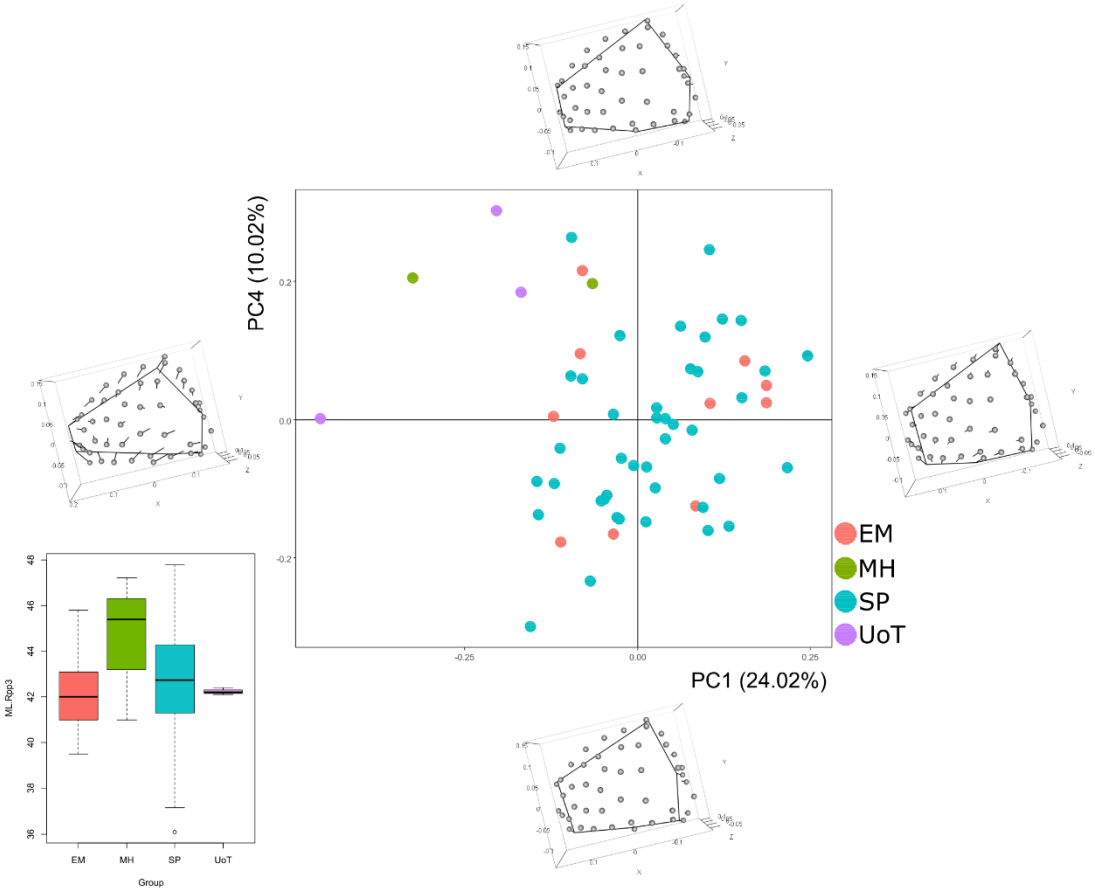
PC4 (10.02%)
PC1 (24.02%)
EM
MH
SP
UoT
ML.Rpp3
Group
EM
MH
SP
UoT

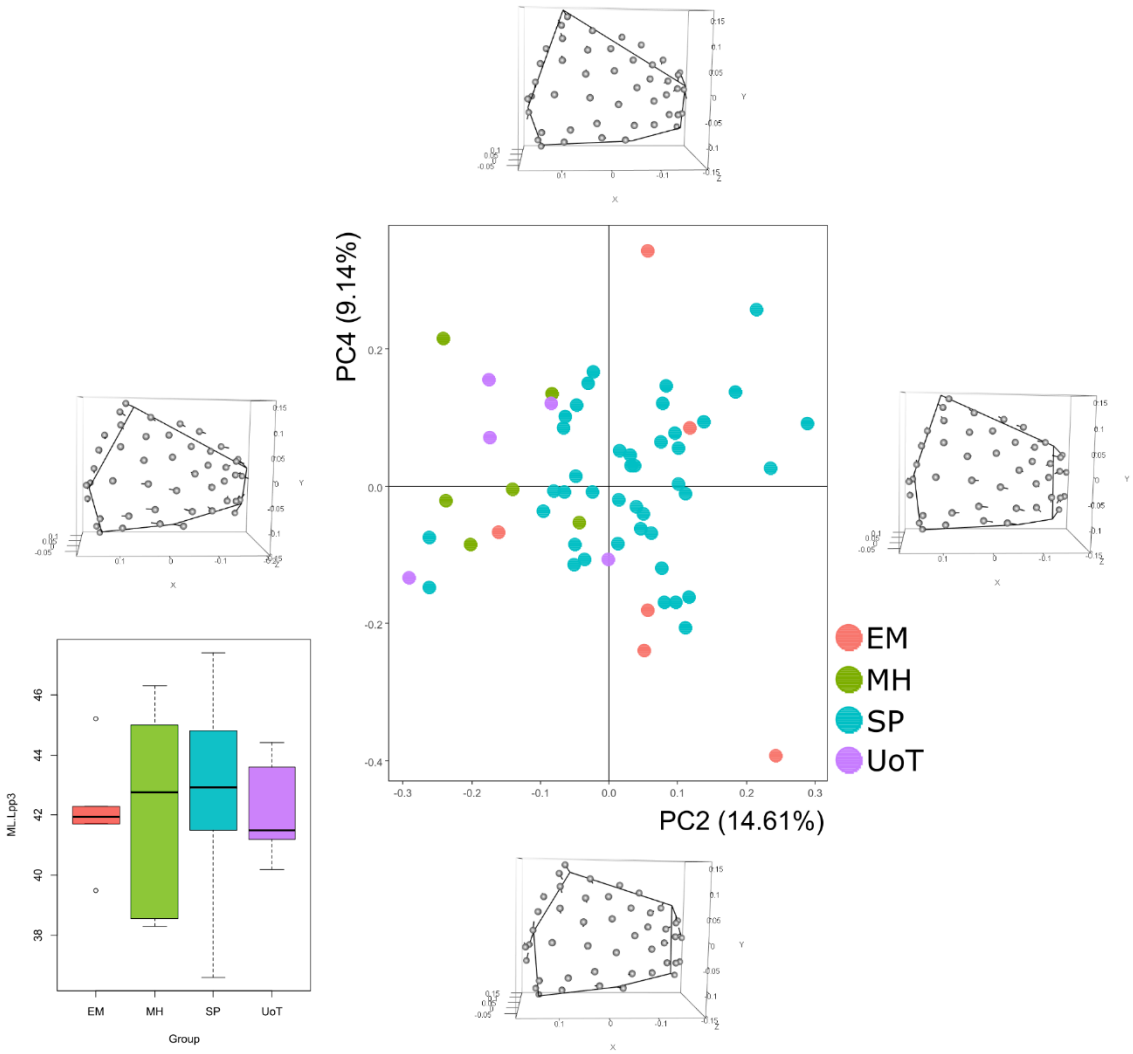
PC4 (9.14%)
PC2 (14.61%)
EM
MH
SP
UoT
ML.Lpp3
Group
EM
MH
SP
UoT

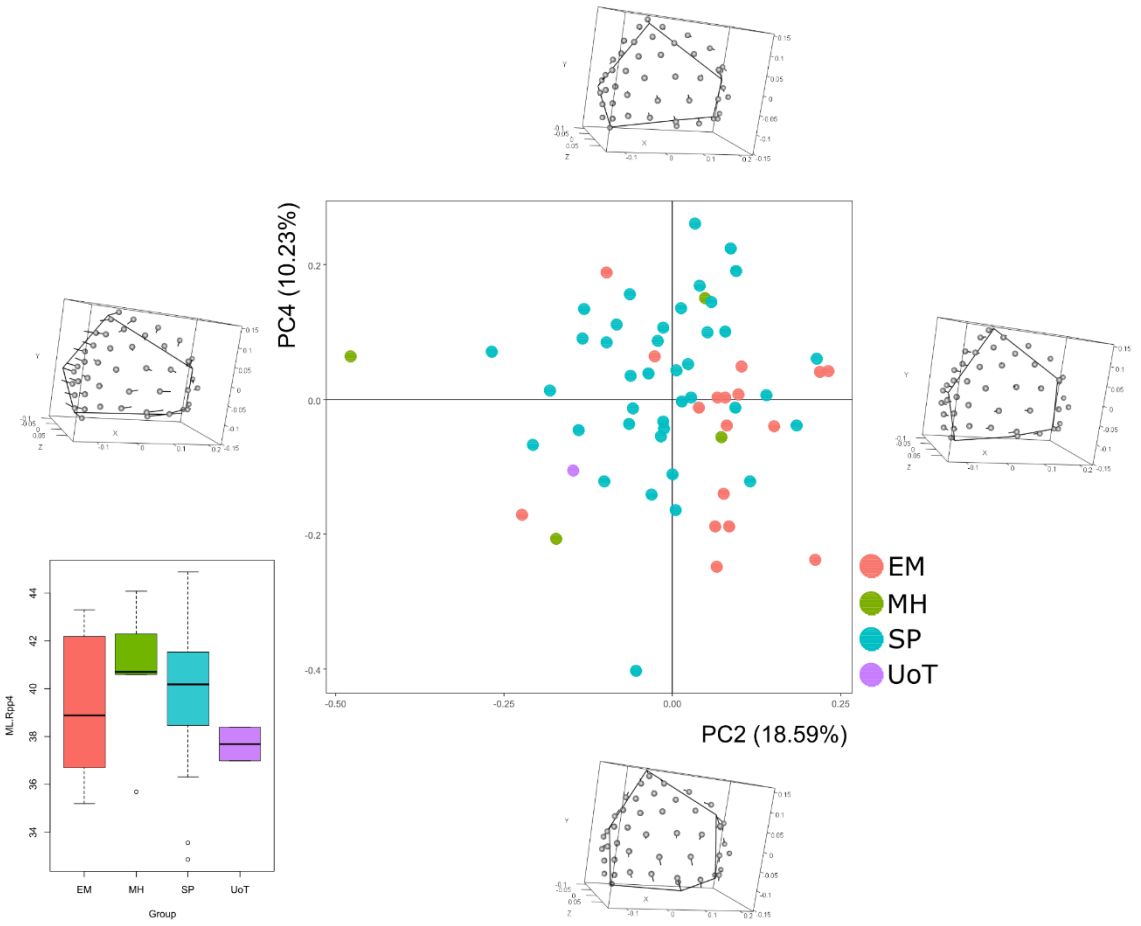
PC4 (10.23%)
PC2 (18.59%)
EM
MH
SP
UoT
ML.Rpp4
Group

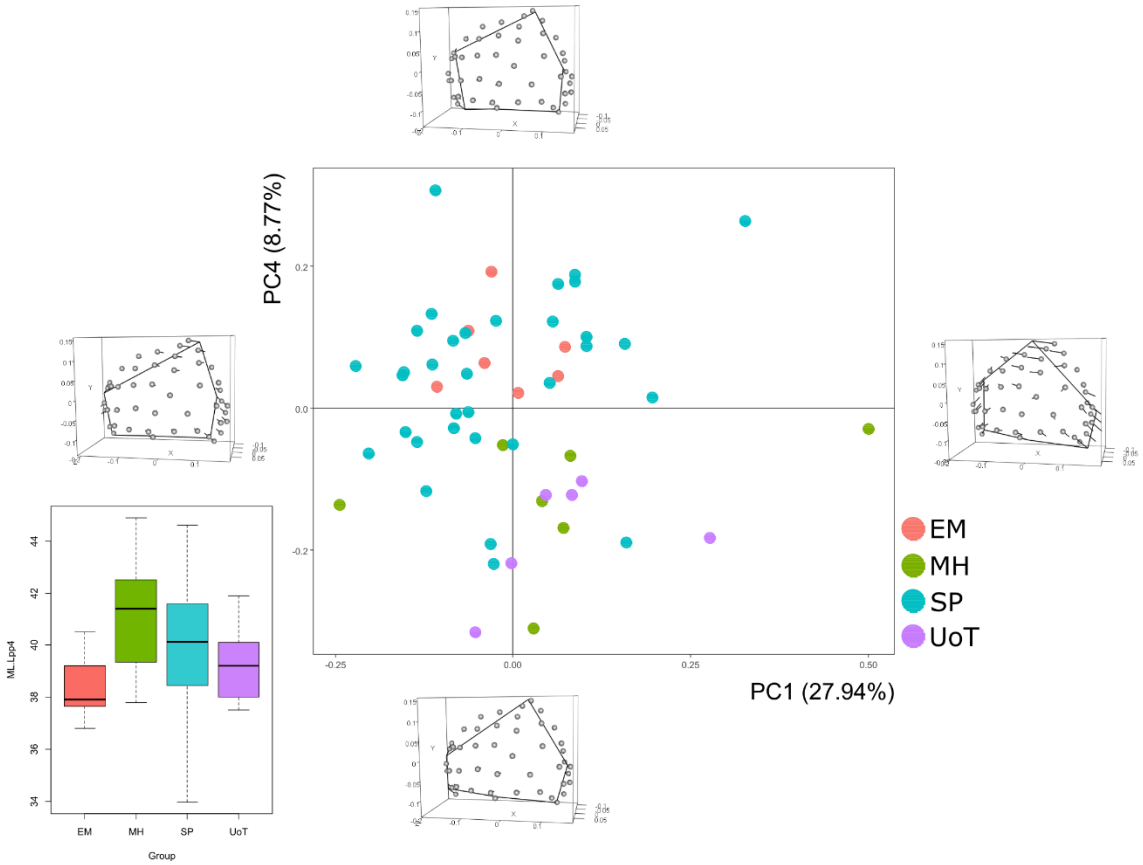
PC4 (8.77%)
PC1 (27.94%)
EM
MH
SP
UoT
MLLpp4
Group

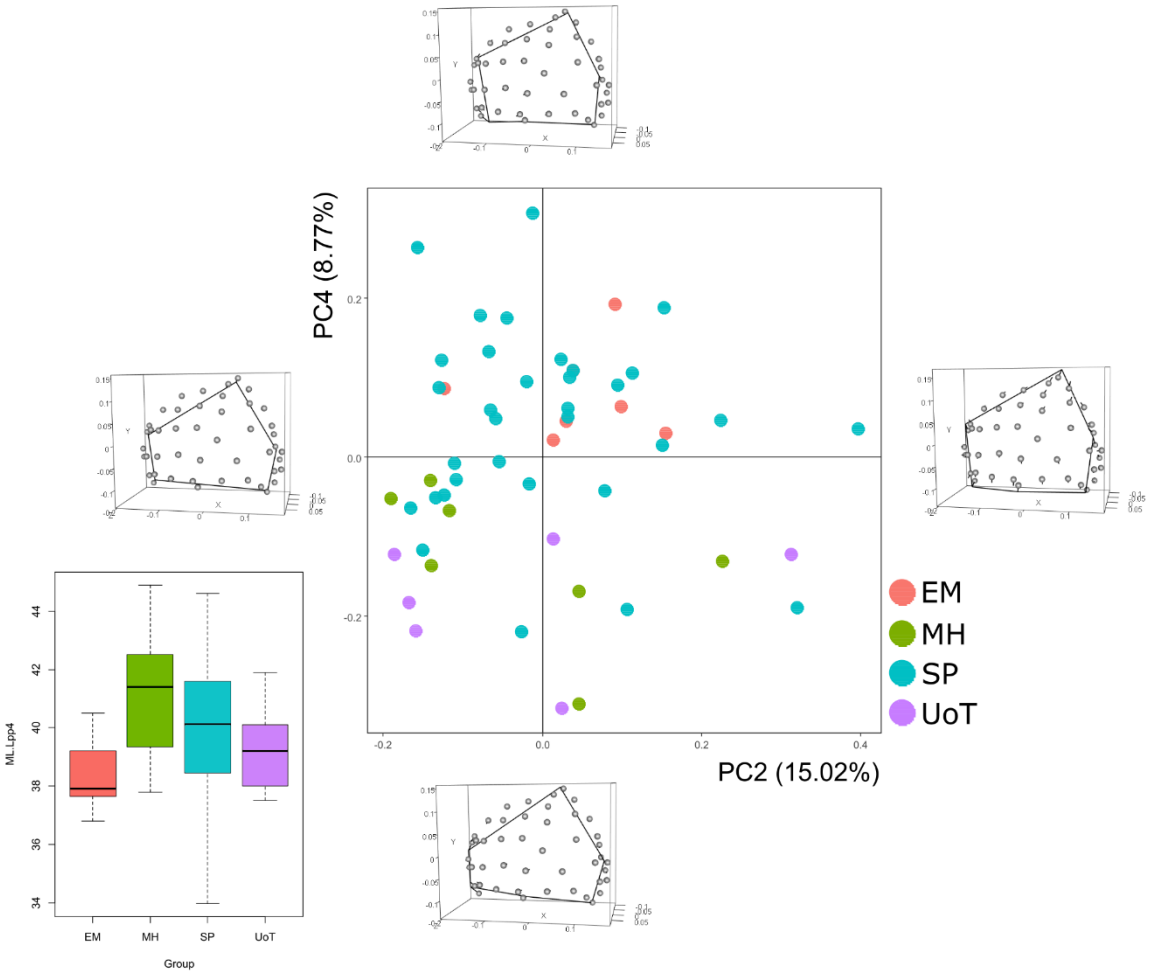
PC4 (8.77%)
PC2 (15.02%)
EM
MH
SP
UoT
ML.Lpp4
Group

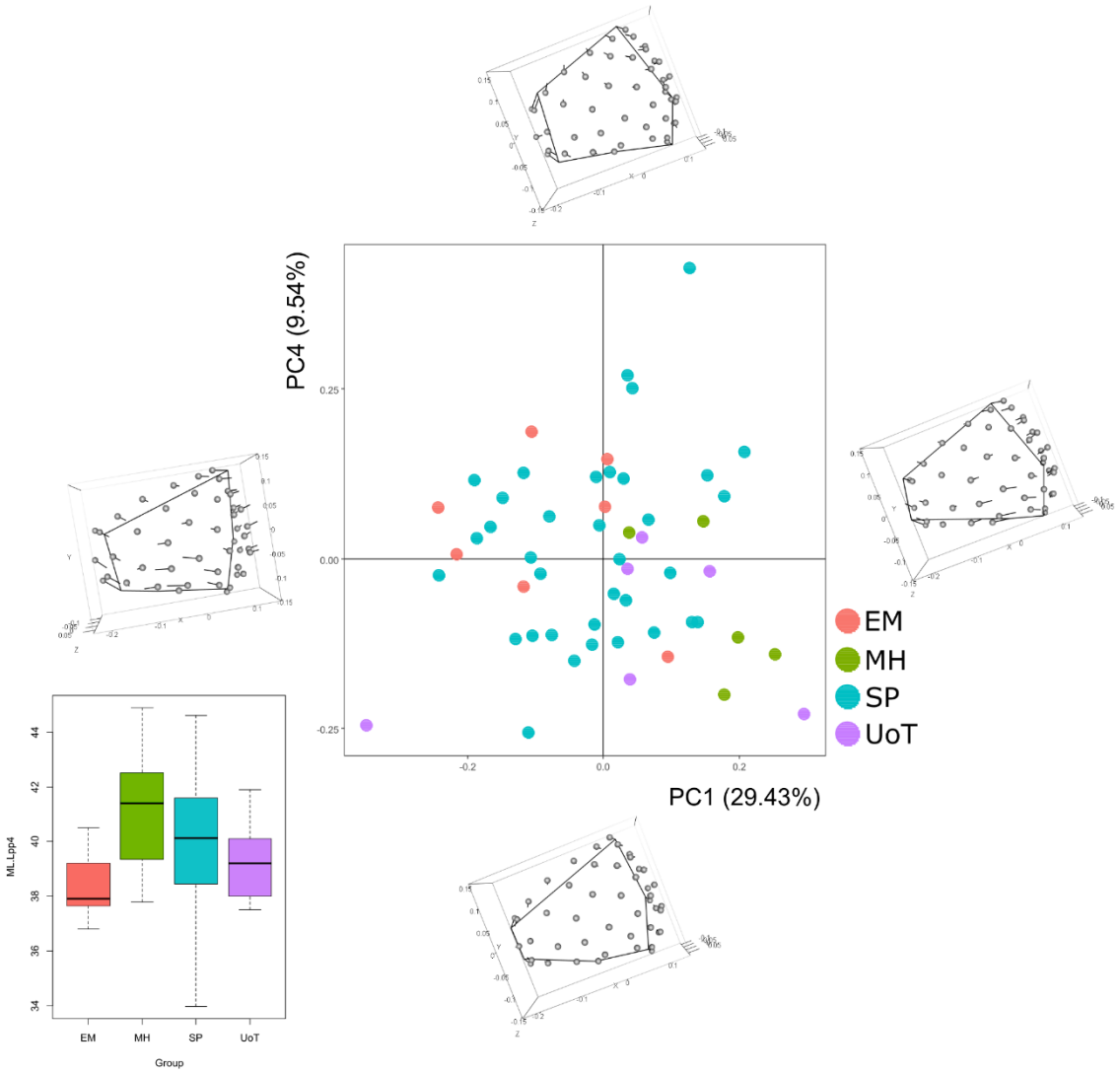
PC4 (9.54%)
PC1 (29.43%)
0.25
0.00
-0.25
-0.2
0.0
0.2
EM
MH
SP
UoT
MtLLpp4
34
36
38
40
42
44
EM
MH
SP
UoT
Group

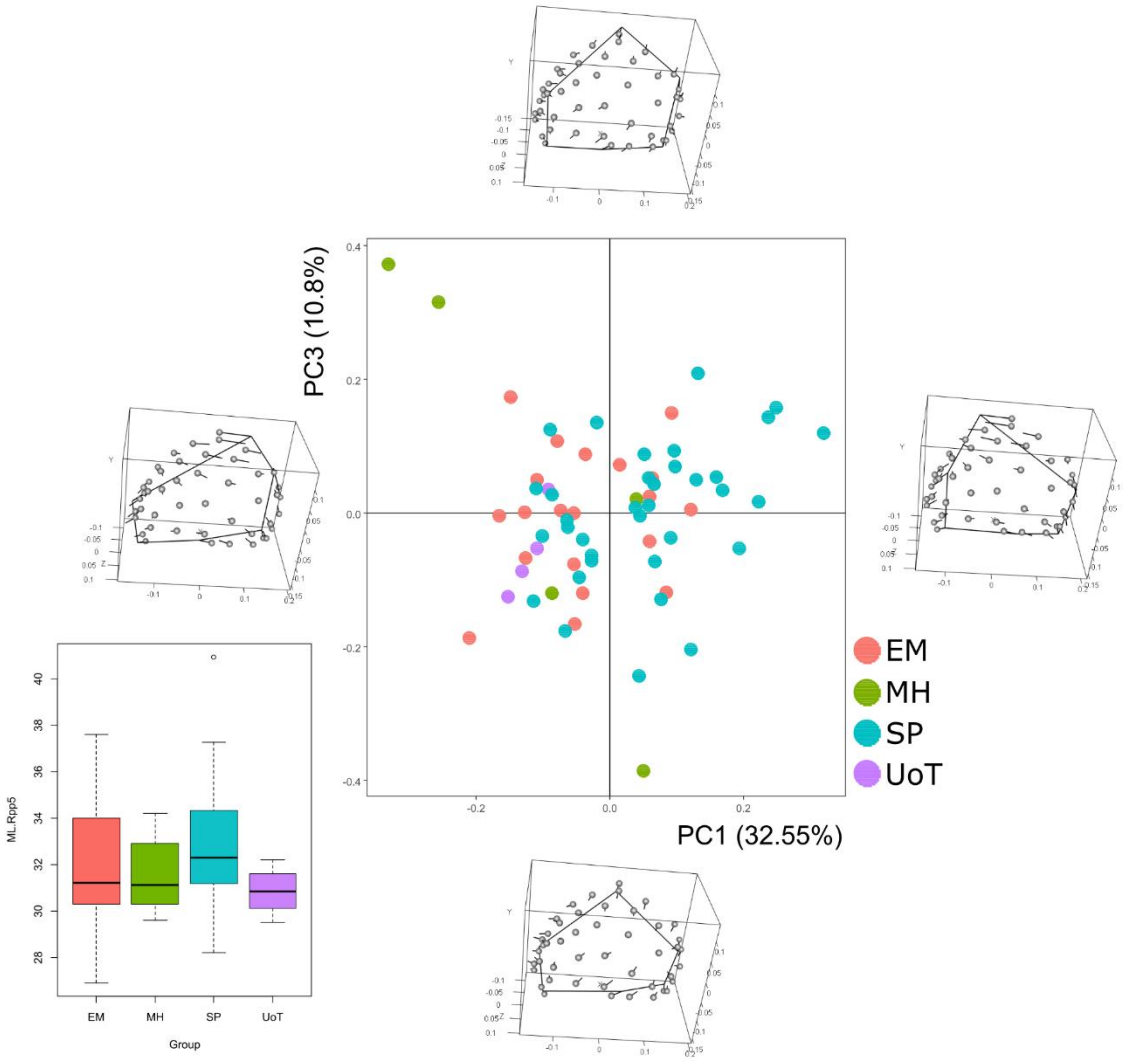
PC3 (10.8%)
PC1 (32.55%)
EM
MH
SP
UoT
ML.Rpp5
Group
EM
MH
SP
UoT

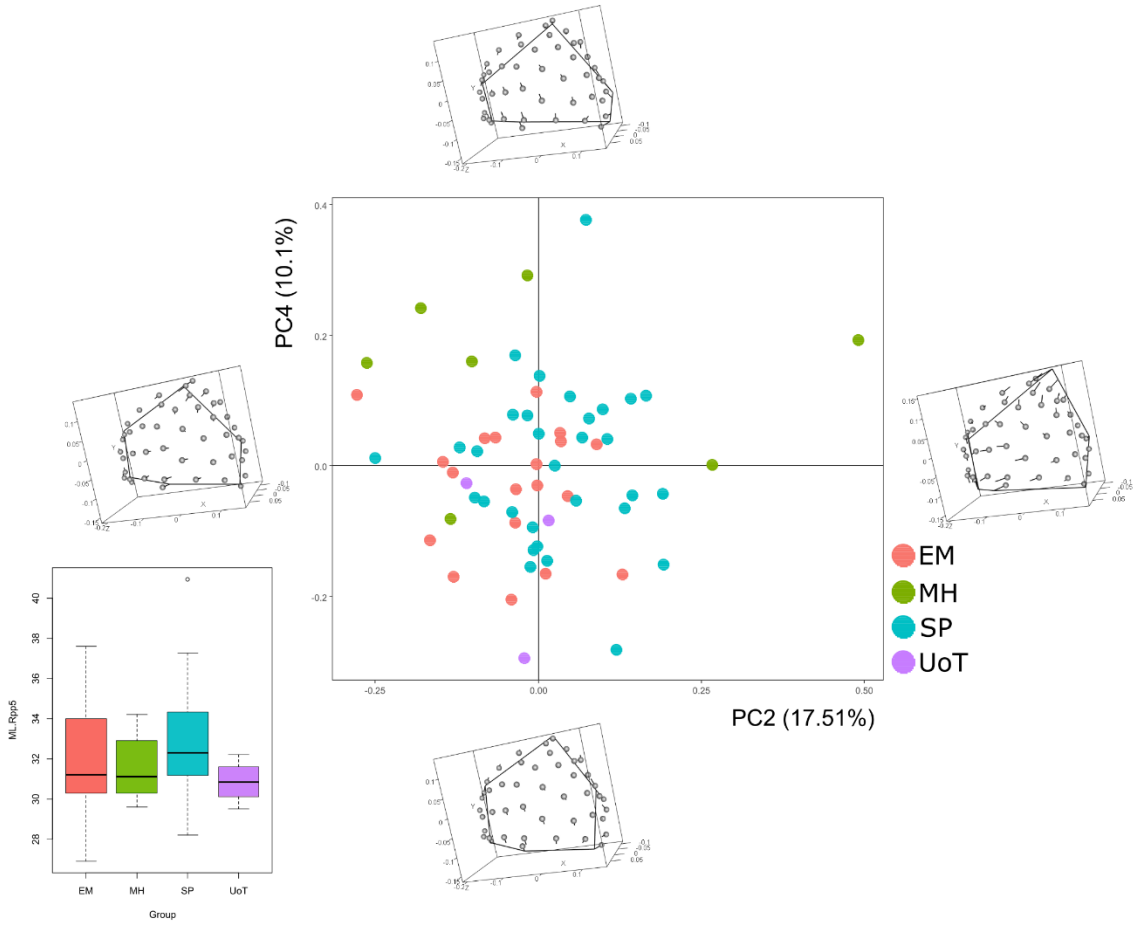
PC4 (10.1%)
PC2 (17.51%)
EM
MH
SP
UoT
ML.Rpo5
Group

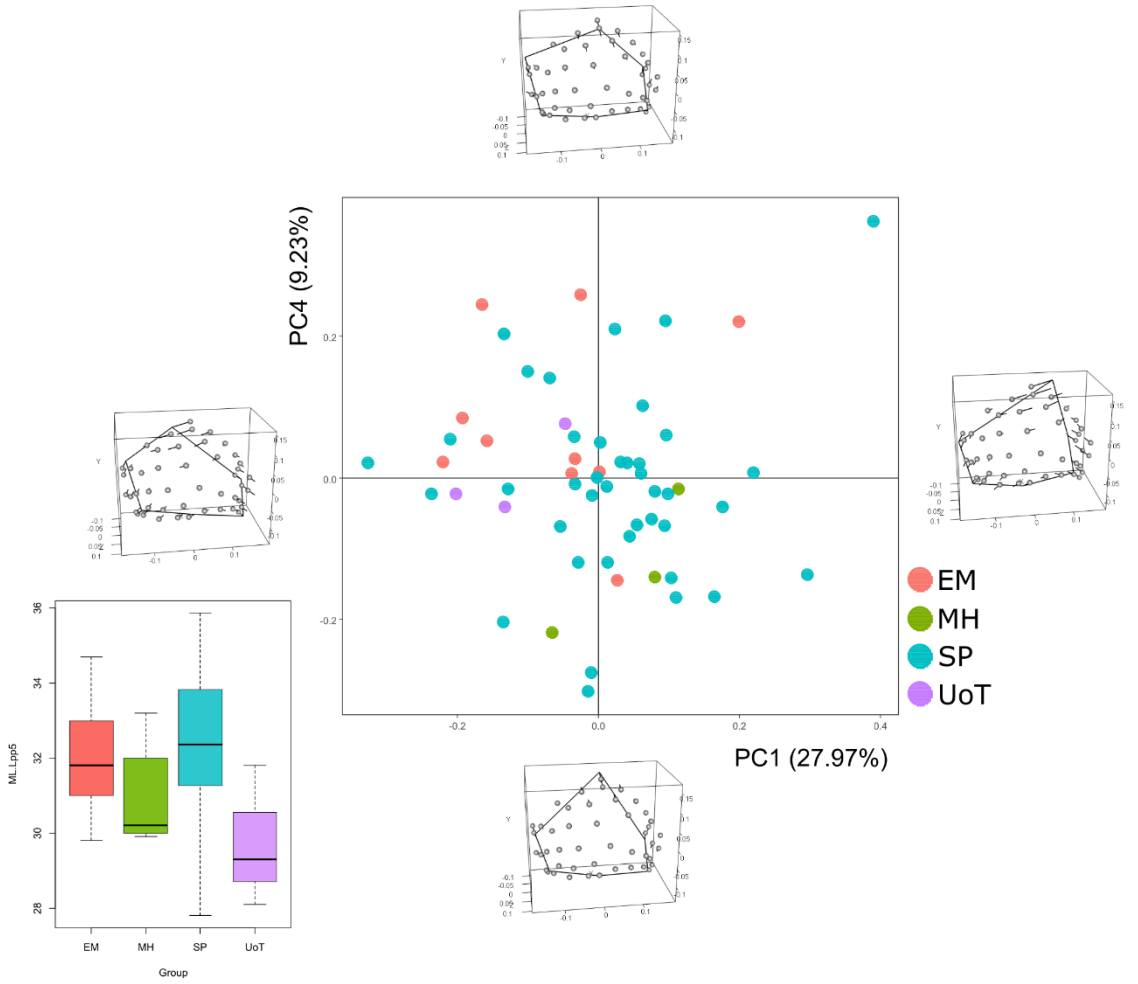
PC4 (9.23%)
PC1 (27.97%)
EM
MH
SP
UoT
MLLppS
Group

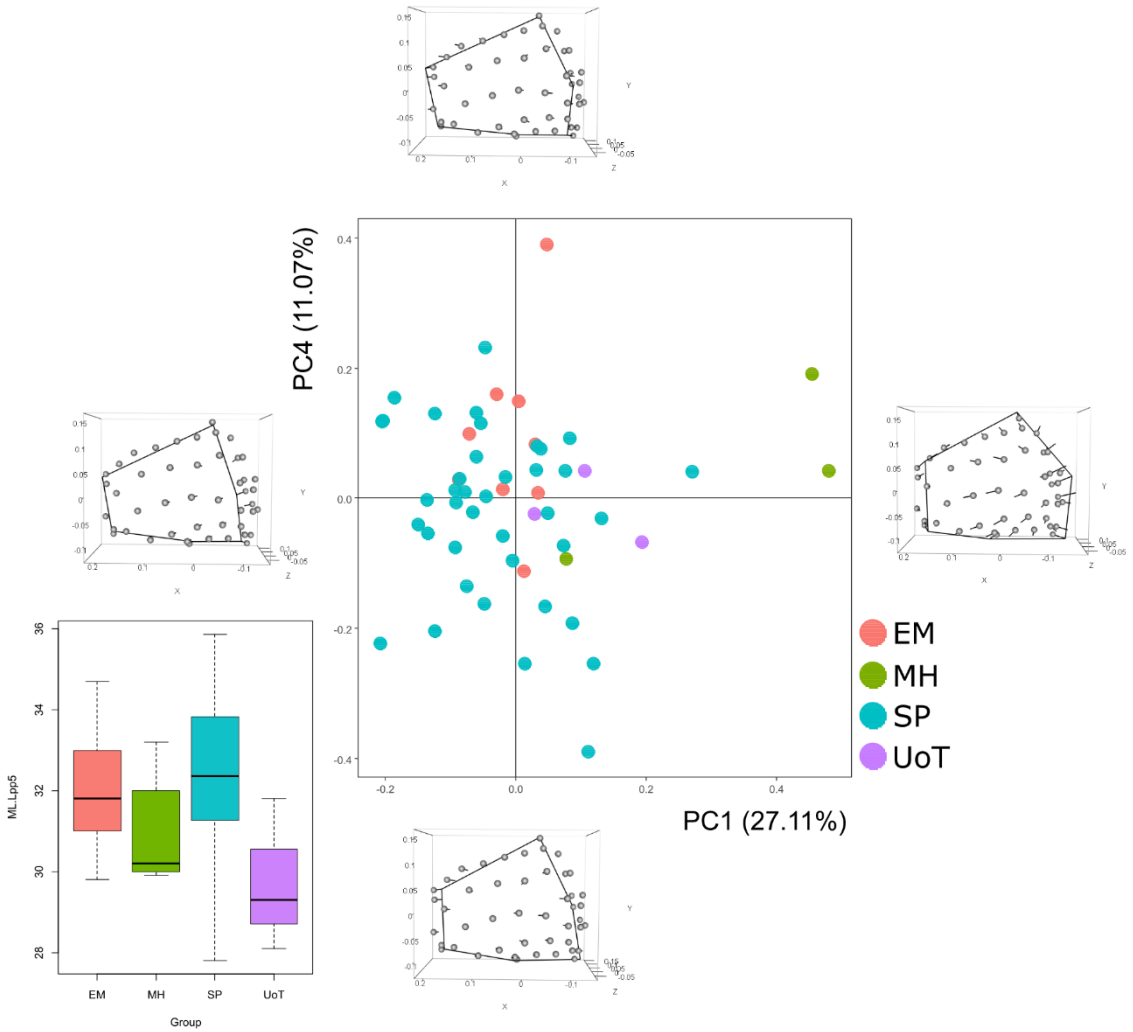
PC4 (11.07%)
PC1 (27.11%)
EM
MH
SP
UoT
ML.bp5
Group
EM
MH
SP
UoT

Index of Illustrations

Figures

Tables